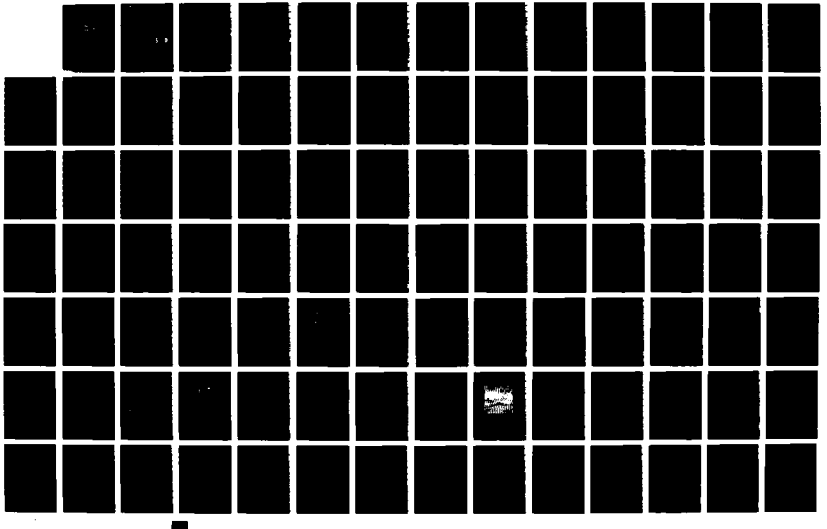
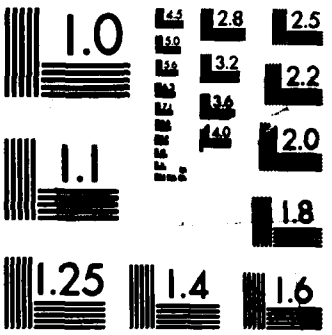
AD-A183 054 AN INTERDISCIPLINARY APPROACH TO PREDICTIVE MODELING OF STRUCTURAL ADHESI..(U) VIRGINIA TECH CENTER FOR ADHESION SCIENCE BLACKSBURG J A SKILES ET AL. JUN 87 1/5

UNCLASSIFIED CAS/CHEM-87-2 F/G 11/1 NL





MICROCOPY RESOLUTION TEST CHART
NATIONAL BUREAU OF STANDARDS-1963-A

DTIC FILE COPY

AD-A183 054

VIRGINIA TECH
CENTER FOR ADHESION SCIENCE

CAS/CHEM-87-2 June 1987

SUMMARY REPORT

AN INTERDISCIPLINARY APPROACH TO PREDICTIVE MODELING OF STRUCTURAL ADHESIVE BONDING

CHROMIC ACID ANODIZED Ti-6Al-4V: ITS CHARACTERIZATION AND ITS SINGLE LAP BOND STRENGTH TO HEAT RESISTANT ADHESIVES

by

Jean Ann Skiles
and
J. P. Wightman

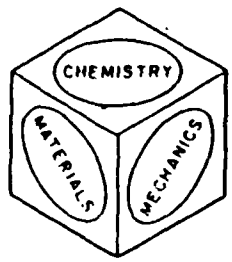
DTIC
ELECTE
JUL 29 1987
S D
D

Prepared under Contract No. N00014-82-0185
Dr. Larry H. Peebles, Jr., Project Monitor
Office of Naval Research
Code 431
800 N. Quincy Street
Arlington, VA 22217

VIRGINIA POLYTECHNIC INSTITUTE
AND STATE UNIVERSITY

216 NORRIS HALL
BLACKSBURG, VIRGINIA 24061

Telephone: (703) 961-6824
TLX: EZLINK 9103331861
VPI-BKS



DISTRIBUTION STATEMENT A
Approved for public release;
Distribution Unlimited

SECURITY CLASSIFICATION OF THIS PAGE

AD-A183054

REPORT DOCUMENTATION PAGE

1a. REPORT SECURITY CLASSIFICATION Unclassified	1b. RESTRICTIVE MARKINGS
2a. SECURITY CLASSIFICATION AUTHORITY	3. DISTRIBUTION / AVAILABILITY OF REPORT Distribution Unlimited
2b. DECLASSIFICATION / DOWNGRADING SCHEDULE	
4. PERFORMING ORGANIZATION REPORT NUMBER(S) CAS/CHEM-87-2	5. MONITORING ORGANIZATION REPORT NUMBER(S)
6a. NAME OF PERFORMING ORGANIZATION Virginia Polytechnic Institute and State University 6b. OFFICE SYMBOL (If applicable)	7a. NAME OF MONITORING ORGANIZATION
6c. ADDRESS (City, State, and ZIP Code) Center for Adhesion Science and Department of Chemistry Blacksburg, VA 24061	7b. ADDRESS (City, State, and ZIP Code)
8a. NAME OF FUNDING / SPONSORING ORGANIZATION Office of Naval Research 8b. OFFICE SYMBOL (If applicable)	9. PROCUREMENT INSTRUMENT IDENTIFICATION NUMBER
8c. ADDRESS (City, State, and ZIP Code) 800 N. Quincy Street Arlington, VA 22217	10. SOURCE OF FUNDING NUMBERS PROGRAM ELEMENT NO. / PROJECT NO. / TASK NO. / WORK UNIT ACCESSION NO.

11. TITLE (Include Security Classification)
An Interdisciplinary Approach to Predictive Modeling of Structural Adhesive Bonding/Chromic Acid Anodized Ti-6Al-4V: Its Characterization and Its Single Life Bond Strength to Heat Resistant Adhesives

12 PERSONAL AUTHOR(S)
Skiles, Jean Ann and Wightman, J. P.

13a. TYPE OF REPORT	13b. TIME COVERED	14. DATE OF REPORT (Year, Month, Day)	15. PAGE COUNT
Summary Report	FROM 1/82 TO 6/87	June 1987	364

16. SUPPLEMENTARY NOTATION

17. COSATI CODES			18. SUBJECT TERMS (Continue on reverse if necessary and identify by block number)
FIELD	GROUP	SUB-GROUP	

19. ABSTRACT (Continue on reverse if necessary and identify by block number)

Single lap bond strength and the fracture mechanism were determined for unprimed and Lica® 44 titanate primed chromic acid/hydrofluoric acid (CA/HF) anodized Ti-6Al-4V/heat resistant bonds. Adhesives tested had reported service temperatures ≥ 423K. Bonds were tested in ambient and also after exposure to thermal aging conditions. Anodic oxide morphology, structure, and thickness were also characterized as a function of anodization procedure.

20. DISTRIBUTION / AVAILABILITY OF ABSTRACT	21. ABSTRACT SECURITY CLASSIFICATION	
☒ UNCLASSIFIED/UNLIMITED ☐ SAME AS RPT. ☐ DTIC USERS		
22a. NAME OF RESPONSIBLE INDIVIDUAL	22b. TELEPHONE (Include Area Code)	22c. OFFICE SYMBOL

DD FORM 1473, 84 MAR 83 APR edition may be used until exhausted. All other editions are obsolete.

SECURITY CLASSIFICATION OF THIS PAGE

CHROMIC ACID ANODIZED Ti-6Al-4V: ITS CHARACTERIZATION AND ITS SINGLE LAP BOND STRENGTH TO HEAT RESISTANT ADHESIVES

(ABSTRACT)

Anodized ~~Ti-6Al-4V~~ Titanium Aluminum Vanadium adhesive bonds exhibit improved corrosion resistance and a higher strength-to-weight ratio compared to conventional metal bonding techniques for primary and/or secondary structural applications. This work was conducted to identify chromic acid (CA) anodization and bond process conditions which produced durable, structural anodized ~~Ti-6Al-4V~~ Titanium Aluminum Vanadium heat resistant single lap bonds and to understand why these conditions were necessary. A structural single lap bond was defined as a bond tested at 298K $\leq$ 0.5 month after bonding and with a strength $\geq$ 6.9 MPa, based upon values reported in structural adhesive manufacturers' product literature. A durable, structural single lap bond was defined as a bond with a strength $\geq$ 6.9 MPa strength at 298K after 9 months aging at 443K. Heat resistant adhesives tested had reported service temperatures greater than 423K, and were: polysulfone; polyethersulfone; polyphenylquinoxaline; polyetherimide, both unfilled and 20% glass filled; and 50% calcium carbonate filled polyimide.

Hydrofluoric acid (HF) added to the CA anodization solution was necessary to produce structural bonds. ~~CA/HF~~ Chromic acid hydrofluoric acid oxide was more porous, and thicker than the CA anodic oxide (140 nm vs. 20 nm); perhaps promoting physical and oxide/adhesive interphase mechan-

Codes
Dist Avail and/or Special
A-1

QUALITY INSPECTED 4

ical interlock. Structural, durable CA/HF anodized Ti-6Al-4V/-adhesive bonds were produced for all adhesives tested except for the filled polyimide (5.5 MPa). The filler may have occluded oxide pores and prevented optimal adhesive/oxide interphase interlock, and there may have been competition of polyimide for calcium carbonate filler and for oxide. Average oxide thickness values of 65 to 410 nm did not affect bond strength; structural bonds were produced in all cases. CA/HF initial current density of 20 Amperes per square meter produced 33% stronger polysulfone bonds than 30 Amperes per square meter. Polysulfone microstructure may have been chemically degraded by the unnecessarily high fluoride concentration in the oxide from the higher current density. Lica® 44 titanate primer did not significantly influence bond strength or durability, except when unfilled polyetherimide was the adhesive. Polyphenylquinoxaline bond processing influenced bond strength. Structural bonds resulted for all the CA/HF anodization and process conditions described above. Single lap bond fracture initiated in the adhesive (polymer) fillet. Fracture propagation in the bond overlap was through the polymer/anodic oxide interphase and/or cohesively in the polymer.

TABLE OF CONTENTS

	Page
ABSTRACT	ii
LIST OF TABLES	xi
LIST OF FIGURES	xvi
Chapter	
I INTRODUCTION	1
A. The Metal-Adhesive Bond: Advantages and Disadvantages	1
B. Research Objectives	5
II LITERATURE REVIEW	13
A. Adhesion Theories	13
B. Factors Which Influence Adhesive Bond Strength	18
C. Oxide Characterization for Chromic Acid/ Hydrofluoric Acid Anodized Ti-6Al-4V . . .	23
D. Chromic Acid with Hydrofluoric Acid Anodized Ti-6Al-4V/Adhesive Bond Characterization and Durability	26
III EXPERIMENTAL	29
A. Chromic Acid Anodization Methods and Materials	29
B. X-Ray Diffraction	41
C. Transmission Electron Microscopy (TEM) and Selected Area Electron Diffraction (SAED) .	41
D. Multiple Beam Interferometry (MBI) Methods and Materials	42

TABLE OF CONTENTS (Continued)

Chapter		Page
III	EXPERIMENTAL (Continued)	
	E. Chromic Acid Anodized Ti-6Al-4V/Heat Resistant Adhesive Single Lap Bond	53
	1. Ti-6Al-4V Adherend	53
	2. Heat Resistant Adhesives	55
	3. Single Lap Bonding Apparatus	62
	4. Single Lap Bonding Methods	64
	5. Single Lap Bond Thermal Aging Conditions	73
	a. Polysulfone Bonds	73
	b. Polyimide Bonds	77
	c. Polyphenylquinoxaline Bonds	78
	d. Polyethersulfone Bonds	79
	e. Polyetherimide Bonds	80
	6. Single Lap Bond Adhesive Thickness Measurement Methods	80
	7. Single Lap Bond Test Method	81
	8. Single Lap Bond Strength Statistical Analyses Methods	84
	9. Photography of the Single Lap Bond Fracture Process	85
	10. Qualitative Image Analysis (QIA) Methods	85
	11. Scanning Electron Microscopy	87
	12. Electron Spectroscopy for Chemical Analysis (ESCA)	89

TABLE OF CONTENTS (Continued)

Chapter		Page
III	EXPERIMENTAL (Continued)	
	13. Auger Electron Spectroscopy	90
IV	RESULTS AND DISCUSSION	92
	A. Anodized Ti-6Al-4V Oxide Characterization	92
	1. Oxide Morphology	92
	a. Scanning Electron Microscopy (SEM) Micrographs	92
	b. Transmission Electron Microscopy (TEM) Micrographs	96
	2. Proposed Model for the CA/HF Anodized Ti-6Al-4V/Adhesive Bond Based upon Anodic Oxide Morphology	101
	3. Oxide Structure	107
	4. Oxide Thickness	108
	a. A Comparison of TEM and MBI Oxide Thickness Methods and Results	108
	b. Influence of Anodization Solution Composition upon Oxide Thickness .	112
	c. Influence of CA/HF Anodization Time upon Oxide Thickness	115
	d. Influence of CA/HF Solution Temperature and Initial Current Density upon Oxide Thickness	115
	B. Anodized Ti-6Al-4V/Heat Resistant Adhesive Single Lap Bond Strength Data Analyses . . .	120
	1. The Interpretation of Single Lap Bond Strength Data	120

TABLE OF CONTENTS (Continued)

Chapter		Page
IV	RESULTS AND DISCUSSION (Continued)	
	2. The Influence of Test Variables upon Single Lap Bond Strength . . .	122
	a. Overview	122
	b. The Influence of Ti-6Al-4V Preanodization Cleaning Treatment upon Bond Strength	122
	c. The Influence of Ti-6Al-4V Chromic Acid Anodization Method upon Bond Strength	124
	1. The Influence upon Bond Strength of Hydrofluoric Acid Added to the Chromic Acid Anodization Solution	124
	2. The Influence of CA/HF Anodization Time upon Bond Strength	128
	3. The Influence of CA/HF Anodization Initial Current Density and Solution Temperature upon Single Lap Bond Strength	128
	d. The Influence of Single Lap Bonding Procedure on CA/HF Anodized Ti-6Al-4V/Polyphenylquinoxaline Bond Strength	144
	e. Thermal Aging Effects upon Single Lap Bond Strength	147
	1. Thermally Aged, Unprimed CA/HF Anodized Ti-6Al-4V/Polysulfone Single Lap Bond Strength . . .	147
	2. Thermally Aged, Unprimed CA/HF Anodized Ti-6Al-4V/50% $CaCO_3$ Filled Polyimide Single Lap Bond Strength	150

TABLE OF CONTENTS (Continued)

Chapter		Page
IV	RESULTS AND DISCUSSION (Continued)	
	3. Thermally Aged, CA/HF Anodized Ti-6Al-4V/Polyphenylquinoxaline Single Lap Bond Strength for Unprimed and Primed Anodized Ti-6Al-4V	153
	4. Thermally Aged, CA/HF Anodized Ti-6Al-4V/Polyethersulfone Single Lap Bond Strengths for Unprimed and Primed Anodized Ti-6Al-4V	158
	5. Thermally Aged, CA/HF Anodized Ti-6Al-4V/Polyetherimide Single Lap Bond Strengths for Unprimed and Primed Anodized Ti-6Al-4V	158
	f. The Influence of the Heat Resistant Adhesive upon Single Lap Bond Strength	167
	C. Failure Analyses for Single Lap Bonds . . .	171
	1. Fracture Initiation	171
	a. Photographic Analyses	171
	b. SEM Analyses	171
	c. Failure Initiation Mechanism . . .	178
	2. Fracture Propagation	179
	a. Proposed Model for the CA/HF Anodized Ti-6Al-4V/Adhesive Bond	179
	b. Visual Analyses of the Fractured Chromic Acid Anodized Ti-6Al-4V/ Adhesive Single Lap Bond . . .	182
	c. Quantitative Image Analyses . . .	199

TABLE OF CONTENTS (Continued)

Chapter		Page
IV	RESULTS AND DISCUSSION (Continued)	
	d. ESCA Analyses	207
	e. Auger Analyses	236
	f. Proposed Model of the Single Lap Fracture Sites and Mechanism Based upon Surface Analysis . .	251
	3. Polymer Fracture Surface Morphology	256
V	SUMMARY	266
VI	RECOMMENDATIONS FOR FUTURE STUDY . . .	270
LITERATURE CITED		271
APPENDIXES		
I	Approximation of the Titanate Monolayer Coverage on the Anodized Ti-6Al-4V Surface	275
II	T-Test Statistical Analysis	279
III	F-Test Statistical Analysis: The One Way Analysis of Variance Test	281
IV	X-Ray Diffraction Spectra for CA/HF Anodized Ti-6Al-4V. Anodization Conditions were: 20 Minutes, 298 ± 2K, 30 ± 2 A/m, 10 Volts . .	284
V	Multiple Beam Interferograms for Anodic Oxide Thickness Determination	289
VI	Anodic Oxide Electrical Property Characterization: Preliminary Results	296
VII	ESCA Data for: (1) Ti-6Al-4V Before and After Anodization; (2) Lica® 44 Titanate Primer; (3) Polysulfone, Polyphenylquinoxaline, Polyethersulfone, 50% Calcium Carbonate Filled Polyimide, Unfilled and 20% Glass	

TABLE OF CONTENTS (Continued)

Chapter Page

APPENDIXES (Continued)

Fiber Filled Polyetherimide; and, (4) Anodized Ti-6Al-4V/Heat Resistant Adhesive Single Lap Bond Fracture Surfaces 329

LIST OF TABLES

Table		Page
I	A Comparison of Total Bond Strengths for Two, 0.025 m by 0.250 m Metal Plates Bonded by Rivets, Spot Welds, and Adhesive	3
II	Creep Moduli for Polymers Studied . . .	10
III	Procedures for Ti-6Al-4V Preanodization Treatments	30
IV	Procedure for Chromic Acid Anodization Without Hydrofluoric Acid	36
V	Procedure for Chromic Acid Anodization With Hydrofluoric Acid	37
VI	Chromic Acid/Hydrofluoric Acid Ti-6Al-4V Anodization and Chromic Acid Ti-6Al-4V Anodization Conditions Tested	38
VII	Post-Anodization Ti-6Al-4V Cleaning Method . .	40
VIII	Polishing Technique for Ti-6Al-4V Interferogram Measurements	43
IX	Interferometry Measurement Technique	47
X	Chemical Structures of Heat Resistant Adhesives Tested	56
XI	T Values and Compression Molding Schedules for Heat Resistant Adhesives Tested	58
XII	Thermal Expansion Coefficients, Vendor, and Chemical Resistance Information for Heat Resistant Adhesives Tested	60
XIII	Polyphenylquinoxaline (PPQ) Stage Dry Method to Remove Solvent From PPQ After PPQ Application to Chromic Acid Anodized Ti-6Al-4V	68

LIST OF TABLES (Continued)

Table		Page
XIV	Bonding Processes for Polyphenylquinoxaline/ Chromic Acid With HF Anodized Ti-6Al-4V Single Lap Bonds	69
XV	Bonding Process for Ablebond® 71-3, 50% $CaCO_3$ Filled Polyimide/Chromic Acid With HF Anodized Ti-6Al-4V Single Lap Bonds	71
XVI	Bonding Process for Victerex® Polyether-sulfone/Chromic Acid With HF Anodized Ti-6Al-4V Single Lap Bonds	72
XVII	Single Lap Bonding Process for Chromic Acid With HF Anodized Ti-6Al-4V Bonded to Either Ultem®1000 Polyetherimide (PEI) or to Ultem® 2200, 20% Glass Filled Polyetherimide (PEIF)	74
XVIII	Bonding Process for Udel® Polysulfone (PS)/ Anodized Ti-6Al-4V Single Lap Bonds	76
XIX	Adhesive Bond Thickness Measured In Situ for Anodized Ti-6Al-4V Single Lap Bonds	83
XX	Comparative Analysis of CA/HF Anodized Ti-6Al-4V Oxide Morphology Characteristics	100
XXI	Chromic Acid Anodized Ti-6Al-4V Oxide Thickness Data	110
XXII	CA/HF Anodized Ti-6Al-4V/Udel® Polysulfone Single Lap Bond Strength Data As a Function of Ti-6Al-4V Preanodization Treatment #1 and #2	123
XXIII	CA/HF Anodized Ti-6Al-4V/Udel® Polysulfone Single Lap Bond Strength and Ti-6Al-4V Anodic Oxide Thickness Data As a Function of Anodization With and Without HF	125
XXIV	CA/HF Anodized Ti-6Al-4V/Udel® Polysulfone Single Lap Bond Strength and Ti-6Al-4V Anodic Oxide Thickness As a Function of 20 Minute, and 60 Minute Anodization	129

LIST OF TABLES (Continued)

Table		Page
XXV	CA/HF Anodized Ti-6Al-4V/Udel® Polysulfone Single Lap Bond Strengths As a Function of Initial Current Density and Solution Temperature	131
XXVI	ESCA Analysis for CA/HF Anodized Ti-6Al-4V, Anodized 20 Minutes, 20 ± 2 A/m, 10 Volts, 283 ± 2K	134
XXVII	ESCA Analysis for CA/HF Anodized Ti-6Al-4V, Anodized 20 Minutes, 30 ± 2 A/m², 10 Volts 298 ± 2K	135
XXVIII	CA/HF Anodized Ti-6Al-4V Oxide Thickness Data as a Function of Selected Anodization Conditions	138
XXIX	Single Lap Bond Strengths for Ti-6Al-4V Anodized Per the Preferred CA/HF Anodization Method at 283 ± 2K and Bonded to Selected Heat Resistant, Structural Adhesives	139
XXX	CA/HF Anodized Ti-6Al-4V/Polyphenylquinoxaline Single Lap Bond Strengths as a Function of Anodization Procedures	142
XXXI	The Influence of Bonding Procedure on CA/HF Anodized Ti-6Al-4V/Polyphenylquinoxaline Single Lap Bond Strength	145
XXXII	Unprimed CA/HF Anodized Ti-6Al-4V/Udel® Polysulfone Single Lap Bond Strength Data as a Function of Thermal Aging	148
XXXIII	Unprimed CA/HF Anodized Ti-6Al-4V/Ablebond® 71-3, 50% $CaCO_3$ Filled Polyimide Single Lap Bond Strength Data as a Function of Thermal Aging	152
XXXIV	CA/HF Anodized Ti-6Al-4V/Polyphenylquinoxaline Single Lap Bond Strength Data as a Function of Thermal Aging for Unprimed and Primed Anodized Ti-6Al-4V	154

LIST OF TABLES (Continued)

Table		Page
XXXV	CA/HF Anodized Ti-6Al-4V/Victerex® Polyethersulfone Single Lap Bond Strength Data as a Function of Thermal Aging for Unprimed and Primed Anodized Ti-6Al-4V	159
XXXVI	CA/HF Anodized Ti-6Al-4V/Ultem® 1000 Unfilled Polyetherimide Single Lap Bond Strength Data as a Function of Thermal Aging for Unprimed and Primed Anodized Ti-6Al-4V	162
XXXVII	CA/HF Anodized Ti-6Al-4V/Ultem® 2200, 20% Glass Fiber Filled Polyetherimide Single Lap Bond Strength Data as a Function of Thermal Aging for Unprimed and Primed Anodized Ti-6Al-4V	164
XXXVIII	Apparent Fracture Sites for Anodized Ti-6Al-4V/Heat Resistant Adhesive Single Lap Bonds, Based Upon Visual Analysis	189
XXXIX	Quantitative Image Analysis for Both Fracture Surfaces of a CA/HF Anodized Ti-6Al-4V/Polysulfone Single Lap Bond	201
XL	Quantitative Image Analysis for One Fracture Surface of a CA/HF Anodized Ti-6Al-4V/Polyphenylquinoxaline Single Lap Bond	204
XLI	Test Apparatus Measurements and the Measurements for Two Parallel Plate Capacitors in Series With the Dielectric Being Anodic Oxide Produced by Chromic Acid Anodization Without HF	315
XLII	Equations to Determine Parallel Plate Capacitance	317
XLIII	C_x, Parallel Plate Capacitance, With the Dielectric Anodic Oxide Produced by Chromic Acid Anodization Without HF	320

LIST OF TABLES (Continued)

Table		Page
XLIV	Test Apparatus Measurements and Measurements for Two Parallel Plates in Series With the CA/HF Anodic Oxide Between the Plates	321

LIST OF FIGURES

Figure		Page
1.	Maximum Continuous Use Temperatures for Polymers Studied	9
2.	Anodization Apparatus Schematic	34
3.	Interferometer Schematic Diagram	45
4.	Interferometer Mount for the Ti-6Al-4V Coupon	46
5.	Interferogram of Fringe Pattern Used to Measure Ti-6Al-4V Anodic Oxide Thickness (28.4X). CA/HF Conditions: 20 Minutes, 278 ± 2K, 10 Volts, 30 ± 2 A/m^2	51
6.	Structure of Lica® 44 Neoalkoxy Titanate Primer	54
7.	Schematic of a Single Lap Bond	63
8.	Schematic of Jig for Single Lap Bonding Process of Anodized Ti-6Al-4V to All Heat Resistant Adhesives Tested Except the 50% $CaCO_3$ Filled Polyimide Adhesive (Top)	65
9.	Schematic of Jig for Single Lap Bonding Process of Anodized Ti-6Al-4V to All Heat Resistant Adhesives Tested Except the 50% $CaCO_3$ Filled Polyimide Adhesive (Bottom)	66
10.	Schematic of Jig for Single Lap Bonding Process of Anodized Ti-6Al-4V to a 50% $CaCO_3$ Filled Polyimide Heat Resistant Adhesive	67
11.	Side View Photograph of Single Lap Bond Used for Adhesive Thickness Measurement (100X)	82
12.	Schematic of Set-up Used to Photograph Single Lap Bond Fracture Process	86
13.	Scanning Electron Micrograph of the Ti-6Al-4V Surface After Preanodization Treatment #1 (1600X)	93

LIST OF FIGURES (Continued)

Figure		Page
14.	Scanning Electron Micrograph of the Ti-6Al-4V Surface After Preanodization Treatment #1 and CA/HF Anodization (3200X)	94
15.	Scanning Electron Micrograph of the Ti-6Al-4V Surface After Preanodization Treatment #1 and CA/HF Anodization (10,000X)	95
16.	Proposed Model of the Interior of an Etch Pit on a CA/HF Anodized Ti-6Al-4V Surface	97
17.	Transmission Electron Micrograph of a Parallel Section of an Anodic Oxide Produced by Twenty Minute CA/HF Anodization at: 283 ± 2K, 20 ± 2 A/m² Initial Current Density, and 10 Volts (200,000X)	98
18.	Transmission Electron Micrograph of a Parallel Section of an Anodic Oxide Produced by Twenty Minute CA/HF Anodization at: 298 ± 2K, 20 ± 2 A/m² Initial Current Density, and 10 Volts (200,000X)	99
19.	Transmission Electron Micrograph of a Cross Section of an Anodic Oxide Produced by Twenty Minute CA/HF Anodization at: 283 ± 2K, 20 ± 2 A/m² Initial Current Density, and 10 Volts (30,000X)	102
20.	Transmission Electron Micrograph of a Cross Section of an Anodic Oxide Produced by Twenty Minute CA/HF Anodization at: 298 ± 2K, 20 ± 2 A/m² Initial Current Density, and 10 Volts (30,000X)	103
21.	Transmission Electron Micrograph of a Cross Section of an Anodic Oxide Produced by Twenty Minute CA/HF Anodization at: 283 ± 2K, 20 ± 2 A/m² Initial Current Density, and 10 Volts (200,000X)	104

LIST OF FIGURES (Continued)

Figure		Page
22.	Transmission Electron Micrograph of a Cross Section of an Anodic Oxide Produced by Twenty Minute CA/HF Anodization at: 298 ± 2K, 20 ± 2 A/m² Initial Current Density, and 10 Volts (200,000X)	105
23.	Proposed Adhesion Model for the CA/HF Anodized Ti-6Al-4V/Adhesive Bond	106
24.	Interferogram of Fringe Pattern Used to Measure Ti-6Al-4V Anodic Oxide Thickness (28.4X). CA/HF Anodization Conditions: 20 Minutes, 283 ± 2K, 10 Volts, 30 ± 2 A/m²	109
25.	Influence of Chromic Acid Anodization Solution Composition upon Anodic Oxide Average Thickness	114
26.	Influence of Chromic Acid/Hydrofluoric Acid Anodization Time upon Anodic Oxide Average Thickness	116
27.	Influence of Chromic Acid/Hydrofluoric Acid Anodization Solution Temperature and Initial Current Density upon Anodic Oxide Average Thickness	117
28.	A Schematic of a Single Lap Bond Under an Applied Tensile Load and a Qualitative Representation of the Stress Distribution	121
29.	Qualitative Representation of the Influence of Oxide Porosity and Thickness upon Single Lap Bond Stress Distribution	127
30.	Single Lap Bond Strengths for Heat Resistant Adhesives Bonded to CA/HF Anodized Ti-6Al-4V Tested After 0.5 Month at 298 ± 5K in a 65 to 80% R.H. Environment	168

LIST OF FIGURES (Continued)

Figure		Page
31.	Single Lap Bond Strengths After 9 Months at 443 ± 5K Followed by 2 Months at 298 ± 5K in a 65 to 80% R.H. Environment for Heat Resistant Adhesives Bonded to Unprimed and Lica® 44 Titanate Primed CA/HF Anodized Ti-6Al-4V	169
32.	High Speed Photographs of the Single Lap Bond Fracture During Test (8X)	172
33.	Photograph of Fractured Single Lap Bond (2X) . .	173
34.	SEM Micrograph of a Fracture Surface for a CA/HF Anodized Ti-6Al-4V/Polyphenylquinoxaline Single Lap Bond (60X)	174
35.	SEM Micrograph of a Fracture Surface for a CA/HF Anodized Ti-6Al-4V/Polysulfone Single Lap Bond (12X)	175
36.	SEM Micrograph of a Fracture Surface for a CA/HF Anodized Ti-6Al-4V/Polyethersulfone Single Lap Bond (30X)	176
37.	SEM Micrograph of a Fracture Surface for a CA/HF Anodized Ti-6Al-4V/20% Glass Fiber Filled Polyetherimide Single Lap Bond (30X)	177
38.	Proposed Model for the Primed, CA/HF Anodized Ti-6Al-4V Adhesive Bond	181
39.	Photograph of a Fracture Surface for a Single Lap Bond Illustrating Apparent Failure I	183
40.	Photograph of a Fracture Surface for a Single Lap Bond Illustrating Apparent Failure II	184
41.	Photograph of a Fracture Surface for a Single Lap Bond Illustrating Apparent Failure III	185
42.	Photograph of a Fracture Surface for a Single Lap Bond Illustrating Apparent Failure IV	186

LIST OF FIGURES (Continued)

Figure		Page
43.	Photograph of a Fracture Surface for a Single Lap Bond Illustrating Apparent Failure V	187
44.	ESCA Concentration Analyses of Ti-6Al-4V Before and After Anodization	210
45.	ESCA Binding Energy Data for Ti-6Al-4V Before and After Anodization	211
46.	ESCA Concentration Analyses of Thermoset and Thermoplastics Used in Chromic Acid/HF Anodized Ti-6Al-4V Single Lap Bonds	213
47.	ESCA Binding Energy Data for a Thermoset and Thermoplastics Used in Chromic Acid/HF Anodized Ti-6Al-4V Single Lap Bonds	214
48.	ESCA Concentration Analyses of Udel® Unfilled Polysulfone As-Received Beads and Compression Molded Film	215
49.	ESCA Concentration Analyses of Fracture Surfaces for Chromic Acid Anodized Ti-6Al-4V/Udel® Unfilled Polysulfone Single Lap Bonds as a Function of Anodization With and Without Hydrofluoric Acid	218
50.	ESCA Concentration Analyses of Fracture Surfaces for Chromic Acid/HF Anodized Ti-6Al-4V/Udel® Unfilled Polysulfone Single Lap Bonds as a Function of Anodization Time	219
51.	ESCA Concentration Analyses of Fracture Surfaces for Chromic Acid/HF Anodized Ti-6Al-4V/Udel® Unfilled Polysulfone Single Lap Bonds as a Function of Anodization Temperature and Initial Current Density	220
52.	ESCA Concentration Analyses of Fracture Surfaces for Chromic Acid/HF Anodized Ti-6Al-4V/Udel® Unfilled Polysulfone Single Lap Unstressed Thermally Aged Bonds	223

LIST OF FIGURES (Continued)

Figure		Page
53.	ESCA Concentration Analyses of Fracture Surfaces for Chromic Acid/HF Anodized Ti-6Al-4V/Unfilled Polyphenylquinoxaline Single Lap Bonds as a Function of Bonding Process	224
54.	Proposed Model of the CA/HF Anodized Ti-6Al-4V/ Polyphenylquinoxaline Isochronally Processed Bond	227
55.	ESCA Concentration Analyses of Fracture Surfaces for Chromic Acid/HF Anodized Ti-6Al-4V/Unfilled Polyphenylquinoxaline Isothermally Processed Single Lap Bonds as a Function of Anodization Solution Temperature and Initial Current Density	229
56.	ESCA Concentration Analyses of Fracture Surfaces for Chromic Acid/HF Anodized Ti-6Al-4V/Unfilled Polyphenylquinoxaline Single Lap Bonds for Primed and/or Aged Bonds	230
57.	ESCA Titanium Binding Energy Analyses of Fracture Surfaces for Chromic Acid/HF Anodized Ti-6Al-4V/ Unfilled Polyphenylquinoxaline Single Lap Bonds for Primed and/or Aged Bonds	231
58.	ESCA Concentration Analyses of a Fracture Surface for Chromic Acid/HF Anodized Ti-6Al-4V/Ablebond® 71-3 50% Calcium Carbonate Filled Polyimide Single Lap Bond	233
59.	ESCA Concentration Analyses of a Fracture Surface for Chromic Acid/HF Anodized Ti-6Al-4V/Ultem® Unfilled Polyetherimide Single Lap Bond	234
60.	ESCA Concentration Analyses of Fracture Surface for a Chromic Acid/HF Anodized Ti-6Al-4V/Ultem® 20% Glass Filled Polyetherimide Single Lap Bond .	235
61.	ESCA Concentration Analyses of a Fracture Surface for Chromic Acid/HF Anodized Ti-6Al-4V/Victerex® Unfilled Polyethersulfone Single Lap Bond	237

LIST OF FIGURES (Continued)

Figure		Page
62	Auger Survey Analyses of a Fracture Surface for a 46.0 MPa CA/HF Anodized Ti-6Al-4V/PPQ Isothermally Processed Single Lap Bond. Side A	239
63	SEM Micrograph of the Fracture Surface for a 46.0 MPa CA/HF Anodized Ti-6Al-4V/PPQ Isothermally Processed Single Lap Bond which was Nitrogen Auger Mapped (60X). Side A	240
64	Nitrogen Auger Map for the Fracture Surface of a 46.0 MPa CA/HF Anodized Ti-6Al-4V/PPQ Isothermally Processed Single Lap Bond (60X). Side A	241
65	Auger Survey Analyses of a Fracture Surface for a 46.0 MPa CA/HF Anodized Ti-6Al-4V/PPQ Isothermally Processed Single Lap Bond. Side B	242
66	SEM Micrograph of the Fracture Surface for a 46.0 MPa CA/HF Anodized Ti-6Al-4V/PPQ Isothermally Processed Single Lap Bond which was Nitrogen Auger Mapped (60X). Side B	243
67	Nitrogen Auger Map for the Fracture Surface of a 46.0 MPa CA/HF Anodized Ti-6Al-4V/PPQ Isothermally Processed Single Lap Bond (60X). Side B	244
68	Auger Survey Analyses of a Fracture Surface for a 16.1 MPa CA/HF Anodized Ti-6Al-4V/PPQ Isochronally Processed Single Lap Bond. Side A .	245
69	SEM Micrograph of the Fracture Surface for a 16.1 MPa CA/HF Anodized Ti-6Al-4V/PPQ Isochronally Processed Single Lap Bond which was Nitrogen Auger Mapped (60X). Side A	246
70	Fluorine Auger Map for the Fracture Surface of a 16.1 MPa CA/HF Anodized Ti-6Al-4V/PPQ Isochronally Processed Single Lap Bond (60X). Side A	247

LIST OF FIGURES (Continued)

Figure		Page
71	Auger Survey Analysis of a Fracture Surface for a 16.1 MPa CA/HF Anodized Ti-6Al-4V/PPQ Isochronally Processed Single Lap Bond. Side B	248
72	SEM Micrograph of the Fracture Surface for a 16.1 MPa CA/HF Anodized Ti-6Al-4V/PPQ Isochronally Processed Single Lap Bond which was Nitrogen Auger Mapped (60X). Side B	249
73	Fluorine Auger Map for the Fracture Surface of a 16.1 MPa CA/HF Anodized Ti-6Al-4V/PPQ Isochronally Processed Single Lap Bond (60X). Side B	250
74	Proposed Model of the Fracture Sites for a CA/HF Anodized Ti-6Al-4V/Adhesive Bond	253
75	Proposed Model of the Fracture Sites for a Lica® 44 Primed CA/HF Anodized Ti-6Al-4V/ Adhesive Bond	254
76	SEM Micrograph of a Polymer Fracture Surface for a CA/HF Anodized Ti-6Al-4V/Udel® Polysulfone Single Lap Bond (10,000X)	257
77	SEM Micrograph of a Polymer Fracture Surface for a CA/HF Anodized Ti-6Al-4V/Victerex® Polyethersulfone Single Lap Bond (10,000X)	258
78	SEM Micrograph of a Polymer Fracture Surface for a CA/HF Anodized Ti-6Al-4V/Ultem® 1000 Polyetherimide Single Lap Bond (10,000X)	259
79	SEM Micrograph of a Polymer Fracture Surface for a CA/HF Anodized Ti-6Al-4V/Ultem® 2200, 20% Glass Filled Polyetherimide Single Lap Bond (500X)	260
80	SEM Micrograph of a Polymer Fracture Surface for a CA/HF Anodized Ti-6Al-4V/Ultem® 2200, 20% Glass Filled Polyetherimide Single Lap Bond (10,000X)	261

LIST OF FIGURES (Continued)

Figure		Page
81	SEM Micrograph of a Polymer Fracture Surface for a CA/HF Anodized Ti-6Al-4V/Polyphenyl-quinoxaline Single Lap Bond (10,000X)	262
82	SEM Micrograph of a Polymer Fracture Surface for a CA/HF Anodized Ti-6Al-4V/Ablebond® 71-3, 50% $CaCO_3$ Filled Polyimide (5,000X)	263
83	Schematic of a Contact Probe	300
84	Schematic of the Template Used to Evaporate Silver Onto Anodized Ti-6Al-4V for the Oxide Bulk Resistivity Determination	302
85	Schematic of the Method for Ti-6Al-4V Anodic Oxide Bulk Resistivity Determination	303
86	Schematic of the Plexiglas Contact Probe Fixture Used in the Anodic Oxide Bulk Resistivity Determination	304
87	Schematic of the Test Apparatus Used in the Ti-6Al-4V Anodic Oxide Bulk Resistivity Determination	305
88	A Schematic of the Template Used to Evaporate Silver Disks Onto Anodized Ti-6Al-4V for the Anodic Oxide Capacitance Determination	307
89	Schematic of the Set-Up for the Ti-6Al-4V Anodic Oxide Capacitance Determination	308
90	Schematic of the Probe Set-Up Used in Ti-6Al-4V Anodic Oxide Capacitance Measurements	309
91	Schematic of the Contact Probe Fixture Used in the Ti-6Al-4V Anodic Oxide Capacitance Determination	311
92	Schematic of the Test Apparatus Used in the Ti-6Al-4V Anodic Oxide Capacitance Determination	312

LIST OF FIGURES (Continued)

Figure		Page
93	Voltage vs. Distance Data Used in Ti-6Al-4V Anodic Oxide Bulk Resistivity Determination. CA/HF Anodization Procedure for Ti-6Al-4V was Used	323

CHAPTER I

INTRODUCTION

A. The Metal-Adhesive Bond: Advantages and Disadvantages

The metal-adhesive-metal bond is nominally composed of five structural elements: *metal/metal oxide-adhesive interphase/adhesive/* adhesive-metal oxide interphase/metal. When joining metal to metal, such an adhesive bond is an alternative to the weld, rivet, or any multi-element mechanical fastener. Major advantages of the metal-adhesive bond, compared to the rivet, which is a mechanical fastener, and welds, are described below.

(1) The metal-adhesive bond promotes laminar air flow, which is important for the proper operation of advanced aircraft wing designs. A screw head, rivet head or weld bead could interrupt such air flow.

(2) The adhesive separation between the metal adherends prevents galvanic corrosion between dissimilar metal adherends. Moreover, the adhesive itself can seal out moisture and contaminants from any one metal adherend surface and thereby prevent environmental corrosion in that area.

(3) Fretting corrosion, which occurs with mechanical fasteners, is eliminated in the metal-adhesive bond.

(4) Notch effects, which result in premature metal fatigue, are eliminated in the metal-adhesive bond. It is recognized that a rivet or screw hole can be reamed to remove inferior metal, or the metal can be annealed after punching or tapping the holes to

eliminate notches and improve metal strength. However, such metal finishing or heat treatment techniques may be too labor intensive for practical consideration.

(5) The metal-adhesive bond, which uses a toughened adhesive, has higher impact or flexural fatigue life and can withstand stresses due to differential thermal expansion better than spot-welded or riveted joints. This is because a toughened adhesive can damp vibrations and distribute impact and flexural stresses better than a mechanical fastener. According to a study conducted by Narmco Materials, both spot-welded and riveted joints in magnesium aircraft skins yielded to fatigue after 12 to 18 million cycles. However, adhesive bonds yielded to fatigue only after 240 million cycles.[1]

(6) The adhesive-metal bond can withstand a larger overall load than riveted or spot-welded bonds. Table I is a comparison of overall bond strengths for two 0.025 m X 0.250 m metal plates bonded by rivets, spot-welds, and adhesive bonds. Typically, four, 0.006 m diameter spot welds could be used to bond such a plate. Each spot weld is capable of a 272.4 Kg load bearing capacity. Or, five, 0.016 m rivets could be used to bond these plates. The equation used to calculate the total strength for the riveted bond was:

$$L = n \times A_r \times S_s \qquad [1\text{-}1]$$

where L is the safe tensile load for the riveted bond, n is the number of rivets, A_r is the cross-sectional area of one rivet and S_s

TABLE I

A Comparison of Total Bond Strengths for Two, 0.025 m by 0.250 m Metal Plates Bonded by Rivets, Spot Welds, and Adhesive

Metal-Metal Bond Description	Bond Method	Typical Total Bond Strength (Kg)
272.4 Kg Weld Strength	Four welds, each 0.006 m in diameter	1,090
Rivet	Five rivets, each 0.016 m in diameter	5,920
13.8 MPa (1.4×10^6 Kg/m^2) Metal-Adhesive Shear Bond Strength	Continuous adhesive bond over the 0.025 m X 0.250 m area	8,796

is the allowable shearing stress for a structural steel rivet and is taken as 58.6 MPa.[2]

Even assuming a relatively low adhesive-metal bond shear strength of 13.8 MPa [1000 psi = 6.9 MPa], the overall metal-adhesive bond strength is 8 times higher than the spot-welded bond and approximately 2 times higher than the riveted bond. This is because the adhesive-metal bond is continuously bonded, and stress concentrations are minimized.

(7) Adhesive-metal bonds have higher strength and are lighter in weight than metal bonds fastened by conventional mechanical methods. The weight consideration is important in aircraft design for fuel economy.

Distinct disadvantages of the metal-adhesive bond are listed as follows.

(1) The metal-adhesive bond is difficult to repair without first removing the adhesive from the metal surface. Typically, structural thermoset adhesives have excellent chemical and solvent resistance, and labor intensive mechanical abrasion of the metal is required to remove adhesive from the metal surface.

(2) Many metal adhesive bonds and the adhesive itself may be weakened by water exposure, high relative humidity, cycling between hot and cold temperatures, or salt immersion.

(3) The service temperature of adhesives can limit applications. Aerospace manufacturers report the need for adhesives with

773K service temperatures. Typically, epoxies have continuous service temperatures of 422 - 450K. Polyimide, the most thermally stable organic polymer, can handle more than 10,000 hours at 589K, and thermal spikes of 811 - 1089K.[3] However, these polyimides are expensive and high bond processing temperatures are required.

B. Research Objectives

In this research, the chromic acid anodized Ti-6Al-4V/heat resistant adhesive single lap bond was the metal-adhesive system studied.

The overall research objectives regarding this metal-adhesive system were twofold. The first objective was to develop a phenomenological model which described the chromic acid anodized Ti-6Al-4V/adhesive bond. The second objective was to further develop the phenomenological model to include the fracture mechanism of the single lap bond as a function of adhesive type and anodization process.

To achieve these objectives, the following research was conducted:

(1) characterize the anodic oxide produced by chromic acid anodization of Ti-6Al-4V in terms of its anodic oxide thickness, surface ($\leq$10 nm) composition, morphology, and structure;

(2) characterize the single lap bond strength after $\leq$ 0.5 month aging at 298 ± 5K in a 65 to 80% relative humidity environment, of chromic acid anodized Ti-6Al-4V to the following heat resistant adhesives:

a) UDEL® unfilled polysulfone (PS),

b) unfilled polyphenylquinoxaline (PPQ),

c) Ablebond® 71-3, 50% calcium carbonate filled polyimide (PI),

d) Ultem® 1000 unfilled polyetherimide (PEI),

e) Ultem® 2200 20% glass filled polyetherimide (PEIF), and

f) Victerex® unfilled polyethersulfone (PES);

(3) characterize the bond strengths after unstressed thermal aging for each adhesive cited above;

(4) characterize the bond strengths after unstressed thermal aging for titanate primed, chromic acid anodized Ti-6Al-4V bonded to selected adhesives cited above; and,

(5) examine the single lap bond as it fractured and also the fracture surfaces to determine:

a) where the fracture occurred, and

b) the failure mechanism, or how and why the crack propagated through the bond.

The metal-adhesive systems studied in this research were chosen for several important reasons. These reasons are cited below.

Titanium alloys have a density 44% less and have a yield and tensile strength equal to or greater than stainless or alloy steels. Ti-6%Al-4%V yield strength is 828 to 1001 MPa, and the ultimate tensile strength is 897 to 1070 MPa. In addition to good strength-to-weight characteristics, Ti-6Al-4V has good temperature resistance up to 703K and good corrosion resistance to salt water, many acids and alkalii.

The Ti-6Al-4V was chromic acid anodized prior to bonding. Chromic acid anodization of Ti-6Al-4V is an accepted method to produce by a controlled process, a durable, porous oxide on the Ti-6Al-4V surface. The porosity may be beneficial for adhesive bonding in that the surface area for physical and/or chemical bonding is increased. Also, the porous oxide may promote mechanical interlock of the adhesive.

The primary criterion for adhesive selection was to include a broad spectrum of polymer types which were heat resistive. Heat resistance was defined as continuous service above 373K. With the exception of the polyimide, the polymers chosen for this study were thermoplastics. Continuous service temperatures are compared in Figure 1 for the polymers used. Underwriters' Laboratory (UL) rated continuous use temperatures were reported where available. The UL value represents the temperature at which 50% of the polymer original physical property measured is retained after 11,000 hours at that temperature.

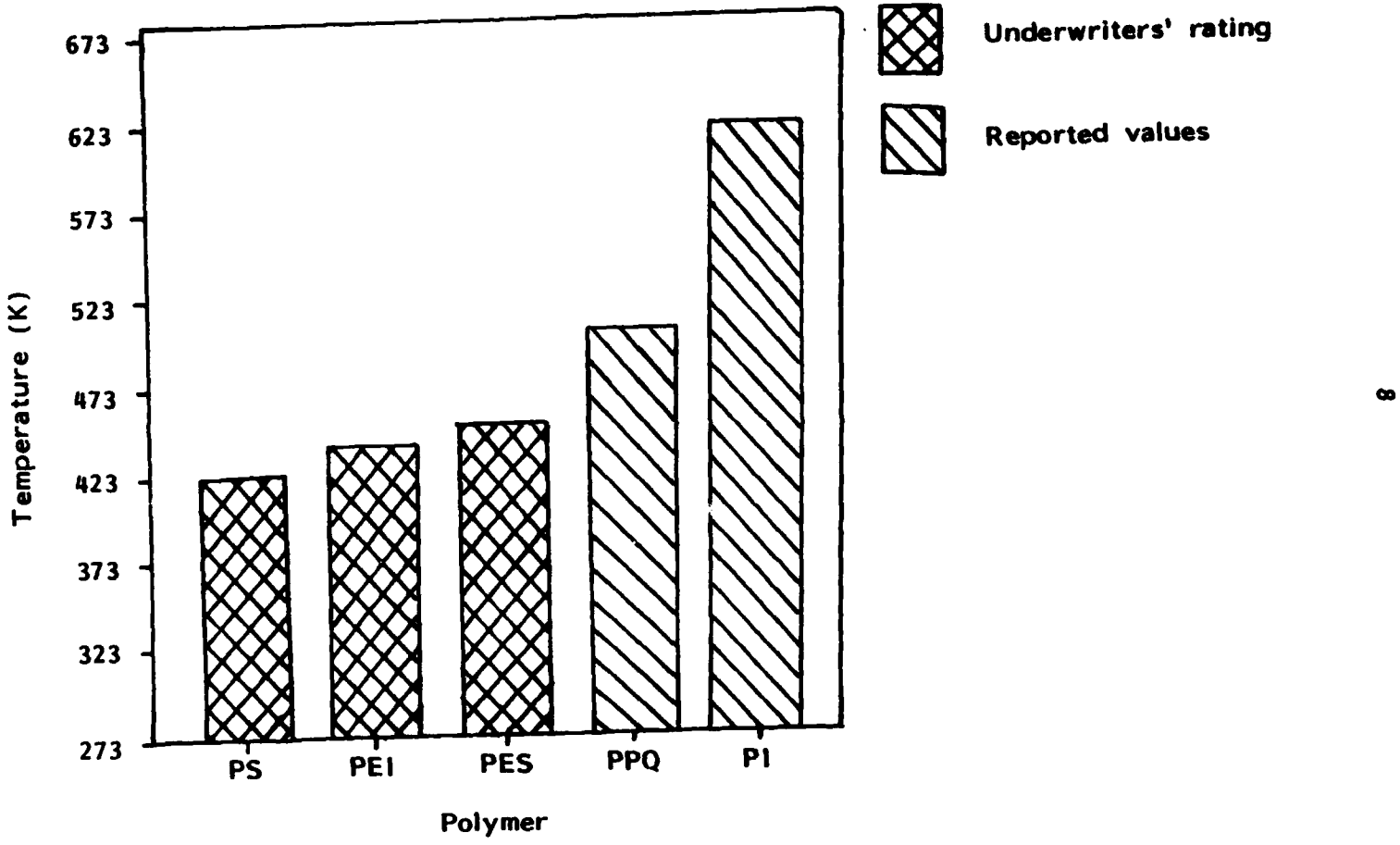


Figure 1. Maximum Continuous Use Temperatures for Polymers Studied.

A secondary criterion for adhesive selection was to select heat resistant adhesives which were also structural adhesives. Generally defined, a structural adhesive must exhibit a high creep modulus for a stress of $\geq$ 6.9 MPa at the specified service temperature. A high creep modulus is a necessary adhesive characteristic for metal-adhesive structural bond dimensional stability.

Creep moduli for the polymers studied are ranked from highest to lowest modulus in Table II. For the 50% $CaCO_3$ filled polyimide studied, specific data was not available; therefore, data for a glass filled polyimide was included in Table II. The polyimide thermoset, which crosslinks upon cure, exhibited the highest reported creep modulus, 18,615 MPa. The thermoplastics exhibited relatively high creep moduli for $\geq$ 6.9 MPa stress at elevated temperatures. Therefore, the polyimide thermoset and these thermoplastics studied could conceivably be used in a structural bond depending upon the elevated service temperatures and bond stress conditions specified.

The single lap bond tested in tension was the test method used to probe the chromic acid anodized Ti-6Al-4V adhesive bond strength. The single lap bond test is primarily a shear test; however, peel and tensile forces are also exerted upon the bond during test. The single lap test has been used extensively to screen adhesives.[7] This test method is representative , in a general sense, of worst case service conditions for metal-adhesive

TABLE II

Creep Moduli for Polymers Studied

Polymer	Test Conditions: Stress (MPa)	Test Conditions: Temperature (K)	Test Conditions: Time (Hours)	Creep Modulus MPa
Polyimide, glass filled	17.2	472	300	18,615.6[4]
Polyphenylquinoxaline	6.9	505	1440	No creep exhibited[5]
Ultem® 2200 Polyetherimide, 20% glass filled	20.7	314	1000	4,826.3[4]
Ultem® 1000 Polyetherimide	20.7	314	1000	2,413.1[4]
Victerex® Polyethersulfone	6.9	422	1000	3,654.2[4]

TABLE II (Continued)

Polymer	Test Conditions Stress (MPa)	Temperature (K)	Time (Hours)	Creep Modulus MPa
Udel® Polysulfone	6.9	422	1440	413.7[6]
Udel® Polysulfone	20.7	372	1000	1,310.0[6]

bonds, which can include all or a combination of any of the following forces: peel, cleavage, shear, and tension forces.

CHAPTER II

LITERATURE REVIEW

A. Adhesion Theories

The following is a review of adhesion theories as they pertain to adhesive bonding to an adherend. The adhesion theories can be classified broadly into the following categories: (1) surface energetics, (2) chemisorption, (3) physisorption, (4) electrostatic forces, (5) hydrogen bonding, (6) diffusion, and (7) mechanical interlock. Whenever possible, these theories will be related to a titanium alloy adherend, which has first undergone surface cleaning and anodization before bonding. Certainly, any one or combination of these theories may be required to best describe bonding to anodized titanium alloy depending upon the type of adhesive.

Before any adhesion forces can develop between the anodized titanium alloy and adhesive, the adhesive must wet and spread on the adherend. An adhesive will wet the anodic oxide if the adhesive has a surface tension , γ_L, less than the anodic oxide critical surface tension, γ_C. This surface energetics description of wetting and spreading was proposed by Zisman[8] and discussed by Schonborn and Sharpe.[9] An adhesive should easily wet and spread onto the anodic oxide of a titanium alloy. The surface free energies range from 0.1 to 3.0 J/m^2 for metals, metal oxides and metal salts.[10] The surface free energy is usually < 0.1 J/m^2 for organic liquids, hot-melt adhesives and thermoplastics.[11]

The surface energetics of wetting and spreading can also be described by the de Bruyne dispersion-polar integration theory.[12] The work of adhesion, W_{ls}, is:

$$W_{ls} = \gamma_l + \gamma_s - \gamma_{ls} \qquad [2\text{-}1]$$

where γ_l is the liquid surface tension, γ_s is the solid surface tension, and γ_{ls} is the interfacial surface tension. The γ_{ls} term can be further defined by the following:

$$\gamma_{ls} = (\gamma_l^d - \gamma_s^d)^2 + (\gamma_l^p - \gamma_s^p)^2 - \Delta ls \qquad [2\text{-}2]$$

where d denotes the dispersion force and p denotes the polar force in surface tension. The Δ is the induction forces and all other forces contributing to surface tension. When the magnitude of the dispersion and polar forces between the adhesive and solid are similar, i.e. both are polar or both are nonpolar, γ_{ls} is reduced. Consequently, the work of adhesion, W_{ls}, is increased. A large W_{ls} value is beneficial to spreading. The spreading of the liquid on the solid occurs when the spreading coefficient, $S_{l/s}$, is large and positive, or the reduction in Gibbs free energy is large. The $S_{l/s}$ is defined as:

$$S_{l/s} = W_{ls} - W_l \qquad [2\text{-}3]$$

where W_l is the work of cohesion, and is defined as:

$$W_l = 2\gamma_l. \qquad [2\text{-}4]$$

Adhesion forces may develop because of chemisorption. The chemical bond provides the strongest adhesion forces possible. Bond strengths are on the order of 120 to 400 kJ/mole. Multilayers of water can adsorb onto the titanium alloy anodic oxide surface.

The metal oxide or any surface impurities, could serve to chemically bond to the adhesive. If the adhesive has acidic or basic functional groups opposite in nature to an oxide site, a covalent chemical bond may be formed between the adhesive and oxide.

In the case of coupling agents or primers applied to the anodized Ti-6Al-4V before bonding, these agents may chemically bond to the anodic oxide. The coupling agent also contains an organic functional end group which can then chemically bond to the adhesive or interact by van der Waals forces with the adhesives.

The chemical bond theory is similar to the attachment site theory proposed by Lewis and Natarajan.[13] Basically, the strength of the interfacial boundary layer is directly proportional to the number of attachment sites and the interfacial area between the adherend and adhesive. The chemical treatment would increase the number of attachment sites according to this theory. If the number is maximized, the boundary can become equal to or greater in strength than the cohesive strength of the adhesive. Increasing the number beyond this point would not improve the bond strength.

Hydrogen bonding may occur between the adhesive and the anodic oxide if polar groups of opposite polarity are present. The hydroxyl groups on the hydrated anodic oxide may hydrogen bond to nitrogen or oxygen from the adhesive. Relatively speaking, hydrogen bonds are weaker than chemical bonds.

Adhesion forces between the adhesive and anodic oxide may also develop due to physisorption. Physisorption forces are known

as van der Waals forces and include London dispersion forces. Van der Waals forces result from permanent dipole attraction between the adhesive and anodic oxide molecules, or dipoles induced by permanent dipoles. Attractive forces between the adherend and anodic oxide can be due to London dispersion forces, which is electron motion alone and is unrelated to dipoles. London dispersion forces are attractive forces present for any type of molecule. In the case of London dispersion forces, a 386.1 MPa shear force has been calculated as the theoretical force to move an adhesive molecule across a surface.[14] And, it has been calculated that fourteen times that value, or 1.38 GPa is required to remove the molecule from the surface.[14] In comparison, physisorption as an adhesion force is weaker than chemical or hydrogen bonds. Even so, as calculated above, physisorption of an adhesive to an adherend should be sufficient to achieve bonding strength which rivals the ultimate strength of the metal in theory.

An electrical double layer between the adhesive and metal oxide may contribute to bond strength. This is known as the electrostatic theory proposed by Derjagin, et al.[12]

The presence and quantity of pores, crevices and capillaries in the oxide film are a function of the chemical pretreatment. Polymer diffusion into the oxide channels, capillaries, and pores may improve bond strength. The polymer molecule or segment diffusion theory of adhesion was first developed by Voyutskii and Vakula.[15] Baun[16] has reported that a porous oxide produces

higher bond strength than nonporous films. It should be noted that there must be mutual solubility of the adhesive into the anodic oxide for interdiffusion to occur.

It has been reported that microrough, porous, and thick oxides promote strong adhesive/Ti-6Al-4V bonds.[17,18,19] Microroughness is characterized by structural protrusions ≤ 0.1 μm. The oxide microroughness and porosity were more prominent in the chromic acid/hydrofluoric acid (CA/HF) anodized Ti-6Al-4V surface than for the phosphate-fluoride (PF) or Turco (Tu) treated surfaces. The CA/HF anodized surface had 40 nm protrusions above the pore cells. The oxide thickness was greatest for the CA/HF oxide. Oxide thickness measurements showed that the CA/HF oxide $>$ PF oxide $>$ Tu oxide.[17] A 10 volt CA/HF anodization potential produced an 80 nm thick anodic oxide. A 5 volt CA/HF anodization potential produced a 40 nm thick anodic oxide. In comparison, the PF oxide was 20 nm thick and the Tu oxide was 17 nm thick.

Of these three characteristics of the CA/HF oxide, the microroughness, or protrusions above the pore cells, is considered to be most important to bond strength by these authors.[17,18,19] Ditchek, et al[17] contend that the anodic oxide, with its high degree of microroughness, can provide a high degree of mechanical interlock to an adhesive. The path of least resistance for crack propagation would be expected to be in the adhesive and not along the bond line. Indeed, his wedge crack extension data supported

this theory. Failure was in the adhesive for the FM 300K/BR 127 adhesive primer system bonded to anodized Ti-6Al-4V.

B. Factors Which Influence Adhesive Bond Strength

Theoretically, high adhesion forces can be developed between an adherend and adhesive, as discussed above. Not even considering the much stronger chemical and hydrogen bonding, theoretical values of 1.38 GPa[14] have been calculated to remove a molecule from an adherend surface, based upon London dispersion forces. However, actual adhesive bond strength is always much lower than this calculated value. Reported values are in the range of 7 MPa to 55 MPa for a metal/adhesive single lap bond joint.

This discrepancy between theoretical and actual bond strength exists because bond strength is determined by more than just adhesion forces. Parameters which can effectively limit any adhesive/metal bond strength are listed and discussed below. They are:

(1) metal surface preparation and cleanliness;

(2) adhesive surface cleanliness;

(3) adhesive viscoelastic response to the applied stresses and temperatures in the bond joint, both before and after any physical aging of the adhesive in the bond joint;

(4) bond joint design;

(5) bond joint residual stresses induced by adhesive shrinkage, thermal coefficient mismatch between adhesive

and metal, and/or air entrapment during bond processing; and,

(6) bond joint environmental stress conditions, such as chemicals, water and temperature.

Metal and surface preparation and cleanliness are important to bond strength. Weak adhesive and adherend boundary layers and/or localized surface contaminants can reduce bond strength, as proposed by Bickerman.[20] Bond strength improvements have been reported after ion etching an adherend such as polyethylene prior to bonding.[21] Ion etching cleaned and removed the weak boundary layer, which was a low molecular weight polymer. Chen, et al.[22] reported that a partial (20%) monolayer of chemisorbed fluorine remained on FPL etched aluminum and resulted in adhesive/oxide failure. An inverse linear relationship between drum peel strength and fluorine surface concentration was reported. Ditchek, et al.[23] reported that Turco treated Ti-6Al-4V exhibited interfacial adhesive bond failure in the wedge test. It was suggested that failure initiated at iron particles introduced during the pretreatment process.

The adhesive viscoelastic response to stress applied to the bond joint and/or test temperatures will, in part,determine bond strength. The adhesive viscoelastic response is the change in the adhesive mechanical properties with frequency and magnitude of the applied stress and/or test temperature conditions.

Ideally, to optimize bond strength, an adhesive should be both a structural component and also a stress relief interlayer for the bond joint under the given test conditions. Such an adhesive would have a viscoelastic response which results in the following mechanical properties for the given test conditions: good impact strength ($\geq$ 214 to 267 J/m), good tensile strength ($\geq$ 55 MPa), a moderately low Young's modulus ($\leq$ 41 MPa), and a low creep rate.

The physical aging of an adhesive in a bond joint will change its viscoelastic response. These changes can be detrimental to bond strength since the adhesive's ability to function as a stress relief interlayer can be reduced and its fracture mechanism may change from ductile to brittle. Tant and Wilkes[24] have published a recent and comprehensive review of polymer physical aging and its effect upon structure and property relationships. The effects of physical aging upon mechanical properties for specific thermoplastics[25,26,27,28] and network epoxies[29] have been reported. Significant polymer physical aging occurs at test temperatures between T_g and T_B, the glass and secondary transition temperatures, respectively. As a result of polymer physical aging, there is a decrease in polymer free volume, impact strength, and creep rate, as well as an increase in tensile and flexural yield stress and Young's modulus. In addition, the fracture mechanism can also change from ductile to brittle fracture.

The bond joint design is also important to bond strength. A design which minimizes stress concentrations is preferred. Bond strength increased as uniformity of bond joint stress increased, as reported by Brett.[30] For epoxy/aluminum clad L-73 bond joints, the average bond strength was 28 MPa for single lap bonds, 50 MPa for double lap bonds and 75 MPa for napkin rings. The single lap bond joint has a parabolic type stress distribution across the overlap, as predicted by Goland and Reissner.[31] As a consequence of this stress distribution, the center of the adhesive contributes less to the bond strength than the edges, and the joint bond strength is consequently lower than it could be.

Single lap bond overlap, adhesive, metal thickness and type of metal also influence bond strength.[32] In the single lap bond, bond strengths and load capacity are proportional to bond width. Single lap bond load capacity increases, but not linearly, with bond overlap. This is because the single lap bond edges carry a relatively higher portion of the load than does the center portion of the overlap. As a result, single lap bond shear strength decreases with bond overlap.

Cagle[32] has also discussed the importance of adherend type and thickness to single lap bond strength. Shear strength increases with adherend thickness and strength. An optimum adhesive thickness for optimum bond strength depends upon the adhesive moduli. The mean single lap bond strength has been

related to the metal thickness and overlap length by means of a joint factor proposed by De Bruyne.[33] De Bruyne has shown that single lap bond strength increases from 7 MPa to 34 MPa as the joint factor increased. The joint factor is the square root of the metal thickness ratioed to the bond overlap length.

Residual stresses in the bond joint due to processing can limit bond strength. Air entrapment during bond processing can limit the adhesive's intrinsic strength and the wetting of the adhesive to the adherend. And, differences in the thermal expansion coefficient of the adherend and adhesive can induce stresses in the bond line and limit bond strength.

Environmental stress conditions can degrade bond strength. Hergenrother and Progar[34] reported that a three day water boil severely degraded the single lap bond strength for phosphate fluoride treated Ti-6Al-4V bonded to a 0.13 mm thick polyphenylquinoxaline adhesive.

Current reported literature for the tensile lap shear strength and wedge crack extension tests indicate that Ti-6Al-4V chromic acid anodization with fluoride produces a stronger and more durable bond than other common Ti-6Al-4V prebond treatments.[18,23,35] Even so, the oxide is amorphous when produced by any one of the commonly used Ti-6Al-4V prebond treatments, and an amorphous oxide can transform to anatase crystalline structure under hydrothermal conditions, 372K water immersion for 210 hours.[19]

If the amorphous to crystalline oxide transformation occurred in the bond line, the resulting stress could cause interfacial failure. To prevent this, Natan, et al.[36] suggest that the amorphous oxide on the titanium alloy should be crystallized to anatase before bonding. Anatase has a lower surface energy and a greater rate of formation than the other possible crystalline titanium oxides, brookite and rutile.[37]

The mechanism which describes how water could penetrate the bond line and cause oxide transformation at high relative humidity is unknown. Data suggest that water is transported along the bond line interface rather than through the adhesive.[38]

Given hydrothermal conditions at the oxide surface of the titanium alloy, oxide transformation mechanisms have been suggested.[36,39] Anatase nucleation from an amorphous oxide on the titanium alloy may be due to structural rearrangement. Anatase growth is attributed to a dissolution-precipitation mechanism in water.

C. Oxide Characterization for Chromic Acid/ Hydrofluoric Acid Anodized Ti-6Al-4V

The oxide surfaces of chromic acid/hydrofluoridic acid (CA/HF) anodized TI-6Al-4V have been characterized using Scanning Transmission Electron Microscopy (STEM) and Scanning

Electron Microscopy (SEM). Ditchek, et al.[17] examined the surfaces by STEM. They described the surfaces in terms of microroughness, which is represented by fine structures ≤ 0.1 μm, and macroroughness, which is characterized by structures ≥ 1.0 μm. The anodic oxide exhibited a low degree of macro and a high degree of microroughness. Protrusions approximately 40 nm above the pore cells were common. The anodic oxide was also described as porous, with a pore cell size of approximately 40 nm. Chen, et al.[40] reported similar surface features for chromic acid anodized Ti-6Al-4V by means of SEM analyses.

Ditchek, et al.[17] reported anodic oxide thickness. The thickness measurements were based upon Auger sputter analysis and confirmed by ellipsometry measurements. Oxide thicknesses were 40 and 80 nm for Ti-6Al-4V anodized at 5 V and 10 V, respectively.

Selected area diffraction patterns of the anodic oxide on CA/HF anodized Ti-6Al-4V have been conducted by Natan and Venables.[41] The anodic oxide was amorphous.

Cheng[42] examined the CA/HF anodic oxide surface, ≤ 10 nm, by means of Electron Spectroscopy for Chemical Analysis (ESCA). Cheng reported a Ti 2p doublet at 458.9 eV and 464.6 eV. The binding energy values and separation indicate TiO_2. Aluminum was reported but no vanadium was found. He suggested that the beta phase of this alloy, which contains the vanadium, was

preferentially etched during HF/HNO_3 acid pickling of the Ti-6Al-4V before anodization or HF acid etching of the Ti-6Al-4V during anodization.

Cheng[42] also reported that pores were present on the anodic oxide only when the fluoride ion was added to the chromic acid solution to control the current density. A smooth, compact film was obtained when HF was not added.

Cheng's work supports a proposed oxide formation method proposed by Marceau[43] and is described as follows. Initially, hydrofluoric acid dissolves the metal's natural oxide and the metal itself. An oxide layer quickly forms on this freshly ionized metal surface. The hydrofluoric acid then continues to etch the metal substrate and the oxide layer is continually added to the metal base. The hydrofluoric acid which etches the metal substrate then tunnels up through the oxide, thereby creating the oxide pores. This oxide formation process continues until the potential across the oxide exceeds the applied potential of the power supply. It must also be recognized that the oxide itself would be expected to have some solubility in the anodization solution. Therefore, oxide dissolution and formation would be occurring at independent rates. The last oxide layer which is formed at the base of the metal appears to be less porous than the preceeding oxide layers. This more dense oxide layer is referred to as a barrier oxide layer.

Oxide cracking or pits may be induced during anodization. These defects could be caused by internal stresses triggered by

metal flaws, contaminants, space charges, migration of ions during oxide growth, compressive and/or tensile oxide stresses, and pressure due to an electric field across the oxide.[42] Cheng[42] reported that under constant current conditions, the potential oscillated in a cyclic fashion. The oscillations were attributed to a cyclic oxide cracking, or pitting, and healing process.

Filbey and Wightman[44,45] have studied the effects of heating on the CA/HF anodized Ti-6Al-4V oxide by ESCA and STEM. ESCA indicated that the oxide surface chemistry was unaffected by exposure to 723K for 10 minutes at 10^{-6} torr. STEM analyses indicated that this high temperature exposure did not affect surface morphology.

D. Chromic Acid with Hydrofluoric Acid Anodized Ti-6Al-4V/ Adhesive Bond Characterization and Durability

No literature reporting bond strengths for polysulfone bonded to CA/HF anodized Ti-6Al-4V was found. Nor was there any literature available from Union Carbide, manufacturer of the Udel® polysulfone used in this study.

Hergenrother and Progar[34] reported CA/HF anodized Ti-6Al-4V/PPQ bond characterization and durability. The adhesive thickness was 0.13 to 0.15 mm. These bonds were exposed to a three day water boil and then tested at a designated temperature. In general, the failed surface exhibited mixed failure modes which

were predominantly cohesive, based upon visual analyses. For four single lap bonds tested at room temperature, the average strength was 24.3 MPa. For four single lap bonds tested at 561K, the average bond strength was reduced to 5.0 MPa. The low bond strength at 561K was attributed to failure of the PPQ. Thermoplastic failure was expected since the T_g of the PPQ was 591K.

No literature reported bond characterizations for polyethersulfone, unfilled or 20% glass filled polyetherimide, or 50% $CaCO_3$ filled polyimide. Further, single lap bond strength data for titanate primed CA/HF anodized Ti-6Al-4V has not been reported.

Data have been reported for titanate primed phosphoric acid anodized aluminum bonded to an unfilled 1-2 polybutadiene modified epoxy.[46] Without titanate primer, single lap bond strength was 9.5 MPa. Bond strength was 20.7 MPa when KR 44 titanate primer (Kenrich Petrochemicals) in a 0.2% concentration in isopropanol was applied to the phosphoric acid (PA) anodized Ti-6Al-4V.

The KR 44 titanate primer was compared to selected silane coupling agents as adhesion promoters for the single lap bond of PA anodized Ti-6Al-4V bonded to the 1-2 polybutadiene modified epoxy.[46] When a Union Carbide A-151 primer was used on the PA anodized Ti-6Al-4V, bond strength was 9.5 MPa. When a Dow Corning X2-8-5066 primer was used, bond strength was 18.0 MPa. As described above, the KR 44 titanate primed bonds resulted in a 20.7 MPa bond strength. It does appear that the KR 44 titanate is

a better adhesion promoter than these selected silane coupling agents for this specific adhesion/adherend system.

III. EXPERIMENTAL

A. Chromic Acid Anodization Methods and Materials

Ti-6Al-4V coupons, 152.4 mm X 25.4 mm X 1.3 mm, were provided by personnel at the NASA-Langley Research Center. All chemicals used for the cleaning and anodization process were purchased from Fisher Scientific. Distilled, deionized water was used to make all solutions.

Ti-6Al-4V was used both as the anode and cathode in the anodization process. Metal surfaces anodized had no previous history of pretreatment or bonding.

Before anodizing, the metal was cleaned per preanodization treatment #1 or preanodization treatment #2. Both methods are described in Table III. Solutions were used to clean six coupons at once; the solutions were not reused.

For preanodization treatment #1, the coupons were glass bead blasted to mechanically abrade and clean the Ti-6Al-4V. A Zero Blast-N-Peen machine from Zero Manufacturing Co. was used with medium size Ferro glass bead abrasives. A 5 minute immersion in a 5% sodium hydroxide solution at 343K was used to remove inorganics from the bead blasted Ti-6Al-4V coupons. An acid pickle, as described in Table III, was used to clean the Ti-6Al-4V anode and cathode as the final cleaning step immediately prior to anodization. The acid pickle etches the metal, thereby removing the natural oxide from the Ti-6Al-4V surface.

TABLE III

Procedures for Ti-6Al-4V Preanodization Treatments

Preanodization Treatment #1

1. Glass bead blast coupons with medium size Ferro glass beads.
2. Immerse 5 minutes in a 343K, 5% NaOH Solution (500 ml of solution for 6 coupons).
3. Rinse in distilled, deionized water.
4. Immerse 5 minutes in 500 ml distilled, deionized water.
5. Repeat Step #4.
6. Pickle at 298K for 5 minutes in a deionized water solution containing 15% by volume of 70% HNO_3, and 3% by volume of 49% HF (100 ml of solution for 6 coupons). Pickle a 50 mm long X 25 mm wide area.
7. Repeat Steps #4 and #5.
8. If pickling procedure results in a white film on the coupon, the surface has not been thoroughly cleaned. Steps #6 and #7 must be repeated using new solutions until no film appears on the surface.
9. Nitrogen dry.

Note: Coupons are anodized immediately after preanodization.

TABLE III (Continued)

Preanodization Treatment #2

1. Vapor degrease in trichloroethylene 10 minutes. Or, vapor degrease in 1,1,1 trichloroethane 15 minutes in vapor of 325K solvent sump, immersed 5 minutes in 298K 1,1,1 trichloroethane, followed by another 5 minutes in the solvent vapor sump.

2. Pickle at 298K for 30 seconds in a deionized water solution containing 15% by volume of 70% HNO_3, and 3% by volume of 49% HF (100 ml of solution for 6 coupons). Pickle a 50 mm long X 25 mm wide area.

3. Immerse 2 minutes in 500 ml distilled, deionized water. Repeat.

4. Repeat Step #3.

5. Nitrogen dry.

Note: Coupons are anodized immediately after preanodization.

Preanodization treatment #2 did not use either the bead blasting or the alkaline cleaning. Instead, preanodization treatment #2 consisted of vapor degreasing the Ti-6Al-4V in either trichloroethylene or 1,1,1 trichloroethane. Vapor degreasing in either of these solvents is a standard industrial method used for cleaning metals. Preanodization treatment #2 used the same type of acid pickle as was used in preanodization treatment #1 immediately prior to anodization. In preanodization treatment #2, the acid pickle was of a shorter duration than for preanodization treatment #1.

Immediately after the Ti-6Al-4V coupons were acid pickled, cleaned and dried, the coupons were anodized. A 5% chromic acid solution with a 0.5 pH was the anodization electrolyte. A Beckman pH meter was used to determine that the chromic acid pH was correct. Technical grade chromium trioxide and distilled, deionized water at 298K were used to make the solution. A 49% solution of hydrofluoric acid (HF) was added as a 2 ml volume addition to many of the 750 ml chromic acid (CA) anodization baths at the beginning of anodization. The hydrofluoric acid was added to obtain the initial anodization current density.

Chromic acid solutions were stored in either Nalgene or polypropylene closed containers. When the anodization solution temperature was either 283K or 278K, the chromic acid solution was first chilled to 276K and then immersed in an ice bath where the temperature was stabilized at the specified anodization temperature.

The anodization solution temperature was checked before and after anodization to verify temperature stability.

The anodization apparatus is depicted in Figure 2. A 0.5 ampere, constant voltage power supply was used. Six Ti-6Al-4V coupons were immersed to a depth of 25.4 mm in the solution and anodized at once. This was done by connecting them in a parallel circuit along a brass conductor. The brass conductor consisted of two, 0.1 mm thick brass shims with a 2.0 mm rubber separator between them. This rubber insert allowed anodization on both sides of each coupon. Air agitation of the bath was used during anodization to insure uniform anodization of both sides of the Ti-6Al-4V surface. Both the bath container and air tube were Teflon because of its excellent chemical resistance to chromic acid and hydrofluoric acid.

Basic equations describing the Ti-6Al-4V anodization process at a given potential are given below. The chromium trioxide in solution can be described by the equation:

$$CrO_3 + 3H_2O \longrightarrow Cr(OH)_6 \qquad [3\text{-}1]$$

Anode electrolytic reactions can be described as follows:

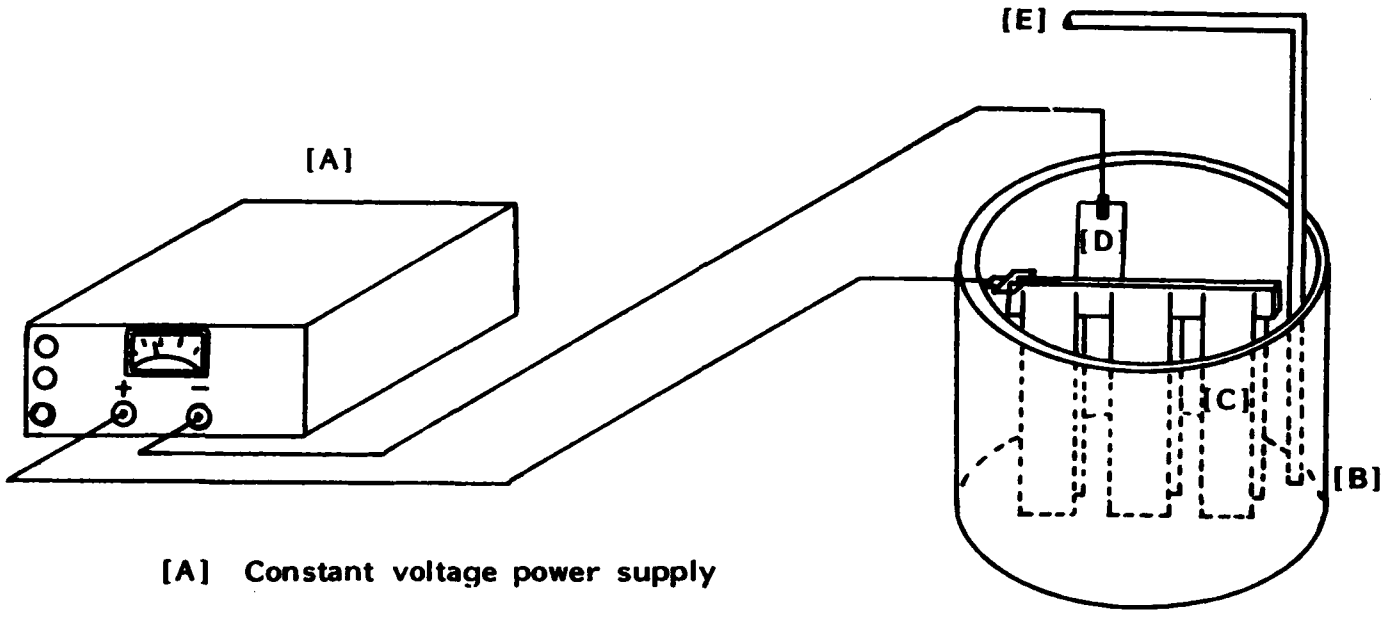
$$2Ti^{\circ} \longrightarrow 2Ti^{+4} + 8e^{-} \qquad [3\text{-}2]$$

and

$$2Ti^{+4} + 8(OH)^{-} \longrightarrow 2TiO_2(4H_2O). \qquad [3\text{-}3]$$

Cathode electrolytic reactions can be described as follows:

$$2H_2O + 2e^{-} \longrightarrow H_2 + 2(OH)^{-} \qquad [3\text{-}4]$$



[A] Constant voltage power supply

[B] Teflon anodization tank

[C] Anodes connected in parallel

[D] Cathode

[E] Teflon tube (for air agitation of solution)

Figure 2. Anodization Apparatus Schematic.

and

$$2Cr(OH)_6 + 6e^- \longrightarrow 2Cr(OH)_3 + 6(OH)^-. \qquad [3\text{-}5]$$

The general procedure used for chromic acid anodization without hydrofluoric acid is described in Table IV. This method was experimentally devised by the author.

The general procedure for chromic acid anodization with hydrofluoric acid is described in Table V. One of the following current densities was used: 20 ± 2 A/m^2, 30 ± 2 A/ m^2, or 54 ± 2 A/m^2.

Seven chromic acid/hydrofluoric acid Ti-6Al-4V anodization conditions were tested and are described in Table VI. The anodization temperature, time and initial current density were varied. After anodization, the coupons were soaked in distilled, deionized water and nitrogen dried, as described in Table VII.

One chromic acid anodization condition was tested and is also described in Table VI. After anodization, the coupons were cleaned and dried as described in Table VII.

B. X-Ray Diffraction

X-ray diffraction was conducted for the following two samples:

(1) Ti-6Al-4V after preanodization treatment #1, and

(2) Ti-6Al-4V after preanodization treatment #1 and 20 minute chromic acid anodization with HF at 298 ± 2K and an initial current density of 30 ± 2 A/m^2.

TABLE IV

Procedure for Chromic Acid Anodization Without Hydrofluoric Acid

1. Immediately after pretreatment, immerse 6 Ti-6Al-4V coupons, connected in a parallel circiut, in 750 ml of a 5% chromic acid solution. Area of immersion was 25 mm X 25 mm. Connect coupons to positive outlet of power supply.

2. Immerse one Ti-6Al-4V coupon in solution and connect to negative outlet of power supply. Cathode should be immersed $\leq$ 6 mm into the solution. This will minimize cathode area and thereby minimize electrolytic reduction of chromic acid at the cathode.

3. Check resistance of circuit with an ohmmeter. Resistance should be $\leq 0.5\ \Omega$ between the anode and the positive outlet of the power supply.

4. Air agitate solution.

5. Increase voltage slowly over a two minute period to 39 V; this prevents localized heating of coupons. Current density should by 30 $\pm$ 2 A/m^2. The voltage must be reduced during anodization to maintain current density.

6. Anodize at 30 $\pm$ 2 A/m^2 for 20 minutes, reducing voltage to 33 V to maintain this current density.

7. Immerse coupons in 500 ml of distilled deionized water for 5 minutes.

8. Repeat Step #7.

9. Nitrogen dry anodized coupons.

TABLE V

Procedure for Chromic Acid Anodization With Hydrofluoric Acid

1. Immediately after pretreatment, immerse 6 Ti-6Al-4V coupons, connected in a parallel circuit, in 5% chromic acid solution. Area of immersion per coupon is 25 mm X 25 mm. Connect coupons to positive outlet of power supply.

2. Immerse one Ti-6Al-4V coupon in solution and connect to negative outlet of power supply. Cathode should be immersed $\leq$ 6 mm into the solution. This will minimize cathode area and thereby minimize electrolytic reduction of chromic acid at the cathode.

3. Resistance should be $\leq 0.5\ \Omega$ between the anode and positive outlet of the power supply.

4. Air agitate solution.

5. Set power supply voltage to 10V.

6. Add hydrofluoric acid dropwise to achieve desired current density (Approximately 2 ml HF/750 ml bath solution results in an initial current density of $30 \pm 2\ A/m^2$).

7. Anodize for either 20 or 60 minutes.

8. Immerse 6 coupons in 1 liter of distilled deionized water for two minutes. Repeat.

9. Immerse 6 coupons in 1 liter of distilled deionized water for 15 minutes.

10. Repeat Step #8.

11. Nitrogen dry anodized coupons.

TABLE VI

Chromic Acid/Hydrofluoric Acid Ti-6Al-4V Anodization and

Chromic Acid Ti-6Al-4V Anodization Conditions Tested

Chromic Acid/Hydrofluoric Acid Ti-6Al-4V Anodization Conditions

Method	Solution Temperature (K ± 2K)	Initial Current Density (A/m^2 ± 2 A/m^2)	Voltage (Volts)	Anodization Time (Minutes)
1	273	30	10	20
2	283	30	10	20
3	283	20	10	20
4	298	54	10	20
5	298	30	10	20
6	298	30	10	60
7	298	20	10	20

Note: For chromic acid/hydrofluoric acid anodization, the hydrofluoric acid was added to obtain the initial current density.

TABLE VI (Continued)

Chromic Acid Ti-6Al-4V Anodization Conditions

Method	Solution Temperature (K ± 2K)	Initial Current Density (A/m^2 ± 2 A/m^2)	Voltage (Volts)	Anodization Time (Minutes)
1	298	30	39	20

TABLE VII

Post-Anodization Ti-6Al-4V Cleaning Method

1. Soak Ti-6Al-4V coupons in a 500 ml volume distilled, deionized water 2 minutes.
2. Soak Ti-6Al-4V coupons in a clean 500 ml volume distilled, deionized water 2 minutes.
3. Soak Ti-6Al-4V coupons in a clean 500 ml volume of distilled, deionized water 15 minutes.
4. Repeat Steps #1 and #2.
5. Nitrogen dry anodized coupons.

NOTE: This procedure is used for cleaning six coupons simultaneously. The coupons were immersed so as to clean the 25.4 square mm of anodized surface area.

A Siemens Type M386-A7 60 KV X-ray diffractometer with a Cu Kα radiation source was used. A 9.5 mm diameter sample was punched from each titanium alloy coupon used in this analysis. The 2θ range was 16° to 75° at a scan speed of 1°/minute. The purpose of the X-ray diffraction analysis was to identify the anodic oxide structure. The X-ray diffraction analysis of the Ti-6Al-4V after preanodization treatment #1 served as the control.

C. Transmission Electron Microscopy (TEM) and Selected Area Electron Diffraction (SAED)

A 38.1 μm thick Ti-6Al-4V foil was purchased from Arnold Subsidiary Magnetics and Electronics, Inc. Ti-6Al-4V preanodization treatment #1 was used to cleaned the foil. Foil sections, each 25.4 mm X 12.0 mm, were anodized by either anodization method #3 or anodization method #7 described in Table VI. TEM analyses of the anodic oxide produced per methods #3 and #7 were conducted. SAED analyses was conducted for the anodic oxide produced per method #3.

The TEM and SAED analyses of the anodic oxide were conducted at Structure Probe, Inc. of West Chester, Pennsylvania. A JEOL 100CX TEM at a 100 kV accelerating voltage was used to obtain both the TEM and SAED micrographs. At Structure Probe, Inc. the anodized Ti-6Al-4V foil was prepared for anodic oxide TEM and SAED analyses as follows. The anodized Ti-6Al-4V foil was embedded in a SPI-PON® 812 epoxy resin and microtomed to

produce ultrathin cross sections and parallel sections of the anodic oxide. A DuPont Sorvall MT2-B Ultramicrotome and diamond knife were used. Sections microtomed were approximately 60 to 80 nm in thickness.

TEM analyses of the oxide in cross section were conducted to elucidate the oxide roughness, morphology and thickness. The anodized Ti-6Al-4V foil to be cross sectioned was gold sputtered prior to epoxy embedding and cross sectioning. The gold sputter coat was used to better define the anodic oxide surface in cross section.

TEM analyses of the oxide in parallel section was conducted to elucidate oxide morphology. Parallel sections were analyzed by SAED to determine oxide structure.

D. Multiple Beam Interferometry (MBI) Methods and Materials

Multiple Beam Interferometry (MBI) was used to measure the Ti-6Al-4V anodic oxide thickness. For these measurements, an anodic oxide was produced on a polished Ti-6Al-4V substrate.

The anodic oxide was produced on a flat (to within $\lambda/4$) substrate to minimize curvature of the multiple beam interferometer fringes. The Ti-6Al-4V coupons were polished prior to anodization as described in Table VIII. The metal substrate portion of each anodized Ti-6Al-4V coupon was masked prior to anodization. The mask was Permatex, a water soluble gasket material. The mask was allowed to dry 24 hours on the coupon before anodization. After

TABLE VIII

Polishing Technique for Ti-6Al-4V Interferogram Measurements

1. Mount Ti-6Al-4V on flat block for support during polishing.
2. Polish in vertical direction on 240 grit (65 μm particle size) silicon carbide wetted with water. Water rinse coupon. Repeat polishing in a horizontal direction. Water rinse.
3. Polish as described in Step #2 using 320 grit (30 μm particle size) wet silicon carbide paper.
4. Polish as described in Step #2 using 400 grit (23 μm particle size) wet silicon carbide paper.
5. Polish as described in Step #2 using 600 grit (16 μm particle size) wet silicon carbide paper.
6. Polish on a lapping wheel using 6 μm diamond paste with oil. Rinse coupon, first in alcohol and then in Freon TF. Light polishing pressure should be used to prevent sample pitting.
7. Polish on a lapping wheel using 1 μm alumina/water solution. Water rinse coupon.
8. Repeat Step #7 using 0.05 μm alumina/water solution. Water rinse.
9. Examine under 30X magnification for scratches. If scratches are present, repeat Steps #5 through #8.

Note: For reference, polishing procedure requires approximately 2 hours per coupon. A minimum of 25 mm^2 surface area was polished on each coupon.

anodization, the Permatex was removed with isopropanol using cotton swabs. This masking technique was necessary in order to obtain a fairly defined anodization line. Given the magnifications used in the interferometer, the interfacial region should be ≤ 0.5 cm wide to obtain the anodic oxide, and interfacial and substrate fringes in one photograph. Microstop, a methylene soluble plating mask, was also tried. However, the Microstop did not adhere well to the polished titanium alloy and the anodization line was not well-defined.

Prior to insertion of the anodized Ti-6Al-4V coupon into the interferometer, 70 nm of silver was evaporated onto the anodic oxide and the adjacent metal substrate to increase the surface reflectivity. The silver evaporation method can be described as follows. A 12.7 cm source-to-anodized Ti-6Al-4V coupon distance was used in the evaporative chamber. A total of 47.5 cm of silver wire, 0.203 mm in diameter, was deposited on the anodized titanium coupon at 0.1 torr.

Figure 3 is a schematic diagram of the interferometer used to measure the Ti-6Al-4V anodic oxide thickness. Figure 4 shows the mount for the Ti-6Al-4V used in the interferometry set-up. The interferometry measurement method is described in Table IX.

The principles and operation of interferometry to measure an oxide thickness are described as follows. In this discussion, direct reference will be made to the interferometer set-up illustrated in Figure 3, and the operation instructions described in Table IX.

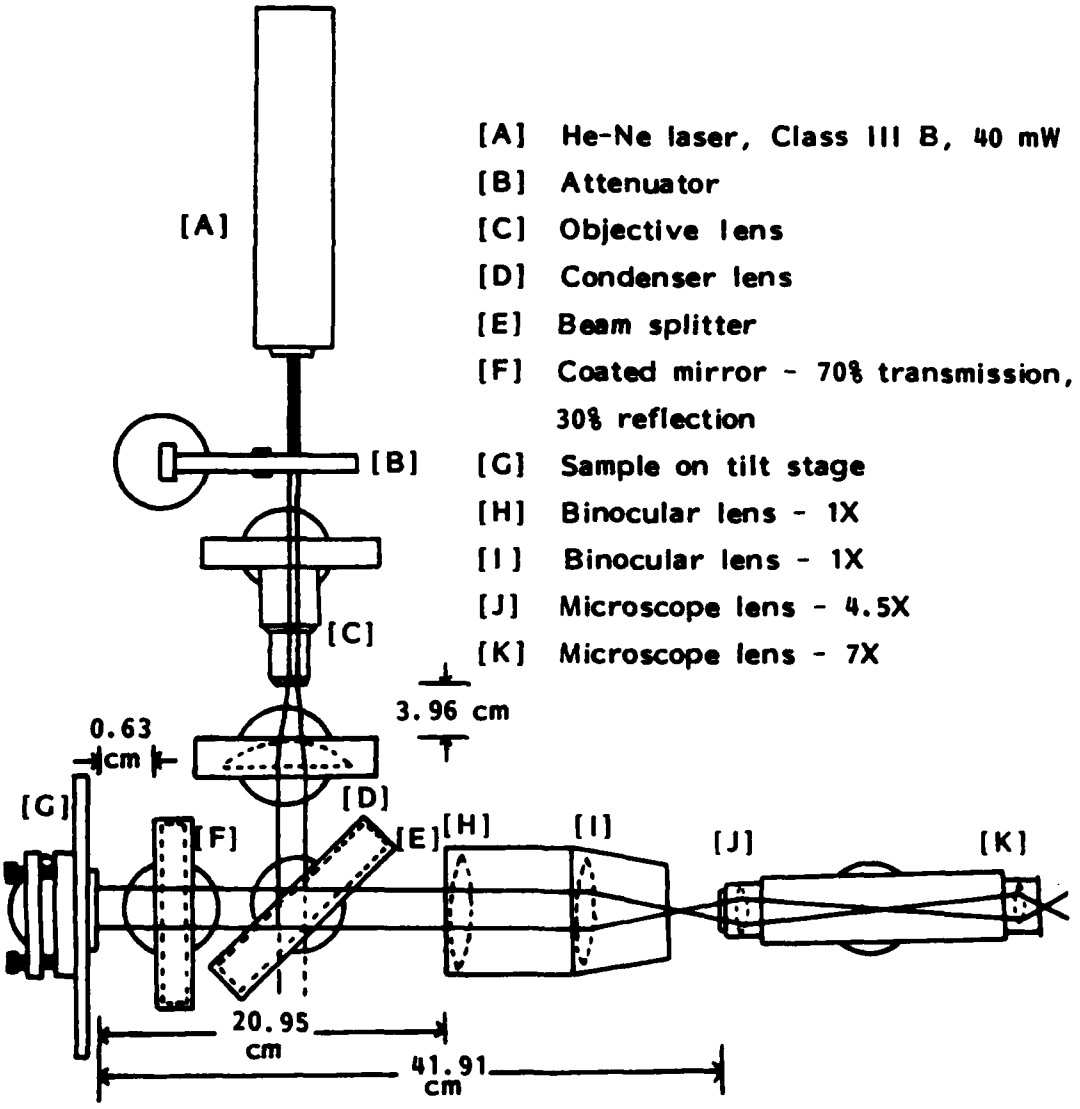


Figure 3. Interferometer Schematic Diagram.

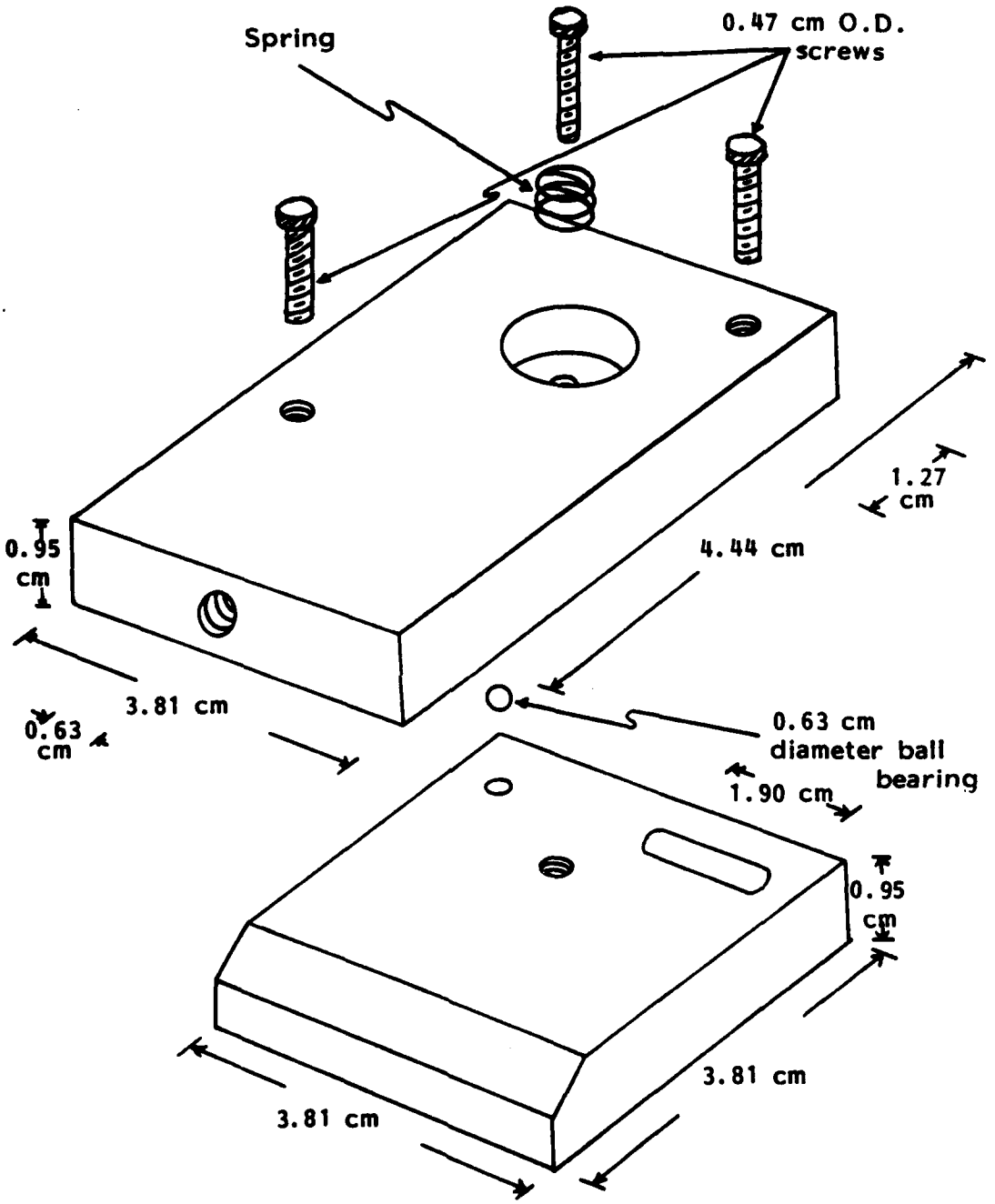


Figure 4. Interferometer Mount for the Ti-6Al-4V Coupon.

TABLE IX

Interferometry Measurement Technique

1. See Figure 3 for interferometric schematic. Mount sample on sample stage and tilt sample.

2. Focus microscope on the oxide/substrate interface using visible light. Turn off visible light source. Microscope lens [J] and lens [K] described in Figure 3 should be used.

3. Collimate the laser beam using the 10X objective lens in component [C] as shown in Figure 3. Attenuate the laser beam to a maximum using a filter.

4. Superimpose reference mirror and sample reflections by tilting sample and adjusting the reference mirror. The two, circular reflections will superimpose when the reference mirror is parallel to the sample surface. The superimposed reflections can be observed by placing a piece of paper in front of the first binocular focusing lens.

5. Fringes should be visible when viewed through microscope.

6. Remove component [J] as described in Figure 3, which is the 7X objective lens in the microscope. Attach in its place the 35 mm camera with extender.

7. Photograph in darkened room with manual shutter speed control. A shutter exposure of approximately 7 seconds was used for 125 ASA black and white film.

The Ti-6Al-4V sample analyzed included three discrete areas: the anodic oxide, the anodic oxide/unanodized Ti-6Al-4V interface, and the unanodized Ti-6Al-4V substrate. All three areas were analyzed simultaneously by interferometry to determine the anodic oxide thickness.

As shown in Figure 3, a reference mirror, which transmitted 70% and reflected 30% of the light, was used. The sample and mirror were tilted and positioned parallel to each other.

The interferometer required a monochromatic, collimated, or parallel, visible light source. A 632.8 nm helium/neon laser was used in this set-up. The laser light, which was attenuated, was focused simultaneously onto the reference mirror and the three discrete areas of the Ti-6Al-4V sample.

Reflected laser light from the reference mirror superimposed with the reflected laser light from each of the 3 discrete areas of the Ti-6Al-4V sample. Because the reference mirror and the Ti-6Al-4V sample were tilted, the reflected light path length varies across the surfaces of the reference mirror, anodic oxide, anodic oxide/unanodized Ti-6Al-4V interface, and the unanodized Ti-6Al-4V. Consequently, superimposition of the reflected light from the tilted reference mirror and the tilted anodic oxide results in alternating bright and dark fringe bands. The bright and dark fringes are due to constructive and destructive interference, respectively. Based upon the same principle, alternating light and

dark fringes exist for the unanodized Ti-6Al-4V surface examined as well as the anodic oxide/unanodized Ti-6Al-4V interface region.

Maximum power, or constructive interference, results in a bright fringe. This occurs when light reflected from the mirror and a discrete region of the sample superimpose to satisfy the following phase condition:

$$(2m + 1)\ \frac{\lambda}{4} \qquad [3\text{-}6]$$

where m = 0, 1, 2, 3, . . .

Minimum power, or destructive interference, results in a dark fringe. This occurs when light reflected from the mirror and sample superimpose to satisfy the following phase condition

$$2m\left(\frac{\lambda}{4}\right) \qquad [3\text{-}7]$$

where m = 0, 1, 2, 3, . . .

The $\lambda/2$ is the minimum distance between the reference mirror and sample to get destructive interference as shown in equation [3-7]. Therefore, $\lambda/2$, where λ = 632.8 nm, is the separation distance between two parallel dark bands. This $\lambda/2$ distance can be measured from photographs of the fringe patterns. This measured separation distance, b, is required to calculate the anodic oxide thickness.

Because of the height of the anodic oxide relative to the unanodized Ti-6Al-4V, the reflected light from the oxide will differ in path length from the reflected light path length from the unanodized Ti-6Al-4V. As a result, the alternating bright and

dark fringes from the anodic oxide will be offset relative to the alternating bright and dark fringes from the unanodized Ti-6Al-4V. This offset distance, a, can be measured from photographs of the fringe patterns and is required to calculate the anodic oxide thickness.

Anodic oxide thickness, n, is calculated from the proportionality equation shown below:

$$n = \frac{a}{b} X \frac{\lambda}{2} \qquad [3\text{-}8]$$

where λ is known to be 632.8 nm and, as described above, a and b are quantities which result from superimposition and can be measured from a photograph of the fringe pattern.

Figure 5 is an interferogram at 28.4X magnification used to measure Ti-6Al-4V anodic oxide thickness. The actual area photographed was 7.6 mm X 5.0 mm.

The interference pattern was photographed in the interferometer set-up using a 35 mm camera with an extender, and ASA 125 black and white film. Photographs were taken in a darkened room using manual timing of the shutter. Photographing the sample required the removal of the 7.0X objective eyepiece in the microscope in order to insert the extender of the camera. The interference photographs were taken at 4.5X magnification and then enlarged 6.3X for accurate oxide thickness measurement.

As shown in Figure 5, alternating bright and dark fringe patterns from the anodic oxide are approximately parallel.

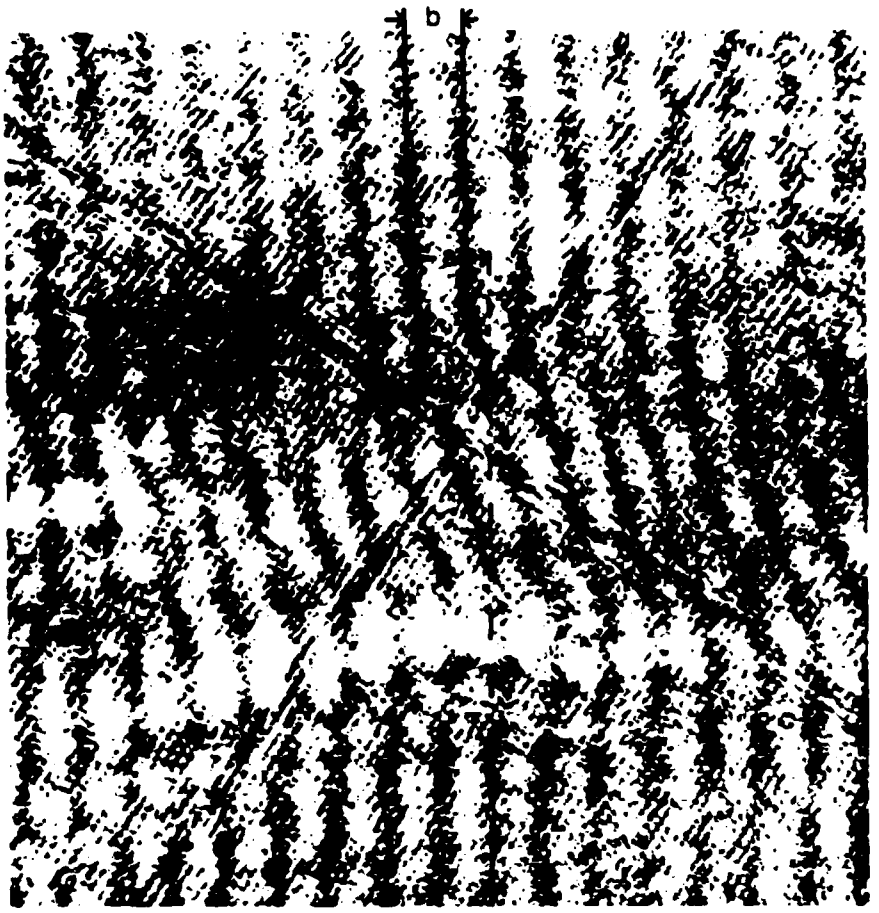


Figure 5. Interferogram of Fringe Pattern Used to Measure Ti-6Al-4V Anodic Oxide Thickness (28.4X). CA/HF Conditions: 20 Minutes, 278 ± 2K, 10 Volts, 30 ± 2 A/m^2.

Similarly, the observed alternating bright and dark fringes from the unanodized Ti-6Al-4V are also approximately parallel. Deviations from parallelism result because the surfaces are not perfectly flat.

As shown in Figure 5, the anodic oxide/unanodized Ti-6Al-4V interface spans a length of approximately 0.5 cm. This is because the Permatex mask applied to the Ti-6Al-4V before anodization was approximately 0.5 cm long. It can also be seen in Figure 5 that the alternating interfacial fringes curve to connect the alternating fringes from the anodic oxide to the alternating fringes from the unanodized Ti-6Al-4V. The fringe curvature results because there is a gradient of anodic oxide thickness in the interface region. These curved interface fringes, which connect the anodic oxide to the unanodized substrate, are a result of the fact that the Permatex mask does not form a perfect seal with the unanodized Ti-6Al-4V. The anodization solution penetrates the masked area and results in a gradient of oxide thickness between the anodic oxide and the unanodized Ti-6Al-4V.

These curved, alternating bright and dark fringes in the interface, which interconnect the anodic oxide and the unanodized Ti-6Al-4V fringes, are important to determine the exact anodic oxide thickness. Without this interconnecting fringe pattern, it would not be possible to distinguish anodic oxide thicknesses $\geq \lambda/2$.

E. Chromic Acid Anodized Ti-6Al-4V/Heat Resistant Adhesive Single Lap Bond

1. Ti-6Al-4V Adherend

The metal used in the single lap bond was Ti-6Al-4V. The dimensions of the Ti-6Al-4V coupons and the anodization procedures have been described earlier in the text.

Some of the CA/HF anodized Ti-6Al-4V coupons were primed with Lica® 44, a neoalkoxy, tri (N ethylamino-ethylamino) titanate primer, prior to application of the heat resistant adhesives in the single lap bonds. The primed, anodized TI-6Al-4V was tested in single lap bonds for the following adhesives: polyphenyl-quinoxaline, Victerex® polyethersulfone, Ultem® 1000 polyether-imide, and Ultem® 2200 glass filled polyetherimide. The Lica® 44 was supplied by Kenrich Petrochemicals, Inc. and the structure is illustrated in Figure 6.

A 0.2% V/V Lica® 44 in reagent grade isopropanol was applied to the anodized Ti-6Al-4V substrate in a single stroke with a 2.54 cm wide and 5.08 cm long sponge brush. The sponge brush was saturated with the titanate solution prior to application to each anodized Ti-6Al-4V surface. The primed Ti-6Al-4V was then stage dried at 338 ± 5K for 0.5 hr.

The selection of Lica® 44 as a primer for anodized Ti-6Al-4V and the method of application were per the recommendation of Dr. Gerald Sugarman, of Kenrich Petrochemicals, Inc. Based upon an

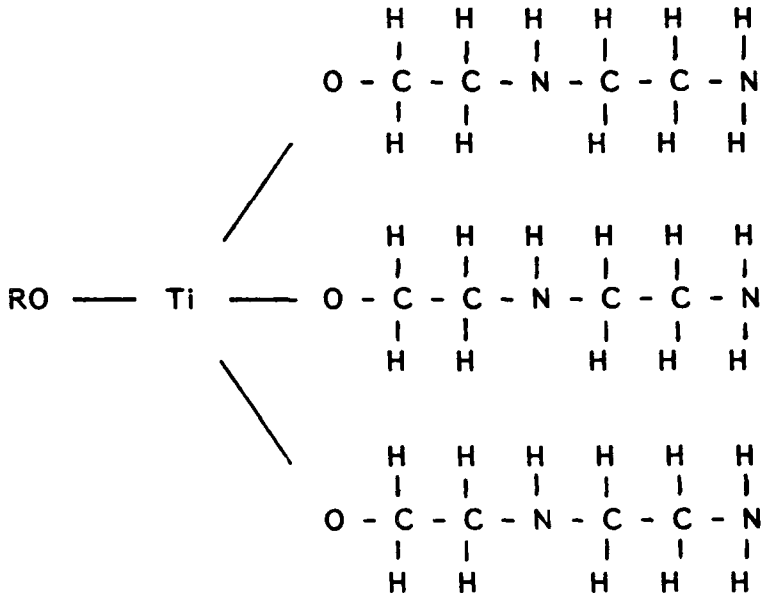


Figure 6. Structure of Lica® 44 Neoalkoxy Titanate Primer

approximation, the application technique resulted in approximately 750 titanate equivalent monolayers on the anodized Ti-6Al-4V surface. This calculation and the necessary assumptions are described in Appendix I.

This titanate is considered beneficial for adhesion of the metal oxide to a thermoplastic. The Lica® 44 RO group chemically reacts with the inorganic hydroxylated metal oxide to form a chemical bond, while the amine terminated end of the titanate provides van der Waals' entanglement due to $(O-C_2H_4-NH-C_2H_4-NH_2)_3$ structure with the thermoplastic. For a thermoset, the amine terminated end of the titanate may chemically react with the curing agent or resin.

2. Heat Resistant Adhesives

Tables X, XI and XII describe the structure and properties of the six heat resistant adhesives tested in single lap bonds. Four of the adhesives were received as polymer beads and were compression molded into an adhesive film for single lap bonding. These polymers which had to be compression molded were: Udel® polysulfone (PS), Victerex® unfilled polyethersulfone (PES), Ultem® 1000 unfilled polyetherimide (PEI), and Ultem® 2200, 20% glass fiber filled polyetherimide (PEIF). The glass fibers were 13.2 μm in diameter. Lengths varied from 200 μm to 500 μm, with 75% being 300 μm long.

TABLE X

Chemical Structures of Heat Resistant Adhesives Tested

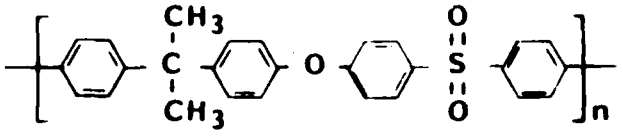
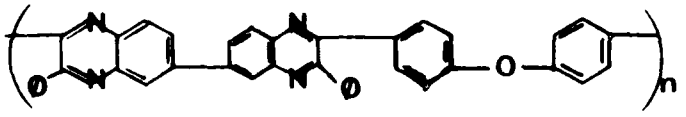
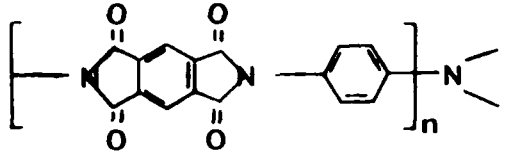
Name	Type	Structure
Udel® P-1700 Polysulfone (PS)	Polysulfone, unfilled, thermoplastic	
Polyphenyl-quinoxaline (PPQ)	Polyphenylquinoxaline, unfilled, thermoplastic, 20% solids in 1:1 mixture in cresol/xylene	
Ablebond® 71-3 Polyimide (PI)	Polyimide, 50% $CaCO_3$, filled, thermoset	

TABLE X (Continued)

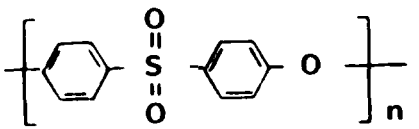
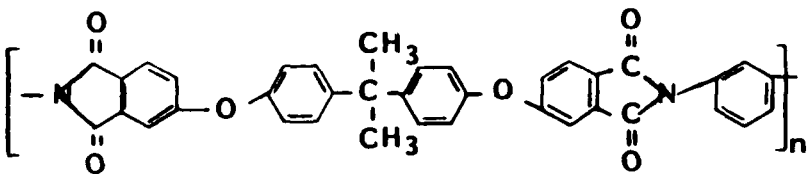
Name	Type	Structure
Victrex® 200P (4100G) Polyethersulfone (PES)	Polyethersulfone, unfilled, thermoplastic	
Ultem® 1000 Polyetherimide (PEI)	Polyetherimide, unfilled, Black 7101, thermoplastic	
Ultem® 2200 Polyetherimide (PEIF)	Polyetherimide, 20% glass filled, Black 7301, thermoplastic	

TABLE XI

T_g Values and Compression Molding Schedules for Heat Resistant Adhesives Tested

Name	Tg (K)	Compression Molding Schedule	Continuous Use Temperature (K)
Udel® P-1700 Polysulfone (PS)	463	20 min preheat 561K 10 min 137.9 MPa 561K Cool under pressure below 423K	422 UL Rated
Polyphenyl-quinoxaline (PPQ)	563	NC	505
Ablebond® 71-3 Polyimide (PI)	513 to 533	NC	623

Note: NC means not compression molded

TABLE XI (Continued)

Name	Tg (K)	Compression Molding Schedule	Continuous Use Temperature (K)
Victerex® 200P (4100G) Polyethersulfone (PES)	498	3 min preheat 644K 5 min 1.4 MPa 644K Cool under pressure below 423K	453 UL Rated
Ultem® 1000 Polyetherimide (PEI)	488	3 min preheat 644K 5 min 1.4 MPa 644K Cool under pressure below 423K	443 UL Rated
Ultem® 2200 Polyetherimide (PEIF)	488 to 496		442 UL Rated

TABLE XII

Thermal Expansion Coefficients, Vendor, and Chemical Resistance

Information for Heat Resistant Adhesives Tested

Name	Thermal Expansion X 10^{-5}/K	Vendor	Chemical Resistance
Udel® P-1700 Polysulfone (PS)	6.2	Union Carbide	Dissolved by chlorinated hydrocarbons. Swollen by esters, ketones or aromatic hydrocarbons.
Polyphenyl-quinoxaline (PPQ)	N/A	NASA	Dissolved by chloroform or xylene.
Ablebond® 71-3 Polyimide (PI)	N/A	Ablestik Laboratories	No known solvent to remove cured polyimide.

Notes: (1) Ti-6Al-4V coefficient of thermal expansion: 1.2 X 10^{-5}/K.

(2) N/A means not available.

TABLE XII (Continued)

Name	Thermal Expansion X 10^{-5}/K	Vendor	Chemical Resistance
Victrex® 200P (4100G) Polyethersulfone (PES)	6.2	ICI	Swollen by xylene, methylene chloride, or N-methyl pyrolidine.
Ultem® 1000 Polyetherimide (PEI)	6.2	General Electric	Dissolved by methylene chloride, or trichloroethane.
Ultem® 2200 Polyetherimide (PEIF)	2.5	General Electric	Dissolved by methylene chloride, or trichloroethane.

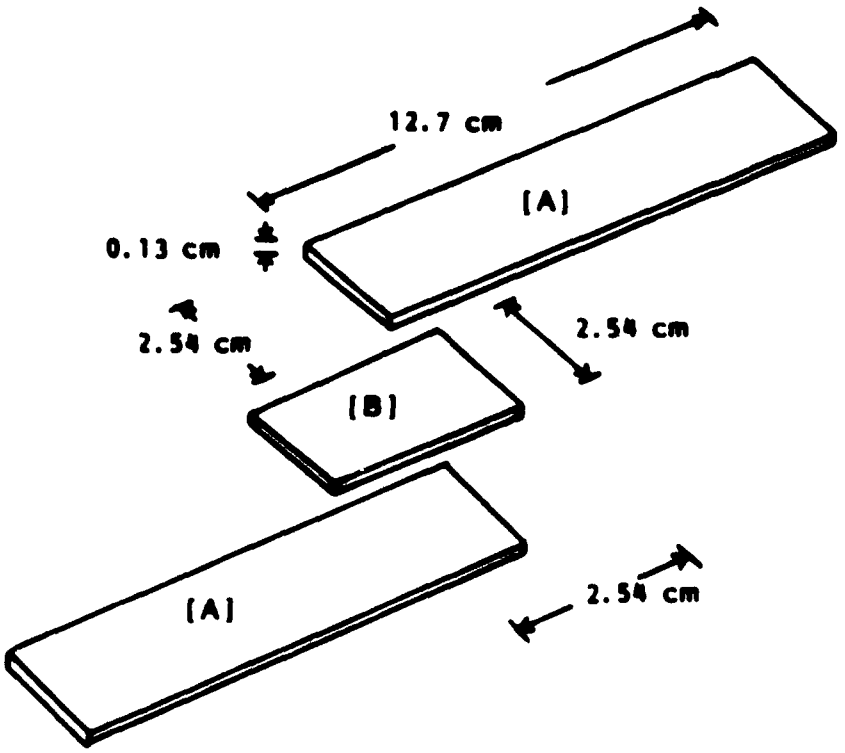
Note: Ti-6Al-4V coefficient of thermal expansion: 1.2 X 10-5/K

The unfilled polyphenylquinoxaline (PPQ) thermoplastic used in the single lap bonds was dissolved in a 1:1 xylene:cresol diluent. The PPQ was supplied by Paul Hergenrother of the NASA Langley Research Center. The PPQ was stored 9 months at 278 ± 5K prior to its use. The PPQ was applied as a liquid to the anodized Ti-6Al-4V surface.

The Ablebond® 71-3 50% $CaCO_3$ filled polyimide (PI) was received as a paste. The $CaCO_3$ particle size was 15 μm. It was stored 9 months at 278 ± 5K prior to its use. It was applied as a paste directly to the anodized Ti-6Al-4V.

3. Single Lap Bonding Apparatus

Figure 7 is a schematic of a single lap bond. The single lap bond configuration was per ASTM D1002, entitled "Strength Properties of Adhesives in Shear by Tension Loading (Metal to Metal)." The bond has a 0.63 cm bond fillet at each bond edge to reduce peel stresses at the bond edges during test in tension. The bond configuration and adhesive thickness were controlled during heat resistant adhesive/anodized Ti-6Al-4V bonding by means of an aluminum alloy jig for all adhesives tested except PPQ and PI. For these two adhesives, the jig was used to control the bond configuration only, since adhesive thickness was controlled by a micrometer-adjusted blade, which will be discussed later in the text. The jig was lined with 22.9 μm thick aluminum foil or 0.08 mm thick glass reinforced Teflon cloth for protection of the jig.



[A] Anodized Ti-6Al-4V coupon

[B] Adhesive

Figure 7. Schematic of a Single Lap Bond.

An aluminum alloy jig was used for the PPQ, PES, PS, PEI and PEIF adhesives bonded to the anodized Ti-6Al-4V. A schematic of the jig is illustrated in Figure 8 and Figure 9.

A second aluminum alloy jig was used solely for the PI bonds, which did not require the platen press pressure bonding. A schematic of this jig is shown in Figure 10.

4. Single Lap Bonding Methods

The PPQ was applied to the anodized Ti-6Al-4V in a 0.10 mm thick layer with a micrometer-adjusted blade. The PPQ coated metal was stage dried in clean ovens as described in Table XIII. The stage drying removed solvents and reduced the 0.10 mm PPQ thickness by approximately 50% as measured with a micrometer. The coupons were then cooled to 298 ± 2K and another 0.10 mm thick PPQ layer was applied and stage dried. The final PPQ thickness on each coupon was 0.15 ± 0.05 mm, as measured by a micrometer.

The PPQ/anodized Ti-6Al-4V coupons were bonded in single lap bonds within 6 hours after PPQ application. The bonds were formed by either an isothermal or isochronal bonding process as described in Table XIV.

The isothermal process and stage drying method were per communication with Paul Hergenrother of the NASA Langley Research Center. The isochronal process was based upon a reported method[46], with two exceptions. A 41.4 MPa bonding

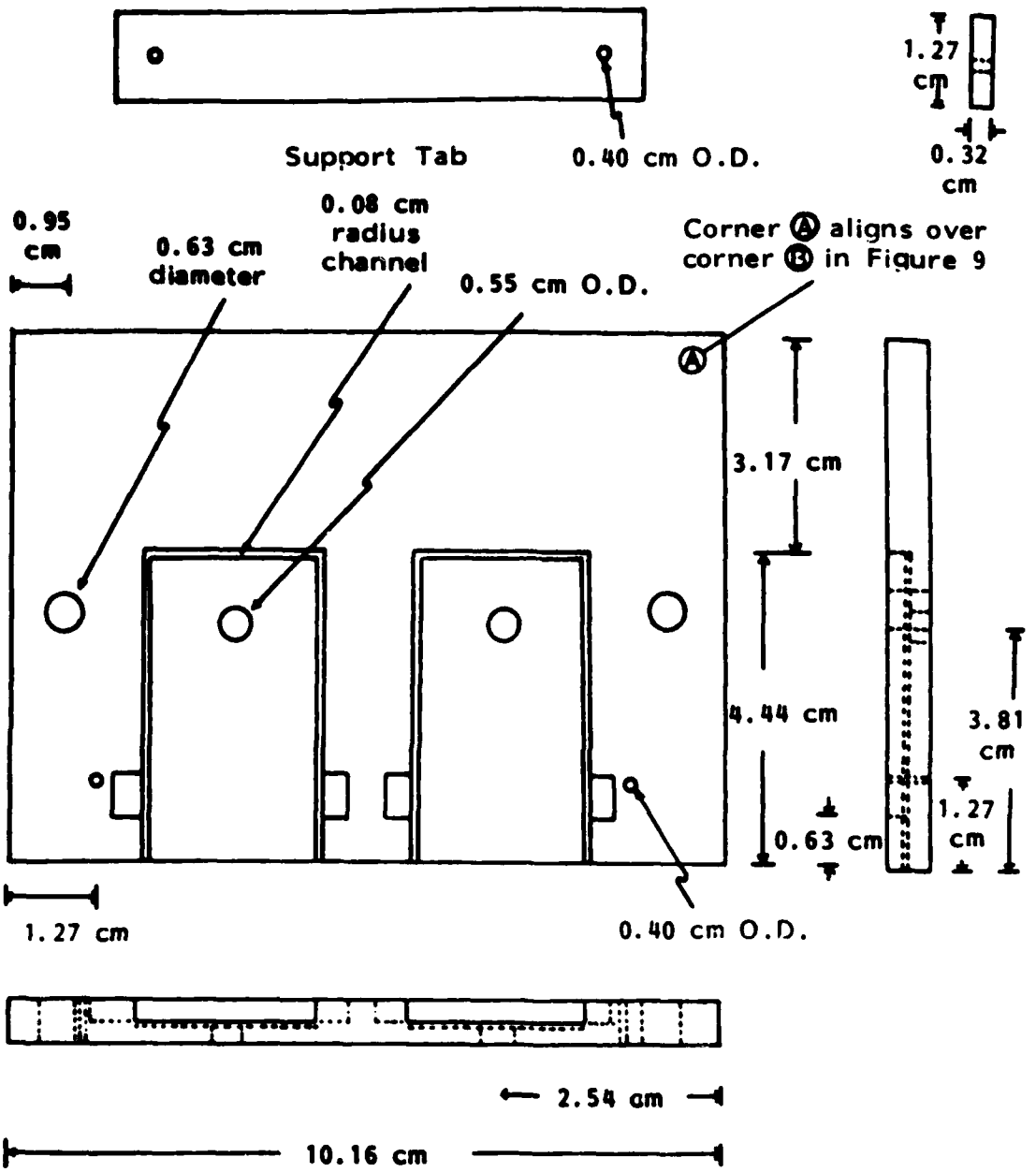


Figure 8. Schematic of Jig for Single Lap Bonding Process of Anodized Ti-6Al-4V to All Heat Resistant Adhesives Tested Except the 50% $CaCO_3$ Filled Polyimide Adhesive (Top).

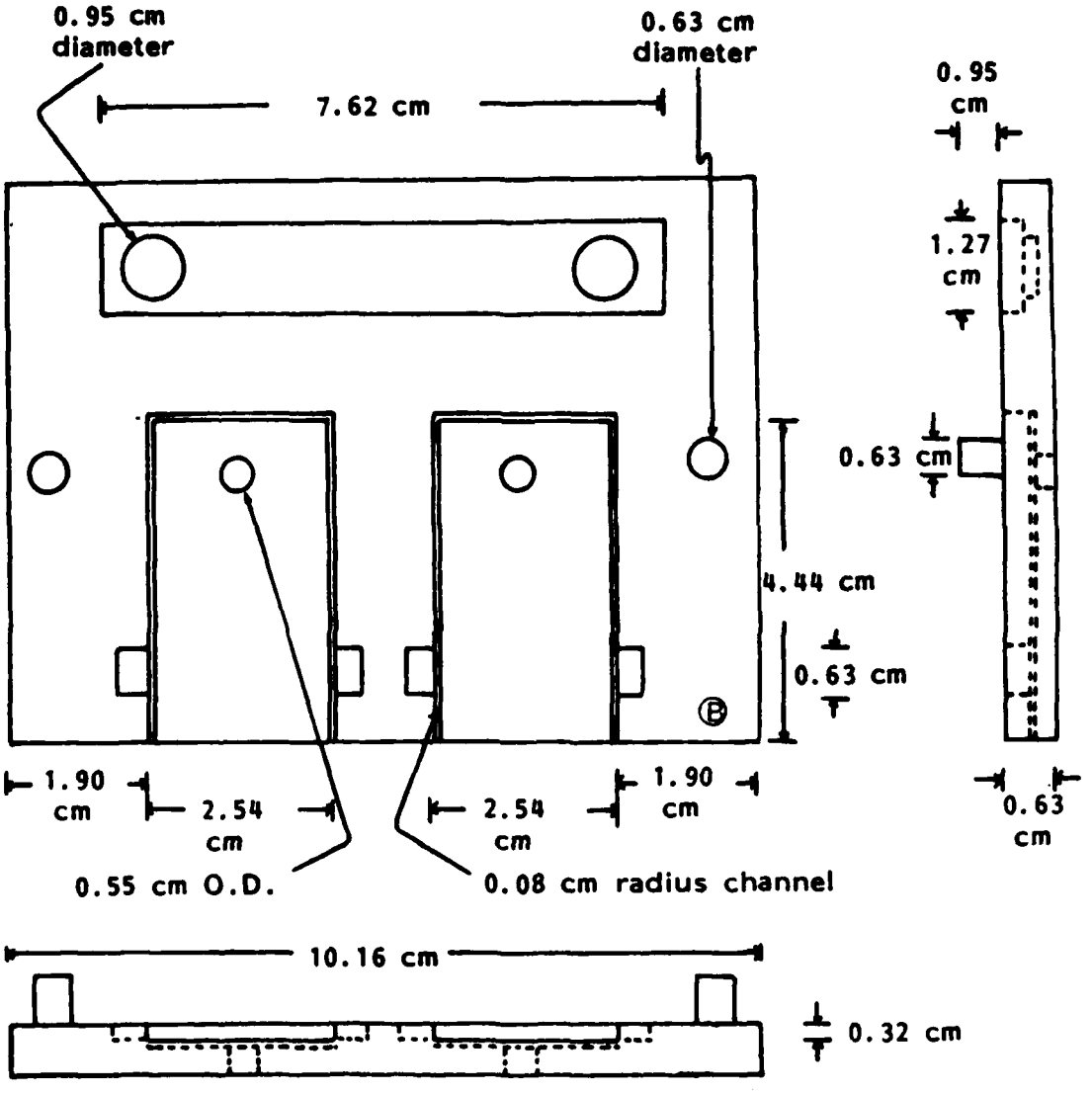


Figure 9. Schematic of Jig for Single Lap Bonding Process of Anodized Ti-6Al-4V to All Heat Resistant Adhesives Tested Except the 50% $CaCO_3$ Filled Polyimide Adhesive (Bottom).

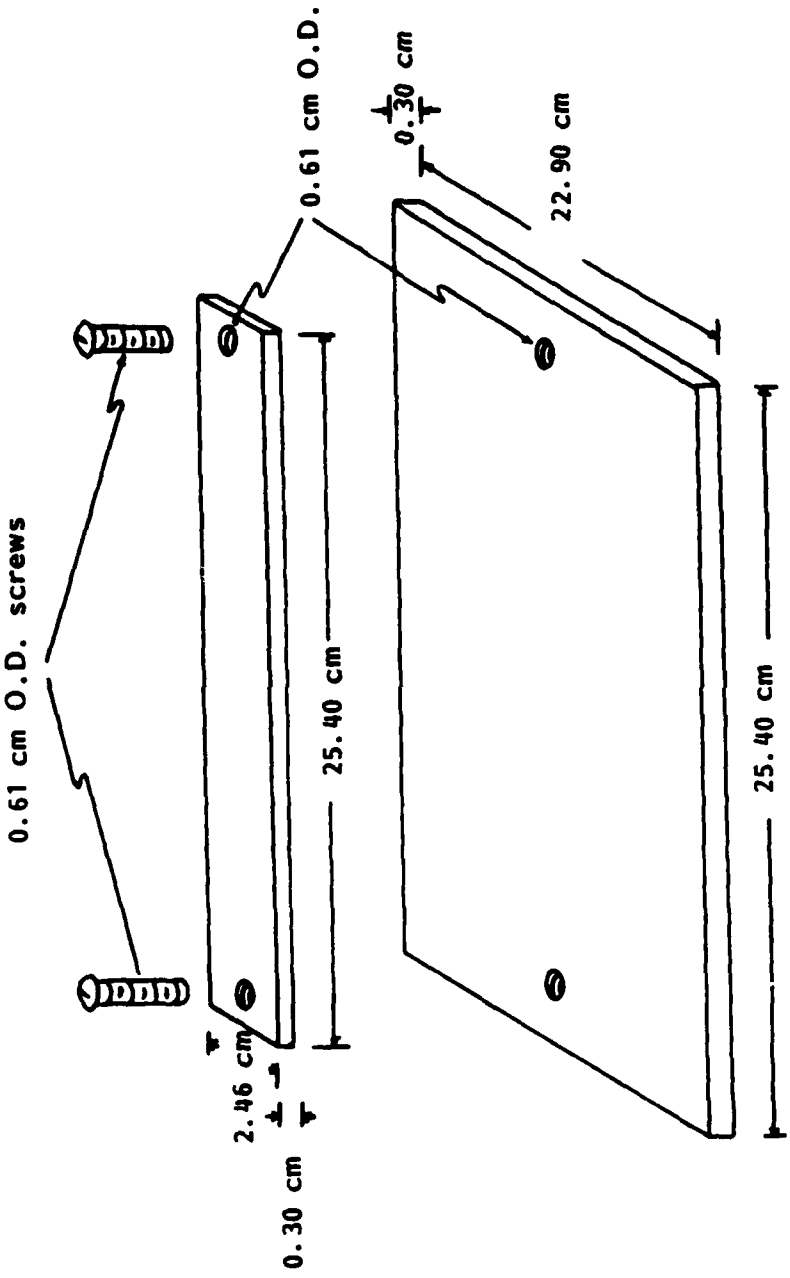


Figure 10. Schematic of Jig for Single Lap Bonding Process of Anodized Ti-6Al-4V to a 50% $CaCO_3$ Filled Polyimide Heat Resistant Adhesive.

TABLE XIII

Polyphenylquinoxaline (PPQ) Stage Dry Method to Remove Solvent From PPQ After PPQ Application to Chromic Acid Anodized Ti-6Al-4V

1. Dry PPQ coated, anodized Ti-6Al-4V coupons 30 minutes in a 373 ± 5K clean oven.
2. Dry coupons 30 minutes in a 433 ± 10K clean oven.
3. Dry coupons 30 minutes in a 473 ± 10K clean oven.

TABLE XIV

Bonding Processes for Polyphenylquinoxaline/Chromic Acid With HF Anodized Ti-6Al-4V Single Lap Bonds

Isothermal Bonding Process

1. Place stage dried PPQ/CA with HF Anodized Ti-6Al-4V coupons in bonding jig and insert jig in platen press which has been preheated to 644K. Heat jig for 3 minutes at 644K.
2. Apply 1.4 MPa at 644K and hold pressure and temperature for 5 minutes.
3. Cool jig under pressure, allowing pressure to decrease slowly as the platen press cools. At 423K, release pressure.
4. Remove jig from platen press.

Isochronal Bonding Process

1. Place stage dried PPQ/CA With HF Anodized Ti-6Al-4V coupons in vacuo at 686 mm and at 453K for 24 hours.
2. Place coupons in bonding jig and insert jig in platen press at room temperature.
3. Apply 1.4 MPa and heat to 672K over a 90 minute period.
4. Increase pressure to 41.4 MPa at 672K and hold for 1 minute.
5. Reduce pressure to 1.4 MPa at 672K and hold for 30 minutes.
6. Cool jig under pressure, allowing pressure to decrease slowly as the platen press cools. At 423K, release pressure.
7. Remove jig from platen press.

pressure was used rather than the reported literature value of 1.4 MPa. Also, a 672K bonding temperature was used rather than the 589K reported literature value. Reasons for these differences will be discussed in the Results and Discussion section.

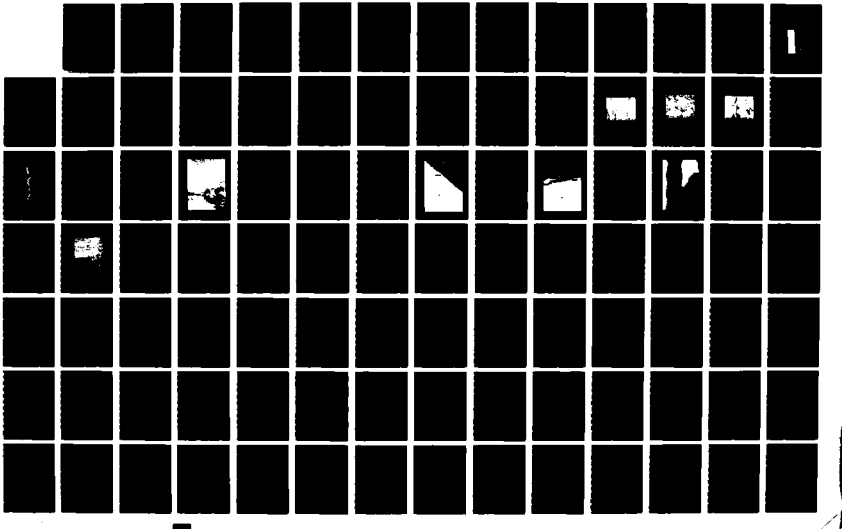
The bond configuration was controlled during bonding by positioning the PPQ/Ti-6Al-4V coupons in the aluminum alloy jig illustrated in Figures 8 and 9. The thickness of each PPQ/anodized Ti-6Al-4V coupon was measured prior to bonding. Aluminum inserts, 0.48 mm thick, were placed in the jig channels to elevate the coupons above them. As a result, the desired 0.15 ± 0.05 mm bond line thickness was obtained by the platen press pressure.

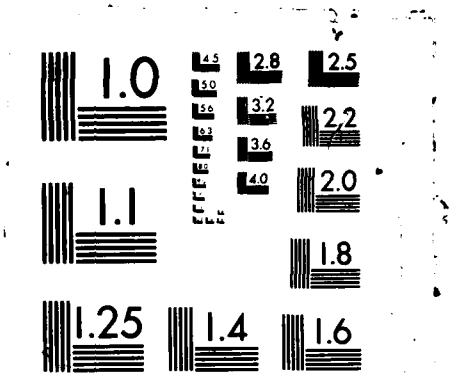
The Ablebond® 71-3, 50% $CaCO_3$ filled polyimide (PI) was also applied to the anodized Ti-6Al-4V surface by means of a micrometer-adjusted blade to allow uniform adhesive thickness. The PI was applied in a 0.35 ± 0.05 mm thickness to each anodized TI-6Al-4V coupon.

The PI/anodized Ti-6Al-4V coupons were bonded in single lap bonds within six hours of PI application. The bonds were processed in the jig illustrated in Figure 10 and per the method described in Table XV. The bonding process was per instructions from Ablestik Laboratories, manufacturers of the PI.

The Victerex® PES was bonded to anodized Ti-6Al-4V per the method described in Table XVI. The as-received PES beads were compression molded into a 0.58 ± 0.06 mm thick film and the film was then processed in the single lap bonds. Molding and

AD-A183 054 AN INTERDISCIPLINARY APPROACH TO PREDICTIVE MODELING OF 2/5
STRUCTURAL ADHESI (U) VIRGINIA TECH CENTER FOR
ADHESION SCIENCE BLACKSBURG J A SKILES ET AL JUN 87
UNCLASSIFIED CAS/CHEM-87-2 F/G 11/1 NL





MICROCOPY RESOLUTION TEST CHART
NATIONAL BUREAU OF STANDARDS-1963-A

TABLE XV

Bonding Process for Ablebond® 71-3, 50% $CaCO_3$ Filled Polyimide/ Chromic Acid With HF Anodized Ti-6Al-4V Single Lap Bonds

1. Place PI/CA with HF anodized Ti-6Al-4V coupons in bonding jig.
2. Insert jig in clean oven at 423 ± 5K. Hold temperature for 0.5 hour.
3. Increase oven temperature from 423 ± 5K to 548 ± 5K at a rate of 4K/minute.
4. Maintain oven at 548 ± 5K for 0.5 hour.
5. Turn heat off and allow jig to cool to 298 ± 5K at a cooling rate of 50K/minute.
6. Remove bonding jig from oven.

TABLE XVI

Bonding Process for Victerex® Polyethersulfone/Chromic Acid

With HF Anodized Ti-6Al-4V Single Lap Bonds

Compression Molding Method to Produce a 0.58 ± 0.06 mm Thick PES Film

1. Vacuum bake PES at 686 mm and 323K for 24 hours. Store PES in desicator until ready for use.
2. Double line two lithographic plates with Teflon 3TB, produced by R. H. Carlson. Teflon 3TB is a 0.08 mm thick glass reinforced release cloth. Use new cloth for each bonding.
3. Place 13 g of PES between the lined plates. Use 0.51 mm thick shim stock spacers to separate the plates.
4. Place plates in 575K preheated platen press. Heat for 7 minutes.
5. Apply a constant 2.1 MPa pressure to plates at 575K; maintain temperature and pressure for 5 minutes.
6. Cool PES, allowing pressure to decrease slowly as the platen press cools. At 397K, release pressure.
7. Remove compression molded PES sheet and store in desicator.

PES/CA With HF Anodized Ti-6Al-4V Bonding Method

1. Preheat platen press to 575K.
2. Place CA/HF anodized Ti-6Al-4V coupons and 25.4 mm^2 of the compression molded film in the bonding jig.
3. Preheat jig in the 575K preheated platen press for 7 minutes.
4. Apply 3.4 MPa pressure to jig at 575K for 5 minutes.
5. Cool under pressure. Maintain the 3.4 MPa pressure as temperature decreases from 575K to 555K. Then allow the pressure to decrease slowly as the platen press cools. At a temperature $\leq$ 422K, release pressure and remove bonds.

processing methods were devised by the author, based upon communication with ICI personnel.

Table XVII describes the single lap bonding process for CA/HF anodized Ti-6Al-4V bonded to either Ultem® 1000 unfilled polyetherimide (PEI) or Ultem® 2200, 20% glass filled polyetherimide (PEIF). The as-received polymer PEI or PEIF beads were compression molded into a film and the film was then processed in the single lap bonds. PEI and PEIF bonding methods were devised by the author, based upon communications with General Electric personnel.

Table XVIII describes the single lap bonding process for chromic acid anodized Ti-6Al-4V bonded to the Udel® polysulfone. The bonding process was used for single lap bonding of chromic acid with HF anodized Ti-6Al-4V and also for chromic acid anodized Ti-6Al-4V. Processing methods were per private communication with Professor Thomas Ward, Department of Chemistry, Virginia Polytechnic Institute and State University.

5. Single Lap Bond Thermal Aging Conditions

a. Polysulfone Bonds

Udel® polysulfone (PS)/CA with HF anodized Ti-6Al-4V single lap bonds were subjected to unstressed thermal aging before testing. The Ti-6Al-4V CA/HF anodization procedure was per method #5 in Table VI: 30 ± 2 A/m^2 initial current density, 10 volts, 298 ± 2K anodization solution temperature, 20 minute

TABLE XVII

Single Lap Bonding Process for Chromic Acid With HF Anodized Ti-6Al-4V Bonded to Either Ultem® 1000 Polyetherimide (PEI) or to Ultem® 2200, 20% Glass Filled Polyetherimide (PEIF)

Compression Molding Method to Produce a 0.84 ± 0.06 mm Thick PEI Film or PEIF Film

1. Vacuum bake PEI or PEIF as-received beads for 40 hours at 323K at 686 mm of Hg. Store PEI in desicator until ready for use.

2. Double line two lithographic plates with Teflon 3TB produced by R. H. Carlson. Teflon 3TB is a 0.08 mm thick glass reinforced Teflon release cloth. Use new cloth for each bonding.

3. Place 13 g of either PEI or PEIF between the lined plates. Use 0.51 mm thick shim stock spacers to separate plates.

4. Place plates in a 575K preheated platen press for 7 minutes.

5. If compression molding PEI films, apply 2.1 MPa constant pressure at 575K to PEI for 5 minutes. Cool PEI, allowing pressure to decrease slowly as the platen press cools. At a temperature $\leq$ 422K, release pressure and remove molded films.

6. If compression molding PEIF films, apply 4.1 MPa constant pressure at 575K to PEIF for 5 minutes. Cool PEIF, allowing pressure to decrease slowly as the platen press cools. At a temperature $\leq$ 422K, release pressure and remove molded films.

TABLE XVII (Continued)

PEI or PEIF/Chromic Acid With HF Anodized Ti-6Al-4V Bonding Process

1. Preheat platen press to 575K.
2. Place CA/HF anodized Ti-6Al-4V and 25.4 mm^2 of the compression molded PEI or PEIF film in the bonding jig.
3. Preheat jig in the 575K preheated platen press for 7 minutes.
4. Apply 3.4 MPa pressure to jig at 575K for 5 minutes.
5. Cool under pressure. Maintain 3.4 MPa pressure as temperature decreases from 575K to 555K. Then allow the pressure to decrease slowly as the platen cools. At a temperature $\leq$ 422K, release pressure and remove bonds.

TABLE XVIII

Bonding Process for Udel® Polysulfone (PS)/

Anodized Ti-6Al-4V Single Lap Bonds

Compression Molding Method to Produce
a 0.50 ± 0.06 mm Thick PS Film

1. Vacuum bake the polysulfone at 686 mm and 378K for 24 hours.
2. Place approximately 15 grams of polysulfone in center of two clean 20 cm^2 lithograph plates.
3. Position 0.51 mm thick brass shims at each corner of the lithograph plate to control polysulfone sheet thickness.
4. Preheat lithograph plates in platen press to 505K for 2 minutes.
5. Apply 137.9 MPa for 10 minutes at 505 - 516K.
6. Cool down under pressure, allowing pressure to gradually decrease as platen press cools
7. At ≤463K, release pressure and remove adhesive film.

Polysulfone/Anodized Ti-6Al-4V Bond Procedure

1. Place anodized Ti-6Al-4V coupons and 25.4 mm^2 of the compression molded PS film in the bonding jig.
2. Preheat jig in platen press to 561K for 2 minutes.
3. Pressurize at 137.9 MPa for 10 minutes at 561K.
4. Cool down under pressure, allowing pressure to gradually decrease as platen press cools.
5. At ≤463K, release pressure and remove bonds.

anodization time in a 5% chromic acid anodization solution with hydrofluoric acid added to control the initial current density. In general, six bonds were subjected to each thermal condition. The thermal aging conditions tested were:

(1) 0.5 month at 298 ± 5K in a 65 to 80% relative humidity (R.H.) environment, or

(2) 2 months at 298 ± 5K in a 65 to 80% R.H. environment, or

(3) 9 months at 298 ± 5K in a 65 to 80% R.H. environment, or

(4) 9 months at 373 ± 5K, followed by 2 months at 298 ± 5K in a 65 to 80% R.H. environment

(5) 9 months at 443 ± 5K, followed by 2 months at 298 ± 5K in a 65 to 80% R.H. environment.

Also, bond strengths were determined as a function of CA anodization parameters, as described earlier in Table VI. Bond strengths were determined for CA/HF anodization methods #1 - 7 and for CA anodization method #1 described in Table VI. These bonds were subjected to unstressed thermal aging at 298 ± 5K for ≤ 0.5 month before testing.

b. Polyimide Bonds

Ablebond® 71-3, 50% $CaCO_3$ filled polyimide(PI)/CA with HF anodized Ti-6Al-4V single lap bonds were subjected to each of the following unstressed thermal aging conditions before testing:

(1) 0.5 month at 298 ± 5K in a 65 to 80% R.H. environment, or

(2) 9 months at 443 ± 5K, followed by 2 months at 298 ± 5K in a 65 to 80% R.H. environment.

Six bonds were subjected to each of these thermal aging conditions. The CA/HF anodization procedure was per method #3 in Table VI: 20 ± 2 A/m² initial current density, 10 volts, 20 minutes anodization time at 283 ± 2K and a 5% CA anodization solution with HF.

c. Polyphenylquinoxaline Bonds

Polyphenylquinoxaline(PPQ)/unprimed CA with HF anodized Ti-6Al-4V single lap bonds were subjected to each of the unstressed thermal aging conditions before testing described as follows:

(1) 0.5 month at 298 ± 5K in a 65 to 80% R.H. environment, or

(2) 11 months at 298 ± 5K in a 65 to 80% R.H. environment, or

(3) 9 months at 443 ± 5K, followed by 2 months at 298 ± 5K in a 65 to 80% R.H. environment, or

(4) 9 months at 505± 10K, air quenched to 298 ± 5K 7X during the 9 month test, followed by aging 2 months at 298 ± 5K in a 65 to 80% R.H. environment.

In addition, Lica® 44 primed, CA/HF anodized Ti-6Al-4V/PPQ bonds were subjected to thermal aging condition #3. For all these

unprimed and primed bonds, the Ti-6Al-4V coupons were CA/HF anodized per method #3 described in Table VI. And the bonds were isothermally processed as described in Table XIV.

Isochronally processed single lap bonds, with unprimed, anodized Ti-6Al-4V, were thermally aged per condition #1 before testing. The Ti-6Al-4V coupons were also anodized per method #3 described in Table VI. The isochronal bonding process is described in Table XIV.

Also, isothermally processed PPQ bonds were tested as a function of CA/HF anodization methods #2, #3 and #5 as described in Table VI. These isothermally processed bonds were subjected to thermal aging condition #1 before testing.

In general, six bonds were tested for each of the above described anodized Ti-6Al-4V/PPQ single lap bond thermal aging tests.

d. Polyethersulfone Bonds

Victerex® polyethersulfone (PES)/CA with HF anodized Ti-6Al-4V single lap bonds were subjected to each of the unstressed thermal aging conditions before testing:

(1) 0.5 month at 298 ± 5K in a 65 to 80% R.H. environment, or

(2) 9 months at 443 ± 5K, followed by 2 months at 298 ± 5K in a 65 to 80% R.H. environment.

In addition, Lica® 44 primed, CA/HF anodized Ti-6Al-4V/PES bonds were subjected to thermal aging condition #2.

Six bonds were subjected to each thermal aging condition. The CA/HF Ti-6Al-4V anodization procedure was per method #3 described in Table VI.

e. Polyetherimide Bonds

Ultem® 1000 polyetherimide (PEI)/CA with HF anodized Ti-6Al-4V single lap bonds were subjected to each of the following unstressed thermal aging conditions before testing:

(1) 0.5 month at 298 ± 5K in a 65 to 80% R.H. environment, or

(2) 9 months at 443 ± 5K, followed by 2 months at 298 ± 5K in a 65 to 80% R.H. environment.

In addition, Lica® 44 primed, CA/HF anodized Ti-6Al-4V/PEI bonds were subjected to thermal aging condition #2.

Ultem® 2200, 20% glass filled polyetherimide (PEIF)/ CA with HF anodized Ti-6Al-4V single lap bonds were also subjected to each of the above described thermal aging conditions. Lica® 44 primed, CA/HF anodized Ti-6Al-4V/PEIF bonds were subjected to thermal aging condition #2.

Six bonds were subjected to each thermal aging condition. The CA/HF Ti-6Al-4V anodization procedure used for these primed and unprimed bonds was method #3 described in Table VI.

6. Single Lap Bond Adhesive Thickness Measurement Methods

The single lap bond adhesive bond thickness was nondestructively measured in situ. A Unitron Metallograph

microscope with a camera attachment was used to photograph the adhesive bond line. The bond thickness was measured for each of the six types of heat resistant adhesives used in this study.

For each single lap bond selected, the adhesive bond line thickness was measured over the entire 12.7 mm long bond overlap region. The side of each measured bond was polished to remove polymer flash; this facilitated focusing during photography. Representative bond line areas were photographed at a magnification of either 100X or 50X. Figure 11 is a representative side view photograph of a bond used for adhesive thickness measurements. A scale, with 10 μm/division, was photographed at 100X and used to measure adhesive bond thickness. Accuracy of the adhesive bond thickness measurement from this type of scale photograph was 10 μm. The adhesive bond thickness varied by as much as 50 μm for any one bond examined.

Adhesive bond thickness data are described in Table XIX. These data are representative of each type of heat resistant adhesive bonded to either CA or CA with HF anodized Ti-6Al-4V single lap bonds included in this study.

7. Single Lap Bond Test Method

Each single lap bond joint was tested in tension per ASTM D1002 entitled: "Strength Properties of Adhesives in Shear by Tension Loading (Metal-to-Metal)." The bonds were tested in tension using an Instron Test Machine.



Figure 11. Side View Photograph of Single Lap Bond Used for Adhesive Thickness Measurement (100X).

TABLE XIX

Adhesive Bond Thickness Measured In Situ for

Anodized Ti-6Al-4V Single Lap Bonds

Adhesive	Adhesive Bond Line Thickness μm ± 50 μm
Polyphenylquinoxaline	160
Ablebond® 71-3, 50% glass filled polyimide	360
Udel® polysulfone	370
Victerex® polyethersulfone	580
Ultem® 1000 polyetherimide	530
Ultem® 2200 20% glass filled polyetherimide	710

The Instron machine was equipped with a universal joint on the crosshead. The universal joint permits alignment of the single lap bond joint with the applied tensile load, thereby reducing stresses in the single lap bond induced by the testing machine design. Measurements were made at 298 ± 5K in a 65 to 80% R.H. environment.

8. Single Lap Bond Strength Statistical Analyses Methods

In general, six single lap bond joints were tested for each anodization processing variable, adhesive, or bond thermal aging condition studied. The t test statistical analysis was used to determine if any one anodization variable, or aging condition tested significantly affected bond strength. Any two groups of data may be compared by using the t test. The t test determines whether or not the sample mean of any one group of single lap bond strength data and the mean of another group of single lap bond strength data come from the same population. The formulas involved in calculating the t statistic are described in Appendix II. In this study, a confidence level of 99% was applied to the t values obtained to compare the two groups of data.

It was also desired to compare the single lap bond strengths of all polymers tested under identical thermal aging conditions. Because more than 2 groups of data were being compared, it was necessary to employ another statistical treatment called the One Way Analysis of Variance. This test is more commonly known as the F

test. The F test examines 3 or more groups of data to determine whether or not all of the groups come from the same population. The formulas involved in calculating the F statistic are described in Appendix III. A 99% confidence level was used.

9. Photography of the Single Lap Bond Fracture Process

The single lap bond fracture process was documented by photographic analyses. The bond overlap region was photographed at 5 frames/second during ASTM D1002 single lap bond testing. A schematic of the photographic set-up used is shown in Figure 12. A 35 mm Nikon camera with motor drive was used for the photography.

10. Qualitative Image Analysis (QIA) Methods

Grey image analyses of a CA/HF anodized Ti-6Al-4V surface was conducted. Also, analyses of typical fracture surfaces for PS/CA with HF anodized Ti-6Al-4V single lap bonds and for PPQ/CA with HF anodized Ti-6Al-4V single lap bonds were conducted. The analyses were conducted to determine, whenever appropriate, the surface area of anodic oxide, bare metal and polymer present on the surface of interest.

An Image Processing System from Kontron, a subsidiary of Carl Zeiss, Inc. was used with a visible light source. The reflected light from each surface was digitalized according to discrete grey levels, which ranged from 0 to 256, for video display or storage in computer memory. There were 512 X 512 pixel points

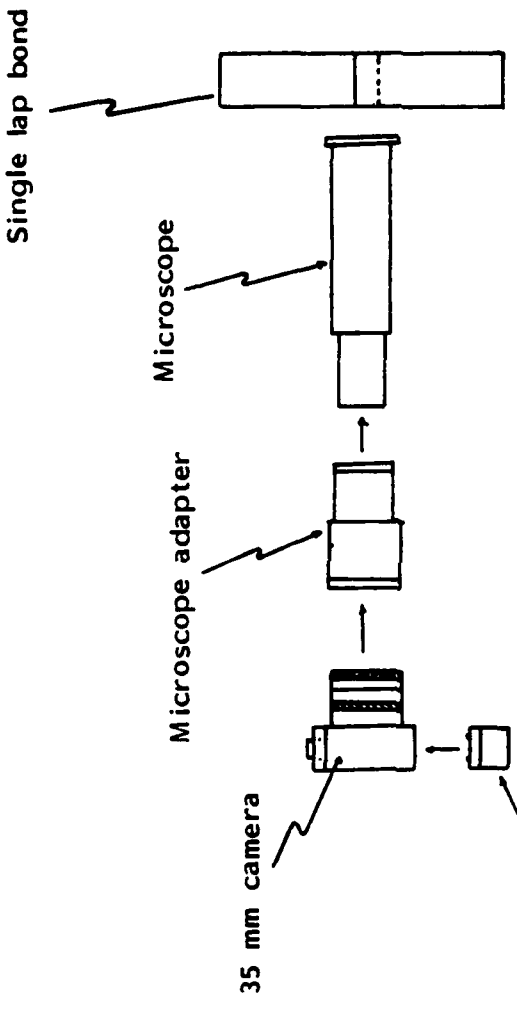


Figure 12. Schematic of Set-up Used to Photograph Single Lap Bond Fracture Process.

for resolution of the video signal and of the image stored in memory. Analyses of the entire fracture surface area was conducted using an automatic scanning mount.

Interactive image analysis, or object identification and contour tracing, was required to differentiate various regions on the fracture surface. Interactive analysis was required because the irregular surface contours on the fracture surface altered the surface reflectivity and differentiation of surfaces on the sole basis of reflectivity was not possible.

Automatic image analysis was used for the anodized Ti-6Al-4V to detect any unanodized regions. This type of analysis, based solely on surface reflectivity, was more time efficient than interactive analysis, and was possible because the unanodized and anodized metal surfaces were relatively smooth.

11. Scanning Electron Microscopy

An AMR 900, 21 kV scanning electron microscope (SEM) was used to characterize the single lap bond fracture surfaces. This analysis was conducted to determine the fracture initiation site and also to characterize the polymer deformation on the fracture surface. The bond overlap and adhesive fillet of he single lap bond fracture surface were examined by SEM. Single lap bond fracture surfaces were examined for:

(1) each Ti-6Al-4V anodization method described in Table VI and tested in a single lap bond;

(2) each of the six types of heat resistant adhesive tested in a single lap bond after 0.5 month thermal aging at 298 ± 5K in a 65 to 80% R.H. environment;

(3) polysulfone/CA with HF anodized Ti-6Al-4V bonds after a) thermal aging at 443 ± 5K for 9 months, followed by 2 months at 298 ± 5K in a 65 to 80% R.H. environment, and b) 9 months at 298 ± 5K in a 65 to 80% R.H. environment;

(4) polyphenylquinoxaline/CA with HF anodized Ti-6Al-4V bonds thermally aged at 443 ± 5K for 9 months, followed by 2 months at 298 ± 5K in a 65 to 80% R.H. environment before testing, for both unprimed and Lica® 44 primed anodized Ti-6Al-4V;

(5) polyphenylquinoxaline/CA with HF anodized Ti-6Al-4V bonds thermally aged 11 months at 298 ± 5K in a 65 to 80% R.H. environment before testing; and,

(6) PPQ/CA with HF anodized Ti-6Al-4V bonds processed per isochronal methods or isothermal methods and aged 0.5 month at 298 ± 5K in a 65 to 80% R.H. environment.

Because of the limited size of the SEM sample chamber, the length of the Ti-6Al-4V coupon was sheared to 2.54 cm after the bond was fractured. The shear zone was outside of the bond overlap and adhesive fillet region to prevent the shearing process from affecting those areas under SEM examination. The fracture surface bond overlap and adhesive fillet region were gold coated

prior to SEM analyses to prevent surface charging during SEM analysis.

A JEOL JSM-36C SEM was used to characterize the following samples:

(1) Ti-6Al-4V after preanodization treatment #1; and,

(2) Ti-6Al-4V after preanodization treatment #1 and CA/HF anodization method #5 described in Table VI.

A 9.5 mm diameter sample, which was punched from each of the titanium alloy coupons and then gold coated, was used in these analyses.

12. Electron Spectroscopy for Chemical Analysis (ESCA)

ESCA surface analysis was conducted using either a Physical Electronics 550 ESCA spectrometer or a Perkin Elmer 5300 ESCA spectrometer at 15 kV. A magnesium X-ray source was used in both spectrometers.

ESCA narrow scan analyses were conducted to determine elements present in the $\leq$ 10 nm of the surface examined, and is sensitive to $\geq$ 1% surface concentration of the element. ESCA multiplex analyses were subsequently conducted to quantify element concentrations and to determine each element binding energy. A 285.0 eV carbon binding energy was used as a reference standard for carbon; ESCA multiplex time was 5 minutes/element.

The spectrometer work function was determined for each sample analyzed. The spectrometer work function is the adjustment

to the measured carbon binding energy necessary for it to equal the 285.0 eV carbon binding energy reference. All subsequent element binding energy values measured in the analyses were then adjusted by this work function.

ESCA surface analyses were conducted for the following samples:

(1) each type of heat resistant polymer adhesive;

(2) Ti-6Al-4V after preanodization treatment #1, and preanodization treatment #2;

(3) anodized Ti-6Al-4V; and,

(4) fracture surfaces of anodized Ti-6Al-4V/heat resistant adhesives which exhibited an apparent adhesive type failure. An apparent adhesive type failure can be defined as either polymer to anodic oxide or anodic oxide to Ti-6Al-4V substrate interphase failure.

A 9.5 mm diameter was punched from the titanium alloy coupons examined by ESCA analyses. For the adhesives, the polymer sample was approximately 4 mm^2. The surface area analyzed by ESCA was approximately 4 mm X 8 mm.

13. Auger Electron Spectroscopy

Auger survey, Auger mapping analyses and SEM micrographs of the Auger mapped areas for fractured bond surfaces were obtained from a Perkin-Elmer Phi 610 Scanning Auger Microprobe. For the Auger survey, a 3.00 kV beam voltage and 0.100 μA

current was used. For the Auger mapping analyses, a 3.00 kV beam voltage and 5 nA current was used to reduce the sample charging effect.

Fracture surfaces analyzed were for CA/HF anodized Ti-6Al-4V/PPQ bonds processed by the isochronal and the isothermal bonding methods.

Auger survey analyses provides element identification for elements present within 10 nm of the surface. Element sensitivity is $\geq$ 1%. High resolution is possible with a small electron beam diameter of approximately 1.5×10^{-6} m.

Auger mapping analysis provides a highly sensitive and resolved method as described above to qualitatively identify the distribution of elements on the sample surface as the beam is rastered across the surface examined. The electron beam raster area was approximately 0.15 cm X 0.15 cm. Auger mapped areas were documented by SEM micrographs.

IV. RESULTS AND DISCUSSION

A. Anodized Ti-6Al-4V Oxide Characterization

1. Oxide Morphology

a. Scanning Electron Microscopy (SEM) Micrographs

Figure 13 is a SEM micrograph of the Ti-6Al-4V surface after preanodization treatment #1 (bead blast, alkaline clean and pickle). The micrograph reveals a nonuniform surface topography.

Figures 14 and 15 are SEM micrographs of Ti-6Al-4V after the preanodization treatment #1 and CA/HF anodization (30 ± 2 A/m^2, 298 ± 2K, 20 minutes, 10 V) of the Ti-6Al-4V surface. Irregularly shaped and nonuniformly distributed structures, which are approximately 2 μm wide and 3 μm long, are apparent on the CA/HF anodized surfaces. These structures have been observed by Hendricks[48] for both phosphoric acid and for CA/HF anodized Ti-6Al-4V. Hendricks referred to these structures as etch pits. It is the opinion of the author of this dissertation that these pits may be the result of: 1) nonuniform etching of the Ti-6Al-4V surface during the preanodization and/or anodization process, 2) oxide cracking during anodization, and/or 3) nonuniform anodization, or even unanodized regions, on the Ti-6Al-4V surface.

The extent to which the inside of the etch pit was anodized could not be determined from the SEM micrographs. It is possible that small breaks in the anodic oxide in the etch pits may exist and

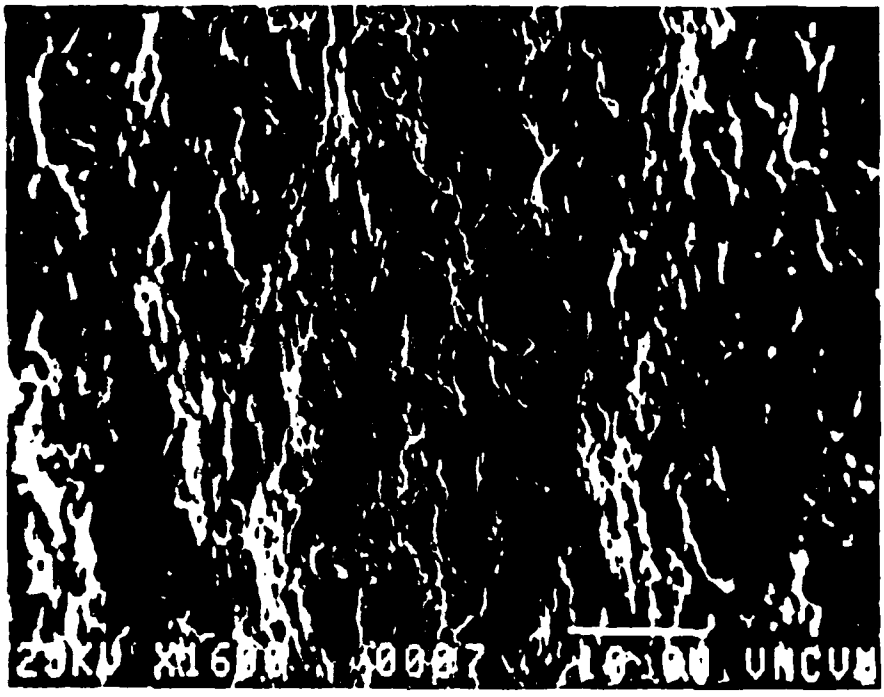


Figure 13. Scanning Electron Micrograph of the Ti-6Al-4V Surface After Preanodization Treatment #1 (1600X).



Figure 14. Scanning Electron Micrograph of the Ti-6Al-4V Surface After Preanodization Treatment #1 and CA/HF Anodization (3200X).



Figure 15. Scanning Electron Micrograph of the Ti-6Al-4V Surface After Preanodization Treatment #1 and CA/HF Anodization (10,000X).

can be visualized as shown in Figure 16.

b. Transmission Electron Microscopy (TEM) Micrographs

Ti-6Al-4V anodic oxide morphology was characterized at Structure Probe by means of thin-section Transmission Electron Microscopy (TEM). Oxides produced by two anodization processes, which differed in solution temperature, were examined. The two solution temperatures examined were 283 ± 2K and 298 ± 2K. The anodization conditions held constant were as follows: 20 minute anodization time, 10 volt potential, and a 5% chromic acid solution with HF added to obtain a 20 ± 2 A/m^2 initial current density.

Figures 17 and 18 are TEM parallel sections of the two oxides examined. The anodic oxide pore diameter and wall thickness were not affected by the choice of either a 283 ± 2K or a 298 ± 2K anodization solution temperature. For both oxides, pore diameters of 30 nm with a 10 nm wall thickness were measured.

Table XX is a comparative analysis of oxide morphology data reported here with work reported by Cheng.[42] Cheng[42] reported a 10 nm to 30 nm pore diameter with a 10 nm wall thickness using STEM. When the oxide was produced by CA/HF of Ti-6Al-4V at 10 V and at a 17 - 27 A/m^2 current density. His results are in good agreement with TEM oxide pore morphology reported here for 20 A/m^2 at either 283 or 298K.

Data in Table XX indicates that a 44K increase in anodization temperature, from 283K to 327K, coupled with a 2.7X increase in

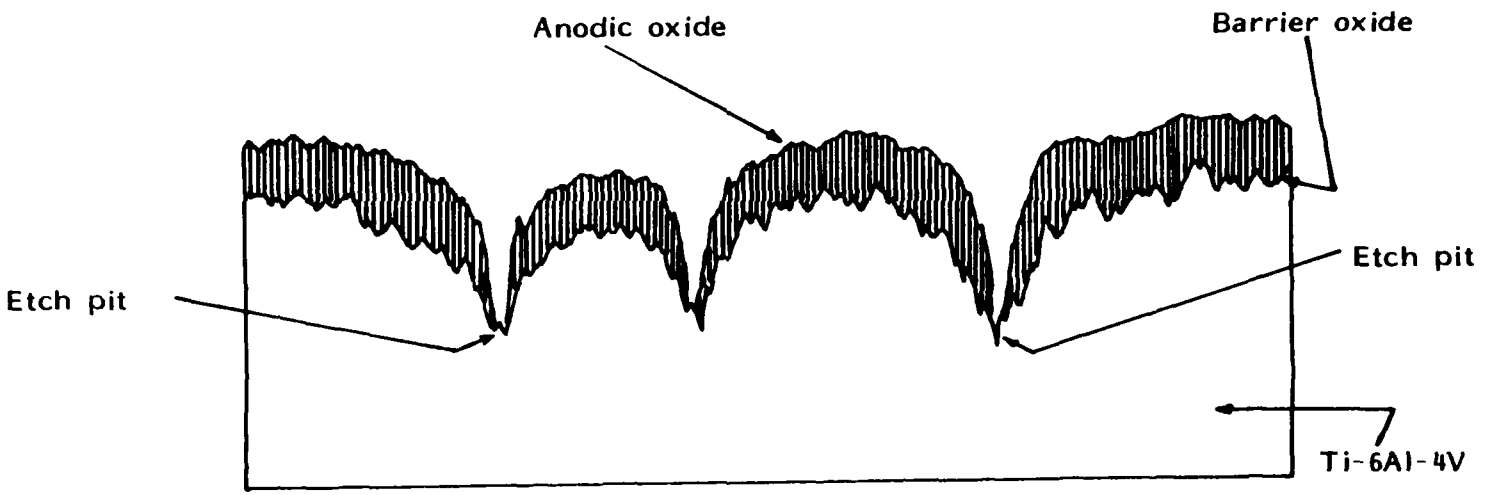


Figure 16. Proposed Model of the Interior of an Etch Pit on a CA/HF Anodized Ti-6Al-4V Surface.

Figure 17. Transmission Electron Micrograph of a Parallel Section of an Anodic Oxide Produced by 20 Minute CA/HF Anodization at: 283 ± 2K, 20 ± 2 A/m^2 Initial Current Density, and 10 Volts (200,000X).

Figure 18. Transmission Electron Micrograph of a Parallel Section of an Anodic Oxide Produced by 20 Minute CA/HF Anodization at: 298 ± 2K, 20 ± 2 A/m^2 Initial Current Density, and 10 Volts (200,000X).



TABLE XX

Comparative Analysis of CA/HF Anodized Ti-6Al-4V

Oxide Morphology Characteristics

Reference	Anodization Solution Temperature (°K)	Anodization Current Density A/m²	Potential (Volts)	Time (Minutes)	Oxide Pore Diameter (nm)	Oxide Wall Thickness (nm)
Cheng[42]	298	17 - 27	10	20	10 - 30	10
Cheng[42]	327	54	10	20	63 - 114	20
Skiles	283	20	10	20	30 - 40	10
Skiles	298	20	10	20	25 - 30	10

the current density, from 20 to 54 A/m^2, affected pore morphology. Oxide pore diameter increased by a factor of 2 to 4 when both the anodization temperature and the current density were increased as such.

Figures 19 and 20 are TEM micrographs of the two oxides examined in cross section. For both oxides examined, the oxide follows the metal substrate contours, and oxide roughness is approximately 170 nm.

Figures 21 and 22 are higher magnification TEM micrographs of the two oxides examined in cross section. The regular, columnar pore structure for both oxides examined is more evident. A thin barrier anodic oxide, or oxide boundary layer, which is approximately 15 nm thick, is apparent at the oxide base.

2. Proposed Model for the CA/HF Anodized Ti-6Al-4V/Adhesive Bond Based upon Anodic Oxide Morphology

Figure 23 illustrates an adhesion model of a CA/HF anodized Ti-6Al-4V/adhesive bond, based upon the TEM micrographs of the oxide. These regular, columnar pores are considered to be beneficial to adhesive-oxide mechanical interlock, or, to provide more surface area for van der Waals bonds to thermoplastics.

The interphase region, as proposed by Sharpe,[49] is proposed to best describe the boundary conditions between bulk metal and this metal oxide, as well as between the metal oxide and polymer. These interphase regions are also shown in Figure 23. The interphase region is a gradual transition region rather than a

Figure 19. Transmission Electron Micrograph of a Cross Section of an Anodic Oxide Produced by 20 Minute CA/HF Anodization at: 283 ± 2K, 20 ± 2 A/m² Initial Current Density, and 10 Volts (30,000X)

[A] Epoxy Mount

[B] Gold Deposit

[C] Oxide

[D] Ti-6Al-4V Substrate

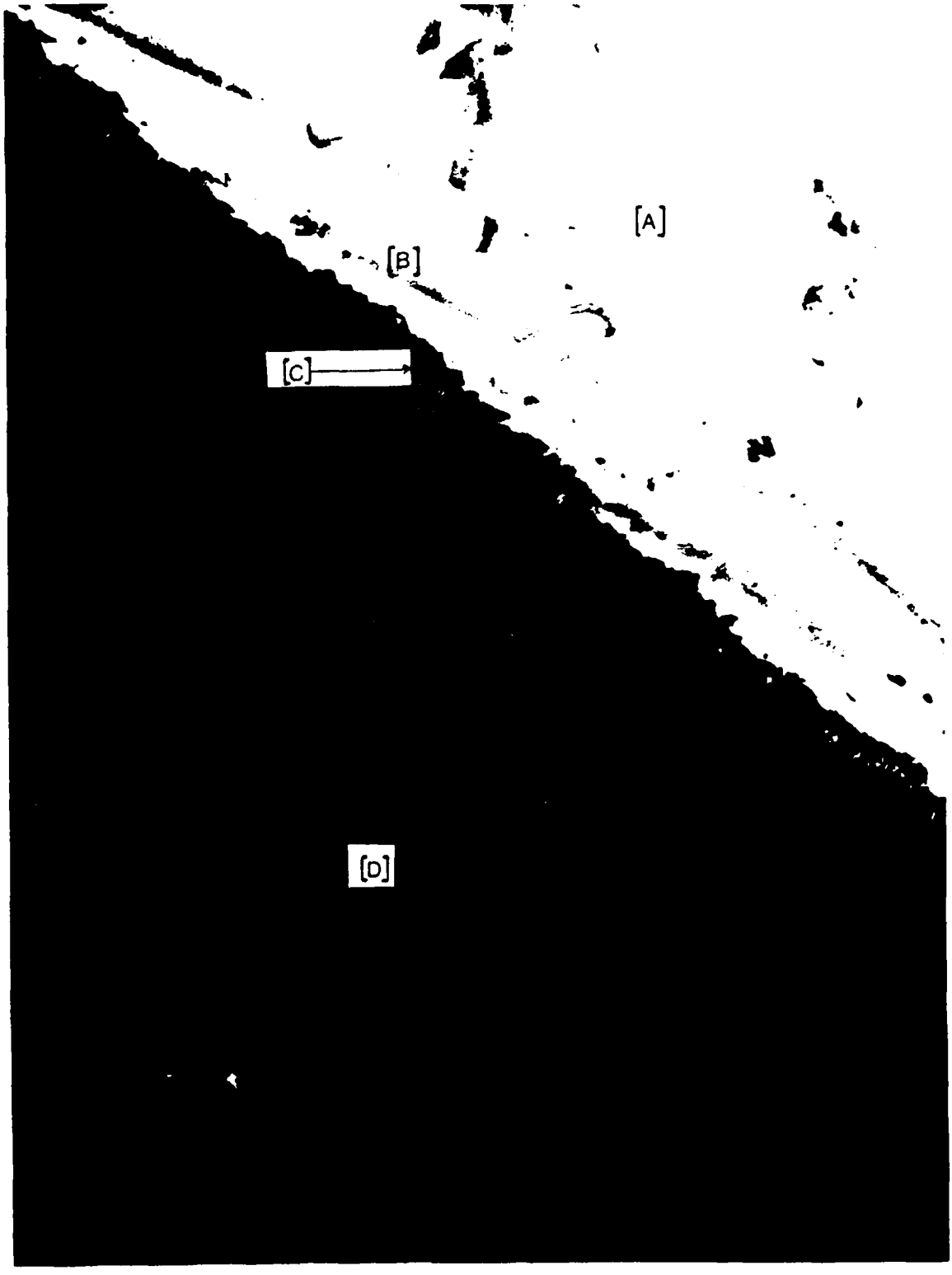

[A]
[B]
[C]
[D]

Figure 20. Transmission Electron Micrograph of a Cross Section of an Anodic Oxide Produced by 20 Minute CA/HF Anodization at: 298 ± 2K, 20 ± 2 A/m² Initial Current Density, and 10 Volts (30,000X)

[A] Epoxy Mount

[B] Gold Deposit

[C] Oxide

[D] Ti-6Al-4V Substrate

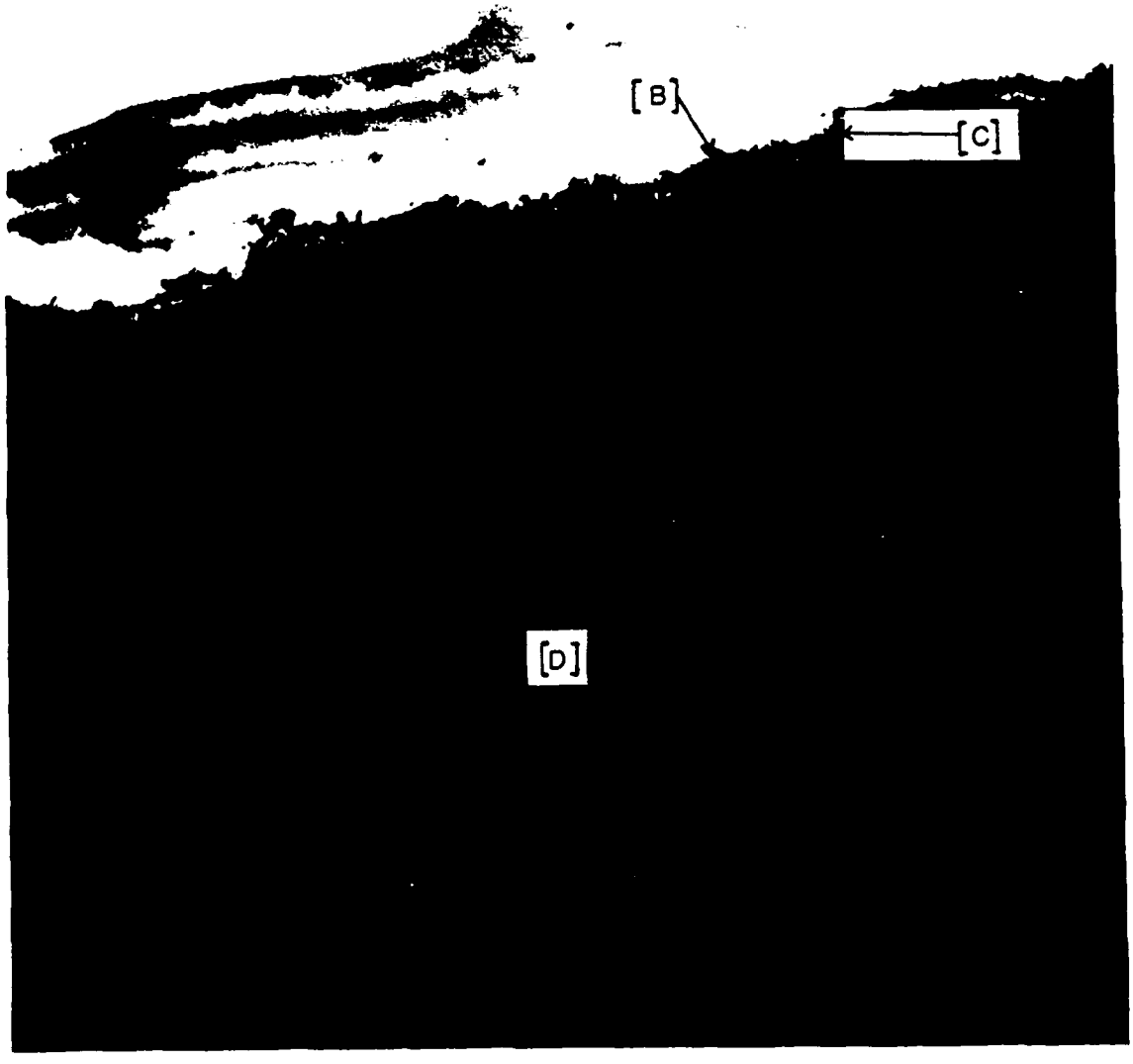

[A]
[B]
[C]
[D]

Figure 21. Transmission Electron Micrograph of a Cross Section of an Anodic Oxide Produced by 20 Minute CA/HF Anodization at: 283 ± 2K, 20 ± 2 A/m² Initial Current Density, and 10 Volts (200,000X)

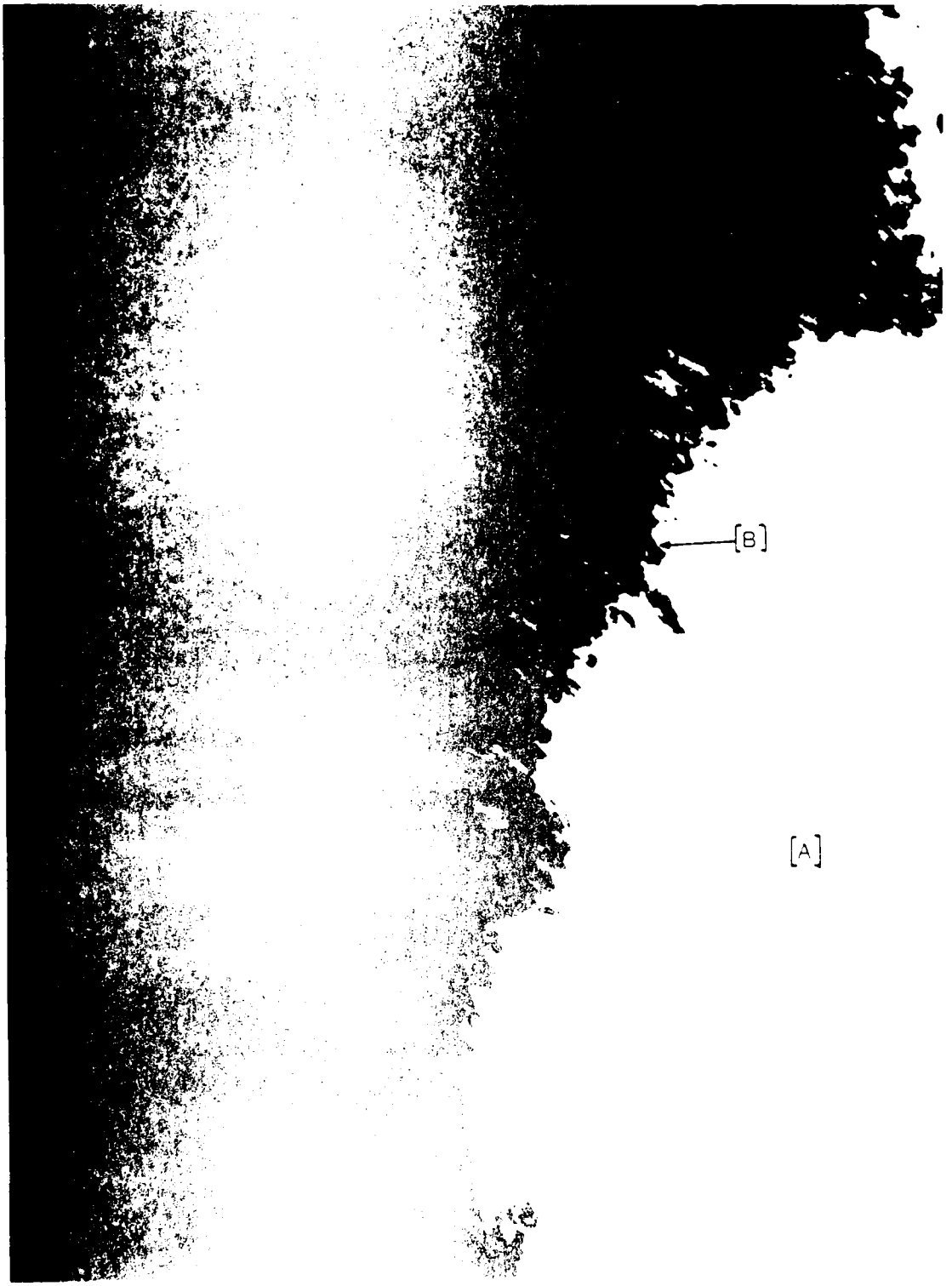
[A] Epoxy Mount

[B] Gold Deposit

[C] Oxide

[D] Oxide Boundary Layer

[E] Ti-6Al-4V Substrate


[B]
[A]

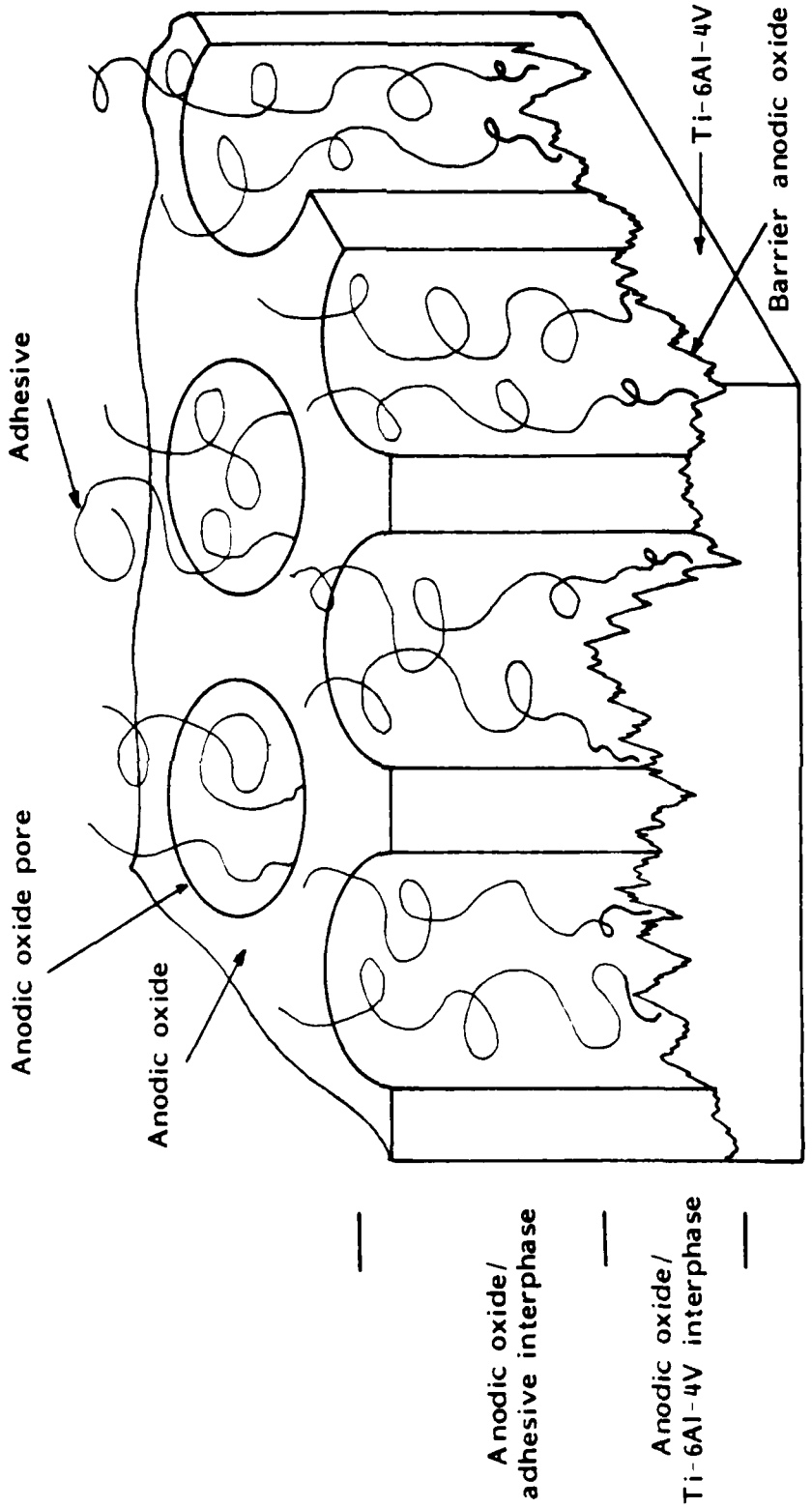


Figure 23. Proposed Adhesion Model for the CA/HF Anodized Ti-6Al-4V/Adhesive Bond.

definitive interfacial boundary. Due to the nature of the anodization process, which erodes the Ti-6Al-4V surface, there is a gradual transition from base metal to anodic oxide, through a region described as the metal-anodic oxide adhesive interphase. Similarly, the flow of adhesive into the anodic oxide columnar structure would result in a transition region of oxide to adhesive, or the anodic oxide-adhesive interphase region. This model is in good agreement with the TEM oxide cross section micrographs which indicate that the anodic oxide columnar pores have irregular surface boundaries.

3. Oxide Structure

Selected Area Electron Diffraction (SAED) analysis was used to determine the structure for an anodic oxide produced on Ti-6Al-4V by the following chromic acid/hydrofluoric acid anodization conditions: 283 ± 2K, 20 A/m^2, 10 volts and 20 minutes. SAED analysis of the oxide in cross section indicated that the oxide was primarily amorphous.

An X-ray diffraction pattern of the Ti-6Al-4V substrate cleaned by preanodization treatment #1 and of the precleaned Ti-6Al-4V anodized 20 minutes with HF at 298 ± 2K and 30 ± 2 A/m^2 were identical. One of the diffraction patterns are shown in Appendix IV. The characteristic peaks, as shown in Appendix IV, indicated that the substrate was Ti-6%Al-1%Mo-4%V. The three measured d-spacings, in order of intensity, were: 2.332, 2.227 and 1.327, which corresponded to the file spectrum for Ti-6AlMo-4V.

The source of the molybdenum is unknown. Because X-ray diffraction is a bulk analysis technique, it was not applicable to thin film oxide structure characterization ($\approx$100 nm).

4. Oxide Thickness

a. A Comparison of TEM and MBI Oxide Thickness Methods and Results

Two direct methods were used to measure oxide thickness: TEM micrographs at 200,000X of the oxide in cross section and/or Multiple Beam Interferogram (MBI) photographs at 28X of the anodized substrate interface. TEM has a resolution of approximately 5 nm; MBI has a resolution of 10 nm at a λ of 632.8 nm.

TEM micrographs of the oxide in cross section have been described earlier as shown in Figures 21 and 22. Typical interferograms are shown in Figures 5 and 24. The remaining interferograms used for oxide thickness calculations are included in Appendix V.

MBI measurements were made on two areas for one Ti-6Al-4V coupon CA/HF anodized at 54 $\pm$ 2 A/m^2, 20 minutes, 298 $\pm$ 2K and 10 V. These results are shown in Table XXI. These average oxide thickness data were comparable to within 10 nm for the two surfaces examined.

The range of oxide thickness values and the average oxide thickness values are reported for each anodic oxide examined in Table XXI. Eight to ten MBI interference shifts were measured to

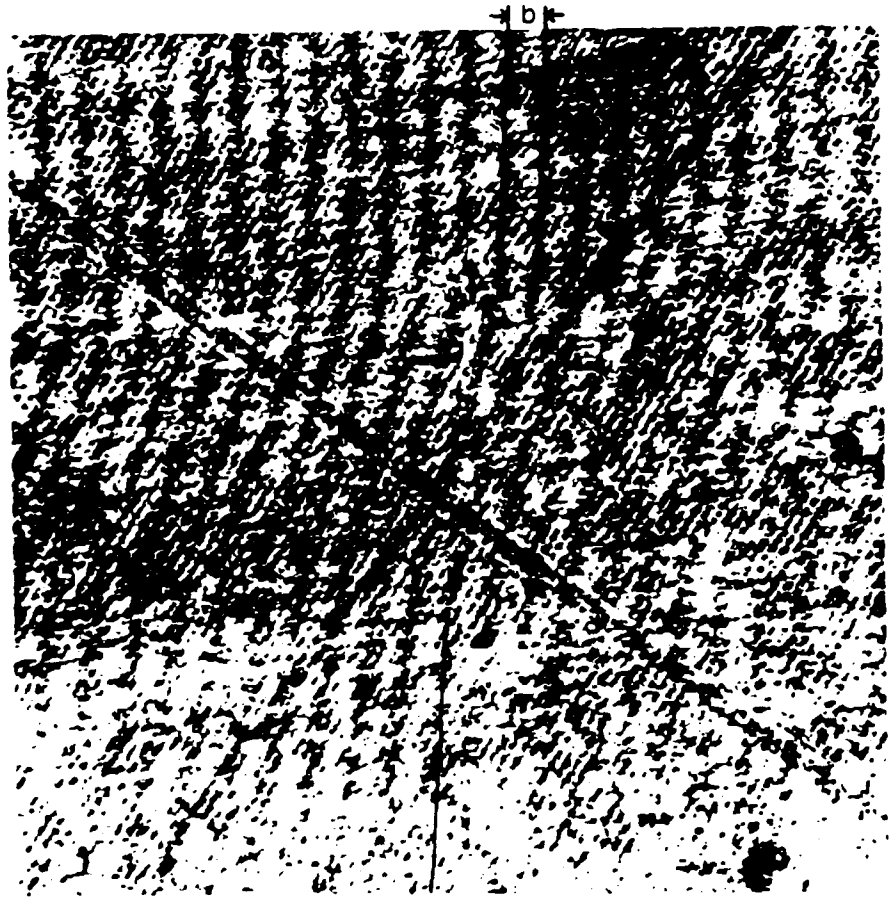


Figure 24. Interferogram of Fringe Pattern Used to Measure Ti-6Al-4V Anodic Oxide Thickness (28.4X). CA/HF Anodization Conditions: 20 Minutes, 283 ± 2K, 10 Volts, 30 ± 2 A/m^2.

TABLE XXI

Chromic Acid Anodized Ti-6Al-4V Oxide Thickness Data

Oxide Thickness Data		Anodization Methods		
Average Oxide Thickness (nm) ± 1 Std. Dev.	Oxide Thickness Range (nm)	Solution Temperature (K ± 2K)	Initial Current Density (A/m^2 ± 2 A/m^2)	Time (Minutes)
I. Ti-6Al-4V Chromic Acid Anodization Without HF at 39 V Initial Potential				
20 ± 10[1]	10 - 40[1]	298	30	20
II. Ti-6Al-4V Chromic Acid Anodization With HF at a Constant 10 V Potential				
80 ± 10[2]	65 - 85[2]	298	20	20
140 ± 10[1]	120 - 160[1]	298	30	20
110 ± 20[1]	90 - 140[1]	298	54	20
120 ± 10[1]	110 - 140[1]	298	54	20

(1) Multiple Beam Interferometry method was used to measure oxide thickness.

(2) Transmission Electron Microscopy was used to measure oxide thickness.

TABLE XXI (Continued)

Oxide Thickness Data		Anodization Methods		
Average Oxide Thickness (nm) ± 1 Std. Dev.	Oxide Thickness Range (nm)	Solution Temperature (K ± 2K)	Initial Current Density (A/m^2 ± 2 A/m^2)	Time (Minutes)
II. Ti-6Al-4V Chromic Acid Anodization With HF at a Constant 10 V Potential (Continued)				
290 ± 20[1]	250 - 300[1]	298	30	60
160 ± 10[1]	150 - 180[1]	283	20	20
120 ± 20[2]	95 - 150[2]	283	20	20
410 ± 20[1]	390 - 440[1]	283	30	20
460 ± 20[1]	430 - 500[1]	278	30	20

(1) Multiple Beam Interferometry method was used to measure oxide thickness.

(2) Transmission Electron Microscopy was used to measure oxide thickness.

obtain the anodic oxide thickness average and range. Also, eight to ten TEM measurements were made to obtain the anodic oxide thickness average and range.

As can be seen in Table XXI, oxide thickness did vary across the anodized Ti-6Al-4V surface. The maximum variation measured was 70 nm.

Both TEM and MBI oxide thickness measurements were made for the oxide produced at CA/HF conditions of 283 ± 2K, 20 ± 2 A/m^2, 10V, and 20 minutes. The comparative results are shown in Table XXI. There was good agreement between the MBI and TEM oxide thickness results. The TEM average oxide thickness was 25% lower than the MBI average oxide thickness. The oxide thickness range was 55 nm based upon TEM measurements and 30 nm based upon MBI measurements.

MBI was the primary method used to measure oxide thickness as a function of anodization method. This is because the interferometer was more readily accessible and less expensive to use than the TEM.

b. Influence of Anodization Solution Composition upon Oxide Thickness

A thin (20 nm) oxide was formed on the Ti-6Al-4V surface when chromic acid anodized without hydrofluoric acid, as shown in Table XXI. In fact, this oxide was the thinnest of all those reported in Table XXI.

Figure 25 is a comparison of oxide thickness for chromic acid anodization with and without hydrofluoric acid. The average oxide thickness decreased from 140 ± 10 nm to 20 ± 10 nm when HF was deleted from the bath in the chromic acid anodization conditions of 30 ± 2 A/m^2 current density and 298 ± 2K solution temperature. When HF was deleted from the bath, the anodization voltage was increased to 39 volts in order to obtain the initial current density.

It is generally accepted that the role of the hydrofluoric acid addition to the Ti-6Al-4V chromic acid anodization solution is to:

1. continue to etch the Ti-6Al-4V substrate and thereby continue oxide formation at the substrate; and,
2. tunnel up through the oxide and thereby create oxide pores.[42]

In the absence of hydrofluoric acid, a thin barrier oxide would be expected to form on the Ti-6Al-4V substrate and oxide formation would stop, for a constant anodization potential. Oxide dissolution at the surface should continue at some rate, however. And the relatively high voltage required for anodization without HF may have increased Joule heating of the oxide and promoted oxide dissolution. Therefore, it would be expected that chromic acid anodization of Ti-6Al-4V without hydrofluoric acid would produce on the Ti-6Al-4V substrate a thin oxide, such as the 20 nm thick oxide measured in this study, with relatively few or no pores.

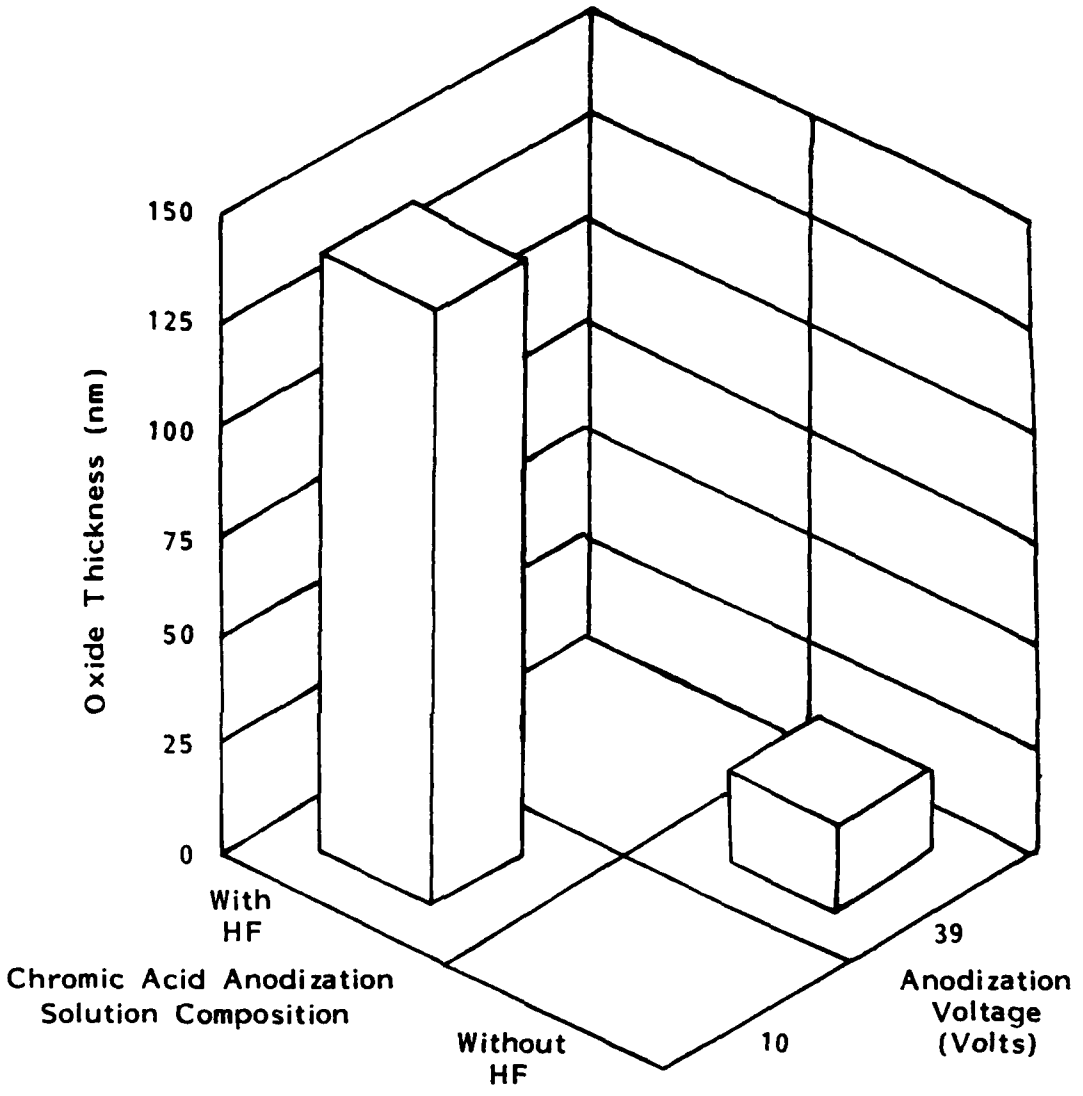


Figure 25. Influence of Chromic Acid Anodization Solution Composition upon Anodic Oxide Average Thickness.

c. Influence of CA/HF Anodization Time upon Oxide Thickness

Increasing the CA/HF anodization time from 20 to 60 minutes approximately doubled the average oxide thickness at CA/HF anodization conditions of 30 ± 2 A/m^2 initial current density and 10 volts. The average anodic oxide thickness increased from 140 to 290 nm when anodization time was increased from 20 to 60 minutes, as shown in Table XXI and Figure 26.

d. Influence of CA/HF Solution Temperature and Initial Current Density upon Oxide Thickness

Figure 27 is a three dimensional graph of selected data from Table XXI which illustrates the influence of solution temperature and initial current density upon average anodic oxide thickness for CA/HF anodized Ti-6Al-4V.

It can be seen from Figure 27 that there is a nonlinear, direct relationship between oxide thickness and current density for the 20 minute, 10 volt, Ti-6Al-4V CA/HF anodization conditions examined. And, there is a nonlinear, indirect relationship between oxide thickness and solution temperature. Apparently, the rate of oxide formation can be increased by an increase in initial current density, up to some limiting value. And, the rate of oxide dissolution can be decreased by a decrease in solution temperature, up to some limiting value.

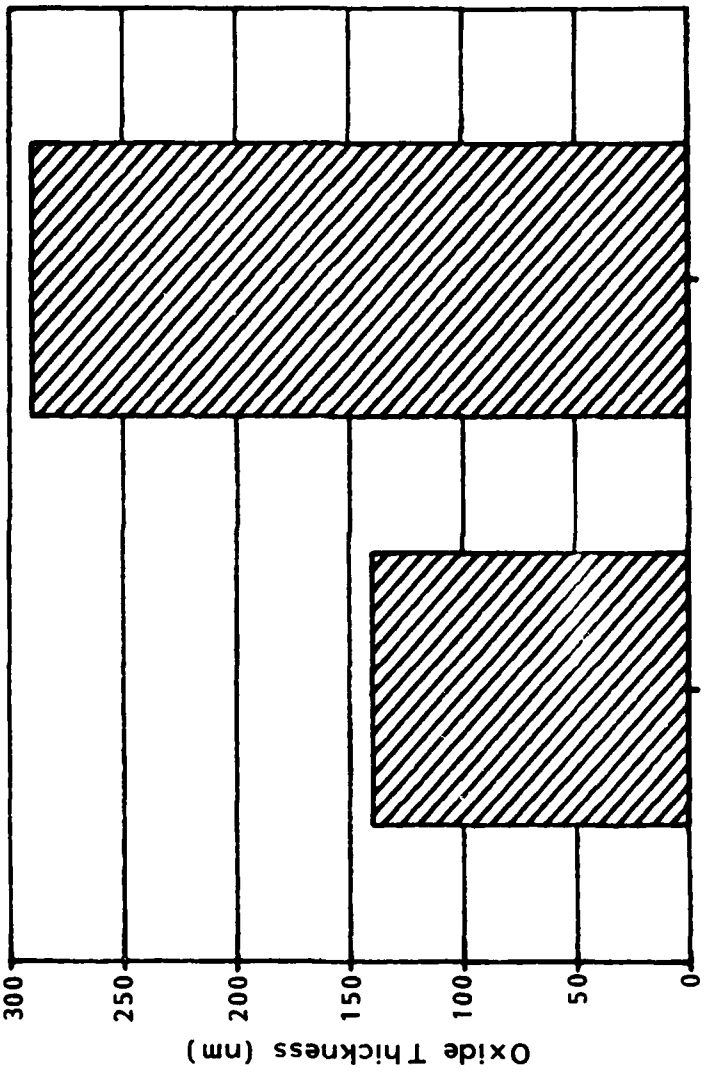


Figure 26. Influence of Chromic Acid/Hydrofluoric Acid Anodization Time upon Anodic Oxide Average Thickness.

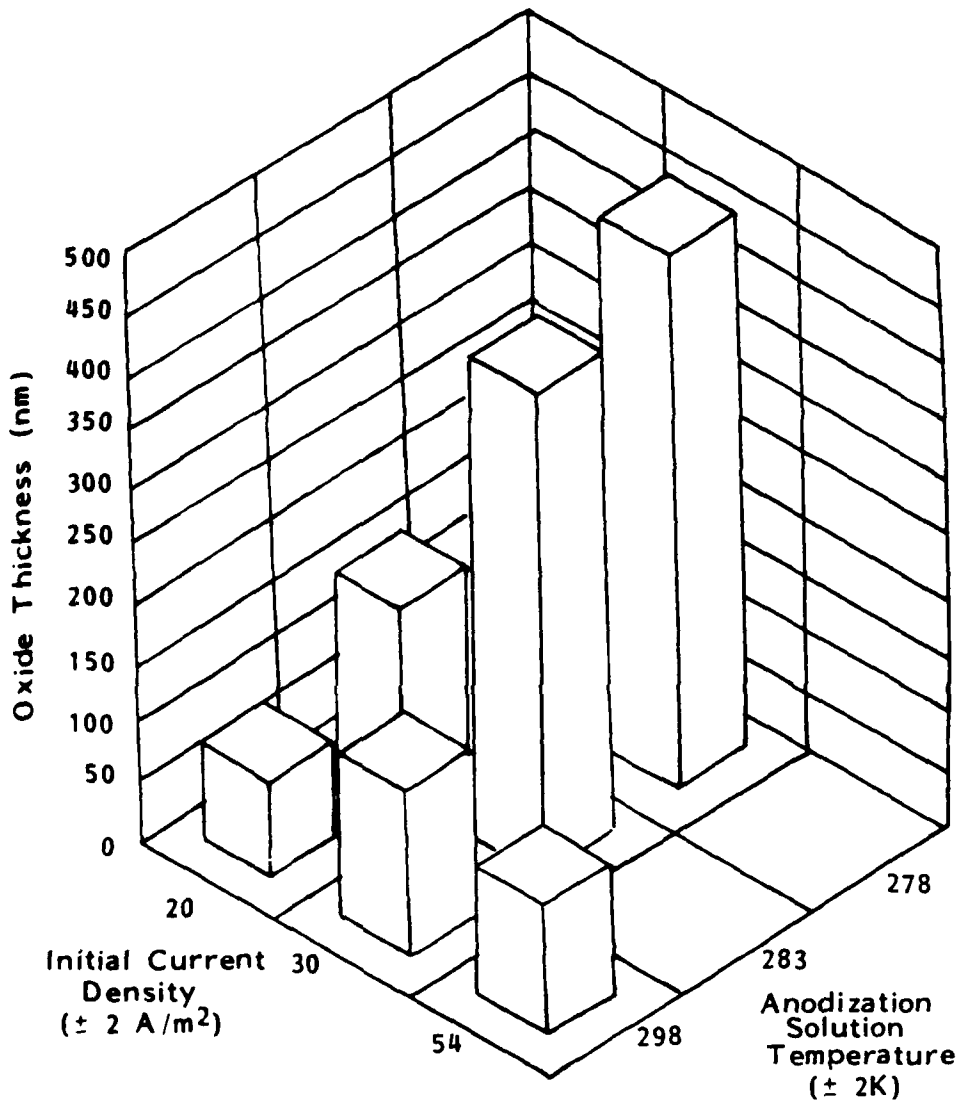


Figure 27. Influence of Chromic Acid/Hydrofluoric Acid Anodization Solution Temperature and Initial Current Density upon Anodic Oxide Average Thickness.

Specific examples of data from Figure 27 are described below which support the observed indirect relationship of initial current density and direct relationship of temperature upon Ti-6Al-4V anodic oxide thickness for 20 minute, 10 volt CA/HF anodization.

At a 30 ± 2 A/m^2 initial current density, average oxide thickness increased by approximately a factor of 3 when the relatively low solution temperature of 283 ± 2K was used rather than 298 ± 2K. Average anodic oxide thickness increased from 140 ± 10 nm to 410 ± 20 nm when temperature was lowered from 298 to 283K. However, a 5K drop in solution temperature from 283 ± 2K to 278 ± 2K did not appreciably change the average oxide thickness from the value obtained at 283 ± 2K. At a 20 ± 2 A/m^2 initial current density, the average oxide thickness increased by a factor of 2 when the solution temperature was 283 ± 2K rather than 298 ± 2K.

For a solution temperature of 298 ± 2K, average anodic oxide thickness increased by approximately a factor of 2 when the 20 A/m^2 initial current density was increased to 30 ± 2 A/m^2. However, a further increase in initial current density from 30 ± 2 A/m^2 to 54 ± 2 A/m^2 did not significantly increase oxide thickness.

The thickest CA/HF anodic oxide measured, on average, was 460 ± 20 nm and was produced at a relatively high initial current density, 30 ± 2 A/m^2, and low solution temperature, 278 ± 2K. And, the thinnest CA/HF measured, on average, was 80 ± 10 nm, and was produced at a relatively low initial current density of 20 ± 2 A/m^2 and relatively high solution temperature of 298 ± 2K.

An anodic oxide thickness is not unique for a set of CA/HF anodization parameters, as shown in Table XXI. An average oxide thickness of 140 ± 10 nm was produced at anodization conditions of 30 ± 2 A/m^2 and 298 ± 2K. Approximately the same average oxide thickness, 160 ± 10 nm, was produced at 20 ± 2 A/m^2 and 283 ± 2K. Apparently, while the rate of oxide formation and dissolution may have differed for these two anodization conditions, the net effect upon oxide thickness was the same.

In addition to its role in adhesive bonding, the anodic oxide may be of value as a dielectric. While a detailed examination of this subject is beyond the scope of this dissertation, preliminary oxide electrical property characterization has been conducted. The details are included in Appendix VI.

B. Anodized Ti-6Al-4V/Heat Resistant Adhesive Single Lap Bond Strength Data Analyses

1. The Interpretation of Single Lap Bond Strength Data

Figure 28 qualitatively illustrates the single lap bond distortion and the combination of peel, shear, and tensile stresses which develop through the single lap bond as a result of the applied tensile load. The bond distorts and these internal stresses develop, ultimately leading to bond failure, when the bond attempts to align more completely with the axis of the applied tensile load.

Because of the nonuniform stress distribution, which is qualitatively depicted in Figure 28, a single lap bond strength value actually represents an average bond strength. The adhesion fillet prevents stress singularities at the bond edges. Even so, when a tensile load is applied to the bond, high peel stresses do develop at the bond edge, resulting in a nonuniform, parabolic single lap bond stress distribution.

As will be discussed in detail in the failure analyses section, it was determined that single lap bond failure initiates in the adhesive fillet. Failure propagates through the anodic oxide/polymer interphase and/or cohesively through the polymer. Single lap bond strength can therefore be used as an indirect measure of the anodic oxide/polymer bond strength and/or polymer cohesive strength. It is recognized that this measure of interphase

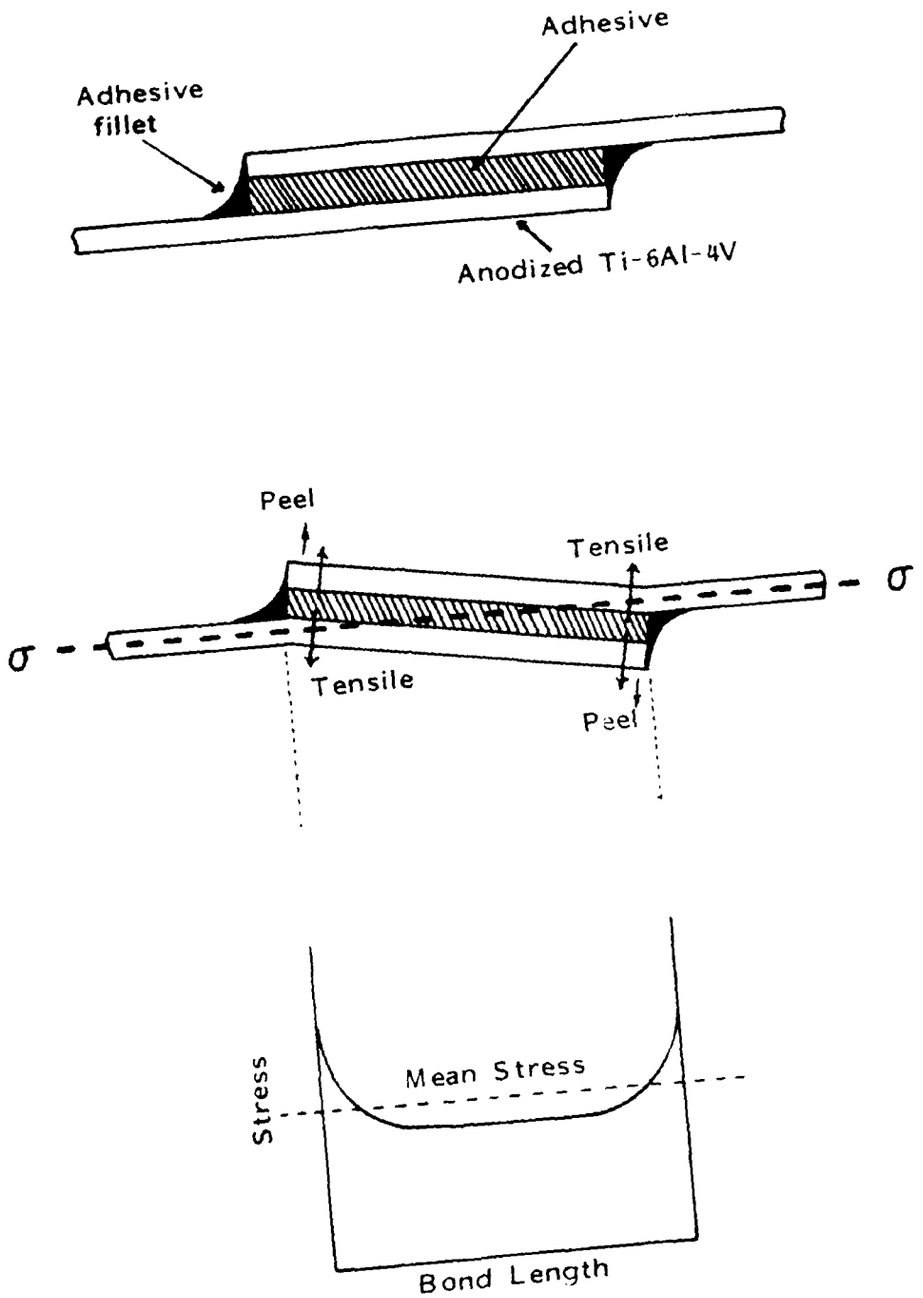


Figure 28. A Schematic of a Single Lap Bond Under an Applied Tensile Load and a Qualitative Representation of the Stress Distribution.(31, 31A)

and/or polymer cohesive strength is specific for the single lap bond geometry and test conditions under evaluation.

2. The Influence of Test Variables upon Single Lap Bond Strength

a. Overview

Single lap bond strengths were used to examine how each of the following variables influenced bond strength:

1. Ti-6Al-4V/preanodization cleaning treatment;
2. Ti-6Al-4V chromic acid anodization treatment;
3. single lap bond processing for anodized Ti-6Al-4V/PPQ bonds;
4. thermal aging of single lap bonds for unprimed and titanate primed anodized Ti-6Al-4V for a specific adhesive; and,
5. the choice of the adhesive

b. The Influence of Ti-6Al-4V Preanodization Cleaning Treatment upon Bond Strength

Table XXII compares the CA/HF Ti-6Al-4V/Udel® polysulfone single lap bond strength for Ti-6Al-4V cleaned by preanodization treatment #1 or preanodization treatment #2 prior to anodization. The Ti-6Al-4V was anodized per CA/HF anodization method #5 described in Table VI.

There was no significant difference between bond strengths for Ti-6Al-4V cleaned by preanodization treatment #1 or #2. Since

TABLE XXII

CA/HF Anodized Ti-6Al-4V/Udel® Polysulfone Single Lap Bond Strength Data

As a Function of Ti-6Al-4V Preanodization Treatment #1 and #2

Ti-6Al-4V Preanodization Treatment	Bond Strength (MPa)	Average Bond Strength (MPa)	Bond Strength Standard Deviation (MPa)
#1	25.3 25.4 26.1 26.2 28.2 28.3	26.6	1.3
#2	21.4 26.4 28.6 28.9	26.3	3.4

Note: Ti-6Al-4V CA/HF anodization procedure was: 20 minute anodization, 10 volts, 30 ± 2 A/m² initial current density, 298 ± 2K solution temperature, and 5% chromic acid solution with hydrofluoric acid.

preanodization treatment #2 is a simpler Ti-6Al-4V cleaning method, it is considered to be a preferred method.

c. The Influence of Ti-6Al-4V Chromic Acid Anodization Method upon Bond Strength

1. The Influence upon Bond Strength of Hydrofluoric Acid Added to the Chromic Acid Anodization Solution

Table XXIII compares the anodized Ti-6Al-4V/polysulfone single lap bond strength for Ti-6Al-4V anodized with and without hydrofluoric acid (HF) in the chromic acid solution. Anodized Ti-6Al-4V oxide thickness data described in section A are also included, for reference, in Table XXIII.

The anodization procedures used are described in Table XXIII. Anodization time, initial current density, anodization solution temperature and concentration of chromic acid solution were held constant for CA/HF and CA anodization of Ti-6Al-4V. In order to obtain the required initial current density, voltage was increased from 10 volts to 39 volts for Ti-6Al-4V anodized without hydrofluoric acid.

Based upon the bond strength data analyses, hydrofluoric acid addition to the chromic acid anodization solution is important to the anodized Ti-6Al-4V/polysulfone bond strength. Anodization with HF increased the mean bond strength by 30%. The t test 99% confidence level analysis indicated a significant difference between

TABLE XXIII

CA/HF Anodized Ti-6Al-4V/Udel® Polysulfone Single Lap Bond Strength and Ti-6Al-4V Anodic Oxide Thickness Data As a Function of Anodization With and Without HF

Ti-6Al-4V Anodization Solution(1)	Bond Strength (MPa)	Average Bond Strength (MPa)	Bond Strength Standard Deviation (MPa)	Anodized Ti-6Al-4V Oxide Thickness (nm)
CA/HF	25.3 25.4 26.1 26.2 28.2 28.3	26.6	1.3	140 ± 10
CA	18.1 18.3 19.9 20.5 21.9 24.3	20.5	2.4	20 ± 10

(1) Ti-6Al-4V anodization procedure was: 20 minute anodization time, 30 ± 2 A/m^2 initial current density, 298 ± 2K solution temperature, 5% chromic acid solution. Voltage was 10 and 39 volts for anodization with and without hydrofluoric acid, respectively. Ti-6Al-4V preanodization treatment #1 was used.

the bond strength data for CA/HF anodized Ti-6Al-4V and for Ti-6Al-4V adherends anodized in chromic acid without the addition of hydrofluoric acid.

Elimination of hydrofluoric acid from the chromic acid anodization solution reduced the anodic oxide thickness by a factor of seven, as shown in Table XXIII. As discussed earlier in Section A, oxide porosity is limited or nonexistent for Ti-6Al-4V anodized without HF.[42,43] For a thin anodic oxide with limited porosity, mechanical interlock of the adhesive into the oxide may be limited. And, for this relatively nonporous oxide, there would be a reduction of surface area, and consequently a reduction in van der Waals forces between the adhesive and the oxide.

The result of this thin, nonporous oxide produced by CA anodization is a lower bond strength, compared to the thicker, more porous CA/HF anodized Ti-6Al-4V oxide. This author suggests that the single lap bond stress distribution at break can be qualitatively depicted as shown schematically in Figure 29. As shown in Figure 29, the single lap bond edges, which are reinforced with the adhesive fillet, should be capable of the same load bearing capacity, regardless of the CA/HF or CA anodization process, until the polysulfone fillet fractures. Once the polysulfone fillet has fractured, it is proposed that the higher the oxide porosity and thickness, the greater the degree of mechanical interlock and van der Waals bonding of the adhesive/oxide bond, and the greater the load bearing capacity and fracture stress.

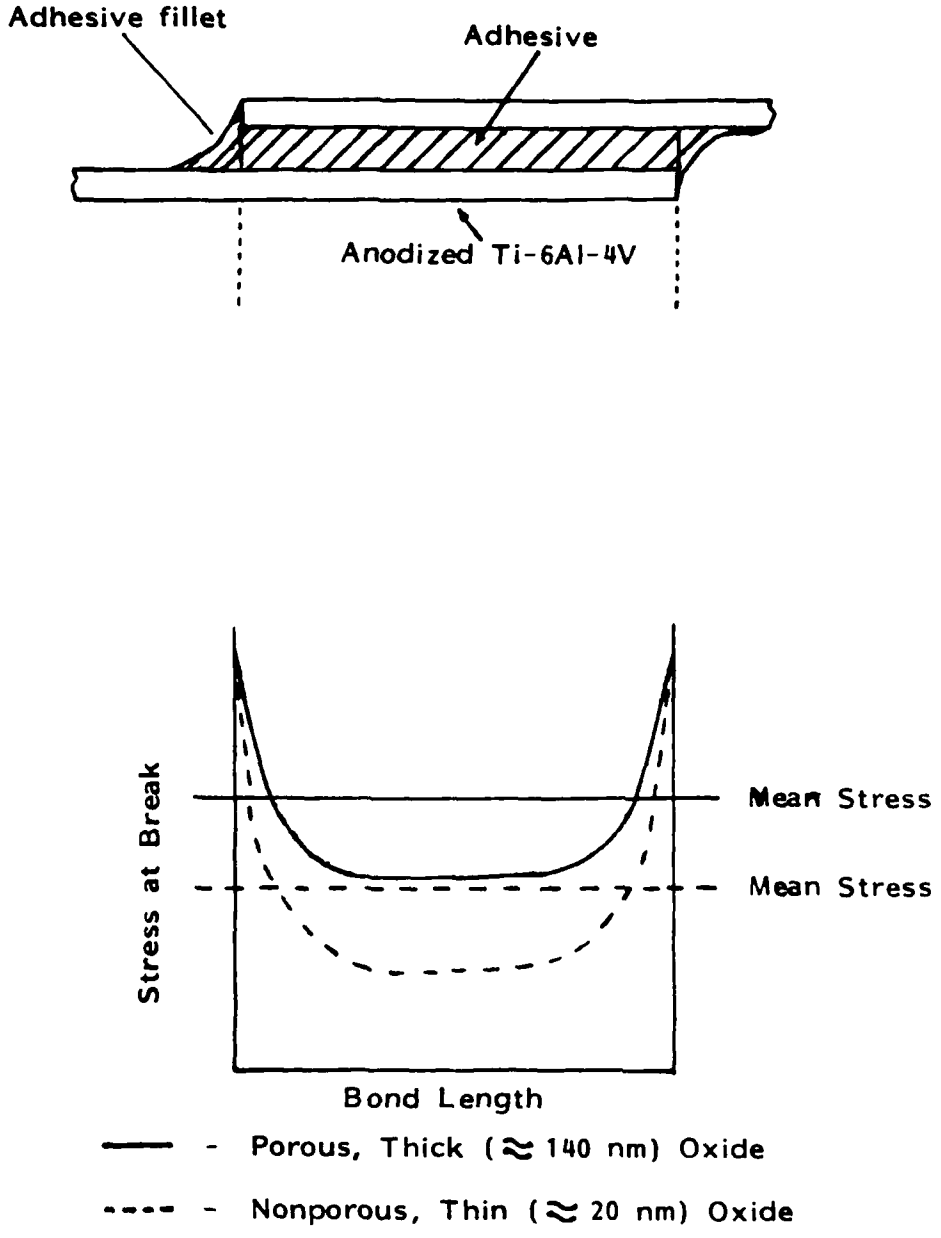


Figure 29. Qualitative Representation of the Influence of Oxide Porosity and Thickness Upon Single Lap Bond Stress Distribution.

2. The Influence of CA/HF Anodization Time upon Bond Strength

Table XXIV compares the anodized Ti-6Al-4V/polysulfone single lap bond strength and the anodic oxide thickness data for CA/HF Ti-6Al-4V anodized 20 minutes and anodized 60 minutes. All other anodization conditions were held constant. There was no significant difference in the bond strength data, based upon the t test analyses at a 99% confidence level. Since there is no difference in bond strengths, the 20 minute CA/HF anodization is preferred over the 60 minute CA/HF anodization, because it is a more time efficient process.

Anodized Ti-6Al-4V oxide thickness data included in Table XXIV indicates that oxide thickness doubled when a 60 minute anodization time, rather than a 20 minute anodization time, was used. Based upon the single lap bond data, this increase in the anodized Ti-6Al-4V average oxide thickness from 140 ± 10 nm to 290 ± 20 nm did not influence bond strength.

3. The Influence of CA/HF Anodization Initial Current Density and Solution Temperature upon Single Lap Bond Strength.

The influence upon single lap bond strengths of the hydrofluoric acid addition to the chromic acid anodization solution was discussed in the preceding paragraphs. Similarly, the influence of CA/HF anodization time upon single lap bond strengths was also

TABLE XXIV

CA/HF Anodized Ti-6Al-4V/Udel® Polysulfone Single Lap Bond Strength and Ti-6Al-4V Anodic Oxide Thickness As a Function of 20 Minute, and 60 Minute Anodization

Ti-6Al-4V Anodization Time (1)	Bond Strength (MPa)	Average Bond Strength Deviation (MPa)	Bond Strength Standard (MPa)	Anodized Ti-6Al-4V Oxide Thickness (nm)
20 Minute	25.3 25.4 26.1 26.2 28.2 28.3	26.6	1.3	140 ± 10
60 Minute	14.5 18.8 24.1 24.9 27.4	21.9	5.2	290 ± 20

(1) Ti-6Al-4V CA/HF anodization procedure was: 30 ± 2 A/m^2 initial current density, 10 volts, 298 ± 2K solution temperature, 5% chromic acid solution. Ti-6Al-4V preanodization treatment #1 was used.

discussed earlier. Both tests were conducted at a 30 ± 2 A/m² anodization initial current density and a 298 ± 2K solution temperature. Because significantly greater bond strengths were achieved for Ti-6Al-4V chromic acid anodized with hydrofluoric acid, all subsequent chromic acid anodizations were conducted with hydrofluoric acid. And, a 20 minute anodization time was chosen for all subsequent CA/HF anodization tests.

Initial current density and solution temperature were varied to determine their respective effects upon CA/HF Ti-6Al-4V/polysulfone single lap bond strength and also upon the CA/HF Ti-6Al-4V/polyphenylquinoxaline single lap bond strength. Anodization time, (20 minutes), voltage, (10 volts), and a 5% chromic acid solution were held constant. The quantity of hydrofluoric acid added to the anodization solution was varied to obtain the initial current density.

CA/HF anodized Ti-6Al-4V/Udel® polysulfone single lap bond strength data, as a function of anodization temperature and initial current density, are shown in Table XXV. A 99% confidence level criteria, the highest possible in the t test, was used to assign the probability that an anodization process variable influenced bond strength. The 20 ± 2 A/m² initial current density did significantly improve the bond strength by about 30%, as compared to the 30 ± 2 A/m² initial current density, at either 283 ± 2K or 298 ± 2 K solution temperature, based upon statistical analyses.

A proposed reason for the significant improvement in the CA/HF anodized Ti-6Al-4V/polysulfone single lap bond strength

TABLE XXV

CA/HF Anodized Ti-6Al-4V/Udel® Polysulfone Single Lap Bond Strengths as a Function of Initial Current Density and Solution Temperature[1]

Initial Current Density[2] ($A/m^2 \pm 2\ A/m^2$)	Solution Temperature ± 2K	Single Lap Bond Strength (MPa ± 0.1 MPa)	Mean Single Lap Bond Strength (MPa)	Standard Deviation (MPa)
20	283	29.4 33.0 33.4 33.8 34.2	32.8	1.9
20	298	30.9 31.6 34.2 35.6 37.1 42.3	35.3	4.2

Notes: (1) Anodization time was 20 minutes and potential was 10 volts in all procedures tested. Preanodization method #2 was used.

(2) Initial current density was based upon the Ti-6Al-4V apparent surface area anodized.

TABLE XXV (Continued)

Initial Current Density[2] ($A/m^2 \pm 2\ A/m^2$)	Solution Temperature ± 2K	Single Lap Bond Strength (MPa ± 0.1 MPa)	Mean Single Lap Bond Strength (MPa)	Standard Deviation (MPa)
30	283	19.7 21.5 23.4 25.6 32.5	24.6	5.0
30	298	21.4 26.4 28.6 28.9	26.3	3.4

Notes: (1) Anodization time was 20 minutes and potential was 10 volts in all procedures tested. Preanodization method #2 was used.

(2) Initial current density was based upon the Ti-6Al-4V apparent surface area anodized.

when a 20 ± 2 A/m² initial current density was used, rather than a 30 ± 2 A/m² initial current density, is described as follows. Udel® polysulfone, in general, has good chemical resistance. However, it is susceptible to chemical degradation by halogenated compounds.[6] Thus, polysulfone would be expected to be susceptible to both fluoride ions and hydrofluoric acid.

The results of ESCA analyses for CA/HF anodized Ti-6Al-4V, anodized at an initial current density of 20 ± 2 A/m² and 30 ± 2 A/m², are listed in Tables XXVI and XXVII, respectively. Fluoride ions are present on the surface of the oxide produced by anodization, based upon the binding energy data. It is assumed that fluoride ions would also be present in the oxide pores. Fluoride ions on the metal oxide surface are a result of the CA/HF anodization process, whereby the initial current density is controlled by hydrofluoric acid addition to the chromic acid solution.

The 30 ± 2 A/m² anodization initial current density is higher than necessary to create the metal oxide pores. Since the Udel® polysulfone polymer chosen for the adhesive bond is susceptible to chemical degradation by fluoride ions, the polymer surface microstructure could be significantly weakened by contact with the oxide surface and inside the metal oxide pores, which contain an excess of fluoride ions and/or hydrofluoric acid. The hydrofluoric acid could result because of adsorbed moisture in the bond joint. The proposed weakened polymer surface microstructure could then

TABLE XXVI

ESCA Analysis for CA/HF Anodized Ti-6Al-4V, Anodized 20 Minutes, 20 ± 2 A/m², 10 Volts, 283 ± 2K

Element	Corrected Binding Energy C: 285.0 eV	Atomic Concentration (%)	% Conc. X / % Conc. Ti
C (1s)	285.0	63	10.5
O (1s)	530.6	25	4.2
F (1s)	685.4	1	0.2
Ti (2p1/2)	464.6	6	1.0
Ti (2p3/2)	458.8		
Cr (2p3/2)	NSP		
V (2p3/2)	NSP		
Al (2p1/2)	74.2	2	0.3
S (2s)	NSP		
S (2p3/2)	NSP		
N (1s)	NSP		
Si (2p3/2)	104.0	3	0.5
Cl (2p3/2)	NSP		
Na (1s)	NSP		

NSP: No Significant Peak

TABLE XXVII

ESCA Analysis for CA/HF Anodized Ti-6Al-4V, Anodized 20 Minutes, 30 ± 2 A/m², 10 Volts, 298 ± 2K

Element	Corrected Binding Energy C: 285.0 eV	Atomic Concentration (%)	% Conc. X / % Conc. Ti
C (1s)	285.0	32	2.3
O (1s)	530.4	49	3.5
F (1s)	685.0	3	0.2
F (A)	596.2		
Ti (2p1/2)	464.4	14	1.0
Ti (2p3/2)	458.8		
Cr (2p3/2)	577.6	1	0.1
V (2p3/2)	NSP		
Al (2p½)	74.6	1	0.1
S (2s)	NSP		
S (2p3/2)	NSP		
N (1s)	NSP		
Si (2p3/2)	NSP		
Cl (2p3/2)	NSP		
Na (1s)	NSP		

NSP: No Significant Peak

explain the observed, significant bond strength reduction for the adhesive/metal oxide bond.

The significantly stronger Udel® polysulfone bonds for Ti-6Al-4V, CA/HF anodized at a 20 ± 2 A/m² initial current density at either a 283 ± 2K or 298 ± 2K solution temperature, as described in Table XXV, may be attributed to this low initial current density, which is proposed to minimize the fluoride ion concentration in and/or at the surface of the metal oxide. ESCA analyses indicated no significant surface element concentration or chemical composition difference between Ti-6Al-4V anodized at the two initial current densities. Also, this difference in bond strength may be attributable to stronger oxide mechanical properties associated with the oxide produced at an initial current density of 20 ± 2 A/m² as compared to 30 ± 2 A/m².

These significantly stronger bonds obtained for Ti-6Al-4V CA/HF anodization at a 20 ± 2 A/m² rather than a 30 ± 2 A/m² initial current density cannot be attributed to associated changes in anodic oxide morphology. Transmission Electron Microscopy analysis of the oxide morphology for Ti-6Al-4V anodized at a 20 ± 2 A/m² initial current density at either a 298 ± 2K or 283 ± 2K solution temperature has been conducted, with the data previously presented in Table XX and Figures 17 through 22. Scanning Transmission Electron Microscopy analyses of the oxide morphology for Ti-6Al-4V anodized at 17 to 27 A/m² and at a 298K solution temperature have been reported by Cheng[42], and are indicated in

Table XX. Both analyses revealed a porous oxide, with comparable pore diameters and pore wall thicknesses.

CA/HF anodized Ti-6Al-4V oxide thickness, as a function of the initial current density and solution temperatures studied, have been previously described and selected data are shown in Table XXVIII. The significantly stronger bonds at 20 ± 2 A/m^2 do not appear to be related to anodic oxide thickness.

In summary, of the CA/HF anodization methods tested, a Ti-6Al-4V CA/HF anodization treatment has been identified as a preferred method, since it produced significantly stronger bonds for polysulfone as the adhesive. For Ti-6Al-4V cleaned of its natural oxide, this preferred anodization process is: 20 minute anodization, at a 10 volt potential, and a 20 A/m^2 initial current density, which is controlled by the volumetric addition of a 49% hydrofluoric acid to a 5% chromic acid solution. The solution temperature can be specified at any value between 283K and 298K and held within ± 2K during anodization. This anodization process will be subsequently referred to as the preferred CA/HF anodization process.

Table XXIX describes bond strength data for a variety of heat resistant, structural adhesives bonded to Ti-6Al-4V anodized per the preferred anodization process. A 283 ± 2K solution temperature was used in all cases. This temperature was chosen rather than the 298 ± 2K temperature to reduce any Joule heating effects upon the oxide, primarily the formation of oxide flaws.

TABLE XXVIII

CA/HF Anodized Ti-6Al-4V Oxide Thickness Data

as a Function of Selected Anodization Conditions

Anodization Procedure[1]	Initial Current Density[2] ($A/m^2 \pm 2\ A/m^2$)	Solution Temperature ± 2K	Oxide Thickness (nm)
1	20	283	160 ± 10[3]
2	20	298	80 ± 10[4]
3	30	283	410 ± 20[3]
4	30	298	140 ± 10[3]

Notes: (1) Anodization time was 20 minutes and potential was 10 volts in all procedures tested.

(2) Initial current density was based upon the Ti-6Al-4V apparent surface area anodized .

(3) Average anodic oxide thickness was determined by interferometry. Accuracy is ± 10 nm.

(4) Anodic oxide thickness was determined by TEM analyses.

TABLE XXIX

Single Lap Bond Strengths for Ti-6Al-4V Anodized Per the Preferred CA/HF Anodization Method at 283 ± 2K and Bonded to Selected Heat Resistant, Structural Adhesives

Adhesive	CA/HF Anodized Ti-6Al-4V/Adhesive Single Lap Bond Strength (MPa ± 0.1 MPa)	Mean Single Lap Bond Strength (MPa)	Standard Deviation (MPa)
Victerex® Polyethersulfone	19.1 23.6 24.3 26.4 28.2 31.4	25.5	4.2
Polyphenyl-quinoxaline(1)	29.2 32.5 32.6 33.6 34.1 34.6	32.8	1.9

Note: (1) Bonds were processed per the isothermal procedure.

TABLE XXIX (Continued)

Adhesive	CA/HF Anodized Ti-6Al-4V/Adhesive Single Lap Bond Strength (MPa ± 0.1 MPa)	Mean Single Lap Bond Strength (MPa)	Standard Deviation (MPa)
Ultem® Polyetherimide	20.9 33.6 35.2 35.2 40.0 42.1	33.2	6.9
Ultem® 20% Glass Filled Polyetherimide	31.2 31.3 32.7 33.4 34.5 35.4	33.1	1.7

These data verify the applicability of this preferred Ti-6Al-4V anodization process for a wide range of adhesives, such as polyetherimide, both filled and 20% glass filled, polyethersulfone and polyphenylquinoxaline.

The preferred Ti-6Al-4V anodization treatment is an effective anodization treatment for structural bonding, not only to plastics with excellent fluoride chemical resistance but also to plastics such as polysulfone susceptible to chemical degradation by fluoride ions. And, this anodization process has a relatively unrestricted anodization solution temperature criteria, which minimizes process controls required and makes this anodization process even more attractive in an industrial processing situation.

CA/HF anodized Ti-6Al-4V/polyphenylquinoxaline (PPQ) single lap bond strength data, as a function of anodization procedure, are shown in Table XXX. Anodization procedures tested were: 298 ± 2K anodization solution temperature at 30 ± 2 A/m^2 or 20 ± 2 A/m^2. Also, a 283 ± 2K anodization solution temperature at 20 ± 2 A/m^2 was tested.

The t test at a 99% confidence level indicates that the choice of a 283 ± 2K or 298 ± 2K anodization solution temperature at 20 ± 2 A/m^2 did not affect the CA/HF Ti-6Al-4V/PPQ bond strength. Recall that this was also the case for CA/HF Ti-6Al-4V/polysulfone bonds.

The t test also indicates that the CA/HF Ti-6Al-4V/PPQ bond strength is independent of the choice of a 20 ± 2 A/m^2 or a 30 ± 2

TABLE XXX

CA/HF Anodized Ti-6Al-4V/Polyphenylquinoxaline Single Lap Bond Strengths

as a Function of Anodization Procedures

Anodization Procedure(1)	Initial Current Density(2) ($A/m^2 \pm 2\ A/m^2$)	Solution Temperature (± 2K)	Single Lap Bond Strength(3) (MPa ± 0.1 MPa)	Mean Single Lap Bond Strength (MPa)	Standard Deviation (MPa)
1	20	283	29.2 32.5 32.6 33.6 34.1 34.6	32.8	1.9
2	20	298	28.2 28.6 28.7 29.5 32.9 37.2	30.9	3.6

Notes: (1) Anodization time was 20 minutes and potential was 10 volts in all procedures tested. Preanodization treatment #2 was used.

(2) Initial current density was based upon the Ti-6Al-4V apparent surface area anodized.

(3) Bonds were isothermally processed and tested after 0.5 month at 298 ± 2K in a 65 to 80% relative humidity environment.

TABLE XXX (Continued)

Anodization Procedure(1)	Initial Current Density(2) ($A/m^2 \pm 2\ A/m^2$)	Solution Temperature ($\pm$ 2K)	Single Lap Bond Strength(3) (MPa $\pm$ 0.1 MPa)	Mean Single Lap Bond Strength (MPa)	Standard Deviation (MPa)
3	30	298	31.2 34.4 37.0 37.2 41.9 46.0	37.9	5.3

Notes: (1) Anodization time was 20 minutes and potential was 10 volts in all procedures tested. Preanodization treatment #2 was used.

(2) Initial current density was based upon the Ti-6Al-4V apparent surface area anodized.

(3) Bonds were isothermally processed and tested after 0.5 month at 298 $\pm$ 2K in a 65 to 80% relative humidity environment.

A/m^2 initial current density at 298 ± 2K solution temperature. This is in contrast to the CA/HF/polysulfone data previously discussed where the choice of a 20 A/m^2 anodization initial current density, which reduced the fluoride concentration at the surface or in the oxide pores, improved its bond strength. This difference is to be expected, given that the chemical resistance of polyphenylquinoxaline to halogenated compounds is greater than for polysulfone.

d. The Influence of Single Lap Bonding Procedure on CA/HF Anodized Ti-6Al-4V/Polyphenylquinoxaline Bond Strength

CA/HF anodized Ti-6Al-4V/PPQ single lap bond strengths for isochronal and isothermal processed bonds are described in Table XXXI. The Ti-6Al-4V coupons were anodized by the same anodization procedure.

The isothermal processed average bond strength was approximately 81% higher than the average isochronal processed bond strength. Also, the t test analyses at a 99% confidence level indicated a significant difference in these bond strengths.

The relatively low isochronal processed bond strength is attributed to both the high bonding pressure of 41.4 MPa and the prolonged exposure to high temperature, 672K for thirty minutes. The isochronal bonding pressure was 1.4 MPa, and the bonding temperature was 28K higher, than is typical for isochronal bonding.[47] The atypically high pressure and temperatures were necessary to mate the two halves of the bonding jig. This was

TABLE XXXI

The Influence of Bonding Procedure on CA/HF Anodized

Ti-6Al-4V/Polyphenylquinoxaline Single Lap Bond Strength

Bonding Process	Bond Strength (MPa)	Average Bond Strength (MPa)	Bond Strength Standard Deviation (MPa)
Isothermal	29.2 32.5 32.6 33.6 34.1 34.6	32.8	1.9
Isochronal	16.1 18.5 18.8 18.9	18.1	1.3

Note: Ti-6Al-4V anodization procedure was: 20 minute anodization time, 20 ± 2 A/m^2 283 ± 2K solution temperature, 10 volts, and 5% chromic acid solution with HF. Preanodization treatment #2 was used.

because the isochronal vacuum stage drying caused hard, elevated areas in the PPQ, apparently the result of solvent evacuation during drying in vacuo.

Two mechanisms to explain why the isothermal processed bonds were stronger than the isochronal processed bonds are described below. Either one or both mechanisms may have contributed to the bond strength differences.

First, the high temperature and pressure used in this isochronal bonding process could have caused the anodic oxide to degrade and collapse. This could have resulted in only partial formation of an anodic oxide/PPQ interphase, causing the low isochronal process bond strength. TEM could verify this theory.

Secondly, the high temperature and pressure could have caused the residual cresol and xylene PPQ diluent to more effectively penetrate and degrade the oxide. This could have reduced the anodic oxide/PPQ interphase strength.

This diluent penetration effect has been proposed by Hill, et al.[50] to explain the oxide separation and relatively low bond strength, 19.9 MPa, for CA/HF anodized Ti-6Al-4V/PPQ bonds. In this study, the bonds were processed isothermally at 648K for 60 minutes. Hill concluded that for good bond strengths, anodized Ti-6Al-4V/PPQ bond processing should not exceed 15 minutes at 648K.

e. Thermal Aging Effects upon Single Lap Bond Strength

1. Thermally Aged, Unprimed CA/HF Anodized Ti-6Al-4V/Polysulfone Single Lap Bond Strength

The single lap bond strength data, as well as the corresponding average and standard deviation data, for thermally aged, unprimed CA/HF anodized Ti-6Al-4V/Udel® polysulfone bonds are described in Table XXXII.

All of the data exceeded the 6.9 MPa bond strength typically required as a minimum for structural bond considerations. In general, the bond strength values were two to three times this value. The 6.9 MPa value was referenced as a typical single lap bond strength for structural adhesives in Professor Thomas Ward's Chemistry 5650, Spring 1985 prepared notes. Also, a 6.2 MPa strength at 450K was the minimum value reported in the general literature for 3M Scotch weld high temperature structural adhesive 2214 bonded to FPL etched aluminum.

All of these thermally aged bond strength data were compared simultaneously using the one-way analysis of variance statistical test, more commonly known as the f test. Based upon this analysis, the following thermal aging conditions had no significant influence upon the single lap bond strength for CA/HF anodized Ti-6Al-4V/Udel® polysulfone bonds:

1. 0.5 month at 298 ± 5K in a 65 to 80% relative humidity (R.H.) environment, or

TABLE XXXII

Unprimed CA/HF Anodized Ti-6Al-4V/Udel® Polysulfone Single Lap

Bond Strength Data as a Function of Thermal Aging

Bond Aging Conditions(1)	Bond Strength(2) (MPa ± 0.1 MPa)	Average Bond Strength (MPa)	Standard Deviation (MPa)
0.5 month at 298 ± 5K	25.3 25.4 26.1 26.2 28.2 28.3	26.6	1.3
2.0 months at 298 ± 5K	25.8 26.5 28.6 29.2 29.7 29.8	28.2	1.7

Note: (1) Ti-6Al-4V anodization procedure was: 20 minutes anodization time, 10 volts 30 ± 2 A/m² initial current density, 298 ± 2K solution temperature, and 5% chromic acid solution with HF. Preanodization treatment #2 was used in all cases except for Ti-6Al-4V for the 0.5 month, 298 ± 5K study.

TABLE XXXII (Continued)

Bond Aging Conditions(1)	Bond Strength(2) (MPa ± 0.1 MPa)	Average Bond Strength (MPa)	Standard Deviation (MPa)
9 months at 298 ± 5K(2)	11.2 20.8 29.1 29.4 32.1 32.3	25.8	8.3
9 months at 373 ± 5K, followed by 2 months at 298 ± 5K(2)	20.2 24.7 25.9 28.7 30.1 31.6	26.9	4.1
9 months at 443 ± 5K, followed by 2 months at 298 ± 5K	18.6 18.8 18.9 19.7 24.5 26.1	21.1	3.3

Notes: (1) Ti-6Al-4V anodization parameters were: 20 minutes anodization time, 10 volts 30 ± 2 A/m^2 initial current density, 298 ± 2K solution temperature, and 5% chromic acid solution with HF. Preanodization treatment #2 was used.

(2) Bonded 2 days after anodization, rather than the usual time interval of $\leq$ 16 hours after anodization.

2. 2 months at 298 ± 5K in a 65 to 80% R.H. environment; or
3. 9 months at 298 ± 5K in a 65 to 80% R.H. environment; or
4. 9 months at 378 ± 5K, followed by 2 months at 298 ± 5K in a 65 to 80% R.H. environment; or,
5. 9 months at 443 ± 5K, followed by 2 months at 298 ± 5K in a 60 to 85% R.H. environment.

The bonds aged 9 months at 298K were bonded two days after Ti-6Al-4V anodization. All other bonds in this study were bonded during the first 16 hours after anodization. Based upon the bond strength data, the 2 day delay in bonding had no significant effect upon bond strength.

It should also be noted that the Ti-6Al-4V was chromic acid/HF anodized at a 30 ± 2 A/m^2 initial current density for these thermally aged studies. These tests were conducted prior to the discovery that a lower initial anodization current density of 20 ± 2 A/m^2 significantly improved CA/HF anodized Ti-6Al-4V/polysulfone bond strength, which was discussed earlier. Therefore, it would be expected that these reported thermally aged bond strengths could have been improved by approximately 25% if the lower initial current density had been used in Ti-6Al-4V anodization.

2. Thermally Aged, Unprimed CA/HF Anodized Ti-6Al-4V/ 50% $CaCO_3$ Filled Polyimide Single Lap Bond Strength

The single lap bond strength data for thermally aged, unprimed CA/HF anodized Ti-6Al-4V/Ablebond® 71-3, 50% $CaCO_3$ filled

polyimide are shown in Table XXXIII. Thermal aging 9 months at 443 ± 5K, followed by 2 months aging at 298 ± 5K did not significantly affect bond strength. Based upon the t test analyses at a 99% confidence level. there was no difference between these bond strength data and the bond strength data for bonds aged only 0.5 month at 298 ± 5K.

This 50% $CaCO_3$ filled polyimide would not be considered for structural type bonding. These bond strengths were less than or only marginally greater than 6.9 MPa. The low bond strength for this polyimide adhesive may be attributed to any or all of the following reasons.

1. As a consequence of both the high filler content and the thermoset crosslinking, the polymer would have been rigid and therefore less able to absorb shock or stress than the thermoplastics included in this study. It shall be discussed in section C that when the polyimide was subjected to the single lap bond test, it exhibited brittle deformation. Therefore, a lower bond strength would be expected for polyimide bonds than for the thermoplastics tested, since the former would be less able to dissipate stress.
2. The filler in the polyimide may have blocked some of the anodic oxide pores, thereby preventing thermoset adhesive flow into the pores. Recall that the oxide pore diameter is approximately 30 nm. The calcium carbonate particles were

TABLE XXXIII

Unprimed CA/HF Anodized Ti-6Al-4V/Ablebond® 71-3, 50% $CaCO_3$ Filled Polyimide

Single Lap Bond Strength Data as a Function of Thermal Aging

..d Aging Conditions(1)	Bond Strength(2) (MPa ± 0.1 MPa)	Average Bond Strength (MPa)	Standard Deviation (MPa)
0.5 month at 298 ± 5K	6.0 7.1 8.0 8.5 8.5 8.5	7.8	1.0
9 months at 443 ± 5K, followed by 2 months at 298 ± 5K	3.0 4.0 5.8 7.0 7.1	5.4	1.8

Notes: (1) Relative humidity at 298K varied from 65 to 80%.

(2) Ti-6Al-4V anodization conditions were: 20 minutes anodization time, 10 volts 20 ± 2 A/m^2 initial current density, 283 ± 2K solution temperature, and 5% chromic acid solution with HF. Preanodization treatment #2 was used.

15 μm in diameter and are 500X larger in diameter than the pore. Pore blockage could reduce bond strength by any one or all of the following mechanisms:

a. a reduction of anodic oxide pore/polyimide mechanical interlock; and/or

b. a reduction in van der Waals forces between the thermoset and the inside of the oxide pores.

3. Shrinkage during the thermoset cure could induce additional stresses in the bond and reduce strength.

3. Thermally Aged, CA/HF Anodized Ti-6Al-4V/Polyphenylquinoxaline Single Lap Bond Strength for Unprimed and Primed Anodized Ti-6Al-4V

The single lap bond strength data analyses for thermally aged, unprimed CA/HF anodized Ti-6Al-4V/polyphenylquinoxaline (PPQ) bonds are described in Table XXXIV. The Lica® 44 titanate primed, anodized Ti-6Al-4V PPQ single lap bond strength data analyses for 443 ± 5K thermally aged bonds are included, also.

All of these thermally aged unprimed bond strengths were compared simultaneously using the f test at a 99% confidence level. Based upon the f test analyses, the following thermal aging conditions had no significant influence upon the single lap bond strength for unprimed CA/HF anodized Ti-6Al-4V/PPQ bonds:

1. 0.5 month at 298 ± 5K in a 65 to 80% R.H. environment; or

TABLE XXXIV

CA/HF Anodized Ti-6Al-4V/Polyphenylquinoxaline Single Lap Bond Strength

Data as a Function of Thermal Aging for Unprimed and Primed Anodized Ti-6Al-4V[1,2]

Anodized Ti-6Al-4V Description	Bond Aging Conditions(3)	Bond Strength (MPa ± 0.1 MPa)	Average Bond Strength (MPa)	Standard Deviation (MPa)
Unprimed	0.5 months at 298 ± 5K	29.2 32.5 32.6 33.6 34.1 34.6	32.8	1.9
Unprimed	11 months at 298 ± 5K	30.8 32.3 33.9 34.2 35.5 38.7	34.2	2.7

Notes: (1) Ti-6Al-4V anodization procedure was: 20 minutes anodization time, 10 volts 20 ± 2 A/m² initial current density, 283 ± 2K solution temperature, and 5% chromic acid solution with HF. Preanodization treatment #2 was used.

(2) Isothermal PPQ bonding process was used.

(3) Relative humidity at 298 ± 5K varied from 65 to 80%.

TABLE XXXIV (Continued)

Anodized Ti-6Al-4V Description	Bond Aging Conditions(3)	Bond Strength (MPa ± 0.1 MPa)	Average Bond Strength (MPa)	Standard Deviation (MPa)
Unprimed	9 months at 443 ± 5K, followed by 2 months at 298 ± 5K	22.4 26.4 30.7 35.3 35.6 35.8	31.0	5.6
Lica® 44 Titanate Primed	9 months at 443 ± 5K, followed by 2 months at 298 ± 5K	22.2 23.6 24.4 28.0 29.1 32.3	26.6	3.8

Notes: (1) Ti-6Al-4V anodization procedure was: 20 minutes anodization time, 10 volts 20 ± 2 A/m² initial current density, 283 ± 2K solution temperature, and 5% chromic acid solution with HF. Preanodization treatment #2 was used.

(2) Isothermal PPQ bonding process was used.

(3) Relative humidity at 298 ± 5K varied from 65 to 80%.

TABLE XXXIV (Continued)

Anodized Ti-6Al-4V Description	Bond Aging Conditions(3)	Bond Strength (MPa ± 0.1 MPa)	Average Bond Strength (MPa)	Standard Deviation (MPa)
Unprimed	Air quenched to 298 ± 5K 7X during 9 month test at 505 ± 10K. Aged 2 months at 298 ± 5K after 9 month test.	14.9 15.9 16.0 16.7 18.2 23.3	17.5	3.0

Notes: (1) Ti-6Al-4V anodization procedure was: 20 minutes anodization time, 10 volts 20 ± 2 A/m² initial current density, 283 ± 2K solution temperature, and 5% chromic acid solution with HF. Preanodization treatment #2 was used.

(2) Isothermal PPQ bonding process was used.

(3) Relative humidity at 298 ± 5K varied from 65 to 80%.

2. 11 months at 298 ± 5K in a 65 to 80% R.H. environment; or
3. 9 months at 443 ± 5K, followed by 2 months at 298 ± 5K in a 65 to 80% R.H. environment.

Lica® 44 titanate primer applied to the anodized Ti-6Al-4V had no significant influence upon bond strength for bonds aged 9 months at 443 ± 5K, followed by 2 months at 298 ± 5K in a 65 to 80% R.H. environment, based upon the t test at a 99% confidence level.

However, there was a significant reduction in bond strength after the following: a 9 month 505 ± 10K aging , which included an air quench to 298 ± 5K seven times during the 9 month period, and a subsequent 2 month 298 ± 5K aging in a 65 to 80% R.H. environment. Average bond strength decreased approximately 50% compared to bonds aged 0.5 month at 298 ± 5K in a 65 to 80% R.H. environment before testing. This thermal aging regime could have reduced bond strength by any one or all of the following mechanisms:

1. the oxide could have cracked or degraded from prolonged 505K exposure; and/or,
2. stress microcracks in the oxide or PPQ could have resulted from the cyclic 505K thermal aging; and/or,
3. the xylene and cresol, PPQ diluents, may have penetrated and degraded the oxide during the prolonged 505K exposure.

It is important to note, however, that all the PPQ bonds, including the 505 ± 10K thermally aged bonds, exhibited good

structural strength. Values exceeded the 6.9 MPa structural bond strength criteria by a factor of 2.1 to 5.5.

4. Thermally Aged, CA/HF Anodized Ti-6Al-4V/Polyethersulfone Single Lap Bond Strengths for Primed and Unprimed Anodized Ti-6Al-4V

The single lap bond strength data for thermally aged CA/HF anodized Ti-6Al-4V/Victerex® polyethersulfone (PES) bonds are included in Table XXXV. Bond strengths for primed and also unprimed anodized Ti-6Al-4V/polyethersulfone bonds are included. All of the PES bonds tested exhibited excellent structural bond strengths. Values exceeded the 6.9 MPA structural bond strength criteria by a factor of 2.6 to 3.7.

T test statistical analyses of the data in Table XXXV was conducted at a 99% confidence level. Thermal aging at 443 ± 5K, followed by 2 months aging at 298 ± 5K did not significantly effect bond strength, when compared to bonds aged 0.5 month at 298 ± 5K. And, the Lica® 44 titanate primer had no significant effect upon bond strength for these 443 ± 5K followed by 298 ± 5K thermally aged bonds.

5. Thermally Aged, CA/HF Anodized Ti-6Al-4V/Polyetherimide Single Lap Bond Strengths for Primed and Unprimed Anodized Ti-6Al-4V

The single lap bond strength data for thermally aged CA/HF anodized Ti-6Al-4V/Ultem® 1000 polyetherimide (PEI) are

TABLE XXXV

CA/HF Anodized Ti-6Al-4V/Victerex® Polyethersulfone Single Lap Bond Strength

Data as a Function of Thermal Aging for Unprimed and Primed Anodized Ti-6Al-4V(1)

Anodized Ti-6Al-4V Description	Bond Aging Conditions(2)	Bond Strength (MPa ± 0.1 MPa)	Average Bond Strength (MPa)	Standard Deviation (MPa)
Unprimed	0.5 months at 298 ± 5K	19.1 23.6 24.3 26.4 28.2 31.4	25.5	4.2
Unprimed	9 months at 443 ± 5k, followed by 2 months at 298 ± 5K	17.7 21.5 21.7 22.3 22.3 25.9	21.9	2.6

Notes: (1) Ti-6Al-4V anodization conditions were: 20 minutes anodization time, 10 volts 20 ± 2 A/m² initial current density, 283 ± 2K solution temperature, and 5% chromic acid solution with HF. Preanodization treatment #2 was used.

(2) Relative humidity at 298 ± 5K varied from 65 to 80%.

TABLE XXXV (Continued)

Anodized Ti-6Al-4V Description	Bond Aging Conditions(2)	Bond Strength (MPa ± 0.1 MPa)	Average Bond Strength (MPa)	Standard Deviation (MPa)
Lica® 44 Titanate Primed	9 months at 443 ± 5K, followed by 2 months at 298 ± 5K	13.5 16.6 17.3 18.7 19.0 21.6	17.8	2.7

Notes: (1) Ti-6Al-4V anodization conditions were: 20 minutes anodization time, 10 volts 20 ± 2 A/m² initial current density, 283 ± 2K solution temperature, and 5% chromic acid solution with HF. Preanodization treatment #2 was used.

(2) Relative humidity at 298 ± 5K varied from 65 to 80%.

included in Table XXXVI. The single lap bond strength data for thermally aged CA/HF anodized Ti-6Al-4V/Ultem® 2200 20% glass fiber filled polyetherimide (PEIF) are included in Table XXXVII. Bond strengths for primed, anodized Ti-6Al-4V bonds are included in each table.

All of the bond strength data for unprimed bonds for PEI in Table XXXVI were compared by means of f test. Similarly, all of the bond strength data for unprimed bond for PEIF in Table XXXVII were compared by means of the f test. All of the data for unprimed bonds for PEI and PEIF adhesives were compared collectively by means of the f test. PEI/anodized Ti-6Al-4V bond strengths and PEIF/anodized Ti-6Al-4V unprimed bond strengths did not differ significantly. All of the unprimed bonds tested exhibited good structural bond strengths, exceeding the 6.9 MPa structural bond strength criteria by a factor of 2.6 to 5.4. Thermal aging at 443 ± 5K, followed by 2 months aging at 298 ± 5K did not affect bond strength.

T test analysis indicated that the Lica® 44 titanate primer had no significant effect upon bond strength for anodized Ti-6Al-4V PEIF bonds thermally aged 9 months at 443 ± 5K followed by 2 months at 298 ± 5K in a 65 to 80% R.H. environment. However, the Lica® 44 titanate primer significantly affected bond strength for the thermally aged anodized Ti-6Al-4V/PEI bonds, based upon the t test analysis. Average bond strength was 37% lower for the thermally aged, primed bonds as compared to the thermally aged, unprimed

TABLE XXXVI

CA/HF Anodized Ti-6Al-4V/Ultem® 1000 Unfilled Polyetherimide Single Lap Bond Strength Data as a Function of Thermal Aging for Unprimed and Primed Anodized Ti-6Al-4V(1)

Anodized Ti-6Al-4V Description	Bond Aging Conditions(2)	Bond Strength (MPa ± 0.1 MPa)	Average Bond Strength (MPa)	Standard Deviation (MPa)
Unprimed	0.5 months at 298 ± 5K	20.9 33.6 35.2 35.2 40.0 42.1	33.2	6.9
Unprimed	9 months at 443 ± 5k, followed by 2 months at 298 ± 5K	23.5 28.4 30.0 32.0 37.2 37.6	31.4	5.4

Notes: (1) Ti-6Al-4V anodization conditions were: 20 minutes anodization time, 10 volts 20 ± 2 A/m² initial current density, 283 ± 2K solution temperature, and 5% chromic acid solution with HF. Preanodization treatment #2 was used.

(2) Relative humidity at 298 ± 5K varied from 65 to 80%.

TABLE XXXVI (Continued)

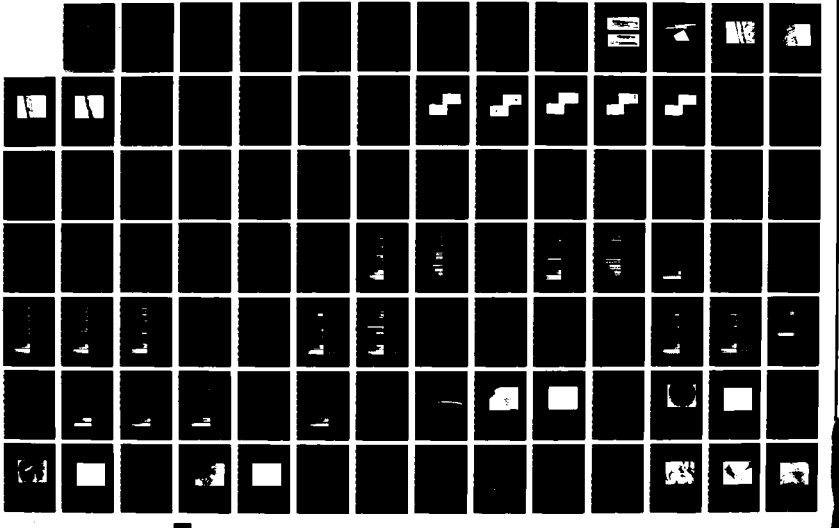
Anodized Ti-6Al-4V Description	Bond Aging Conditions(2)	Bond Strength (MPa ± 0.1 MPa)	Average Bond Strength (MPa)	Standard Deviation (MPa)
Lica® 44 Titanate Primed	9 months at 443 ± 5K, followed by 2 months at 298 ± 5K	12.3 19.2 19.9 21.3 26.8	19.9	5.0

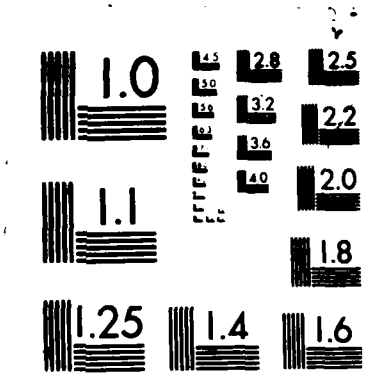
Notes: (1) Ti-6Al-4V anodization conditions were: 20 minutes anodization time, 10 volts 20 ± 2 A/m² initial current density, 283 ± 2K solution temperature, and 5% chromic acid solution with HF. Preanodization treatment #2 was used.

(2) Relative humidity at 298 ± 5K varied from 65 to 80%.

AD-A183 054 AN INTERDISCIPLINARY APPROACH TO PREDICTIVE MODELING OF STRUCTURAL ADHESI (U) VIRGINIA TECH CENTER FOR ADHESION SCIENCE BLACKSBURG J A SKILES ET AL JUN 87 CAS/CHEM-87-2 F/G 11/1 NL

UNCLASSIFIED





MICROCOPY RESOLUTION TEST CHART
NATIONAL BUREAU OF STANDARDS-1963-A

TABLE XXXVII

CA/HF Anodized Ti-6Al-4V/Ultem® 2200, 20% Glass Fiber Filled Polyetherimide Single Lap Bond Strength Data as a Function of Thermal Aging for Unprimed and Primed Anodized Ti-6Al-4V(1)

Anodized Ti-6Al-4V Description	Bond Aging Conditions(2)	Bond Strength (MPa ± 0.1 MPa)	Average Bond Strength (MPa)	Standard Deviation (MPa)
Unprimed	0.5 months at 298 ± 5K	31.2 31.3 32.7 33.4 34.5 35.4	33.1	1.7
Unprimed	9 months at 443 ± 5k, followed by 2 months at 298 ± 5K	27.8 29.9 32.7 33.6 35.4 37.2	32.8	3.5

Notes: (1) Ti-6Al-4V anodization conditions were: 20 minutes anodization time, 10 volts 20 ± 2 A/m² initial current density, 283 ± 2K solution temperature, and 5% chromic acid solution with HF. Preanodization treatment #2 was used.

(2) Relative humidity at 298 ± 5K varied from 65 to 80%.

TABLE XXXVII (Continued)

Anodized Ti-6Al-4V Description	Bond Aging Conditions(2)	Bond Strength (MPa ± 0.1 MPa)	Average Bond Strength (MPa)	Standard Deviation (MPa)
Lica® 44 Titanate Primed	9 months at 443 ± 5K, followed by 2 months at 298 ± 5K	27.7 28.0 28.9 31.9 35.5 39.8	32.0	4.8

Notes: (1) Ti-6Al-4V anodization conditions were: 20 minutes anodization time, 10 volts 20 ± 2 A/m² initial current density, 283 ± 2K solution temperature, and 5% chromic acid solution with HF. Preanodization treatment #2 was used.

(2) Relative humidity at 298 ± 5K varied from 65 to 80%.

bonds, as shown in Table XXXVI. Even so, the thermally aged, primed anodized Ti-6Al-4V PEI bonds had good structural strength; the average strength was 19.9 MPa.

Lica® 44 may have reduced van der Waals forces between the PEI adhesive and the primed anodized Ti-6Al-4V, thereby reducing bond strength. Repulsion forces between the nitrogen in the adhesive imide linkage and the nitrogen in the amine end groups of the titanate may have developed. Since van der Waals forces are highly sensitive to intermolecular distances, the repulsion force between adhesive and adherend would reduce van der Waals forces and bond strength would be reduced. In the case of the primed adherend bonded to the PEIF adhesive, which is 20% glass filled, physical forces between the titanate primed adherend and glass may have developed, resulting in good bond strength, comparable to the unprimed bonds for PEIF.

Unprimed and primed PEIF bond strengths and the unprimed PEI bond strengths were comparable. Apparently, the flow of the thermoplastic resin into the anodic oxide was not hindered by the 20% by weight glass fiber filler.

The use of a 20% glass fiber filled polyetherimide, rather than unfilled polyetherimide, could be especially beneficial in structural bonds where thermal expansion mismatch must be minimized between the titanium alloy and polymer. Recall from Table XII that the thermal expansion coefficient of PEI is $6.2 \times 10^{-5}/K$,

whereas for PEIF it is 2.5 X 10^{-5}/K. The titanium alloy thermal expansion coefficient is 1.2 X 10^{-5}/K.

f. The Influence of the Heat Resistant Adhesive upon Single Lap Bond Strength

Figure 30 illustrates the CA/HF anodized Ti-6Al-4V single lap bond strength data for the six heat resistant adhesives tested after 0.5 month at 298 ± 5K in a 65 to 80% R.H. environment. The anodization conditions were held constant. The preferred anodization method was used at a solution temperature of 283 ± 2K.

These data in Figure 30 were compared by means of the f test analysis. Good single lap bond strengths, which were similar in values, were measured for the following heat resistant adhesives:

1. Udel® polysulfone (PS),
2. polyphenylquinoxaline (PPQ),
3. Ultem® 1000 unfilled polyetherimide (PEI),
4. Ultem® 2200, 20% glass filled polyetherimide (PEIF), and
5. Victerex® polyethersulfone (PES).

The Ablebond® 71-3, 50% $CaCO_3$ filled polyimide bond strengths were significantly lower than for any of the adhesives tested. This polyimide would not be considered for structural type bonding to CA/HF anodized Ti-6Al-4V. In retrospect, reasons for the low bond strengths discussed earlier should also include competition of the polyimide for $CaCO_3$ and the oxide.

Figure 31 illustrates the unprimed and Lica® 44 primed CA/HF anodized Ti-6Al-4V single lap bond strength data for the six

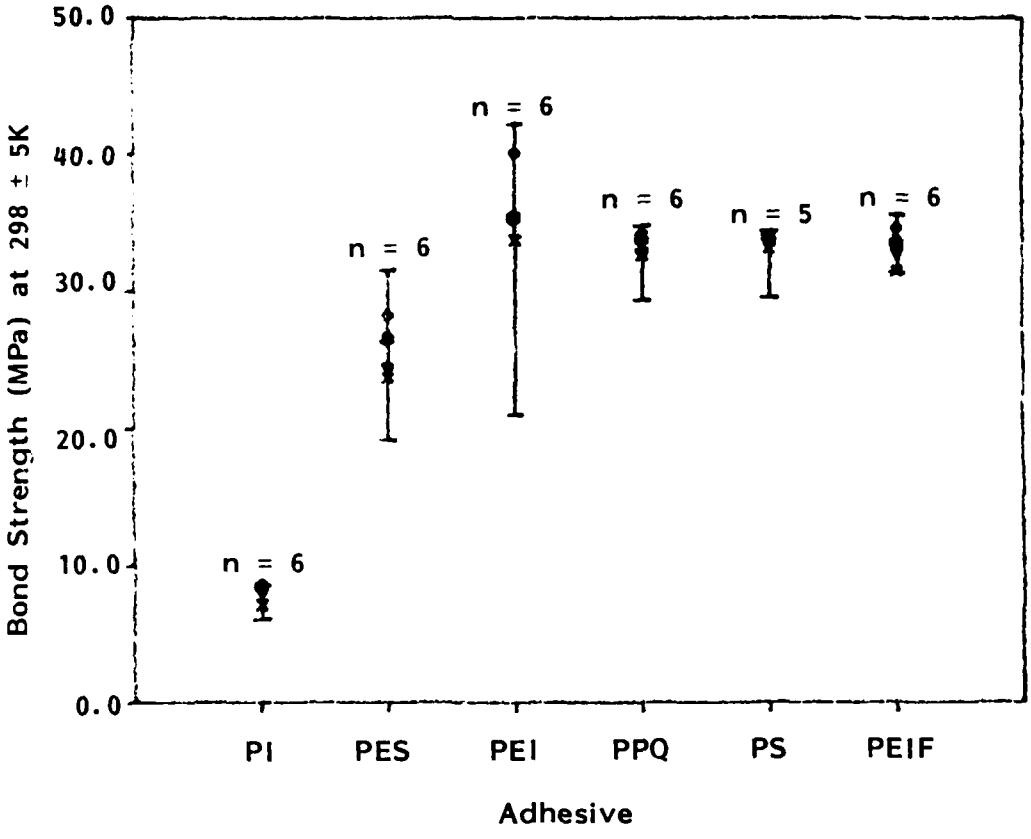


Figure 30. Single Lap Bond Strengths for Heat Resistant Adhesives Bonded to CA/HF Anodized Ti-6Al-4V Tested After 0.5 mo. at 298 ± 5K in a 65 to 80% R.H. Environment.

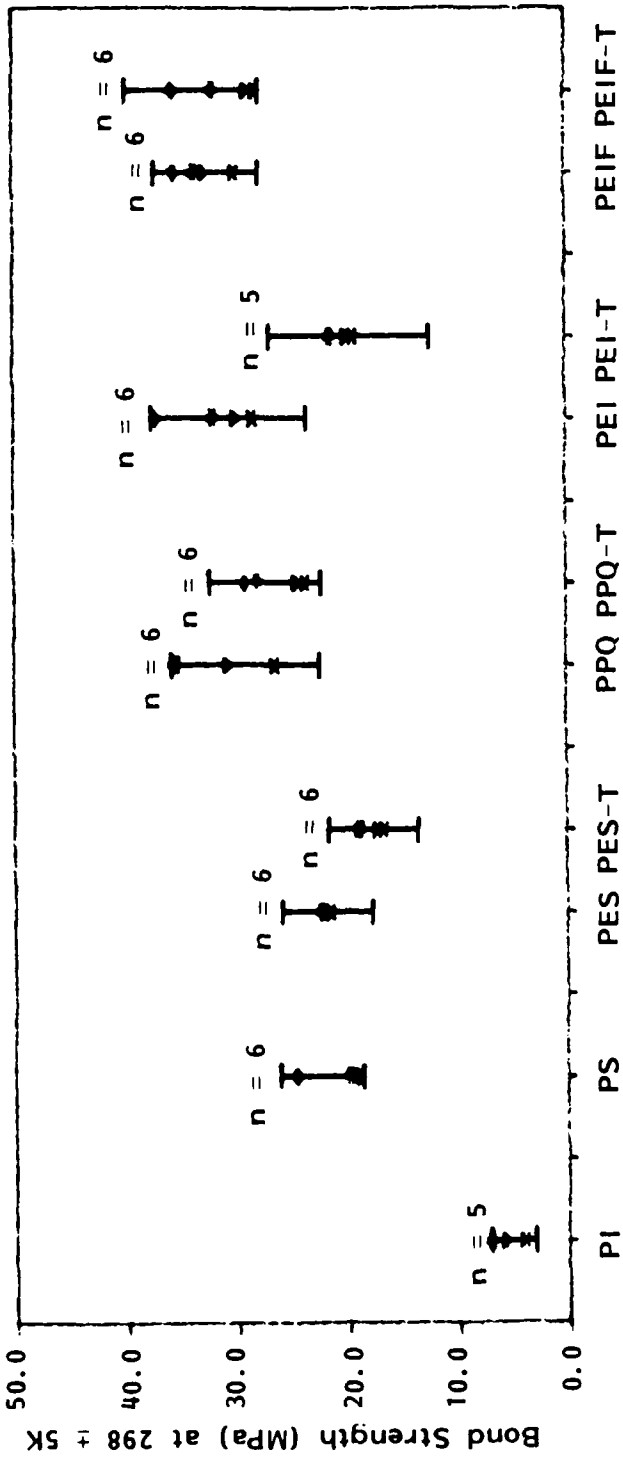


Figure 31. Single Lap Bond Strengths After 9 Months at 443 ± 5K Followed by 2 Months at 298 ± 5K in a 65 to 80% R.H. Environment for Heat Resistant Adhesives Bonded to Unprimed and to Lica® 44 Titanate Primed CA/HF Anodized Ti-6Al-4V.

heat resistant adhesives tested. These bonds were tested after 9 months at 443 ± 5K, followed by 2 months at 298 ± 5K in a 65 to 80% R.H. environment. The preferred Ti-6Al-4V anodization process at 283 ± 2K was used for all except for the polysulfone bonds. As discussed earlier, the PS bonding was conducted prior to the development of the preferred anodization process.

The unprimed bond strength data for all six adhesives tested after the 443 ± 5K/298 ± 5K thermal aging were compared by the f test analysis. The best bond strengths, which were statistically similar, were for PPQ, PEI, and PEIF. Bond strengths were statistically similar for PS and PES adhesives, and lower than for PPQ, PEI and PEIF. The filled PI had the lowest, and the only nonstructural, average bond strength.

The primed bond strength data for the four adhesives tested after the 443 ± 5K/298 ± 5K thermal aging were compared by means of the f test analysis. The best primed bond strengths, which were statistically similar, were for the PPQ and PEIF adhesives. The PES and PEI adhesives produced bond strengths which were statistically similar, but lower than for PPQ and PEIF adhesives.

C. Failure Analyses for Single Lap Bonds

1. Fracture Initiation

a. Photographic Analyses

Figure 32 illustrates sequential, high speed photographs of the fracture of a single lap bond during testing. These photographs suggest that fracture initiated in the polymer, or adhesive, fillet. These photographs definitely show fracture propagating into the bond overlap.

Figure 33 is a photograph of a single lap bond after initial failure has occurred, but prior to complete separation of the fracture surfaces. It can be seen that fracture has initiated in each of the two adhesive fillets for the single lap bond. And, it appears that fracture propagated from both bond edges through the bond, in a diagonal path, to the center of the bond. This fracture pattern is expected since even with the adhesive fillet, there are high peel stresses at the bond edges.

b. SEM Analyses

Low magnification SEM micrographs of fractured bond surfaces, specifically for the region of the bond overlap adjacent to adhesive fillet, are shown in Figures 34 through 37. These micrographs illustrate that fracture initiated in the adhesive fillet for the CA/HF anodized Ti-6Al-4V/adhesive single lap bond and the cracks in the single lap adhesive which propagate toward the bond

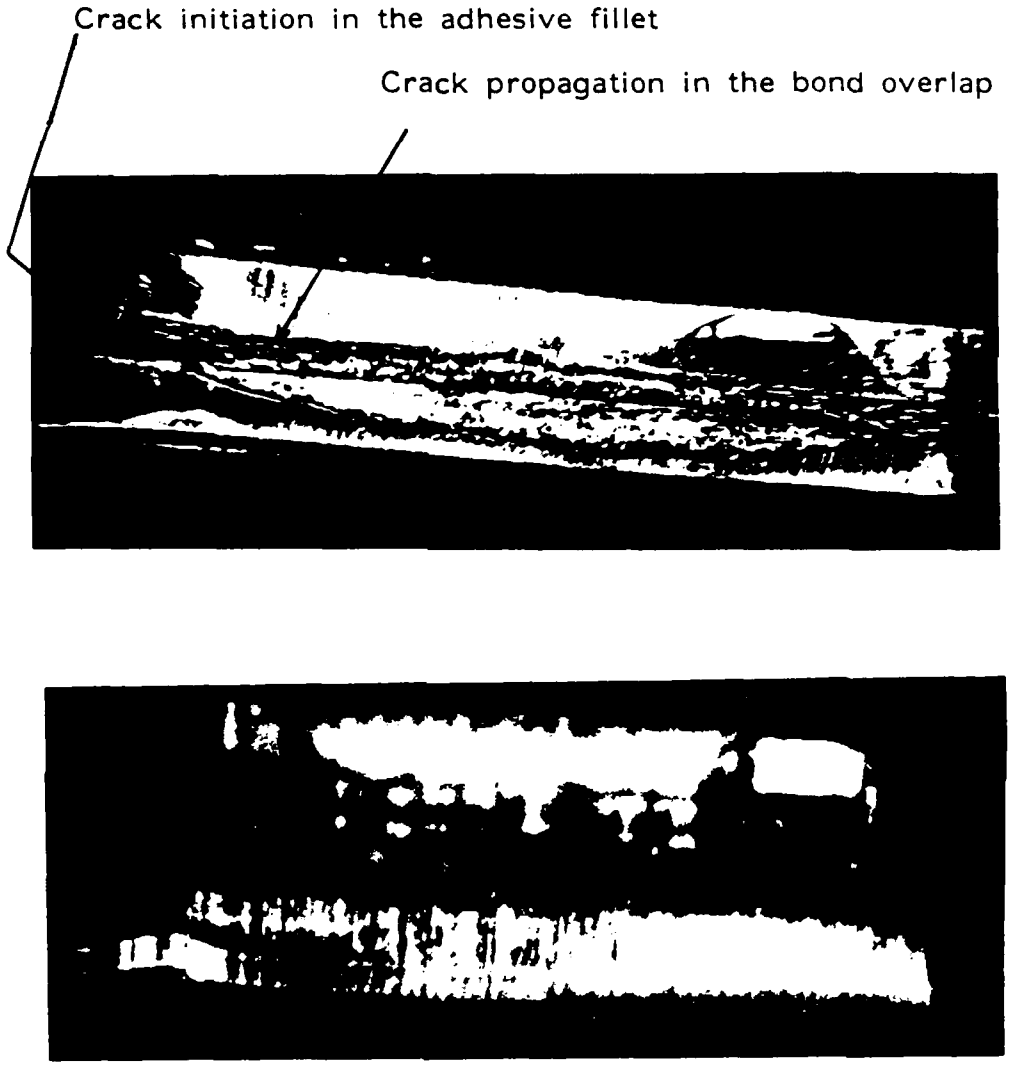


Figure 32. High Speed Photographs of the Single Lap Bond Fracture During Test (8X).

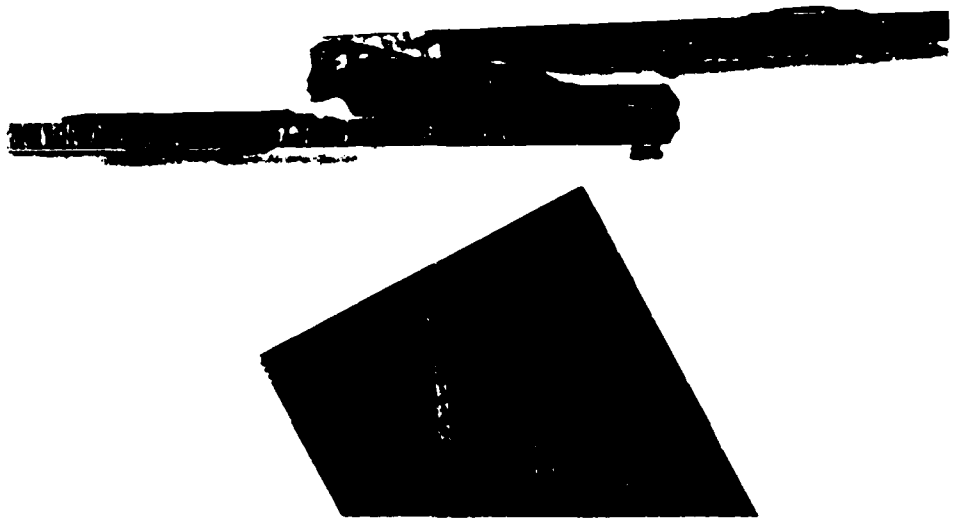


Figure 33. Photograph of Fractured Single Lap Bond (2X).

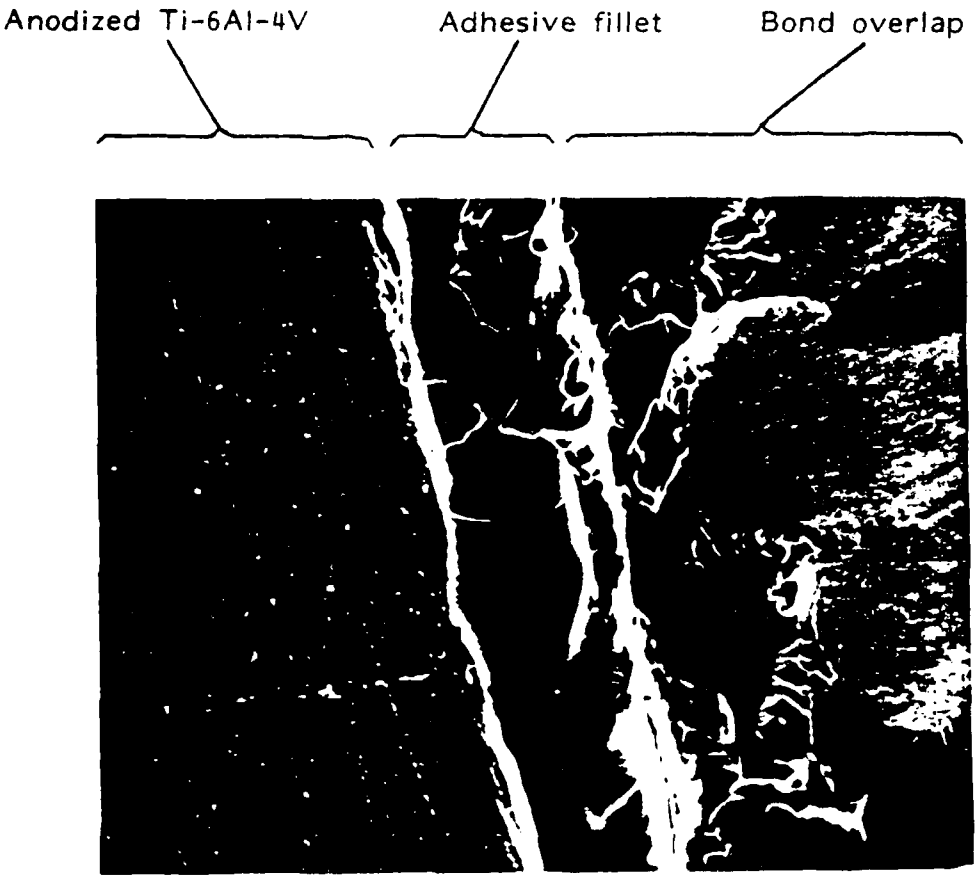


Figure 34. SEM Micrograph of a Fracture Surface for a CA/HF Anodized Ti-6Al-4V/Polyphenylquinoxaline Single Lap Bond (60X).

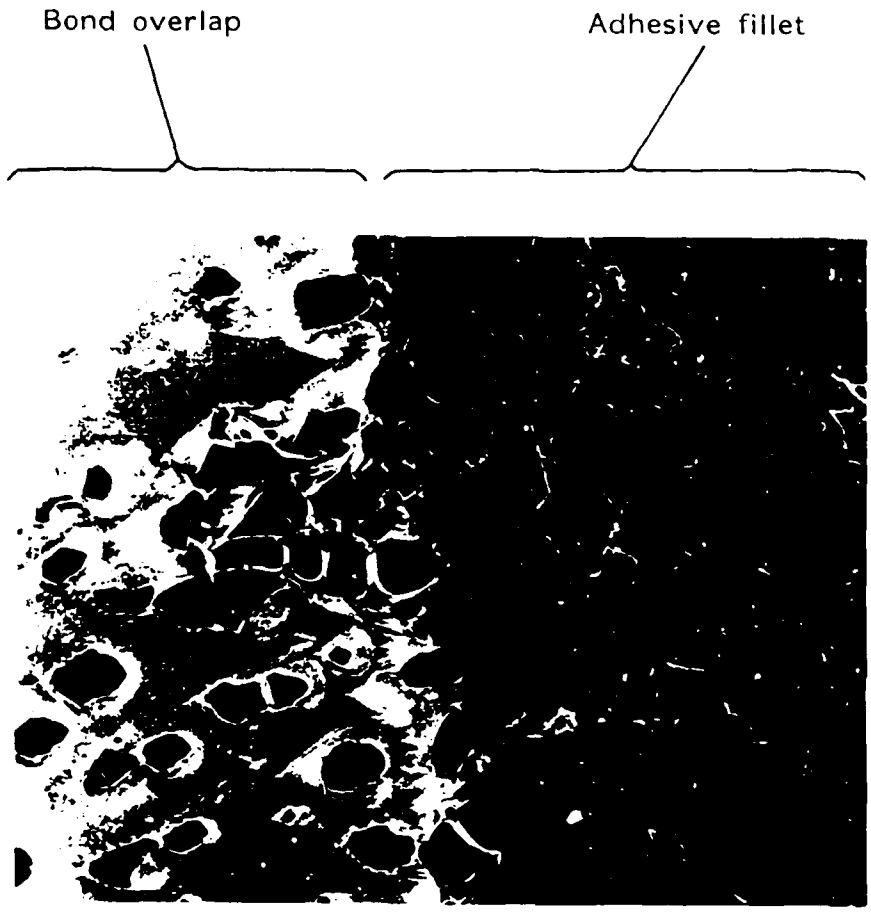


Figure 35. SEM Micrograph of a Fracture Surface for a CA/HF Anodized Ti-6Al-4V/Polysulfone Single Lap Bond (12X).

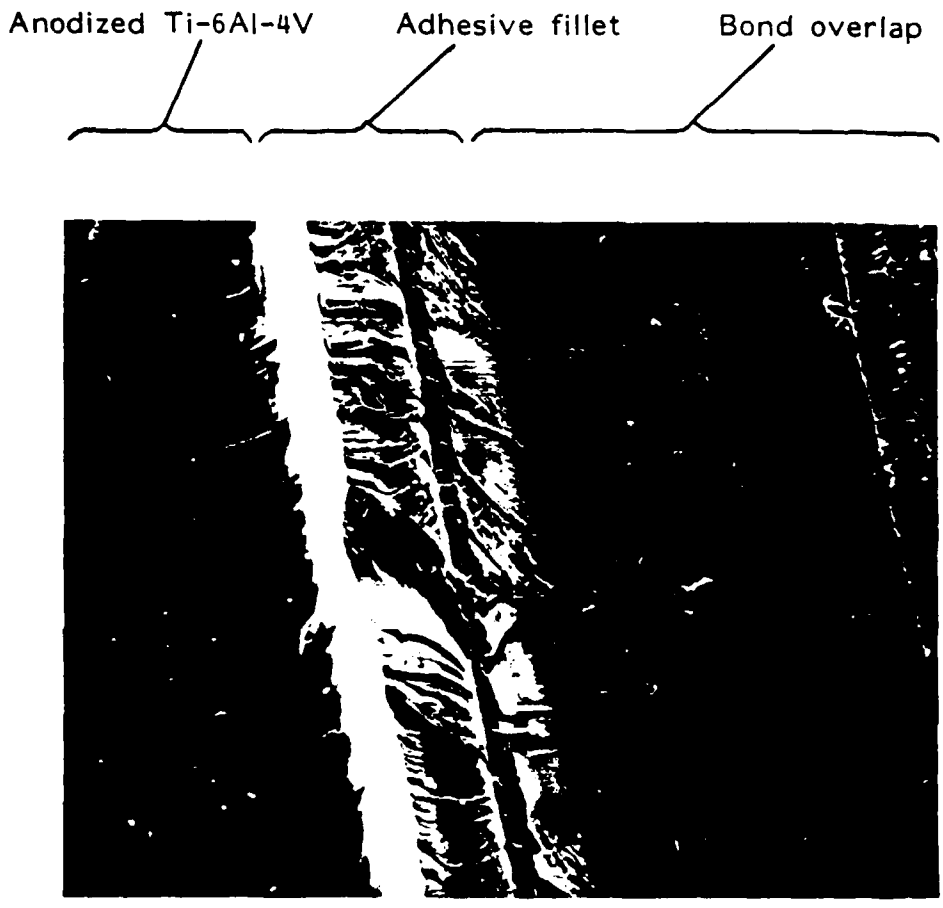


Figure 36. SEM Micrograph of a Fracture Surface for a CA/HF Anodized Ti-6Al-4V/Polyethersulfone Single Lap Bond (30X).

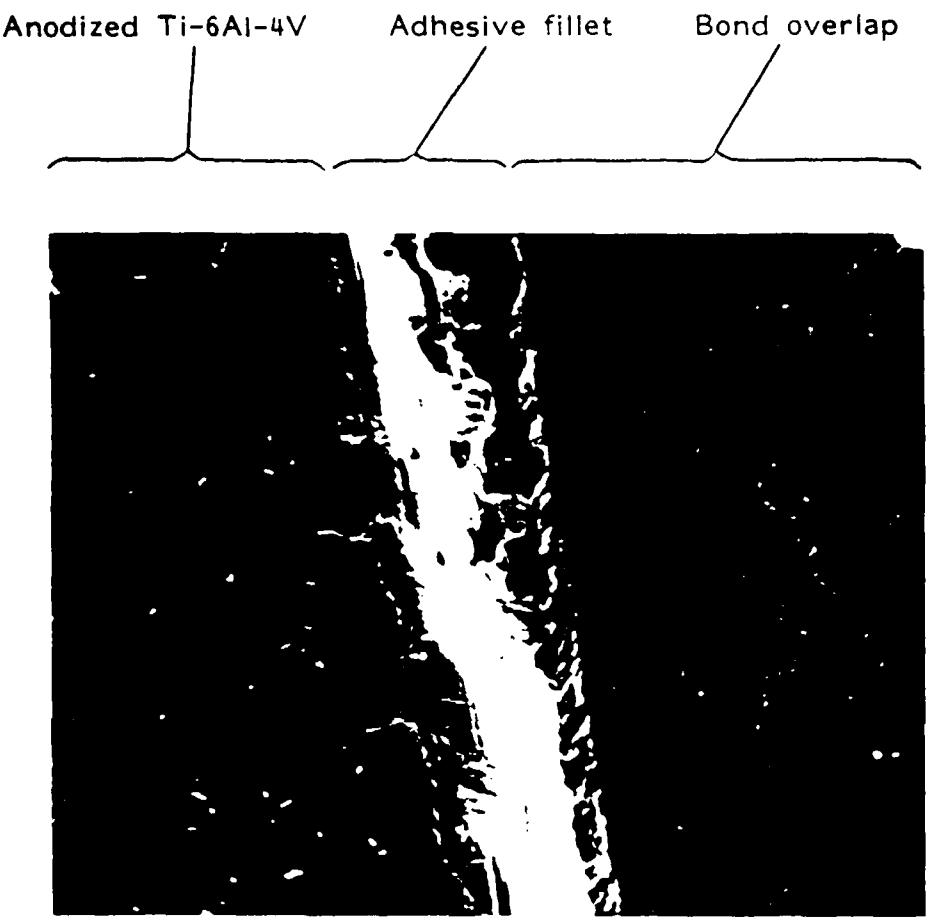


Figure 37. SEM Micrograph of a Fracture Surface for a CA/HF Anodized Ti-6Al-4V/20% Glass Fiber Filled Polyetherimide Single Lap Bond (30X).

overlap area. At the bond overlap adjacent to the fillet, polymer has been deformed in the direction of the applied test load, away from the fillet region, as would be expected if failure initiated in the fillet.

c. Failure Initiation Mechanism

As shown in the SEM micrographs previously described, fracture initiated in the adhesive fillet for the single lap bond. The mechanics of this fracture initiation are described below.

Figure 28 illustrates the forces -- tensile, shear, and peel -- acting upon the single lap bond during test. A qualitative representation of the stress distribution across the bond is also shown in Figure 28. It can be seen that stresses increase parabolically at the ends of the bond overlap and in the polymer fillet, primarily due to peel stress concentrations.

Peel and tensile stresses develop at the end of the bond overlap when a tensile load is applied to the single lap bond. This is because the single lap bond attempts to maximize its alignment with the axis of the applied tensile load, as shown in Figure 28. The peel stresses also cause a tensile stress to develop in the bond overlap and in the adjacent adhesive fillet. Because the adhesive fillet is outside the bond overlap, stress is greatest in this region, causing fracture initiation in the adhesive fillet.

It is recognized that the stress at which fracture initiation in the single lap bond adhesive fillet occurs, on a microscopic level,

may vary for each single lap test, due to varying stress concentrations. Although it was not observed in this study, it is possible that microscopic deformities in the adhesive fillet may develop due to air bubble entrapment in the adhesive, and this may be a source of both stress concentration and failure initiation in the adhesive. Also, thermal mismatch between the metal jig, metal adherend, and polymer, and/or nonuniform polymer cooling, could also induce stress concentrations and fracture in the adhesive fillet when the single lap bond is tested.

2. Fracture Propagation

a. Proposed Model for the CA/HF Anodized Ti-6Al-4V/ Adhesive Bond

Figure 23 represents a model of adhesion for the single lap joint. Interphase regions, rather that definitive interfacial boundaries, are incorporated into this model. The interphase region,[49] best describes the boundary conditions between bulk metal, metal oxide and polymer. Due to the nature of the anodization process, which erodes the Ti-6Al-4V surface, there is a transition from base metal to anodic oxide. Adhesive is assumed to flow into the anodic oxide columnar structures; this results in an interphase transition region which is included between the bulk metal and the bulk adhesion.

Based upon this model, there are four possible failure paths for the single lap bond. The failure paths are:

1. metal cohesive;
2. metal - anodic oxide interphase;
3. anodic oxide - polymer interphase; and,
4. polymer cohesive.

Fracture could occur at any one or all of these locations for the single lap bond.

For a primed anodized Ti-6Al-4V/heat resistant adhesive bond, the model for adhesion must be modified slightly. The modified adhesion model is depicted in Figure 38. Possible failure sites listed earlier, three additional failure sites are:

1. metal cohesive;
2. metal - primed anodic oxide interphase;
3. primed anodic oxide - polymer interphase;
4. primer cohesive;
5. primer - polymer interphase; and,
6. polymer cohesive.

The models in Figures 23 and 38 are suited to describe a thermoplastic bond to either primed or unprimed anodic oxide where van der Waals and H-bonding forces, and/or mechanical interlock forces are possible. These models are equally well suited to describe a thermoset/anodic oxide bond, where chemical bonding of the thermoset and oxide is possible. The models assume that polymer viscosity is sufficiently low during the bonding process to achieve flow to the bottom of the oxide pores, and if necessary, displace primer not chemically bonded to the oxide pore walls.

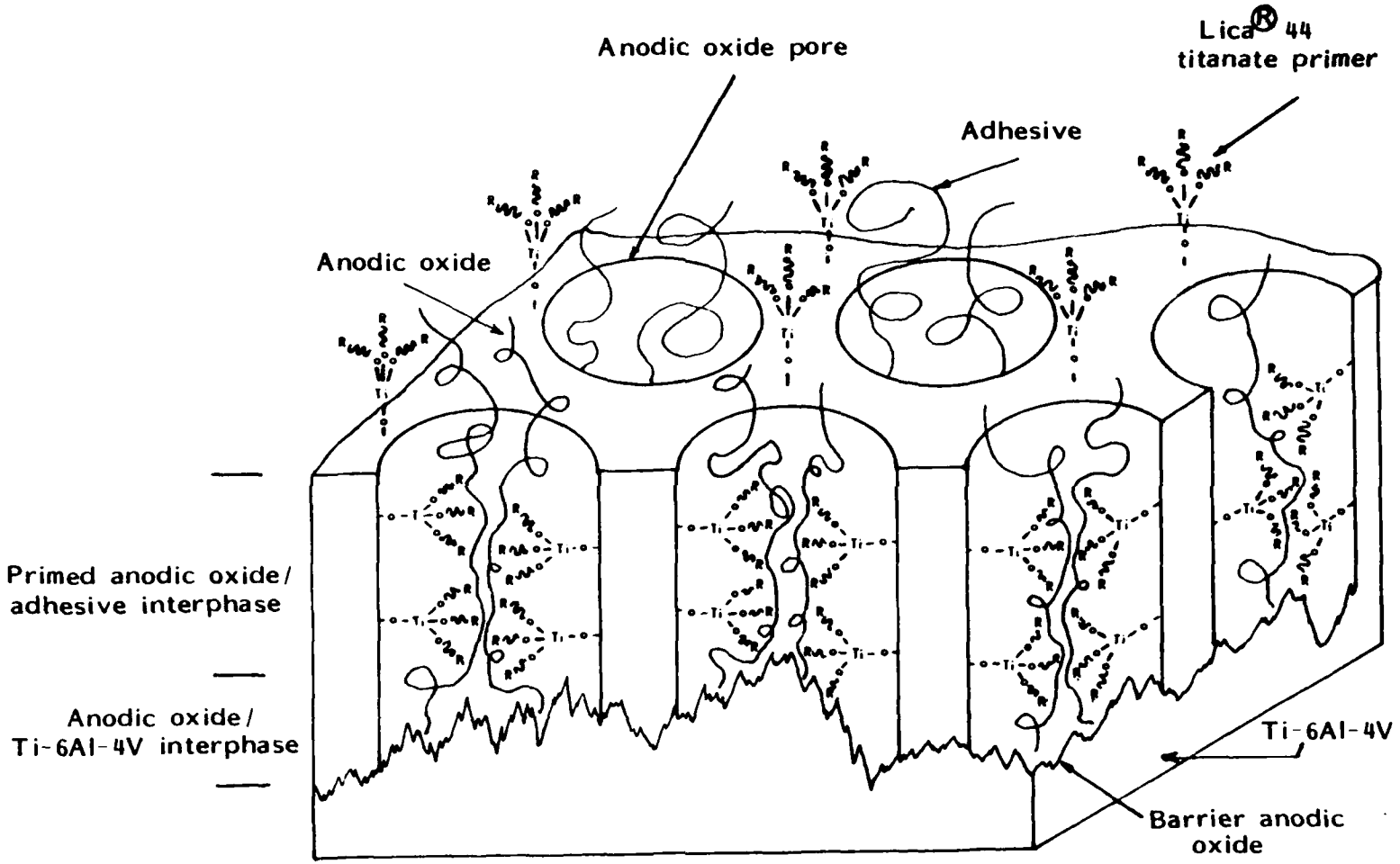


Figure 38. Proposed Model for the Primed, CA/HF Anodized Ti-6Al-4V Adhesive Bond.

The models of adhesion depicted in Figures 23 and 38 are central to the understanding of failure propagation for the anodized Ti-6Al-4V/heat resistant adhesive single lap bond. Once the bond failure paths are determined and described by the model, then a failure mechanism can be proposed. Most of the remaining text is dedicated to the description of the bond failure sites and the bond failure mechanism.

b. Visual Analyses of the Fractured Chromic Acid Anodized Ti-6Al-4V/Adhesive Single Lap Bond

Figures 39 through 43 are photographs of the five visually distinguishable, apparent fracture paths for the unprimed chromic acid anodized Ti-6Al-4V/adhesive single lap bond. These fractured bonds were selected so as to best illustrate the visually apparent fracture sites, irrespective of the heat resistant adhesive or the anodization procedure. Apparent failure sites illustrated by these photographs can be described as follows.

Apparent failure I is an apparent polymer/anodic oxide interphase failure that is confined to one of the two fracture surfaces. This is often referred to as apparent "polymer slick-off" failure.

Apparent failure II is a random distribution on both fracture surfaces of both apparent polymer/anodic oxide interphase failure and polymer cohesive failure.

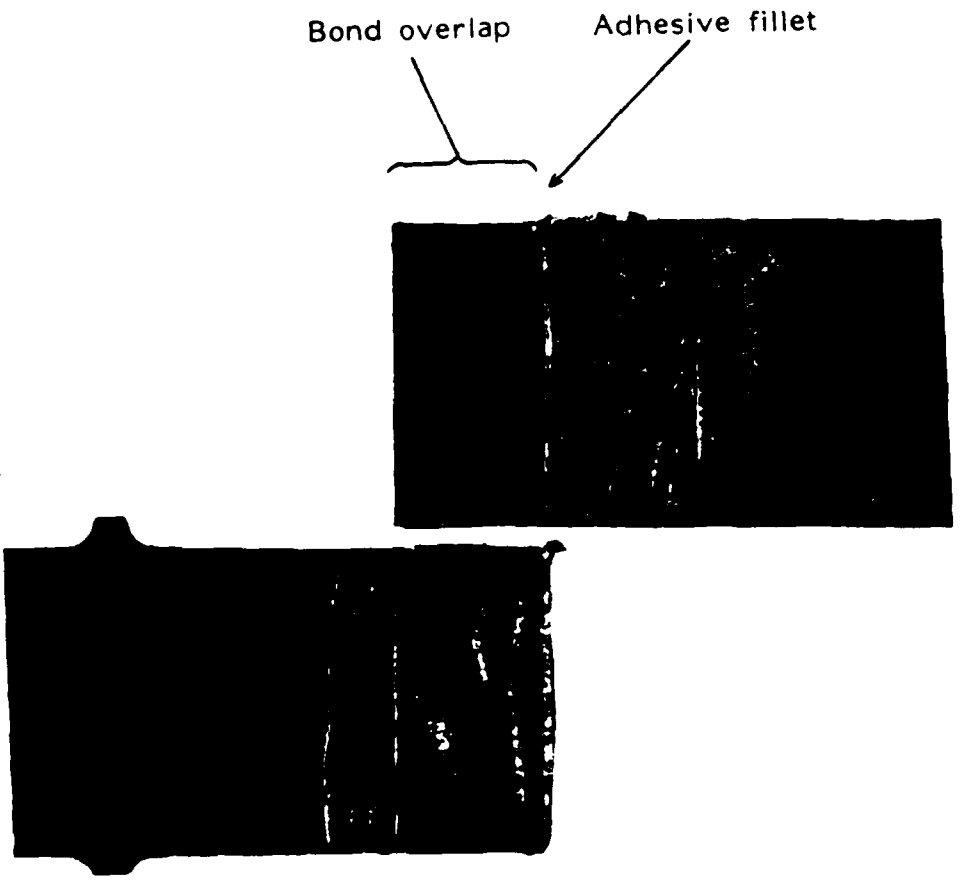


Figure 39. Photograph of a Fracture Surface for a Single Lap Bond Illustrating Apparent Failure I.

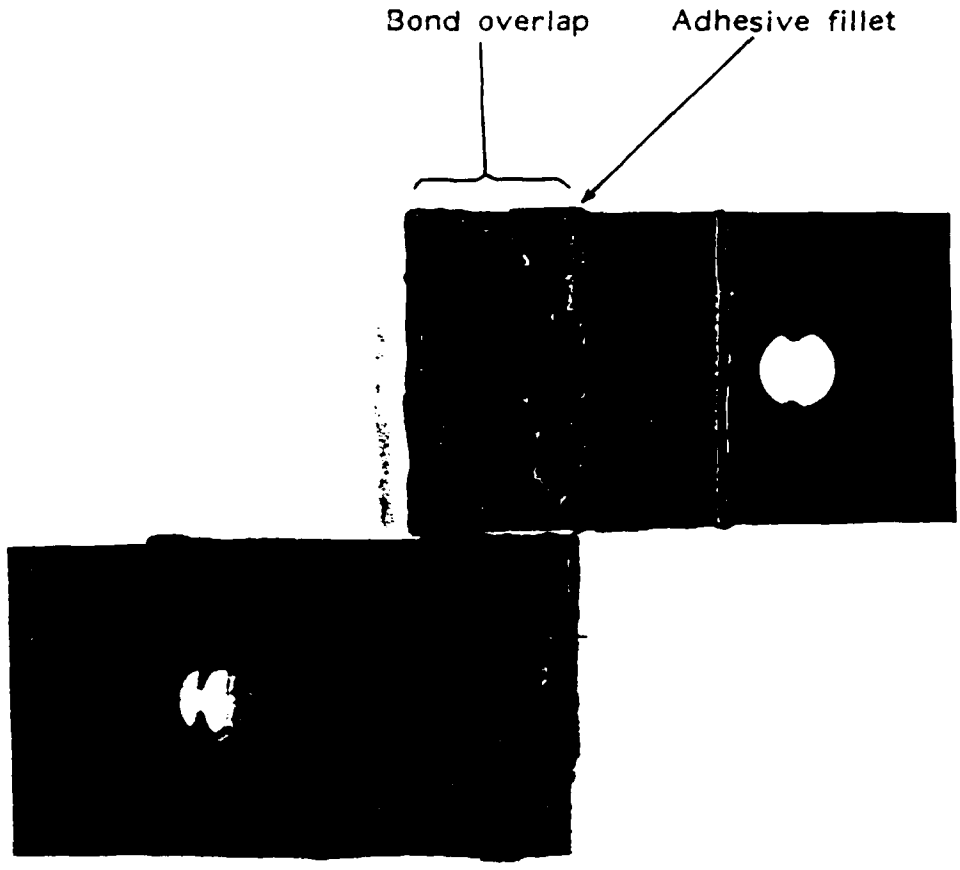


Figure 40. Photograph of a Fracture Surface for a Single Lap Bond Illustrating Apparent Failure II.

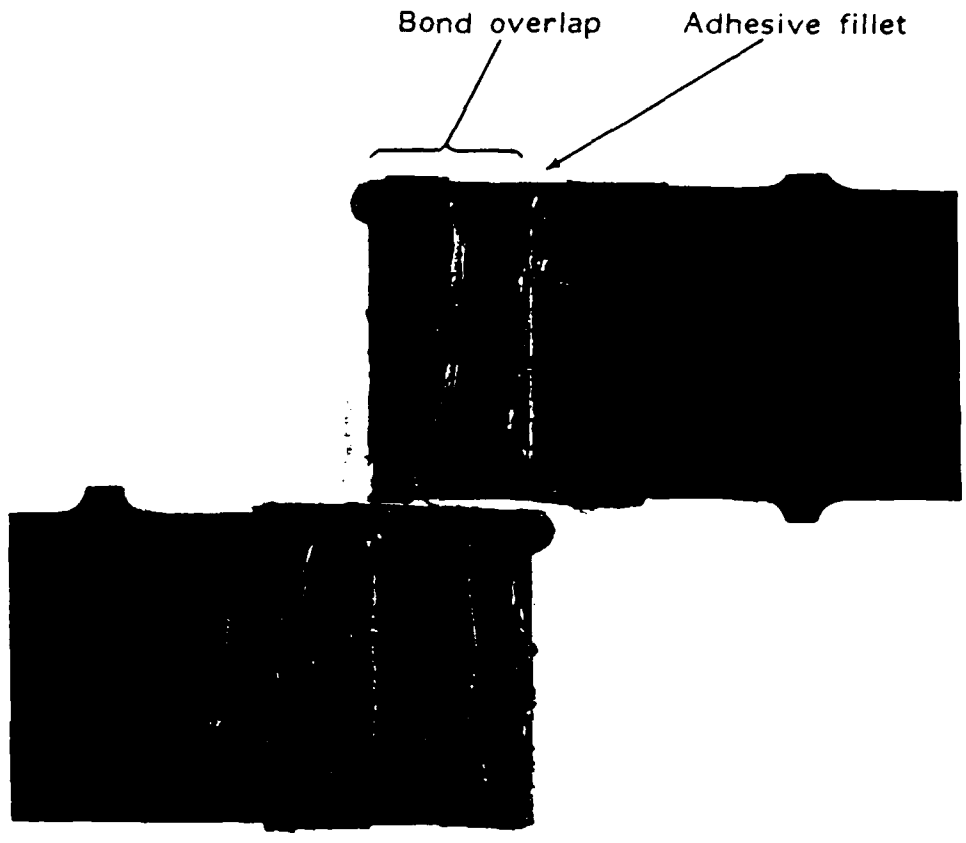


Figure 41. Photograph of a Fracture Surface for a Single Lap Bond Illustrating Apparent Failure III.

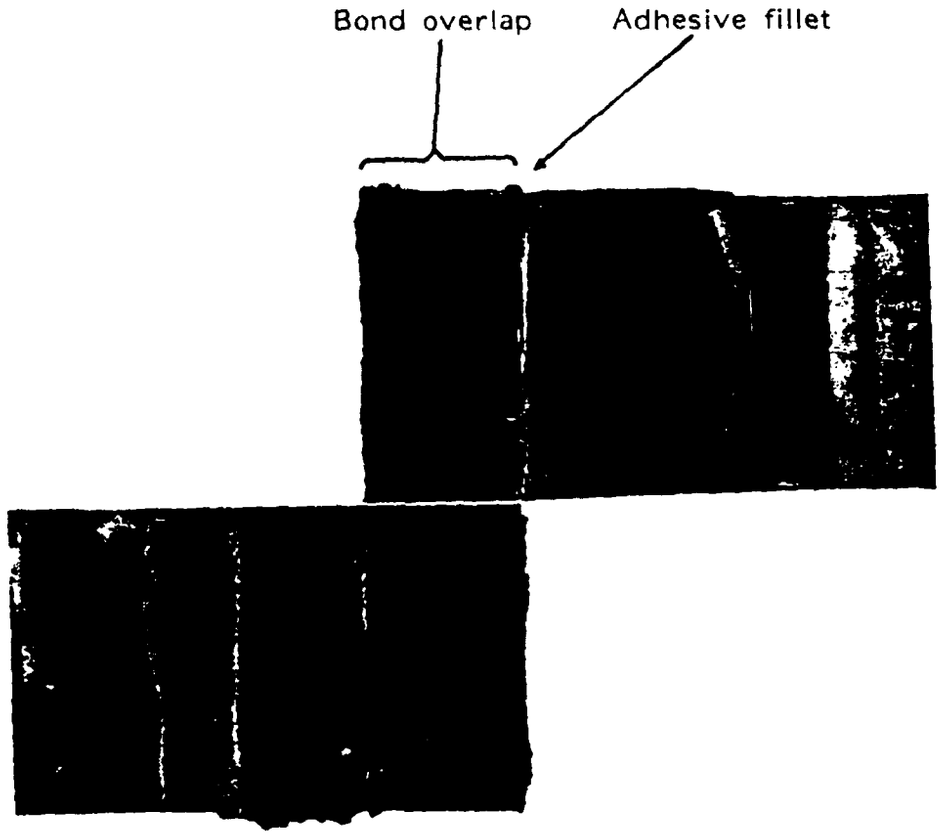


Figure 42. Photograph of a Fracture Surface for a Single Lap Bond Illustrating Apparent Failure IV.

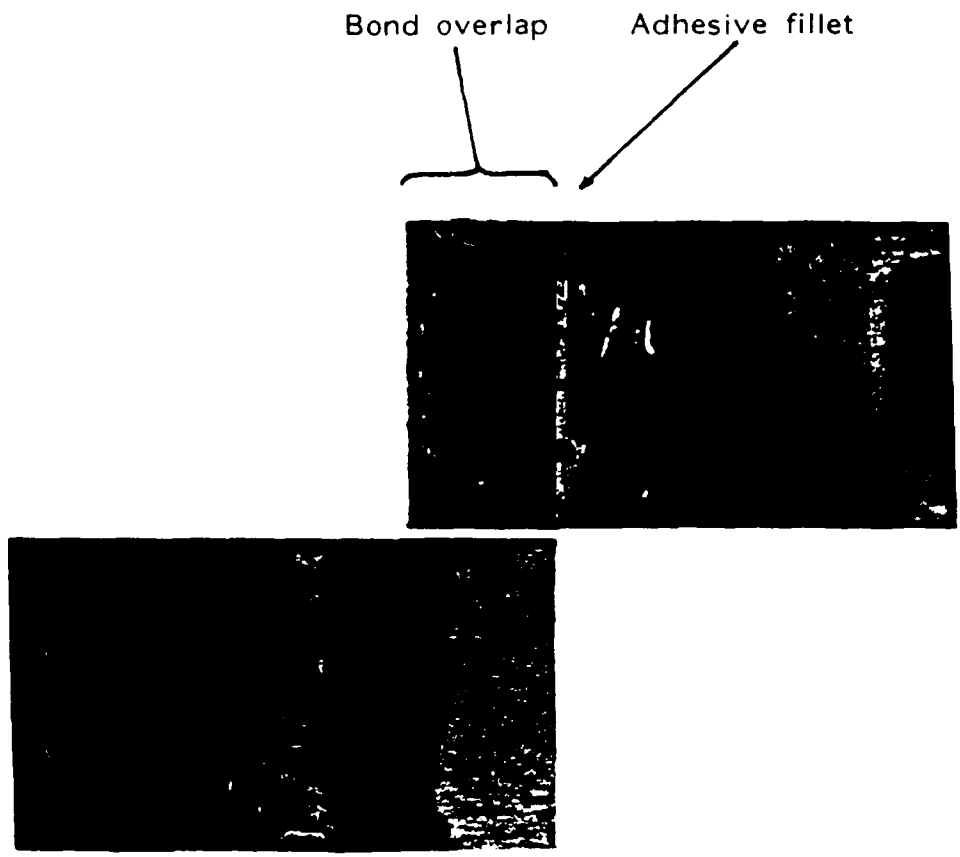


Figure 43. Photograph of a Fracture Surface for a Single Lap Bond Illustrating Apparent Failure V.

Apparent failure III is a definitive, patterned distribution on both fracture surfaces of apparent polymer/anodic oxide interphase failure and polymer cohesive failure.

Apparent fracture IV is an apparent metal/anodic oxide interphase failure that is confined to one of the two fracture surfaces. This failure mechanism could be referred to as apparent "anodic oxide slick-off."

Apparent failure V is a combination of both apparent polymer cohesive failure and apparent metal/anodic oxide interphase failure. This failure mode was confined to one of two fracture surfaces of a single lap bond.

Each fractured chromic acid anodized Ti-6Al-4V/heat resistant adhesive single lap bond was visually examined and each fracture surface categorized as described above. These data are described in Table XXXVIII. An apparent failure site (path) was not unique to any one heat resistant adhesive tested in the single lap bonds. Nor was an apparent failure unique to any one Ti-6Al-4V chromic acid anodization procedure tested.

The predominant failure can be described by apparent failure II, which was a random distribution on both fracture surfaces of both polymer/anodic oxide interphase failure and polymer cohesive failure.

TABLE XXXVIII

Apparent Fracture Sites for Anodized Ti-6Al-4V/Heat Resistant Adhesive

Single Lap Bonds, Based Upon Visual Analysis

Preanodization Treatment	Ti-6Al-4V Anodization Procedure	Bond Aging Conditions	Number of Bonds Tested	Percentage of Bonds Exhibiting Failure I-V				
				I	II	III	IV	V
Heat Resistant Adhesive: Polysulfone								
1	30 A/m^2, 39V 298K, no HF	0.5 month at 298K	6	50	50			
1	30 A/m^2, 298K Anodized 60 min.	0.5 month at 298K	5		100			
1	30 A/m^2, 298K	2 months at 298K	6		100			
1	30 A/m^2, 298K	9 months at 298K	6		100			

Notes: (1) A chromic acid/HF acid solution and 10 volt potential was used in all cases except for the one case indicated above.

(2) A 20 minute chromic acid/HF anodization time was used, except for the one case indicated above.

(3) Current density reported is the initial current density.

TABLE XXXVIII (Continued)

Preanodization Treatment	Ti-6Al-4V Anodization Procedure	Bond Aging Conditions	Number of Bonds Tested	Percentage of Bonds Exhibiting Failure I-V				
				I	II	III	IV	V
Heat Resistant Adhesive: Polysulfone (Continued)								
1	30 A/m², 298K	9 months at 373K	6	20	80			
1	30 A/m², 298K	9 months at 443K	6	50		50		
1	30 A/m², 298K	0.5 month at 298K	6		100			
2	30 A/m², 298K	0.5 month at 298K	4		100			

Notes: (1) A chromic acid/HF acid solution and 10 volt potential was used in all cases except for the one case indicated above.

(2) A 20 minute chromic acid/HF anodization time was used, except for the one case indicated above.

(3) Current density reported is the initial current density.

TABLE XXXVIII (Continued)

Preanodization Treatment	Ti-6Al-4V Anodization Procedure	Bond Aging Conditions	Number of Bonds Tested	Percentage of Bonds Exhibiting Failure I-V				
				I	II	III	IV	V
Heat Resistant Adhesive: Polysulfone (Continued)								
2	30 A/m², 283K	0.5 month at 298K	5					100
2	20 A/m², 283K	0.5 month at 298K	5		100			
2	20 A/m², 298K	0.5 month at 298K	6		100			

Notes: (1) A chromic acid/HF acid solution and 10 volt potential was used in all cases except for the one case indicated above.

(2) A 20 minute chromic acid/HF anodization time was used, except for the one case indicated above.

(3) Current density reported is the initial current density.

TABLE XXXVIII (Continued)

Preanodization Treatment	Ti-6Al-4V Anodization Procedure	Bond Aging Conditions	Number of Bonds Tested	Percentage of Bonds Exhibiting Failure I-V				
				I	II	III	IV	V
Heat Resistant Adhesive: Polyphenylquinoxaline								
2	30 A/m², 298K	0.5 month at 298K	6			100		
2	30 A/m², 283K	0.5 month at 298K	6			100		
2	20 A/m², 283K	0.5 month at 298K	6		100			
2*	20 A/m², 283K	0.5 month at 298K	4					100
2	20 A/m², 283K	11 month at 298K	6		70	30		

Notes: (1) Isothermal bonding process was used in all cases except for the one case noted above with an asterisk.

(2) A chromic acid/HF acid solution and 10 volt potential was used in all cases.

(3) Current density reported is initial current density.

TABLE XXXVIII (Continued)

Preanodization Treatment	Ti-6Al-4V Anodization Procedure	Bond Aging Conditions	Number of Bonds Tested	Percentage of Bonds Exhibiting Failure I-V				
				I	II	III	IV	V
Heat Resistant Adhesive: Polyphenylquinoxaline (Continued)								
2	20 A/m², 283K	9 mo. @ 443K followed by 2 mo. @ 298K	6			100		
2	20 A/m², 283K	Lica® 44 Primed, 9 mo. @ 443K followed by 2 mo. @ 298K	6			100		
2	20 A/m². 283K	Air quenched to 298K 7X during 9 mo. @ 505K, followed by 2 mo. @ 298K	6	20	80			

Notes: (1) Isothermal bonding process was used in all cases except for the one case noted above with an asterisk.

(2) A chromic acid/HF acid solution and 10 volt potential was used in all cases.

(3) Current density reported is initial current density.

TABLE XXXVIII (Continued)

Preanodization Treatment	Ti-6Al-4V Anodization Procedure	Bond Aging Conditions	Number of Bonds Tested	Percentage of Bonds Exhibiting Failure I-V				
				I	II	III	IV	V
Heat Resistant Adhesive: 50% $CaCO_3$ Filled Polyimide								
2	20 A/m², 283K	0.5 mo. @ 298K	6		100			
2	20 A/m², 283K	9 mo. @ 443K followed by 2 mo. @ 298K	6		100			
Heat Resistant Adhesive: Polyethersulfone								
2	20 A/m², 283K	0.5 mo. @ 298K	6		100			
2	20 A/m², 283K	9 mo. @ 443K followed by 2 mo. @ 298K	6	20	30	50		

Notes: (1) A chromic acid/HF acid solution and 10 volt potential was used in all cases.

(2) Current density reported is initial current density.

TABLE XXXVIII (Continued)

Preanodization Treatment	Ti-6Al-4V Anodization Procedure	Bond Aging Conditions	Number of Bonds Tested	Percentage of Bonds Exhibiting Failure I-V				
				I	II	III	IV	V
Heat Resistant Adhesive: Polyethersulfone (Continued)								
2	20 A/m², 283K	Lica® 44 Primed, 9 mo. @ 443K, followed by 2 mo. @ 298K	6	20	20	60		
Heat Resistant Adhesive: Unfilled Polyetherimide								
2	20 A/m², 283K	0.5 mo. @ 298K	6	30			70	
2	20 A/m², 283K	9 mo. @ 443K followed by 2 mo. @ 298K	6	30	70			

Notes: (1) A chromic acid/HF acid solution and 10 volt potential was used in all cases.

(2) Current density reported is initial current density.

TABLE XXXVIII (Continued)

Preanodization Treatment	Ti-6Al-4V Anodization Procedure	Bond Aging Conditions	Number of Bonds Tested	Percentage of Bonds Exhibiting Failure I-V				
				I	II	III	IV	V
Heat Resistant Adhesive: Unfilled Polyetherimide (Continued)								
2	20 A/m², 283K	Lica® 44 Primed, 9 mo. @ 443K, followed by 2 mo. @ 298K	5	30	70			
Heat Resistant Adhesive: 20% Glass Filled Polyetherimide								
2	20 A/m², 283K	0.5 mo. @ 298K	6			20	80	
2	20 A/m², 283K	9 mo. @ 443K followed by 2 mo. @ 298K	6			100		

Notes: (1) A chromic acid/HF acid solution and 10 volt potential was used in all cases.

(2) Current density reported is initial current density.

TABLE XXXVIII (Continued)

Preanodization Treatment	Ti-6Al-4V Anodization Procedure	Bond Aging Conditions	Number of Bonds Tested	Percentage of Bonds Exhibiting Failure I-V				
				I	II	III	IV	V
Heat Resistant Adhesive: 20% Glass Filled Polyetherimide (Continued)								
2	20 A/m², 283K	Lica® 44 Primed, 9 mo. @ 443K, followed by 2 mo. @ 298K	6		70	30		

Notes: (1) A chromic acid/HF acid solution and 10 volt potential was used in all cases.

(2) Current density reported is initial current density.

It is noteworthy that in no case was it visually apparent that polymer cohesive failure was the sole fracture site for any fractured single lap bond. There was always an apparent interphase failure visible on the fractured surfaces.

It should be noted that these categories discussed above are specific for the unprimed chromic acid anodized Ti-6Al-4V/adhesive fracture surfaces. Fracture surfaces for primed bonds were also described by these categories. Since the Lica® 44 primer is clear, it would be indistinguishable on the fracture surfaces. Therefore, visual distinction of primer cohesive failure from polymer/primed anodic oxide interphase failure was not possible. These particular surfaces were arbitrarily categorized as exhibiting polymer/anodic oxide, more specifically, primed anodic oxide, interphase failure.

Visual analysis of the bond fracture sites is only a first approximation of the actual fracture sites. Various analytical methods were used to determine if the failure sites visually observed were valid. These analytical techniques were:

1. optical quantitative imaging analysis,
2. ESCA analysis, and
3. Auger analysis.

Specifically, ESCA and Auger analyses were used to determine if polymer/anodic oxide interphase failure did occur. The results of these analyses are described below.

c. Quantitative Image Analyses

Single lap bond fracture surfaces were examined by Quantitative Image Analysis (QIA). The purpose of the analysis was to determine, based upon surface reflectivity differences, whether any or all of the following could be identified and quantified on the fracture surface:

1. Ti-6Al-4V metal,
2. apparent anodic oxide/polymer interphase, and
3. adhesive.

QIA was first conducted for Ti-6Al-4V and also for CA/HF anodized Ti-6Al-4V. It was determined that bare metal was indistinguishable from the anodic oxide by QIA. Reflectivity was similar for both surfaces. Apparently, incident light transmitted through the thin anodic oxide underwent second surface reflections off the underlying base Ti-6Al-4V metal. These second surface reflections rendered the anodic oxide indistinguishable from bare metal in image analysis.

The isochronally bonded CA/HF anodized Ti-6Al-4V/PPQ single lap bond fracture surfaces were image analyzed. This fracture surface exhibited apparent failure V described earlier. It appeared as if the anodic oxide/polymer interphase from the opposing fracture surface had been transferred to the adhesive on the fracture surface examined by QIA. When the apparent anodic oxide/polymer interphase was on top of the adhesive on the fracture surface, QIA could not distinguish between apparent anodic oxide/

polymer interphase and the adhesive beneath the oxide. Only the adhesive underneath the anodic oxide/polymer interphase was detected. This is because of second surface reflections from the adhesive.

QIA was useful to identify and quantify the surface area of cohesively fractured polymer on the anodized Ti-6Al-4V single lap bond fracture surfaces. The QIA analyzed polymer surface area data are shown in Tables XXXIX and XL for:

1. both fracture surfaces for a CA/HF anodized Ti-6Al-4V/polysulfone bond with a 33.4 MPa bond strength; and,
2. one fracture surface for a CA/HF anodized Ti-6Al-4V/PPQ isothermally bonded specimen with a 27.7 MPa bond strength.

The surface area calculation was based upon the total pixel number with an associated reflectivity threshold. To determine the polymer area on the fracture surface, it was easier to measure the apparent anodic oxide/polymer interphase area on the fracture surface. This is because of the high reflectivity of the base metal underlying this interphase surface. The polymer surface area was then calculated based upon the total number of pixels examined and the fraction examined which represented the apparent anodic oxide/polymer interphase surface area.

The data indicated that polymer cohesive failure was the primary failure mechanism for these fracture surfaces examined.

TABLE XXXIX

Quantitative Image Analysis for Both Fracture Surfaces of a CA/HF Anodized Ti-6Al-4V/Polysulfone Single Lap Bond

Frame	Number of Pixels Associated with Apparent Anodic Oxide/Polymer Interphase
	Fracture Side A
1	14,512
2	9,196
3	8,032
4	3,308
5	6,155
6	6,000
7	5,903
8	10,066
9	8,782
10	14,022
11	18,143
12	29,255
13	33,319
14	7,230
15	18,279
16	24,261
17	40,999
18	15,047
19	22,287
20	34,341
21	17,252
22	11,254
23	29,753
24	3,484
25	10,216
26	16,945
27	22,138
28	3,822
29	20,646
30	27,525
31	9,183
32	28,941

TABLE XXXIX (Continued)

Frame	Number of Pixels Associated with Apparent Anodic Oxide/Polymer Interphase
Fracture Side A (Continued)	
33	18,140
34	6,889
35	0
36	0
Total Apparent Anodic Oxide/ Polymer Interphase Pixels:	555,328
Total Pixels:	9,437,184
Surface Area of Apparent Anodic Oxide/Polymer Interphase:	5.9%
Surface Area of Polymer:	94.1%

Frame	Number of Pixels Associated with Apparent Anodic Oxide/Polymer Interphase
Fracture Side B	
1	11,144
2	15,097
3	36,936
4	19,071
5	19,603
6	4,362
7	1,947
8	17,346
9	13,270
10	15,013

TABLE XXXIX (Continued)

Frame	Number of Pixels Associated with Apparent Anodic Oxide/Polymer Interphase
Fracture Side B (Continued)	
11	14,691
12	3,696
13	16,955
14	16,497
15	8,889
16	17,792
17	17,427
18	2,760
19	7,938
20	16,242
21	24,597
22	18,599
23	21,344
24	20,340
25	20,827
26	8,137
27	19,270
28	18,219
29	895
30	6,202
31	3,020
32	908
33	2,235
34	0
35	0
36	0
37	0
Total Apparent Anodic Oxide/ Polymer Interphase Pixels:	441,270
Total Pixels:	9,699,328
Surface Area of Apparent Anodic Oxide/Polymer Interphase:	4.5%
Surface Area of Polymer:	95.5%

TABLE XL

Quantitative Image Analysis for One Fracture Surface of a CA/HF Anodized Ti-6Al-4V Polyphenylquinoxaline Single Lap Bond

Frame	Number of Pixels Associated with Apparent Anodic Oxide/Polymer Interphase
1	0
2	0
3	0
4	0
5	2,743
6	0
7	0
8	0
9	5,712
10	0
11	0
12	0
13	0
14	0
15	806
16	0
17	0
18	3,140
19	0
20	0
21	0
22	997
23	0
24	0
25	421
26	0
27	0
28	1,992
29	2,741
30	2,122
31	1,632
32	47,966
33	2,047
34	10,716

TABLE XL (Continued)

Frame	Number of Pixels Associated with Apparent Anodic Oxide/Polymer Interphase
35	9,733
36	31,177
37	84,560
38	26,525
39	137,570
40	97,260
41	74,240
42	69,929
43	72,751
44	16,644
45	14,968
46	932
47	0
48	24,500
49	86,280
50	173,182
51	198,747
52	257,810
53	233,124
54	243,594
55	236,404
56	192,054
57	229,665
58	167,492
59	203,451
60	110,339
61	104,148
62	169,317
63	135,041
64	133,100
65	178,900
66	156,400
67	129,700
68	145,700
69	27,493
70	67,560
71	3,180

TABLE XL (Continued)

Total Apparent Anodic Oxide/ Polymer Interphase:	4,326.505
Total Pixels:	18,612,224
Surface Area of Apparent Anodic Oxide/Polymer Interphase:	23.2%
Surface Area of Polymer:	76.8%

Seventy seven percent or greater of the fracture surface area was composed of the respective polymer. These QIA data confirmed the qualitative visual analyses of the fracture sites

Fracture surfaces for only these two types of chromic acid/HF anodized Ti-6Al-4V/adhesive single lap bonds were examined by QIA because of the previously described limitations of the image analysis technique for the fracture surface, which is the inability to distinguish the anodic oxide from either the underlying metal substrate or the underlying adhesive.

d. ESCA Analyses

The purpose of the ESCA surface analyses was to examine fracture surfaces so as to determine if the apparent interphase failures, as described by visual analyses and described earlier in the text, were valid on a microscopic scale. For these ESCA analyzed surfaces, there was little or no polymer observed. ESCA analyses are confined to the first 10 nm of the surface analyzed and are sensitive to approximately a 1% concentration of an element. ESCA identifies and quantifies the surface elements for the entire surface; the element location on the surface is not identified.

Approximately 10% of the total fracture surface area from a given single lap bond was analyzed. In general, only one half of any selected single lap bond pair was analyzed.

ESCA was conducted not only for chromic acid anodized Ti-6Al-4V/heat resistant adhesive single lap bonds which exhibited

apparent interphase failure, but also for appropriate controls. These controls were: Ti-6Al-4V cleaned per preanodization treatment #1 or #2, anodized Ti-6Al-4V, Lica® 44 titanate primer, and each of the heat resistant adhesives.

These ESCA data were tabulated in Appendix VII. These tabulated data include the element identity, average quantity, and the binding energy of elements detected on the surface analyzed. Based upon these binding energy data, the chemical state of detected elements were also determined.

Selected concentration and binding energy data from Appendix VII are graphically shown in Figures 44 through 53 and 55 through 61. These data in Figures 44 through 53 and 55 through 61 typify the data in Appendix VII and should be referred to in the following discussion. These graphs include ESCA data for cleaned Ti-6Al-4V, anodized Ti-6Al-4V, the heat resistant adhesives included in this study, and single lap bond fracture surfaces for all of the heat resistant adhesives tested.

As shown in these graphs, carbon and oxygen are the major surface constituents and result in part from atmospheric exposure or from the adhesive primer. Aluminum and silicon were detected on many, but not all, of the surfaces analyzed. The aluminum is attributed to the ESCA aluminum sample mount and not to the base Ti-6Al-4V metal. The silicon may be due to contamination in the ESCA analyzer itself.

Nitrogen was detected on both the cleaned, and anodized Ti-6Al-4V surfaces and fracture surfaces. For the fracture surfaces, there were two possible nitrogen sources - nitrogen chemisorbed from the atmosphere and/or nitrogen from the PPQ, PEI or PI adhesive, when used. Since both types of nitrogen had the same corrected binding energy, this could not be used to determine the nitrogen source. However, based upon nitrogen concentration, it was possible to assign the nitrogen source, as will be discussed later in this text.

Based upon the data in Figures 44 and 45, Ti-6Al-4V, cleaned per preanodization treatment #1 or #2, and cleaned and anodized Ti-6Al-4V were characterized by ESCA as follows.

1. The Ti-6Al-4V preanodization treatments did not introduce a contaminant to the Ti-6Al-4V surface.
2. The cleaned and anodized Ti-6Al-4V surfaces contained TiO_2. The Ti 2p1/2 and Ti 2p3/2 corrected binding energies and the 5.7 to 5.8 eV separation between the Ti 2p1/2 and Ti 2p3/2 peaks indicated a TiO_2 chemical state.
3. The chromic acid anodized Ti-6Al-4V surface and chromic acid/HF anodized Ti-6Al-4V surfaces differed in one respect. Low levels of fluorine, $\leq$ 3%, were detected on the chromic acid/HF anodized surface but not on the chromic acid anodized surface. Both organic and inorganic fluorine were present, as

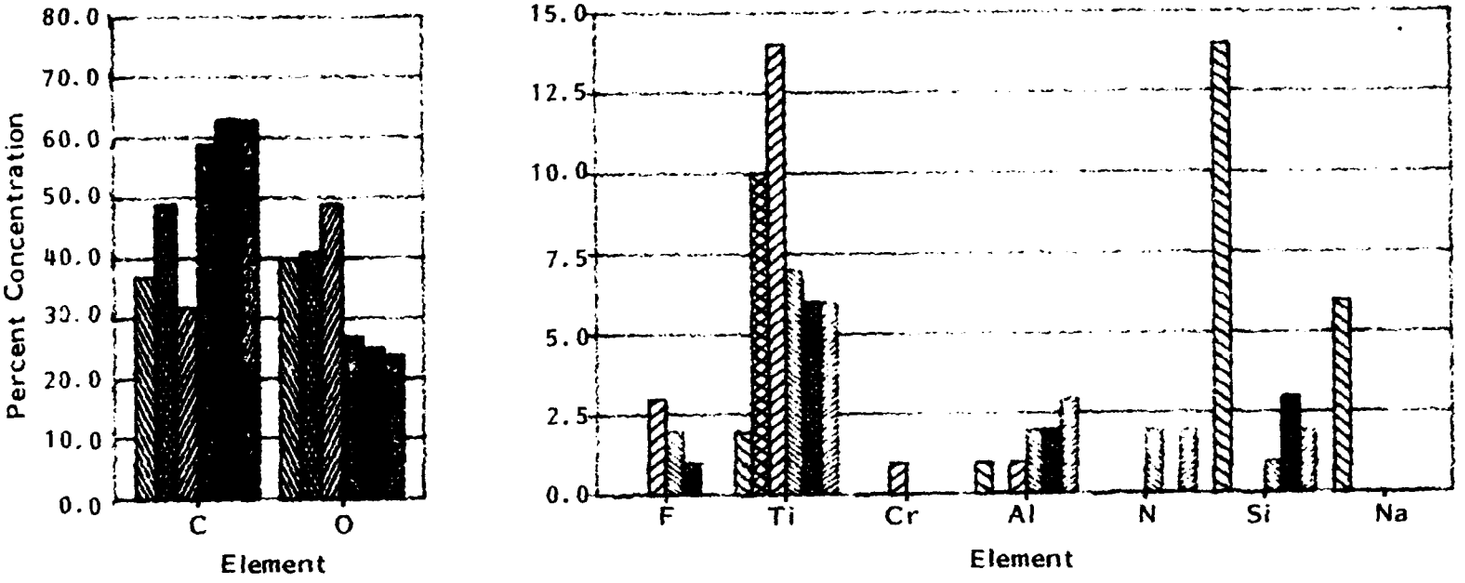
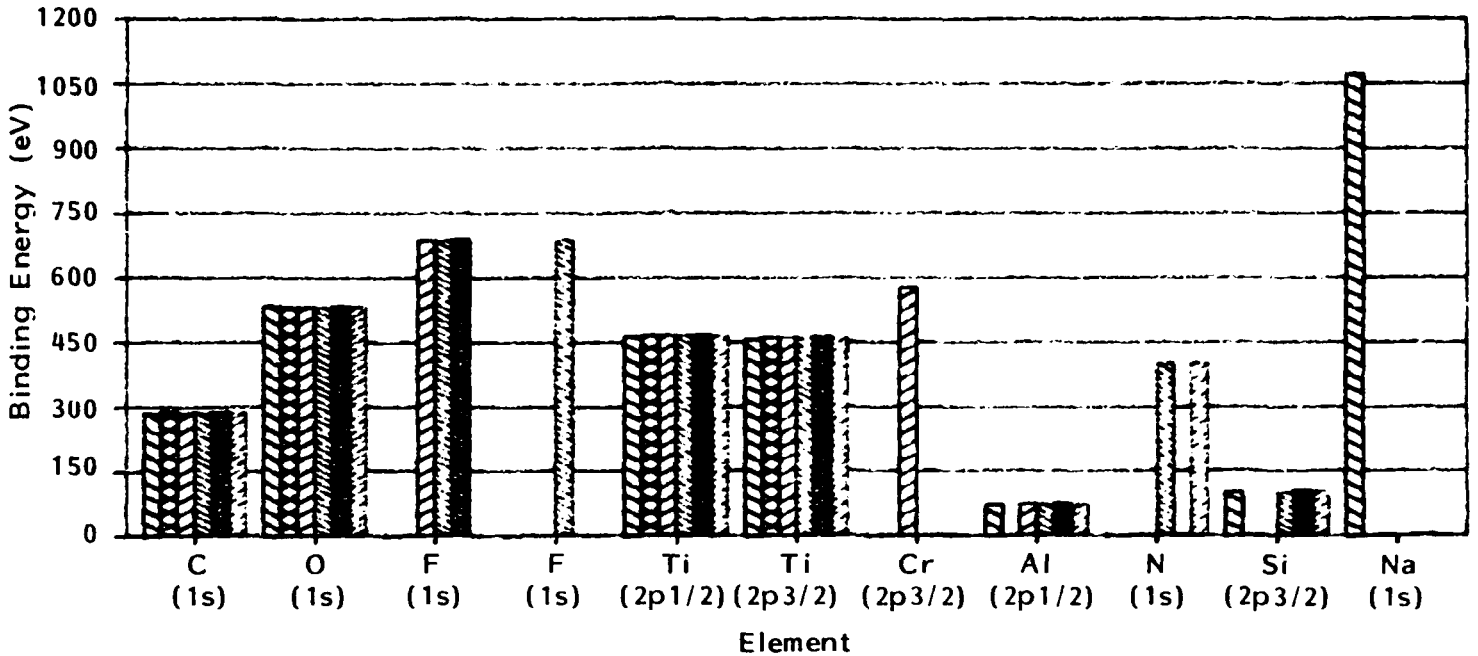


Figure 44. ESCA Concentration Analyses of Ti-6Al-4V Before and After Anodization.



- Ti-6Al-4V After Preanodization Treatment #1
- Ti-6Al-4V After Preanodization Treatment #2
- Chromic Acid/HF Anodized Ti-6Al-4V, 20 Minutes, 30 A/m^2, 10 V, 298K
- Chromic Acid/HF Anodized Ti-6Al-4V, 60 Minutes, 30 A/m^2, 10 V, 298K
- Chromic Acid/HF Anodized Ti-6Al-4V, 20 Minutes, 20 A/m^2, 10 V, 283K
- Chromic Acid/No HF Anodized Ti-6Al-4V, 20 Minutes, 30 A/m^2, 39 V, 298K

Figure 45. ESCA Binding Energy Data for Ti-6Al-4V Before and After Anodization.

indicated by the 688.8 eV and 685.0 eV corrected binding energies, respectively.

4. Neither the chromic acid/HF anodized Ti-6Al-4V element concentrations or binding energies were influenced by altering the range of anodization times, initial current densities or solution temperatures examined.

ESCA characterization of the compression molded Udel® polysulfone, Victerex® polyethersulfone, both unfilled and 20% glass filled Ultem® polyetherimide, the neat samples of 50% $CaCO_3$ filled Ablebond® 71-3 polyimide, and polyphenylquinoxaline are graphed in Figures 46 and 47. For the Udel® PS, the as-received polymer beads were also analyzed by ESCA and compared to the compression molded film in Figure 48. The compression molded thermoplastics and the neat PPQ and PI samples examined are representative of the polymers as they were applied to the anodized Ti-6Al-4V. The analyses of the data are described below.

1. Compression molded PS, PEI, PEIF and PES had varying levels of organic fluorine. Fluorine was not detected on either the as-received PS, or the PPQ, or the PI neat polymer samples. The fluorine on the compression molded samples is attributed to the Teflon-glass reinforced release cloth used in the compression molding process.

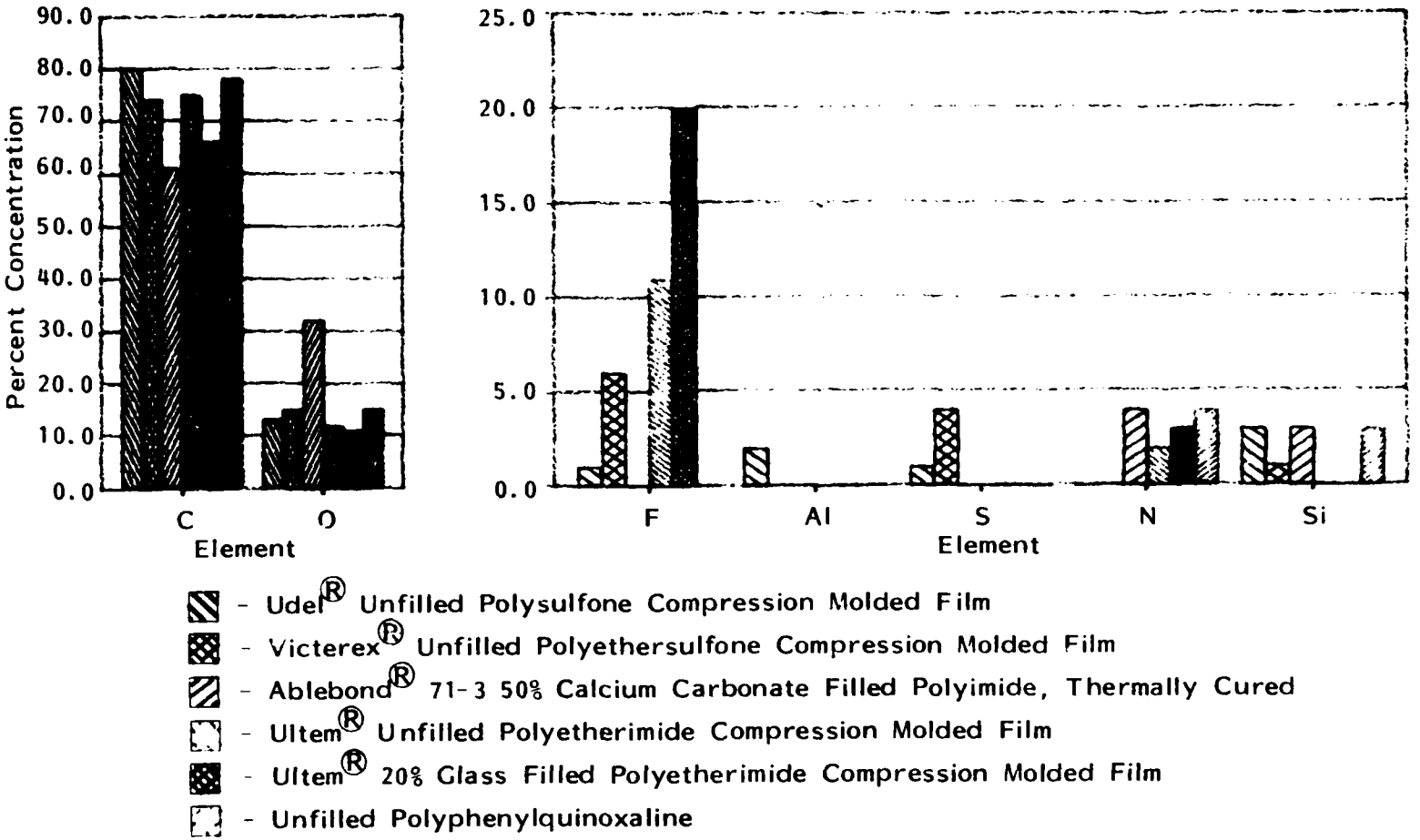


Figure 46. ESCA Concentration Analyses of Thermoset and Thermoplastics Used in Chromic Acid/HF Anodized Ti-6Al-4V Single Lap Bonds.

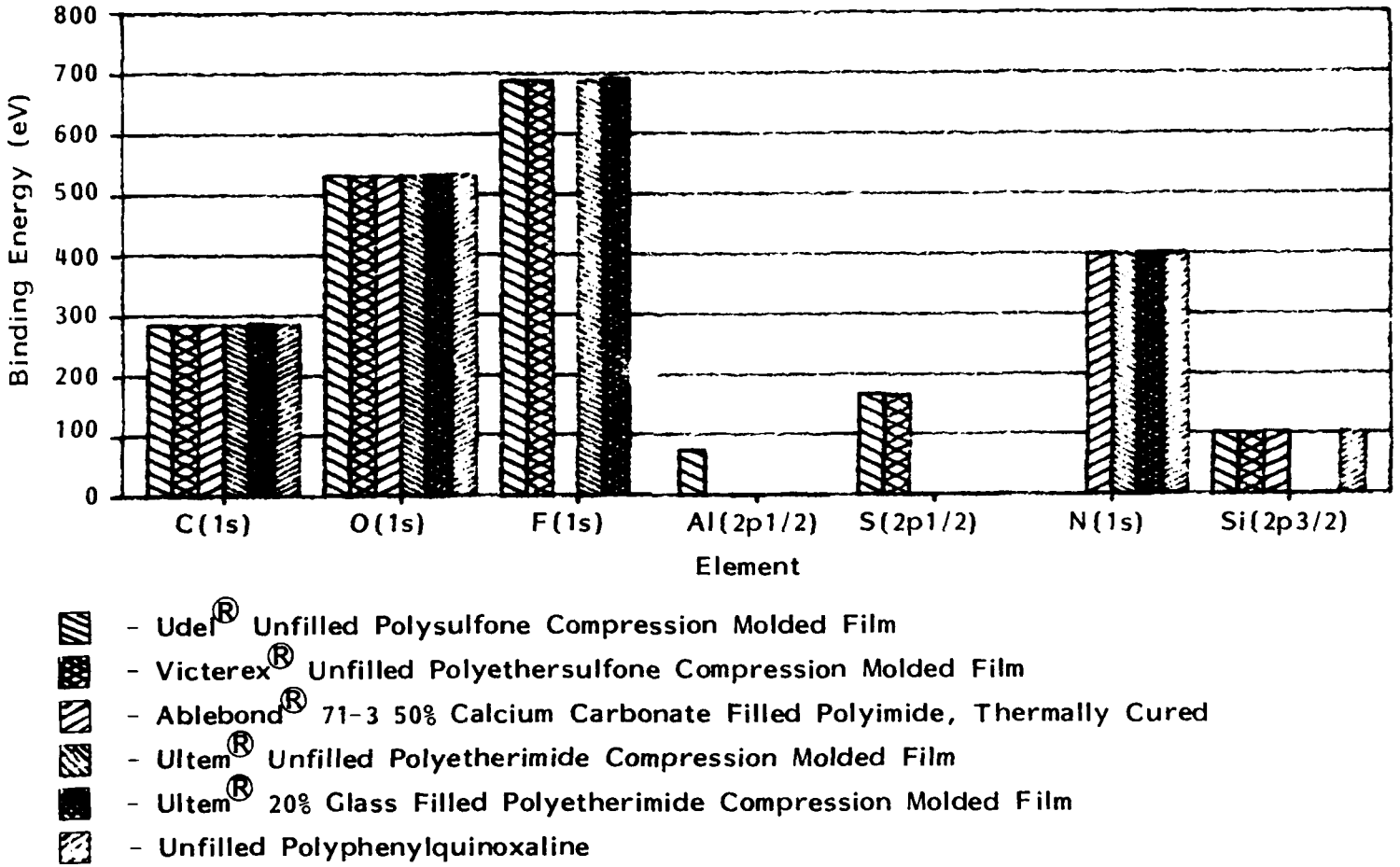


Figure 47. ESCA Binding Energy Data for a Thermoset and Thermoplastics Used in Chromic Acid/HF Anodized Ti-6Al-4V Single Lap Bonds.

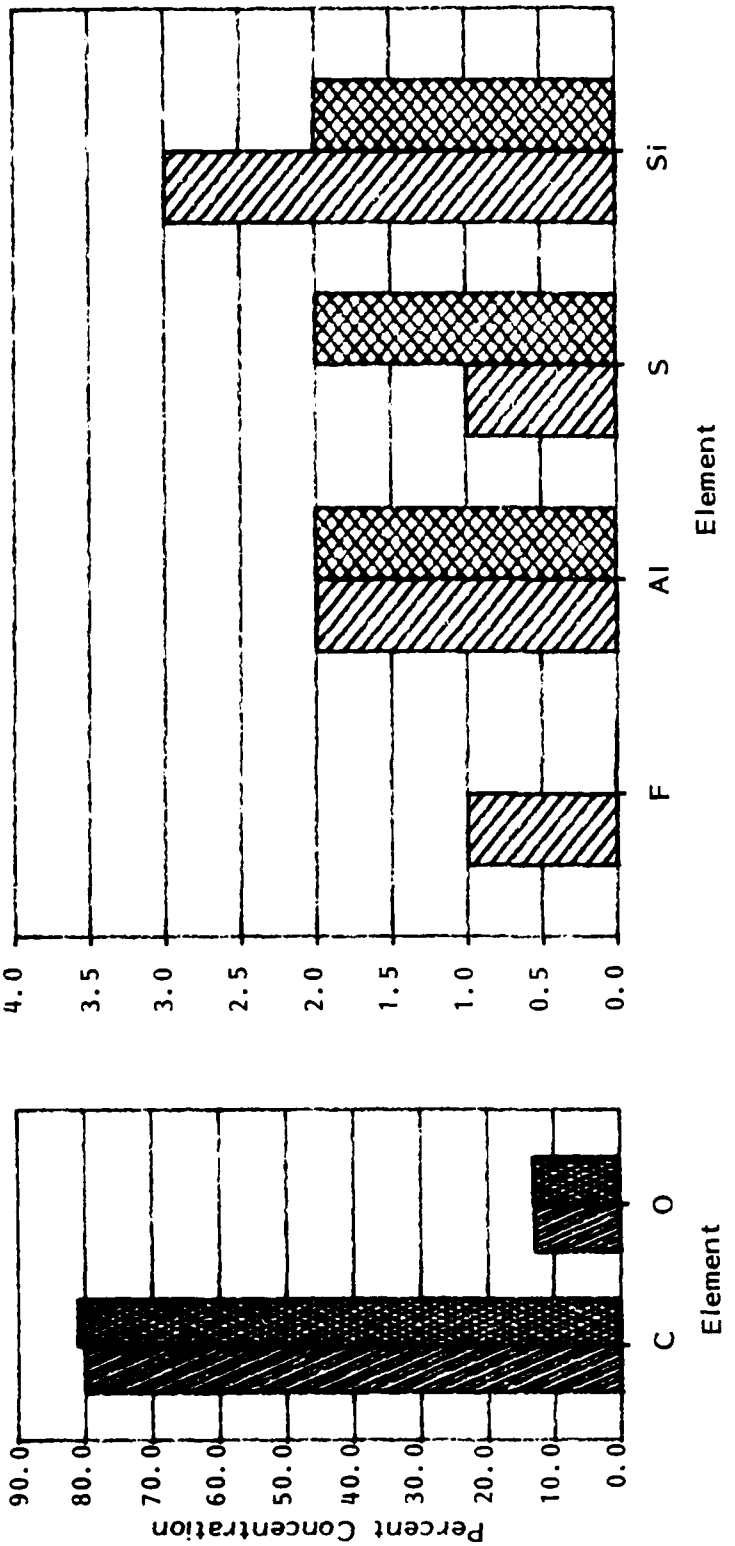


Figure 48. ESCA Concentration Analyses of Udel® Unfilled Polysulfone As-Received Beads and Compression Molded Film.

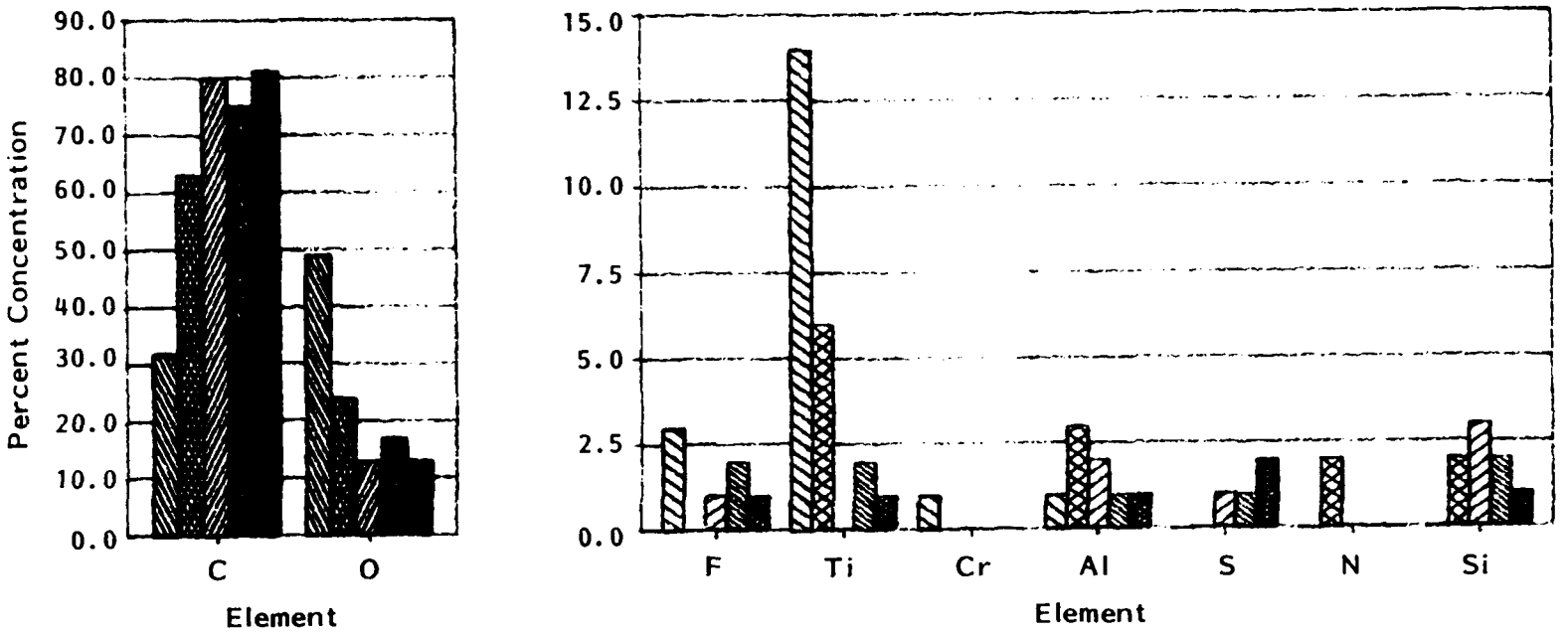
2. Sulfur was detected in 2% and 4% concentrations on PS and PES, respectively, at approximately the same binding energy, characteristic of a sulfone group. Based upon these data, sulfur concentrations of $\geq$ 2% on a fracture surface, where either PS or PES was the adhesive used, was taken as an indicator of that respective adhesive.
3. Nitrogen was detected on the PEIU, PEIF, PPQ and PI compression molded or neat polymer surfaces in concentrations of 2% to 4% where any of these adhesives were used. Based upon these data, nitrogen in $\geq$ 2% concentrations on the analyzed fracture surfaces was taken as an indicator of adhesive on these fracture surfaces.

Figures 49 through 53 and 55 through 61 are the ESCA surface concentration data for the single lap bond fracture surfaces. ESCA analyses for anodized Ti-6Al-4V as well as the adhesive are included on the bar graphs for reference. Element binding energy data for fracture surfaces are not illustrated here, since they do not differ significantly from the respective anodized Ti-6Al-4V and adhesive binding energy data shown earlier in Figures 45 and 47. Bond failure sites based upon these ESCA data are described as follows.

1. ESCA data for anodized Ti-6Al-4V/PS fracture surfaces were compared as a function of anodization

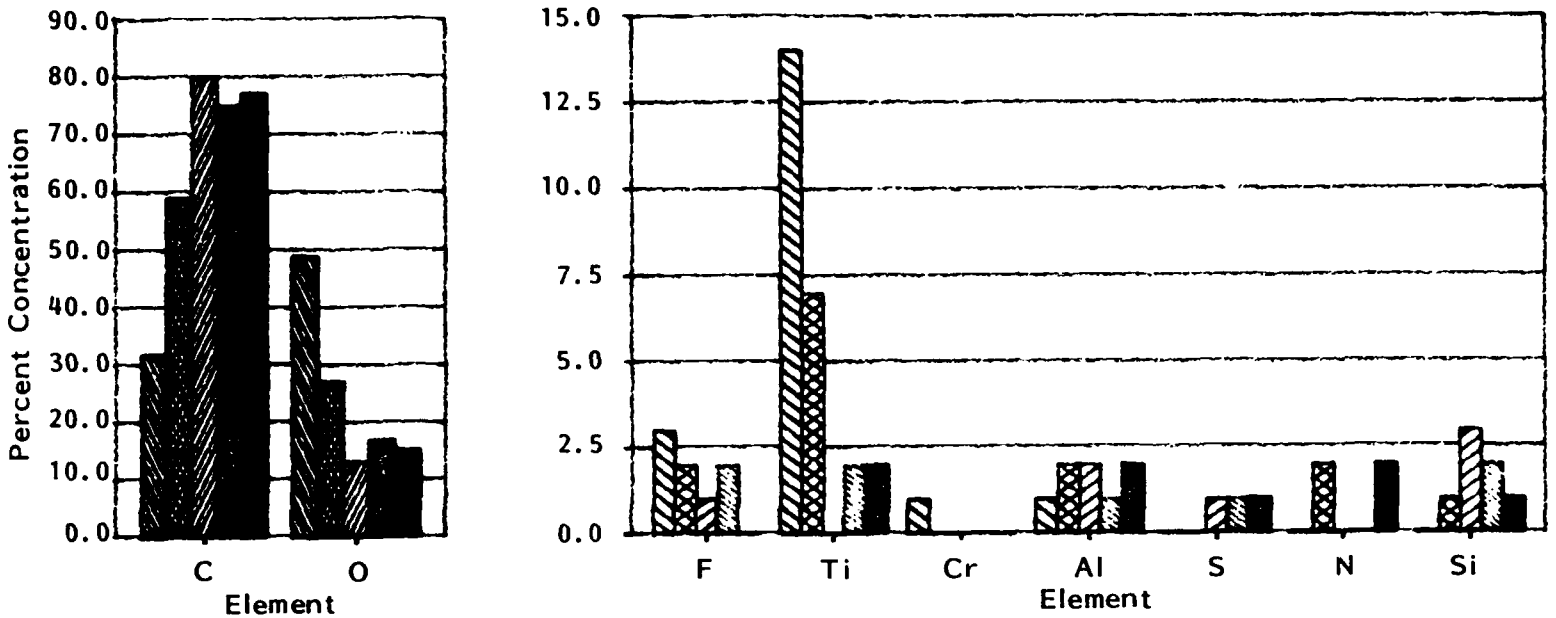
with and without hydrofluoric acid, as shown in Figure 49. For anodized Ti-6Al-4V/PS, with or without the presence of HF in the anodization bath, fracture was in the anodic oxide/PS interphase. Both titanium and sulfur concentrations were approximately equivalent on the fracture surface. This suggests that the fracture occurred in the anodic oxide/PS interphase for both CA/HF anodized Ti-6Al-4V and also CA anodized Ti-6Al-4V bonds. The ESCA analysis of this fracture surface examined was in good agreement with the visual analysis of this surface.

2. ESCA data of fracture surfaces for chromic acid/HF anodized Ti-6Al-4V/PS bonds as a function of 20 minute or 60 minute anodization time are shown in Figure 50. Anodic oxide/PS interphase failure occurred, as evidenced by approximately equivalent titanium and sulfur concentrations for the fracture surfaces. The ESCA analysis of this fracture surface was in good agreement with the visual analysis of the failure site.
3. ESCA data for chromic acid/HF anodized Ti-6Al-4V/PS fracture surfaces as a function of anodization initial current density and of solution temperature are shown in Figure 51. ESCA data analyses indicated anodic oxide/PS interphase failure for all these fracture



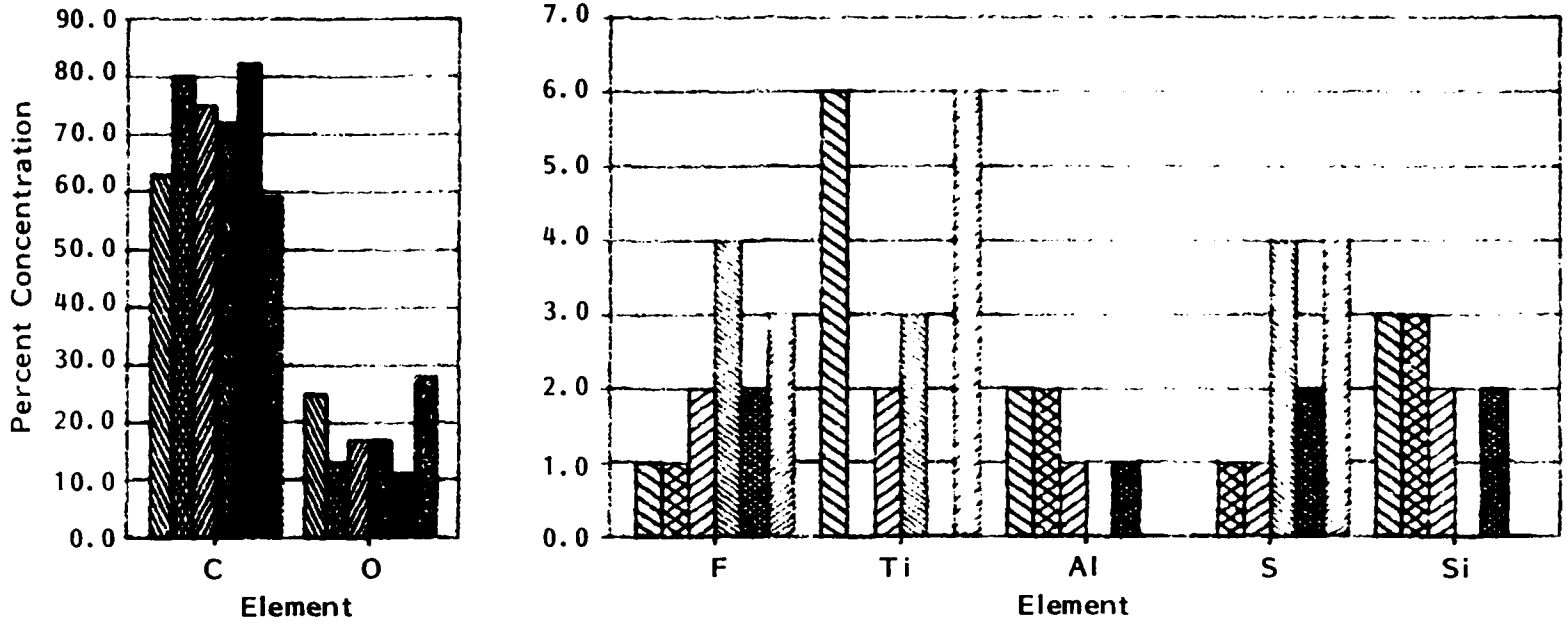
- Chromic Acid/HF Anodized Ti-6Al-4V, 20 Minutes, 30 A/m^2, 10 V, 298K
- Chromic Acid/No HF Anodized Ti-6Al-4V, 20 Minutes, 30 A/m^2, 39 V, 298K
- Polysulfone Compression Molded Film
- Fracture Surface, Anodization: 20 Minutes, 30 A/m^2, 10 V, 298K
- Fracture Surface, Anodization: 20 Minutes, 30 A/m^2, 39 V, 298K

Figure 49. ESCA Concentration Analyses of Fracture Surfaces for Chromic Acid Anodized Ti-6Al-4V/Udel® Unfilled Polysulfone Single Lap Bonds as a Function of Anodization With and Without Hydrofluoric Acid.



- Chromic Acid/HF Anodized Ti-6Al-4V, 20 Minutes, 30 A/m^2, 10 V, 298K
- Chromic Acid/HF Anodized Ti-6Al-4V, 60 Minutes, 30 A/m^2, 10 V, 298K
- Polysulfone Compression Molded Film
- Fracture Surface, Anodization: 20 Minutes, 30 A/m^2, 10 V, 298K
- Fracture Surface, Anodization: 60 Minutes, 30 A/m^2, 10 V, 298K

Figure 50. ESCA Concentration Analyses of Fracture Surfaces for Chromic Acid/HF Anodized Ti-6Al-4V/Udel® Unfilled Polysulfone Single Lap Bonds as a Function of Anodization Time.



- Chromic Acid/HF Anodized Ti-6Al-4V, 20 Minutes, 30 A/m^2, 10 V, 283K
- Udel® Polysulfone Compression Molded Film
- Fracture Surface, Anodization: 20 Minutes, 30 A/m^2, 10 V, 298K
- Fracture Surface, Anodization: 20 Minutes, 20 A/m^2, 10 V, 298K
- Fracture Surface, Anodization: 20 Minutes, 20 A/m^2, 10 V, 283K
- Fracture Surface, Anodization: 20 Minutes, 30 A/m^2, 10 V, 283K

Figure 51. ESCA Concentration Analyses of Fracture Surfaces for Chromic Acid/HF Anodized Ti-6Al-4V/Udel® Unfilled Polysulfone Single Lap Bonds as a Function of Anodization Temperature and Initial Current Density.

surfaces, except for one. The exception was the fracture surface for Ti-6Al-4V anodized at the preferred anodization conditions previously discussed, which were a relatively low initial current density of 20 A/m^2 and a solution temperature of 283K. Polysulfone cohesive failure occurred for this surface. Apparently, for the Ti-6Al-4V anodized per the preferred method, the anodic oxide/polysulfone interphase bond was stronger than the bulk polysulfone for this area on the fracture surface. The polysulfone cohesive failure, coupled with the excellent bond strength data for the Ti-6Al-4V anodized by the preferred method previously discussed, further supports the conclusion that low current density Ti-6Al-4V anodization is beneficial to the anodized Ti-6Al-4V/PS bond. As was discussed earlier, the low current density would be expected to minimize the fluoride concentration in the oxide. Minimizing fluoride concentration in the oxide would be beneficial since fluoride could cause polysulfone to microcrack and weaken the interphase bond.

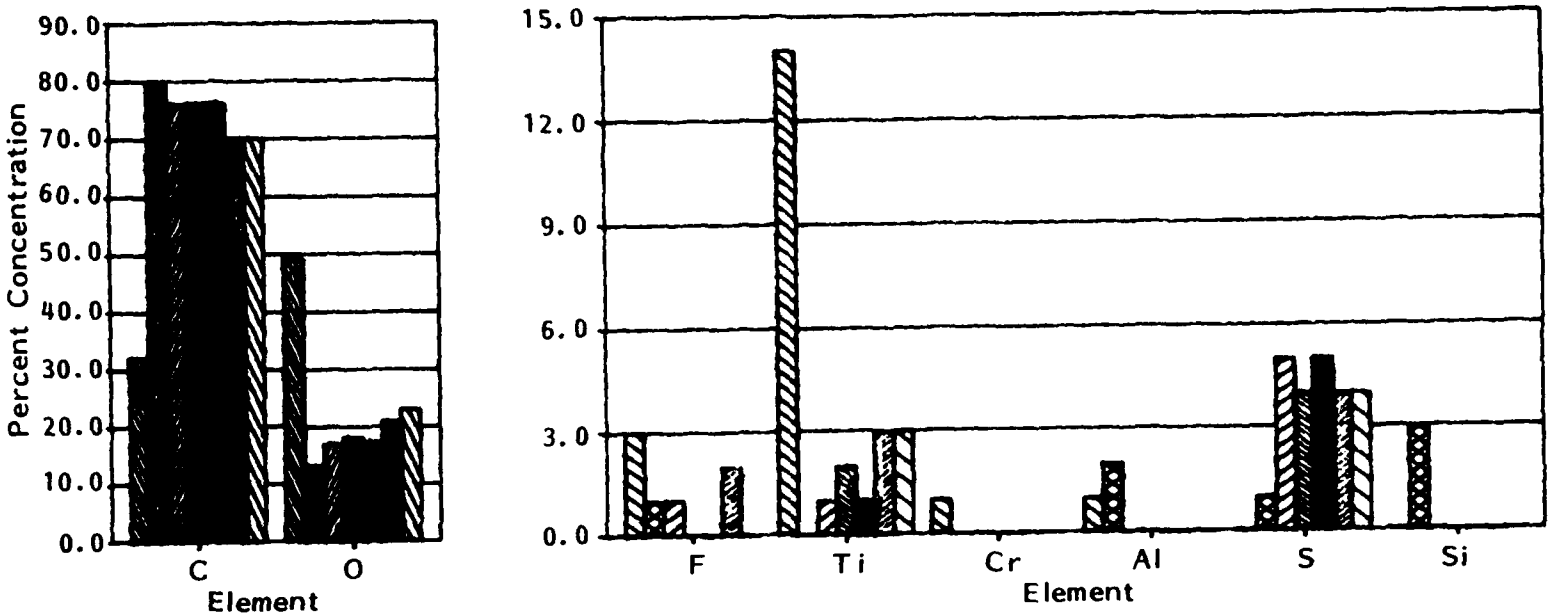
In general, there was good agreement between failure sites as determined by ESCA data and the visual analysis of the fracture area examined by ESCA. The one exception was for the Ti-6Al-4V

anodized at 30 A/m^2 and 298K. Based upon the fracture surface's metallic appearance, visual analysis indicated that an apparent anodic oxide/metal interphase failure had occurred. However, ESCA data suggests polysulfone/anodic oxide interphase failure occurred for this area examined, hence refuting the visual analysis.

4. ESCA analysis of fracture surfaces for chromic acid/HF anodized Ti-6Al-4V/PS bonds as a function of thermal aging are shown in Figure 52. Based upon visual analysis, this area of the fracture surface exhibited apparent anodic oxide/adhesive interphase failure. Based upon the ESCA data, this area of the fracture surface exhibited anodic oxide/PS interphase failure, since the titanium and sulfur concentrations were approximately equivalent on each sample.

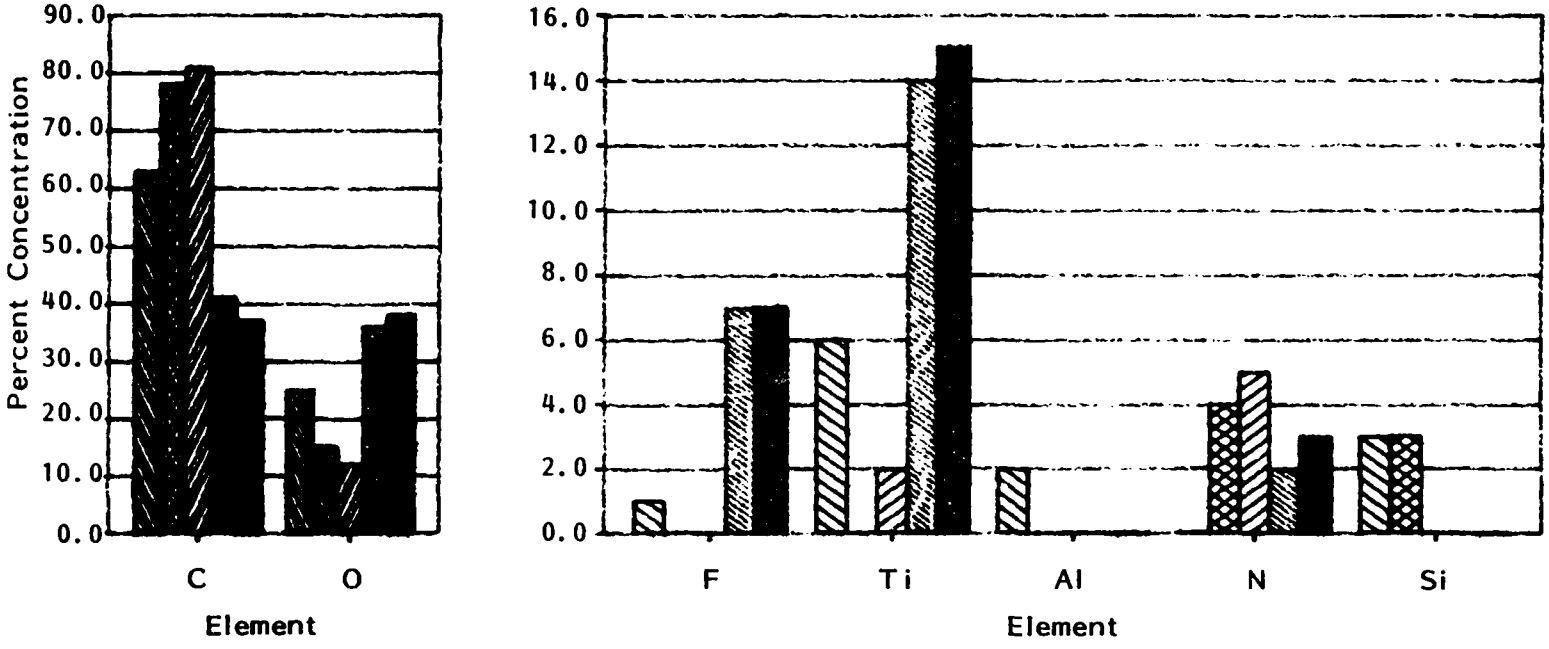
5. ESCA analysis of fracture surfaces for chromic acid/HF anodized Ti-6Al-4V/PPQ bonds as a function of isochronal and isothermal bonding processes are shown in Figure 53. ESCA analysis indicated anodic oxide/PPQ interphase failure for both bonding processes. Both nitrogen and titanium were detected on the fracture surfaces in concentrations $\geq$ 2%.

Recall that visual analysis indicated an apparent anodic oxide/PPQ interphase failure for the



- Chromic Acid/HF Anodized Ti-6Al-4V, 20 Minutes, 30 A/m^2, 10 V, 298K
- Udel® Polysulfone Compression Molded Film
- Bonds Aged 2 Months at 298K Before Fracture
- Bonds Aged 9 Months at 298K Before Fracture
- Bonds Aged 11 Months at 298K Before Fracture
- Bonds Aged 9 Months at 378K Before Fracture
- Bonds Aged 9 Months at 443K Before Fracture

Figure 52. ESCA Concentration Analyses of Fracture Surfaces for Chromic Acid/HF Anodized Ti-6Al-4V /Udel® Unfilled Polysulfone Single Lap Unstressed Thermally Aged Bonds.



- Chromic Acid/HF Anodized Ti-6Al-4V, 20 Minutes, 20 A/m^2, 10 V, 283K
- Unfilled Polyphenylquinoxaline
- Fracture Surface, Isothermally Processed
- Fracture Surface, Side #1, Isochronally Processed
- Fracture Surface, Side #2, Isochronally Processed

Figure 53. ESCA Concentration Analyses of Fracture Surfaces for Chromic Acid/HF Anodized Ti-6Al-4V/Unfilled Polyphenylquinoxaline Single Lap Bonds as a Function of Bonding Process.

isothermal bonds. This visual analysis is in good agreement with these ESCA results. However, the ESCA analysis refuted the visual analysis of failure for the isochronal processed bonds. The isochronal processed bonds exhibited an apparent metal/anodic oxide interphase failure, based upon the metallic appearance of the fracture surface. Apparently, the isochronal processed bonds fractured close to the base of the anodic oxide in the anodic oxide/PPQ interphase region, giving it the appearance of a metal/anodic oxide failure.

Nitrogen, in the range of 2 to 5%, was observed on all fracture surfaces. For the isochronal bond, there was a 14 to 15% titanium signal on both fracture surfaces examined. There was a 2% titanium surface concentration for the isothermal bond fracture surface examined. One reason for the low titanium signal on the isothermally bonded fracture surface may be due to the high concentration of carbon. As shown in Appendix VII, the carbon concentration for the isothermally bonded fracture surface was twice the value for the isochronally bonded fracture surface. Another reason for the differences in the titanium surface concentration for the isochronal and isothermal processed bonds, just like their bond

strength differences discussed earlier, can be attributed to the high isochronal bonding temperature and pressure. Because of the relatively high temperature and pressure used in the isochronal bonding process, the columnar oxide structure may have been degraded and collapsed, as shown in Figure 54. Or, the relatively high temperature and pressure, in concert with the PPQ diluent's penetration of the oxide, may have caused oxide degradation and collapse. This oxide degradation or collapse would have resulted in only partial formation of an anodic oxide/PPQ interphase. Consequently, a relatively higher surface area of anodic oxide would be exposed on the fracture surfaces for the isochronally processed bond relative to the isothermally processed bond. This model of the isochronal bond described in Figure 54 would therefore explain a titanium signal on both fracture surfaces of the isochronally processed bond which was 7X higher than for the isothermal processed bonds. And, this adhesive model for the isochronally processed bond, which illustrates an oxide morphology that occludes adhesive penetration, would explain the low isochronally bond strengths, as compared to the isothermally processed bond strengths.

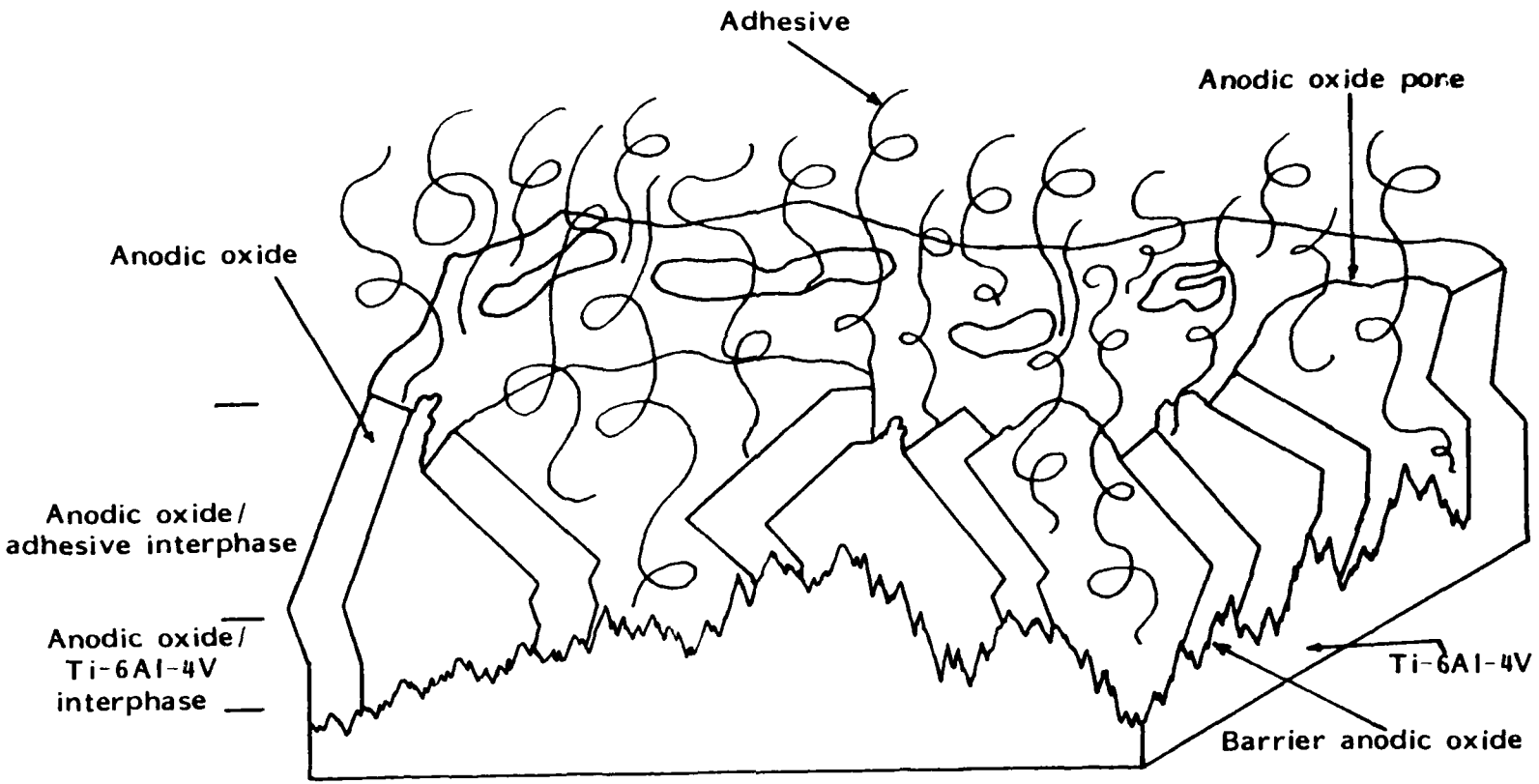
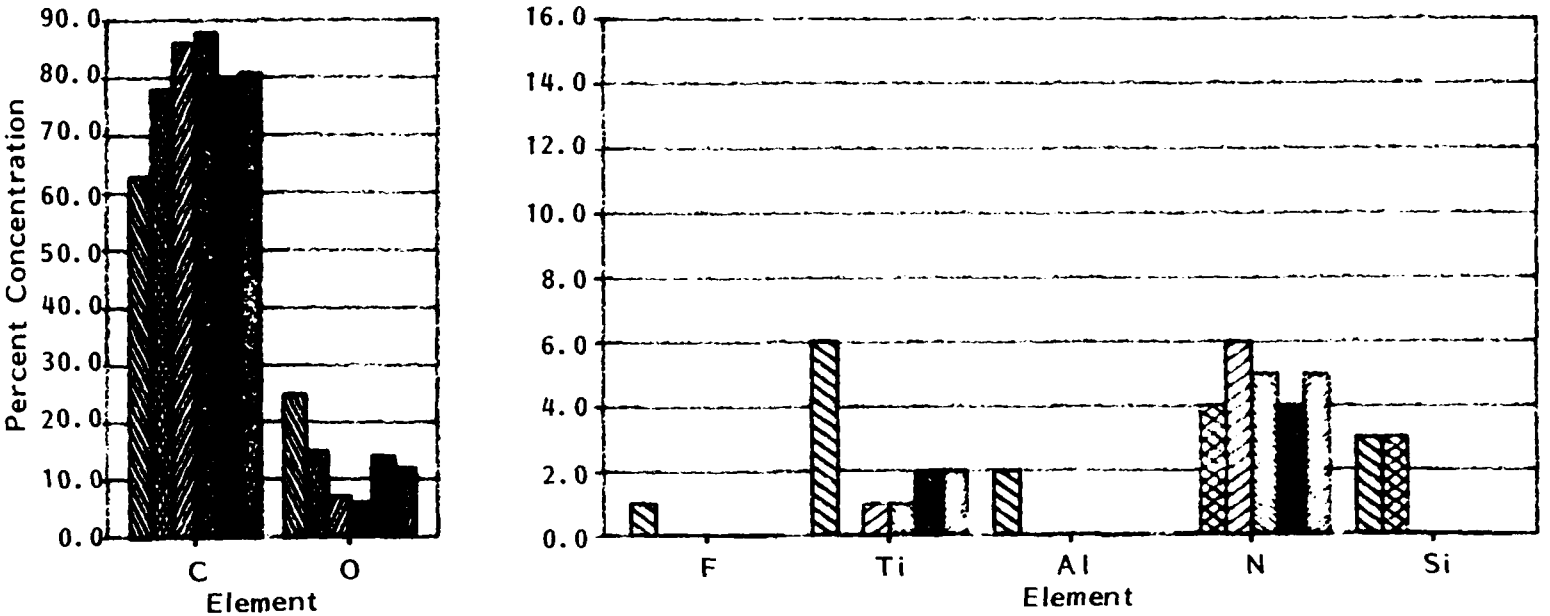


Figure 54. Proposed Model of the CA/HF Anodized Ti-6Al-4V/Polyphenylquinoxaline Isochronally Processed Bond.

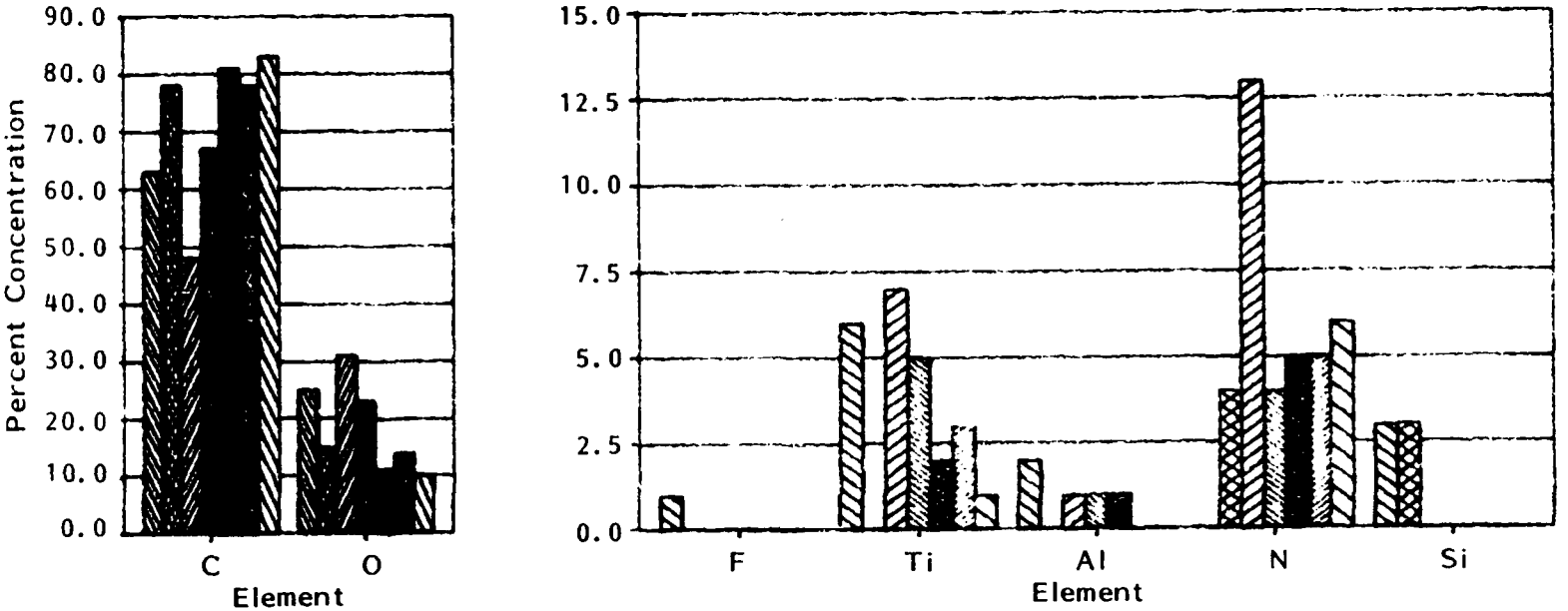
6. ESCA analysis of fracture surfaces for chromic acid/HF anodized Ti-6Al-4V/PPQ bonds as a function of anodization current density and anodization solution temperature are shown in Figure 55. Varying the current density from 20 A/m^2 to 30 A/m^2, or varying temperature from 283K to 298K, did not affect the failure mechanism. All bonds exhibited anodic oxide/PPQ interphase failure. The ESCA analysis and visual analyses of the fracture sites were in good agreement.
7. Anodic oxide/PPQ interphase failure was evident for thermally aged bonds at 298K, 443K or 505K, as shown in Figure 56. This ESCA failure analysis was in good agreement with the visual analysis.
8. ESCA data in Figures 56 and 57 were used to deduce the failure site for Lica® 44 titanate primed anodic oxide/PPQ bonds, thermally aged 9 months at 443K and 2 months at 298K before fracture. Failure in the primed anodic oxide/PPQ interphase was evident. This was deduced based upon the approximately equivalent nitrogen and titanium concentrations on the fracture surface, and the presence of nitrogen in $\geq$ 2% concentrations.

   As shown in Figure 57, the titanium binding energy for the primer was 1.3 eV lower than for the



- Chromic Acid/HF Anodized Ti-6Al-4V, 20 Minutes, 20 A/m^2, 10 V, 283K
- Unfilled Polyphenylquinoxaline
- Fracture Surface, Side #1, Anodization: 20 Minutes, 30 A/m^2, 10 V, 298K
- Fracture Surface, Side #2, Anodization: 20 Minutes, 20 A/m^2, 10 V, 298K
- Fracture Surface, Anodization: 20 Minutes, 30 A/m^2, 10 V, 283K
- Fracture Surface, Anodization: 20 Minutes, 20 A/m^2, 10 V, 283K

Figure 55. ESCA Concentration Analyses of Fracture Surfaces for Chromic Acid/HF Anodized Ti-6Al-4V/Unfilled Polyphenylquinoxaline Isothermally Processed Single Lap Bonds as a Function of Anodization Solution Temperature and Initial Current Density.



- Chromic Acid/HF Anodized Ti-6Al-4V, 20 Minutes, 20 A/m^2, 10 V, 283K
- Unfilled Polyphenylquinoxaline
- Lica® 44 Titanate Primer
- Bonds Aged 11 Months at 298K Before Fracture
- Lica® 44 Titanate Primed Bonds Aged 9 Months at 443K Before Fracture
- Bonds Aged 9 Months at 443K Before Fracture
- Bonds Aged 9 Months at 505K and Thermally Cycled 7 Times Before Fracture

Figure 56. ESCA Concentration Analyses of Fracture Surfaces for Chromic Acid/HF Anodized Ti-6Al-4V/Unfilled Polyphenylquinoxaline Single Lap Bonds for Primed and/or Aged Bonds.

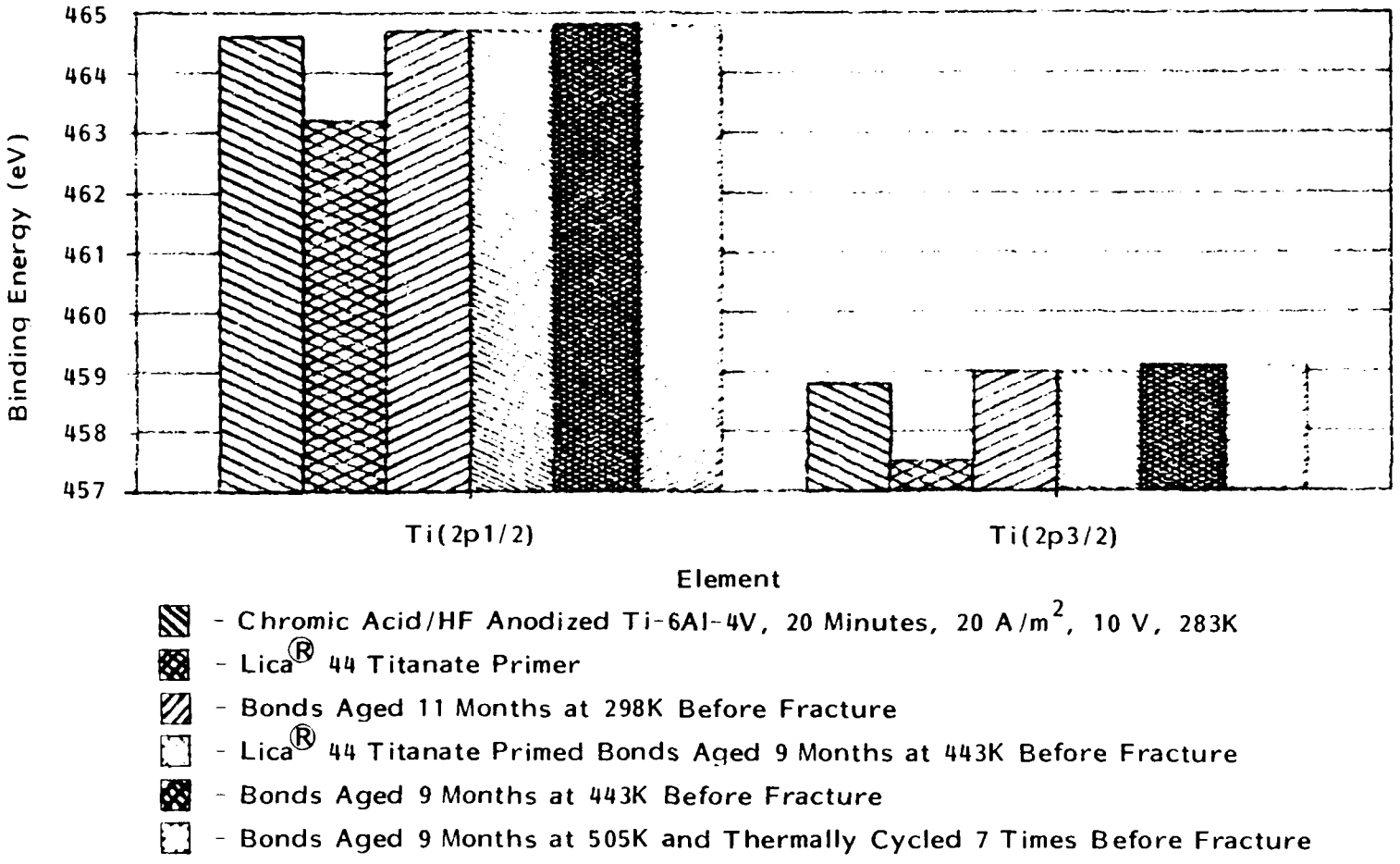
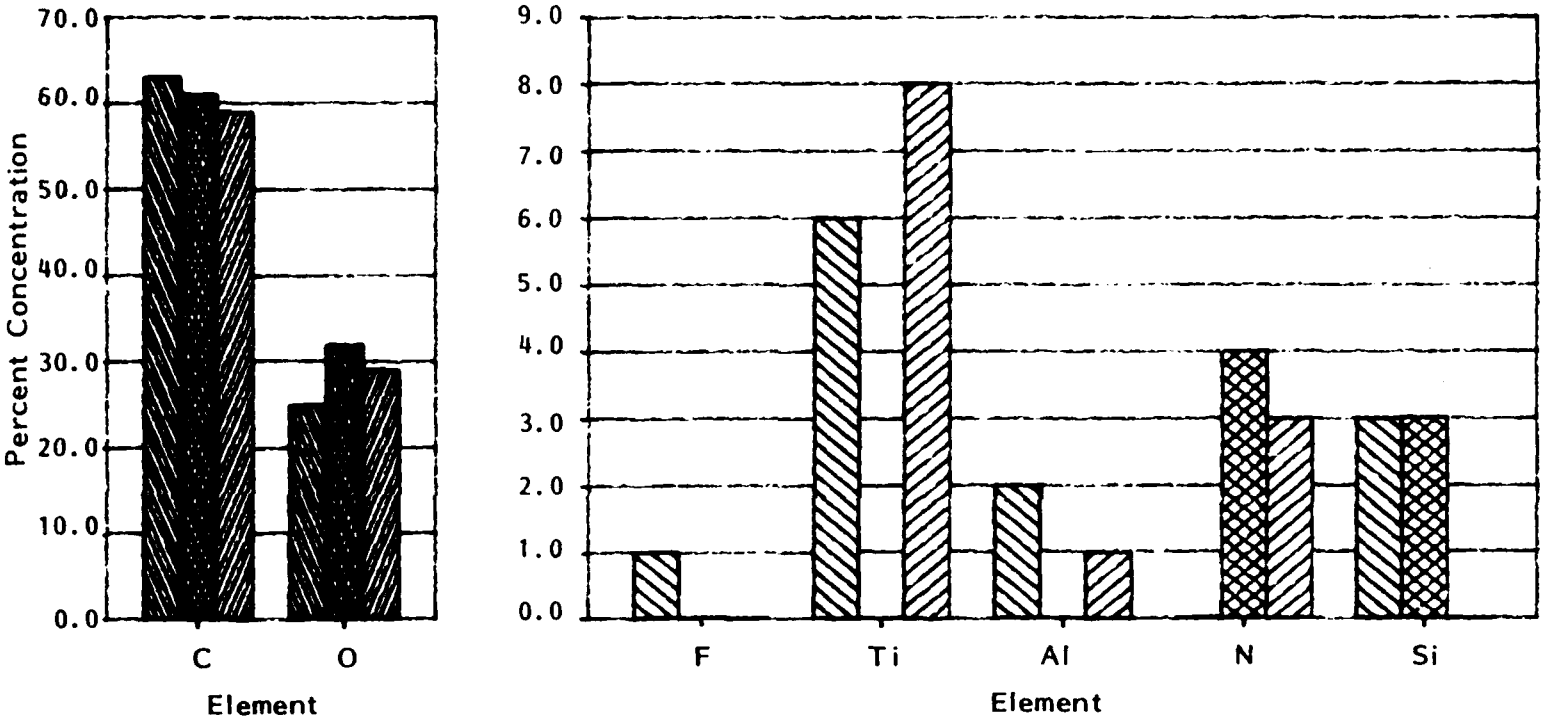


Figure 57. ESCA Titanium Binding Energy Analyses of Fracture Surfaces for Chromic Acid/HF Anodized Ti-6Al-4V/Unfilled Polyphenylquinoxaline Single Lap Bonds for Primed and/or Aged Bonds.

titanium binding energy of the anodic oxide. The titanium 2p1/2 and 2p3/2 binding energies were 463.2 eV and 457.5 eV, respectively, for the neat primer. The titanium 2p1/2 and 2p3/2 binding energies were 464.5 and 458.7 eV, respectively, for the CA/HF anodized Ti-6Al-4V surface. As a result of fracture, large areas of unprimed oxide surface area could be exposed. And, it is conceivable that the primed oxide exposed could be below the ESCA detectable limits, resulting in no primer detected on the fracture surface.

9. ESCA analysis of fracture surfaces for CA/HF anodized Ti-6Al-4V/Ablebond® 50% $CaCO_3$ filled PI single lap bonds are shown in Figure 58. Anodic oxide/PI interphase failure is evident, as indicated by the presence of nitrogen in $\geq$ 2% and the approximately equivalent nitrogen and titanium signals. The ESCA analysis and visual analysis of the failure sites were in good agreement.

10. ESCA analysis of fracture surfaces for chromic acid/HF anodized Ti-6Al-4V bonded to either unfilled Ultem® PEI or 20% glass filled Ultem® PEI are shown in Figures 59 and 60. The fracture sites for both were anodic oxide/PEI interphase, as determined by ESCA. It was interesting to note that silicon was not



- Chromic Acid/HF Anodized Ti-6Al-4V, 20 Minutes, 20 A/m^2, 10 V, 283K
- Ablebond® 71-3 50% Calcium Carbonate Filled Polyimide, Thermally Cured
- Fracture Surface

Figure 58. ESCA Concentration Analyses of a Fracture Surface for Chromic Acid/HF Anodized Ti-6Al-4V/Ablebond® 71-3 50% Calcium Carbonate Filled Polyimide Single Lap Bond.

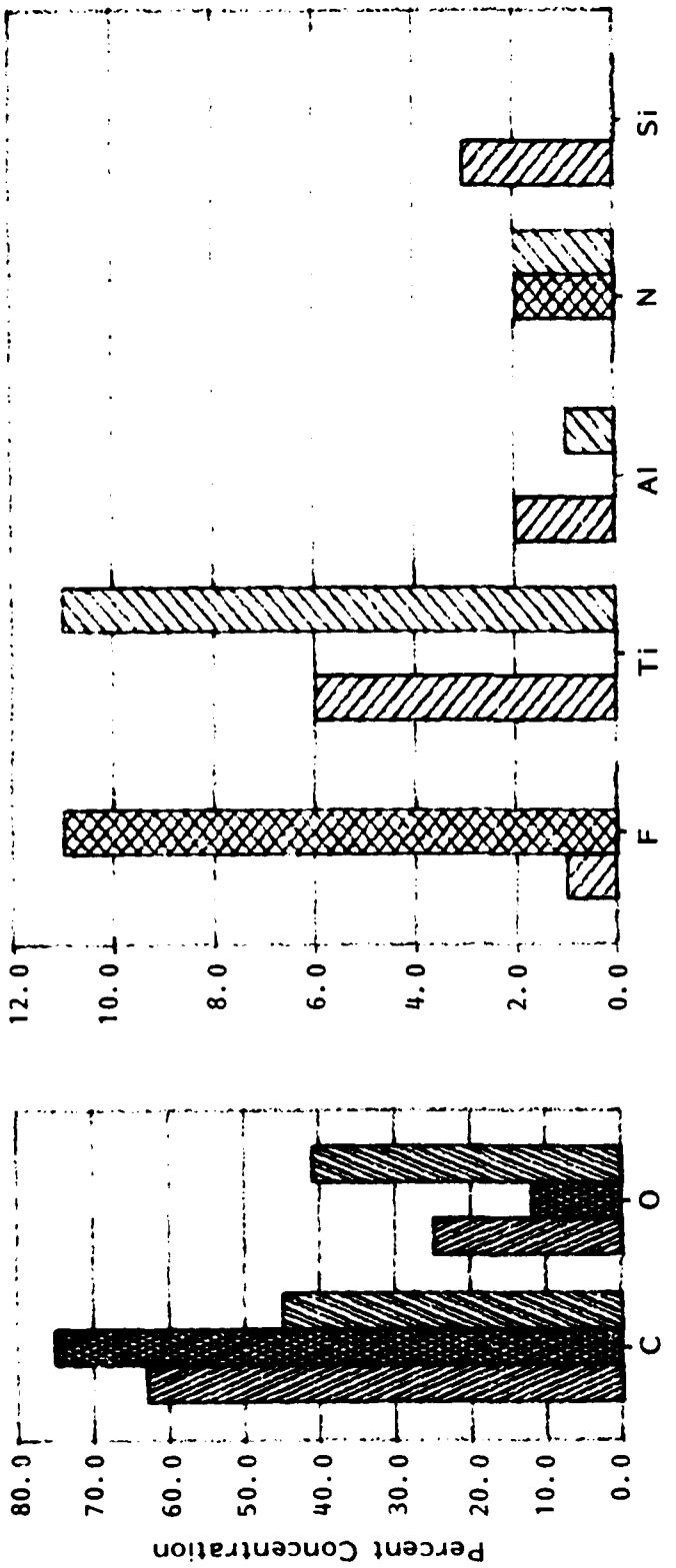


Figure 59. ESCA Concentration Analyses of a Fracture Surface for Chromic Acid/HF Anodized Ti-6Al-4V/Ultem® Unfilled Polyetherimide Single Lap Bond.

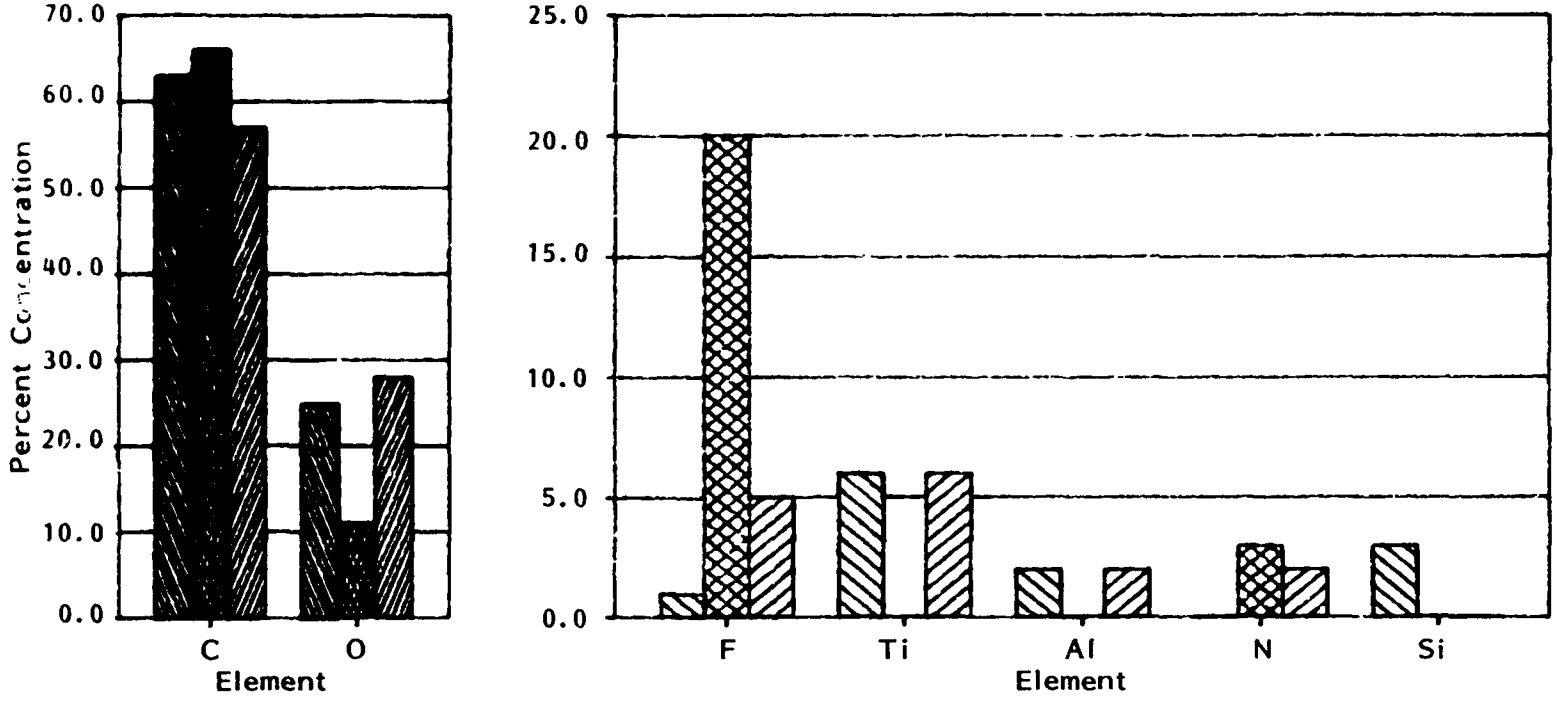


Figure 60. ESCA Concentration Analyses of Fracture Surface for a Chromic Acid/HF Anodized Ti-6Al-4V/Ultem® 20% Glass Filled Polyetherimide Single Lap Bond.

detected on any fracture surface for glass filled PEI or, for that matter, on the compression molded PEI control. Apparently, there was good adhesion of the PEI to the glass filler. The ESCA fracture analysis refuted the visual analysis of these fracture surfaces. Visually, the surfaces appeared to fracture in the anodic oxide/metal interphase, since the fracture fracture surface appeared metallic.

11. ESCA analysis of the fracture surface for Victrex® PES/chromic acid/HF anodized Ti-6Al-4V bonds are shown in Figure 61. Data indicate an anodic oxide/PES interphase failure. The ESCA analysis is in good agreement with the visual analysis of the failure site.

e. Auger Analysis

Auger mapping analyses for selected PPQ-chromic acid/HF anodized Ti-6Al-4V single lap bond fracture surfaces was conducted. This was used to supplement the ESCA analysis previously described to determine the fracture mechanism for only selected PPQ single lap bonds studied. Auger mapping provided a photographic representation of the surface concentration and distribution of each element on the fracture surface, whereas ESCA provided an average element concentration based upon the surface area examined. Given the dimensions of the single lap bond used

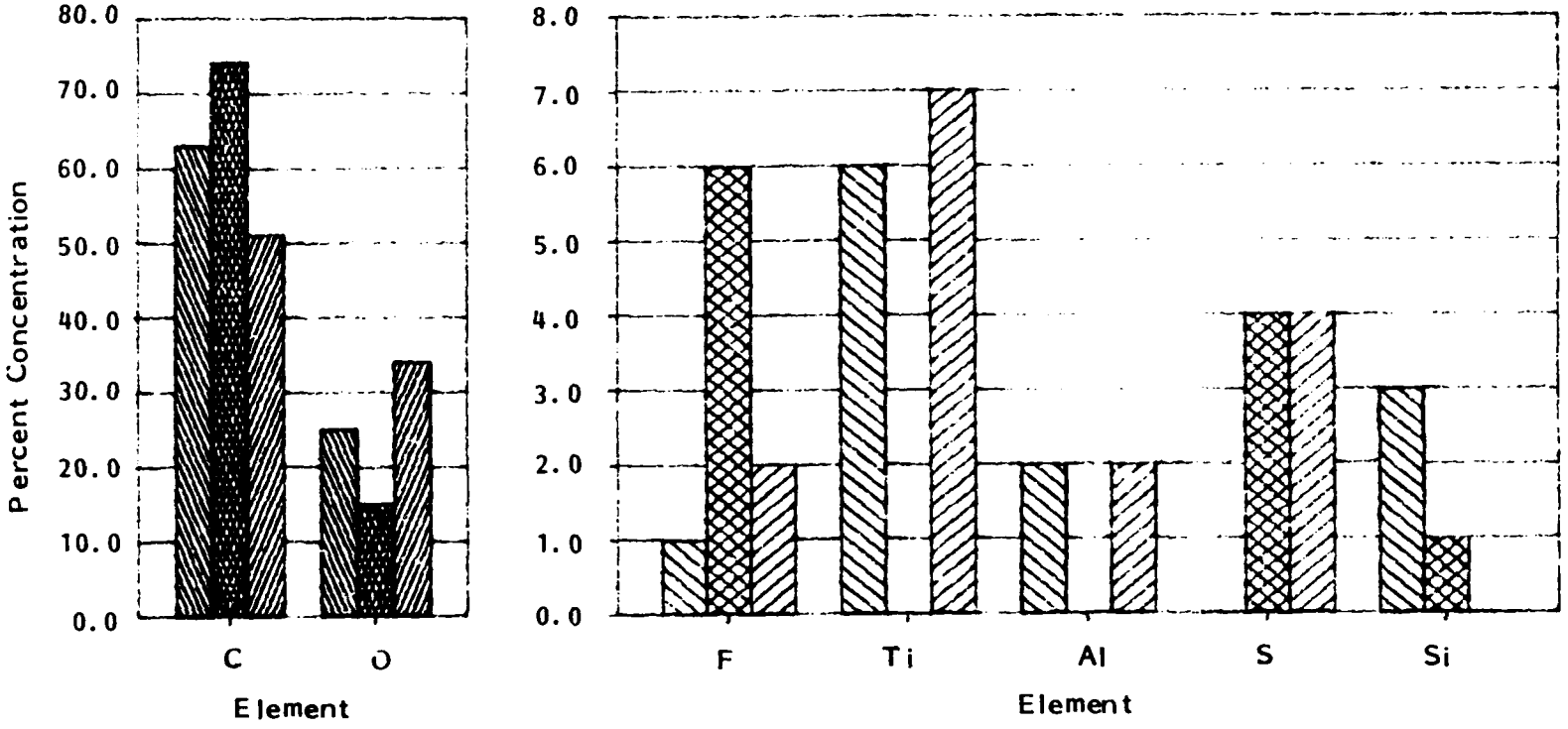


Figure 61. ESCA Concentration Analyses of a Fracture Surface for Chromic Acid/HF Anodized Ti-6Al-4V/Victerex® Unfilled Polyethersulfone Single Lap Bond.

in this study, only 0.3% of the total fracture surface can be analyzed at any one time using Auger mapping analysis. Therefore, thirty separate Auger maps would be necessary to analyze the same fracture surface area analyzed by ESCA analysis. As a result, it was cost prohibitive to use Auger mapping as a primary method to determine fracture sites for all the single lap bonds studied.

Auger survey, Auger mapping analysis and SEM micrographs of the Auger mapped areas for opposing single lap bond fracture surfaces are shown in Figures 62 through 73. These fracture surface data are for PPQ isochronally bonded to chromic acid/HF anodized Ti-6Al-4V, and for PPQ isothermally bonded to chromic acid/HF anodized Ti-6Al-4V. Three spots on each fracture surface were Auger mapped so that approximately 1% of the total fracture surface was examined. Data shown in Figures 62 through 73 are typical of all the Auger map data obtained for each bond type.

Auger survey analysis indicated that the isothermally bonded PPQ/anodized Ti-6Al-4V fracture surfaces were composed of only carbon, nitrogen and oxygen. Nitrogen was distributed over the entirety of opposing fracture surfaces mapped. Nitrogen was strongly detected in specific regions of the Auger map, which corresponded to visible PPQ adhesive on the SEM micrograph. These data support the conclusion, based upon ESCA analysis, that anodic oxide/PPQ interphase fracture occurred.

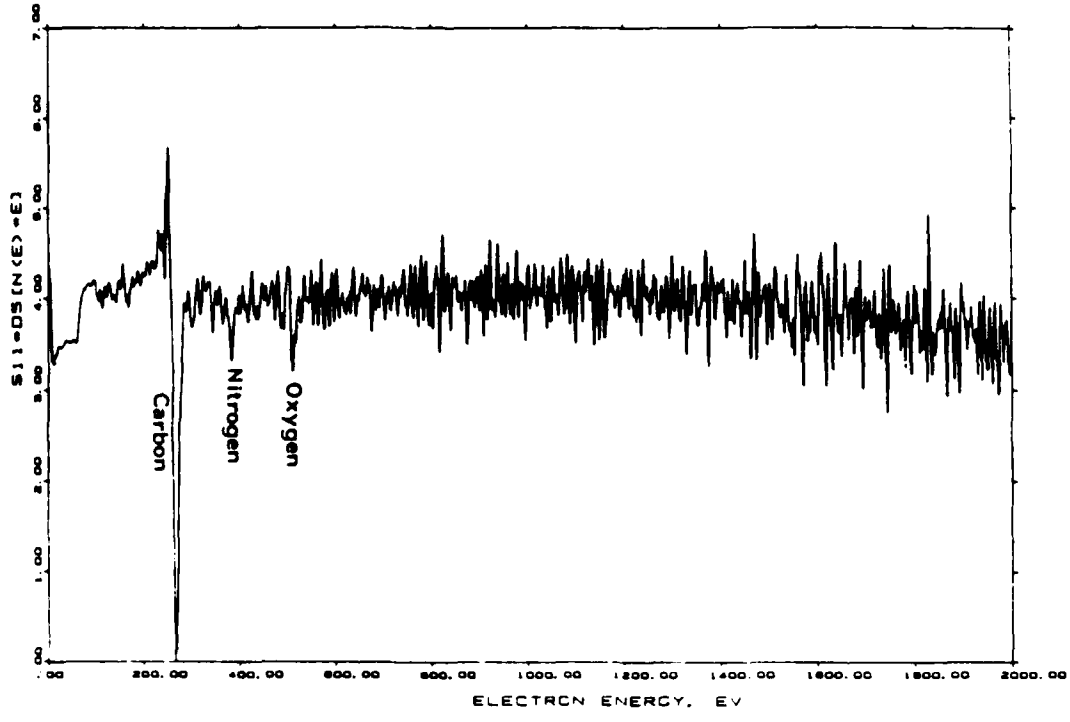


Figure 62. Auger Survey Analysis of a Fracture Surface for a 46.0 MPa CA/HF Anodized Ti-6Al-4V/PPQ Isothermally Processed Single Lap Bond. Side A.



Figure 63. SEM Micrograph of the Fracture Surface for a 46.0 MPa CA/HF Anodized Ti-6Al-4V/PPQ Isothermally Processed Single Lap Bond which was Nitrogen Auger Mapped (60X). Side A.

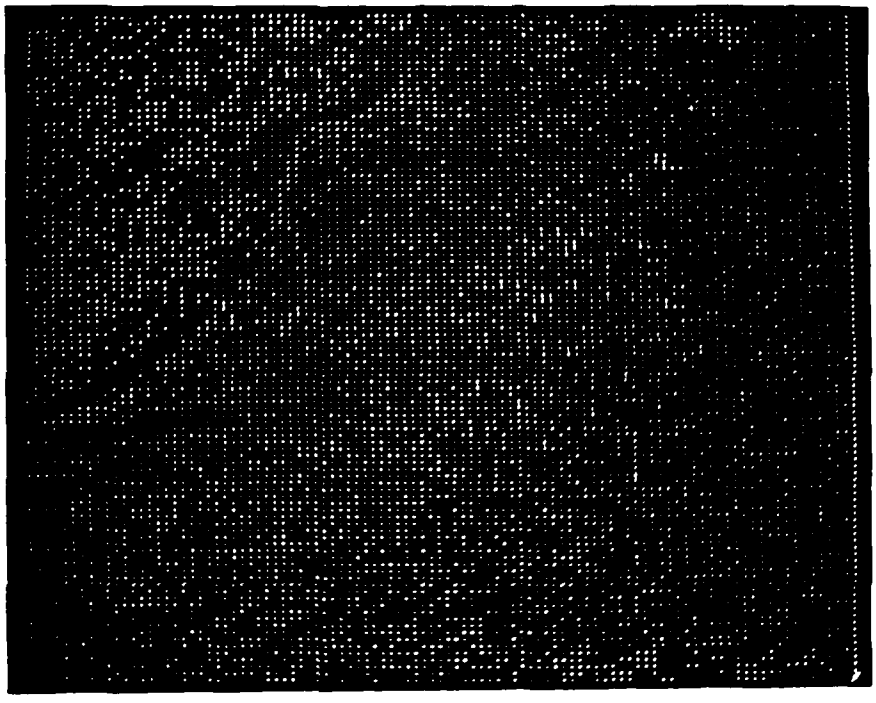


Figure 64. Nitrogen Auger Map for the Fracture Surface of a 46.0 MPa CA/HF Anodized Ti-6Al-4V/PPQ Isothermally Processed Single Lap Bond (60X). Side A.

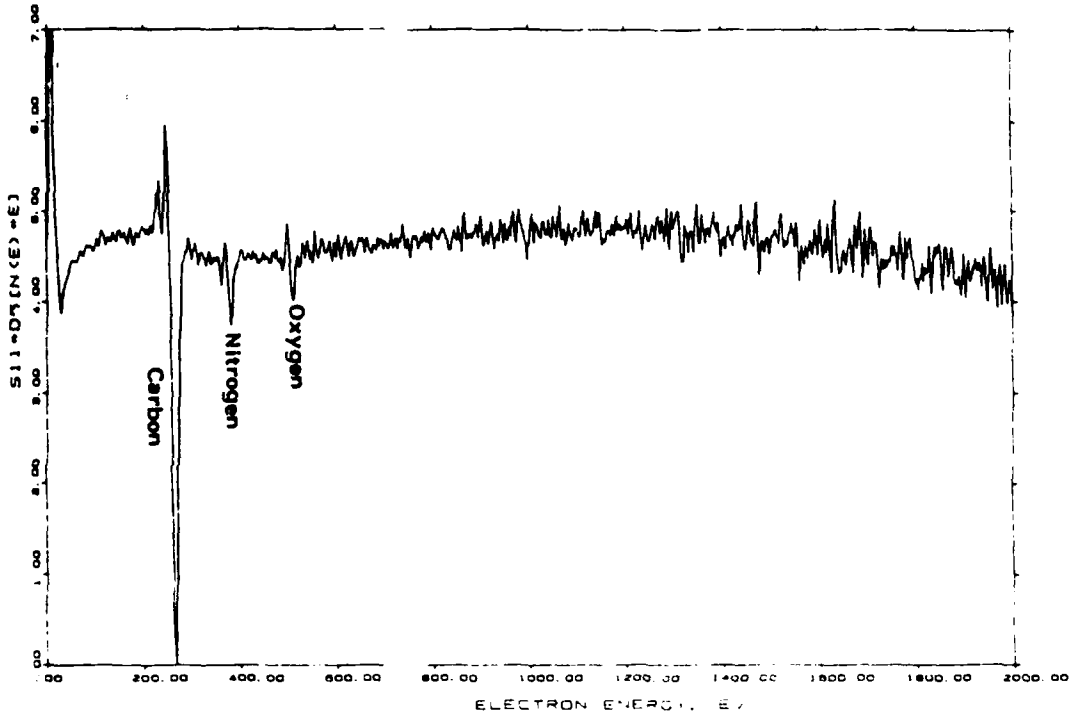


Figure 65. Auger Survey Analysis of a Fracture Surface for a 46.0 MPa CA/HF Anodized Ti-6Al-4V/PPQ Isothermally Processed Single Lap Bond. Side B.

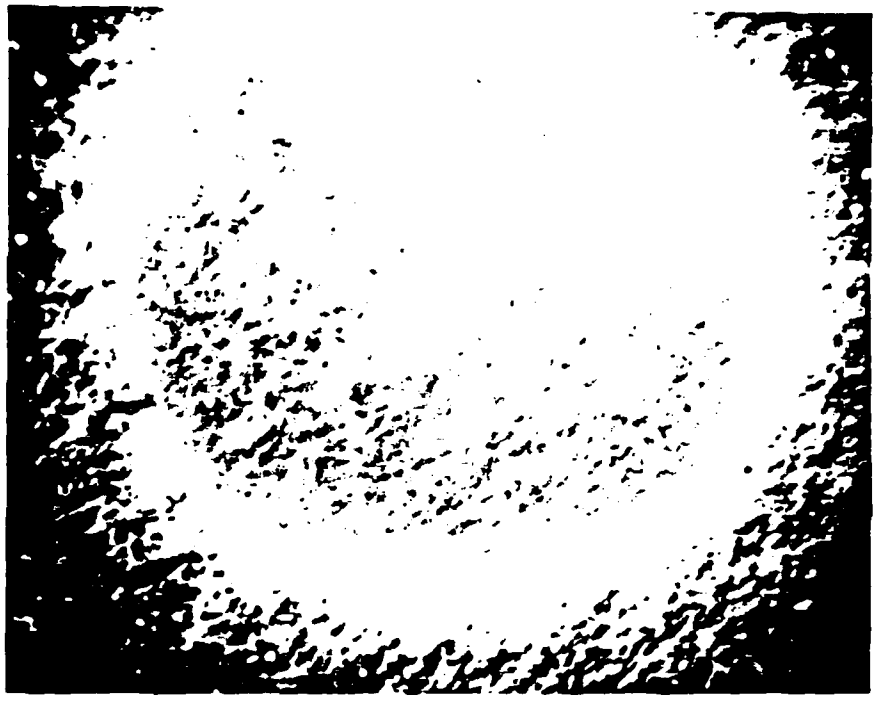


Figure 66. SEM Micrograph of the Fracture Surface for a 46.0 MPa CA/HF Anodized Ti-6Al-4V/PPQ Isothermally Processed Single Lap Bond which was Nitrogen Auger Mapped (60X). Side B.

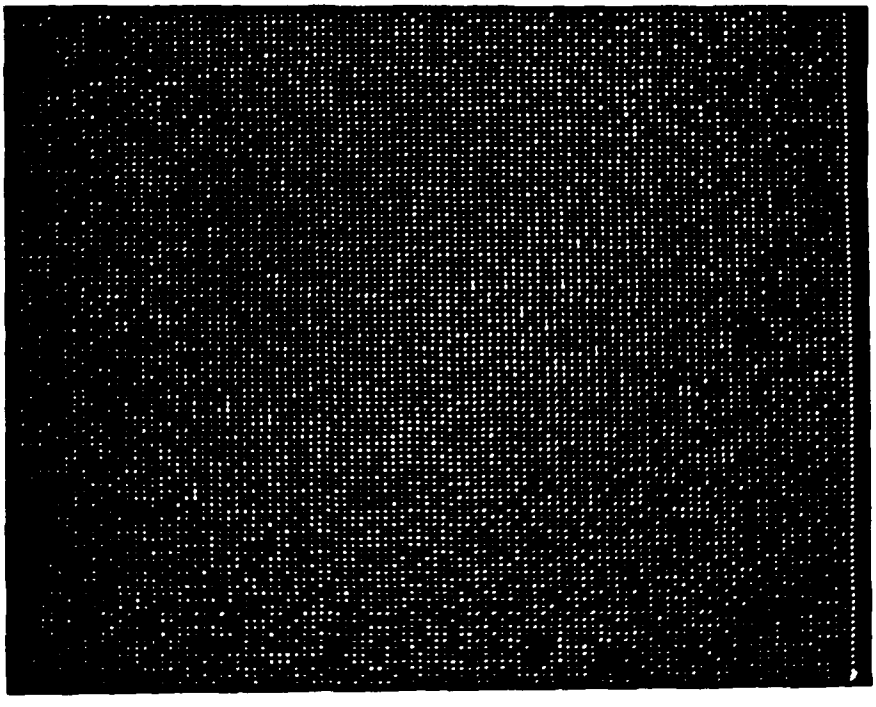


Figure 67. Nitrogen Auger Map for the Fracture Surface of a 46.0 MPa CA/HF Anodized Ti-6Al-4V/PPQ Isothermally Processed Single Lap Bond (60X). Side B.

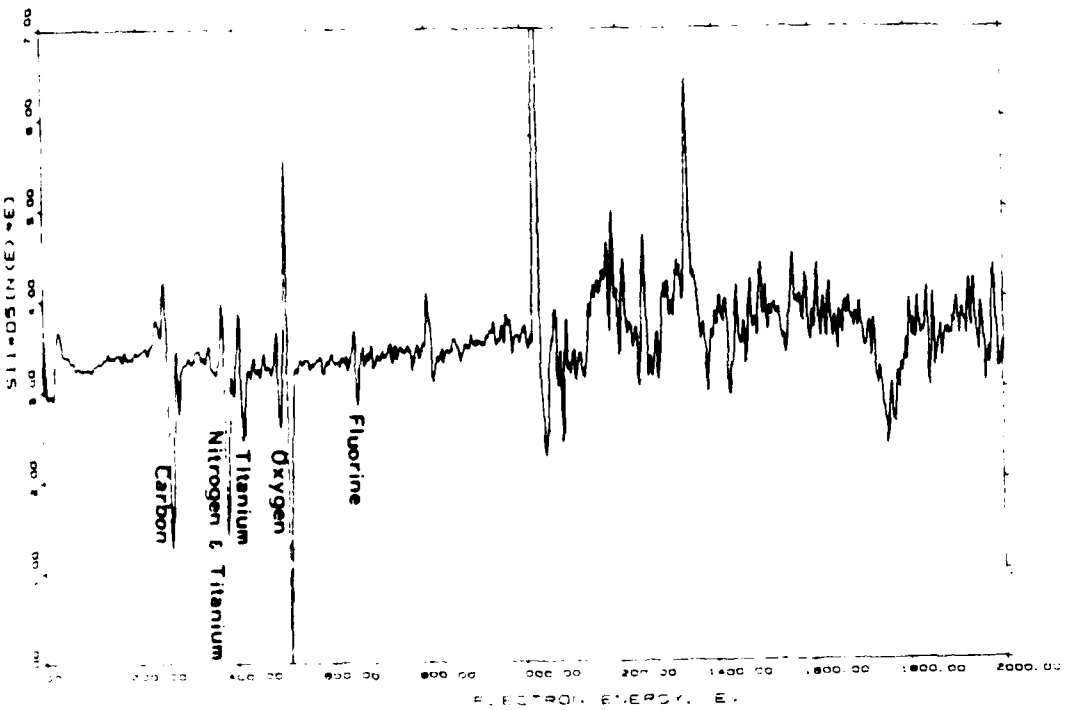


Figure 68. Auger Survey Analysis of a Fracture Surface for a 16.1 MPa CA/HF Anodized Ti-6Al-4V/PPQ Isochronally Processed Single Lap Bond. Side A.



Figure 69. SEM Micrograph of the Fracture Surface for a 16.1 MPa CA/HF Anodized Ti-6Al-4V/PPQ Isochronally Processed Single Lap Bond which was Nitrogen Auger Mapped (60X). Side A.



Figure 70. Fluorine Auger Map for the Fracture Surface of a 16.1 MPa CA/HF Anodized Ti-6Al-4V/PPQ Isochronally Processed Single Lap Bond (60X). Side A.

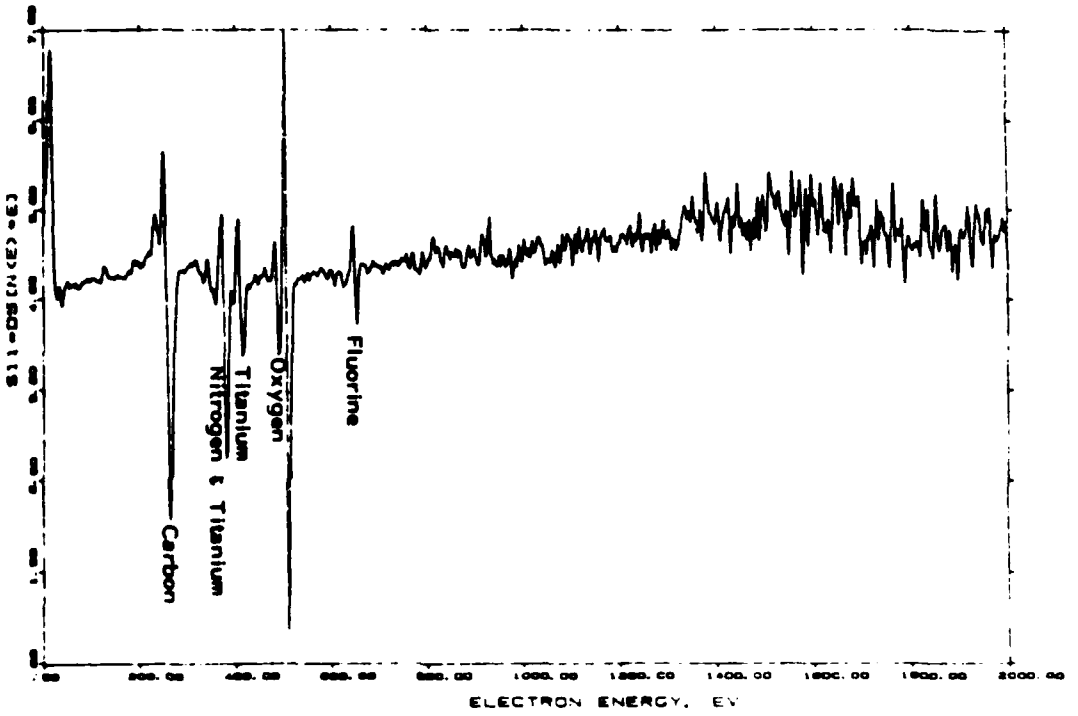


Figure 71. Auger Survey Analysis of a Fracture Surface for a 16.1 MPa CA/HF Anodized Ti-6Al-4V/PPQ Isochronally Processed Single Lap Bond. Side B.



Figure 72. SEM Micrograph of the Fracture Surface for a 16.1 MPa CA/HF Anodized Ti-6Al-4V/PPQ Isochronally Processed Single Lap Bond which was Nitrogen Auger Mapped (60X). Side B.

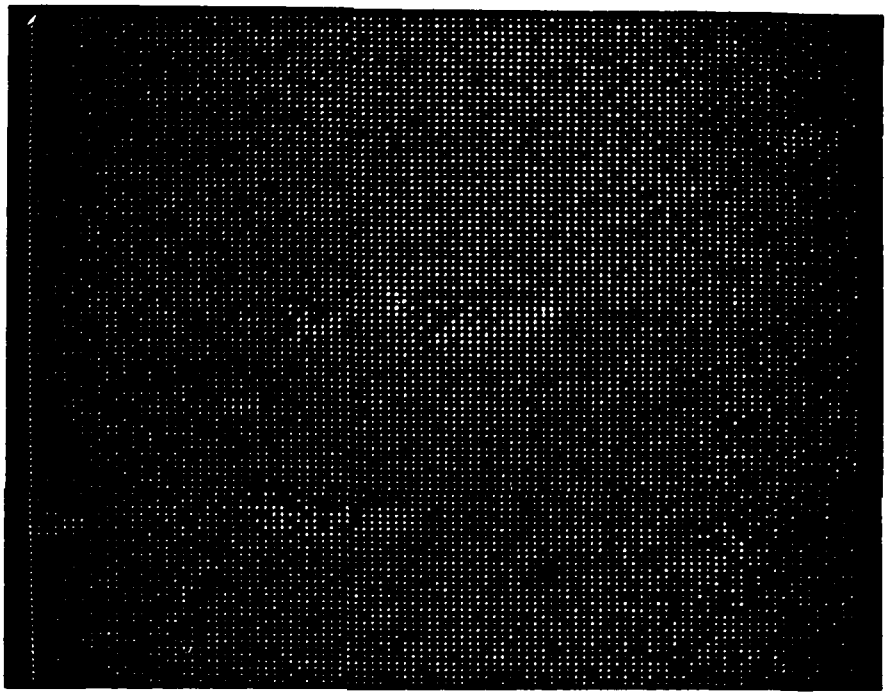


Figure 73. Fluorine Auger Map for the Fracture Surface of a 16.1 MPa CA/HF Anodized Ti-6Al-4V/PPQ Isochronally Processed Single Lap Bond (60X). Side B.

For the isochronally bonded CA/HF anodized Ti-6Al-4V/PPQ, the Auger survey indicated carbon, oxygen, fluorine, titanium and nitrogen. The ratio of 387 eV peaks to 418 eV peaks was not 1:1, as would be expected for titanium. The high 387 eV signal was attributed to the presence of nitrogen. As discussed above, it is not possible to distinguish nitrogen from titanium in Auger mapping. Therefore, fluorine mapping was used as an indicator of the anodic oxide on the fracture surface. As discussed earlier, low levels of fluorine, $\leq$ 3%, were detected by ESCA on the CA/HF anodized Ti-6Al-4V. Fluorine was detected over the entire Auger map for opposing fracture surfaces for the isochronally bonded PPQ/anodized Ti-6Al-4V. One surface had a stronger overall fluorine signal, as shown in Figure 73. These data support the conclusions based upon ESCA analysis that anodic oxide/PPQ interphase fracture occurred.

f. Proposed Model of the Single Lap Bond Fracture Sites and Mechanism Based upon Surface Analysis

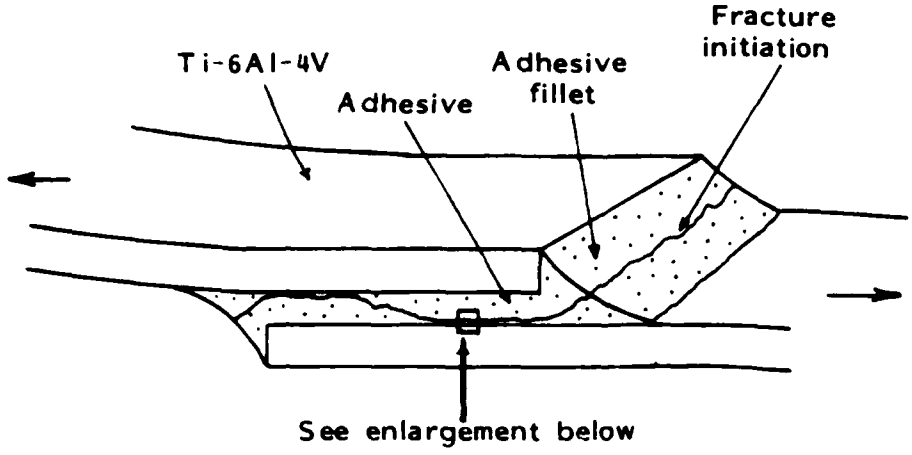
Based upon visual observations of the fracture surfaces, the typical failure surface observed exhibited anodic oxide/polymer interphase failure, in tandem with polymer cohesive failure in either a random or patterned distribution over the fracture surface. In general, ESCA and Auger analyses supported the visual observation of apparent anodic oxide/polymer interphase failure on the fracture surface. There was one exception. Visual observation of one

fracture surface indicated apparent anodic oxide/polymer interphase failure; however, ESCA analysis indicated polymer cohesive failure had occurred.

A few of the fracture surfaces exhibited one of the following three failure mechanisms, based upon visual observation: 1) apparent anodic oxide/polymer interphase failure only, or 2) apparent anodic oxide/metal interphase only, or 3) apparent anodic oxide/metal interphase failure, in tandem with polymer cohesive failure in a random distribution over the fracture surface. Based upon ESCA and Auger analyses, there was no microscopic evidence to support the visual observation of anodic oxide/metal interphase failure.

Figure 74 is a proposed model of the predominant fracture path for anodized Ti-6Al-4V/heat resistant adhesive bonds. Figure 75 is a proposed model of the predominant fracture path for the Lica® 44 primed, anodized Ti-6Al-4V/heat resistant adhesive bond. These models are based upon the fracture analyses which indicated anodic oxide/polymer interphase and/or polymer cohesive failure.

A model of the single lap bond fracture mechanism, or where and why failure occurred, can be described as follows, based upon failure analyses. Fracture initiated in the adhesive fillet and the polymer failed cohesively outside the bond overlap due to high peel stresses in the fillet. Fracture propagated in the bond overlap in two locations, cohesively in the polymer and also in the polymer/anodic oxide interphase. The bulk polymer cohesive



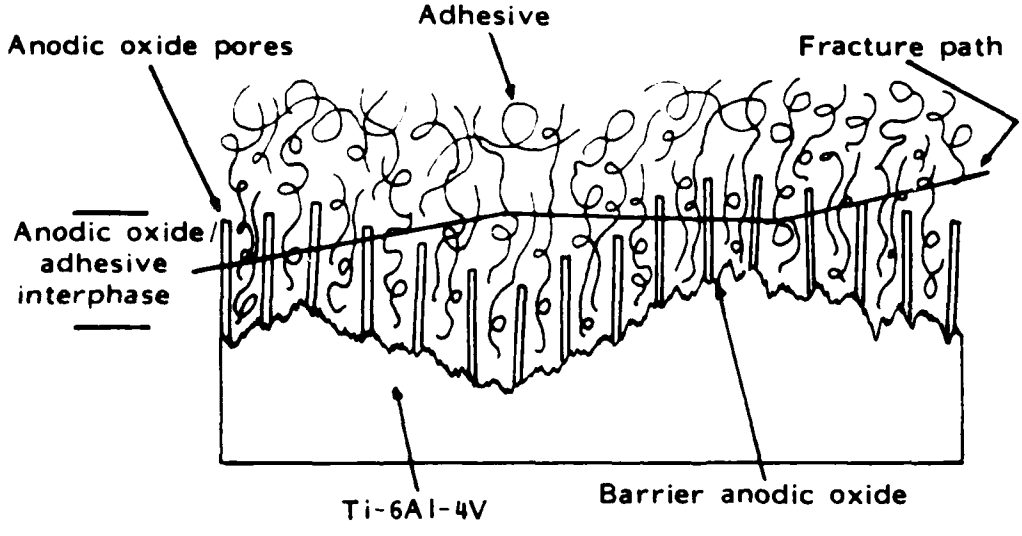
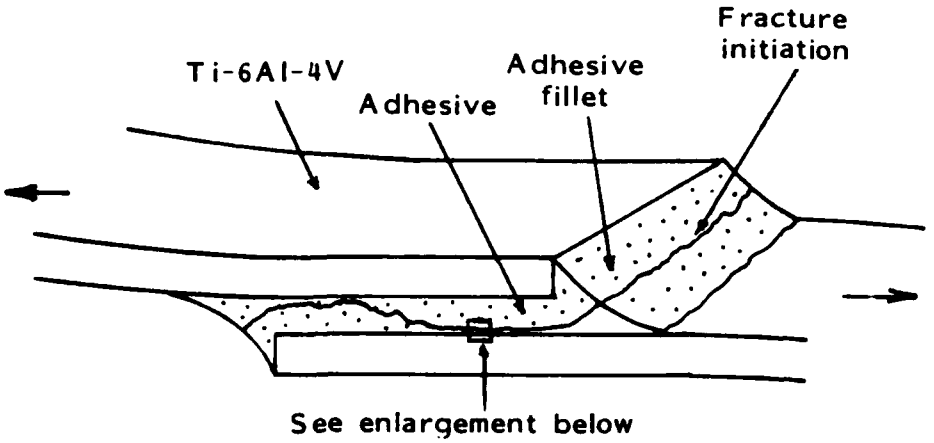


Figure 74. Proposed Model of the Fracture Sites for a CA/HF Anodized Ti-6Al-4V/Adhesive Bond.



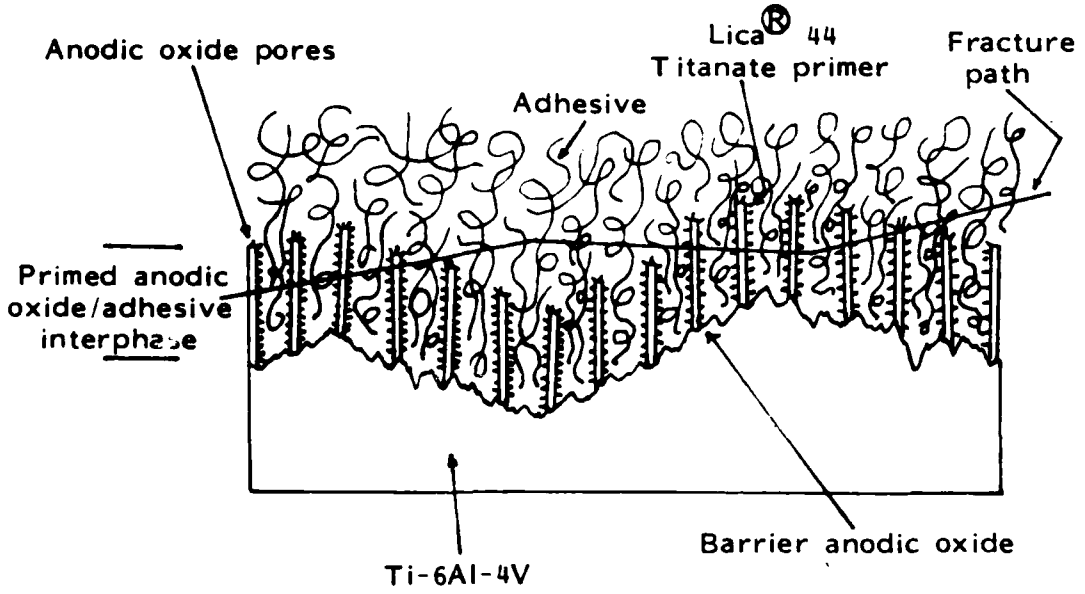


Figure 75. Proposed Model of the Fracture Sites for a Lica® 44 Primed CA/HF Anodized Ti-6Al-4V /Adhesive Bond.

strength and the polymer/anodic oxide interphase strength were the limiting factors in the single lap bond strength. The polymer/anodic oxide bond, due to van der Waals forces, was not the limiting factor in the single lap bond strength. Nor were the strengths of the anodic oxide/metal interphase or the metal cohesive strength limiting factors.

Localized stresses could be induced in the polymer and also in the anodic oxide/polymer interphase due to:

(1) thermal mismatch of the oxide and polymer during bond processing or thermal aging of the bond;

(2) adhesive shrinkage and/or voids due to bond processing or thermal aging of the bond;

(3) thermal mismatch of the polymer and filler during polymer processing; and/or,

(4) oxide flaws and/or contaminants from the anodization process or bonding process.

The single lap bond stresses, which are a combination of shear, tensile and peel, in concert with the localized stresses induced in the bulk polymer and the polymer/anodic oxide interphase due to processing, could exceed the critical stress required for crack initiation. Therefore, a crack can initiate and propagate either cohesively in the bulk polymer, in the anodic oxide or in the polymer of the anodic oxide/polymer interphase.

It is recognized that covalent bonds in the polymer chain backbone are inherently stronger than metallic bonds in the

Ti-6Al-4V alloy. However, based upon the failure analyses, failure did not occur cohesively in the metal. Secondary bonds, which are approximately 1/100th the strength of covalent bonds, interconnect the polymer chains. The localized stresses induced by bond processing or bond thermal aging could break these secondary bonds and cause the bulk polymer or the polymer in the anodic oxide/polymer interphase to fracture cohesively. It is also recognized that localized stresses due to bond or anodization processes would be induced in the anodic oxide/metal interphase. Fracture was not detected in this area, however. Therefore, it can be concluded that the critical stress required for crack initiation in this anodic oxide/metal interphase is higher than, and/or the level of induced stresses is lower than, for the anodic oxide/polymer interphase.

3. Polymer Fracture Surface Morphology

Figures 76 through 82 are high magnification SEM micrographs of the single lap bond fracture surface. The micrographs illustrate the polymer deformation up to fracture. Polymer morphology for each different heat resistant adhesive tested in the single lap bond study are included in these micrographs. These surfaces are representative of the surfaces examined for all bonds included in this study.

These SEM micrographs were used to categorize the polymer deformation up to fracture into one of three categories. These



Figure 76. SEM Micrograph of a Polymer Fracture Surface for a CA/HF Anodized Ti-6Al-4V/Udel® Polysulfone Single Lap Bond (10,000X).



Figure 77. SEM Micrograph of a Polymer Fracture Surface for a CA/HF Anodized Ti-6Al-4V Victrex^{R} Polyethersulfone Single Lap Bond (10 000X).

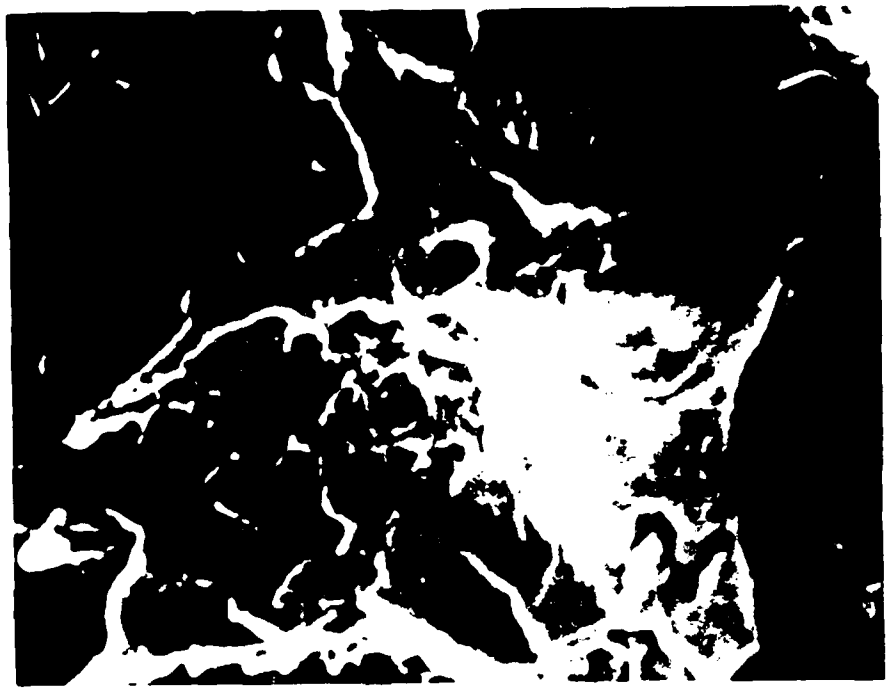
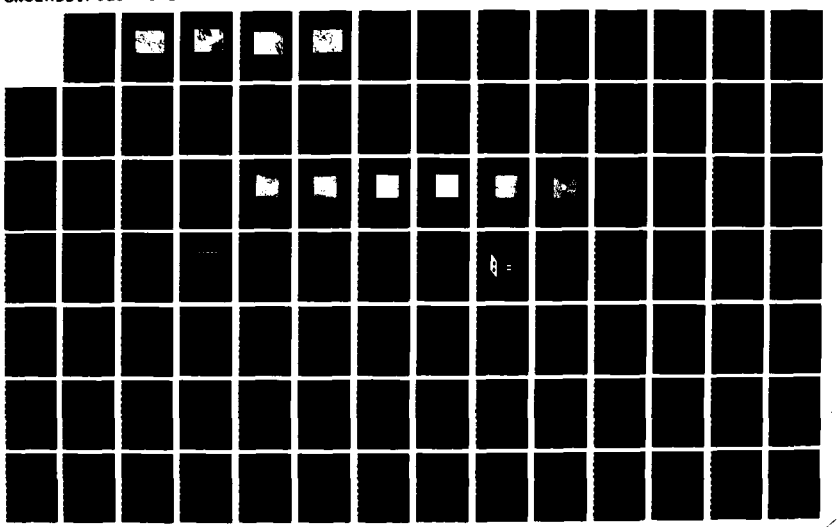
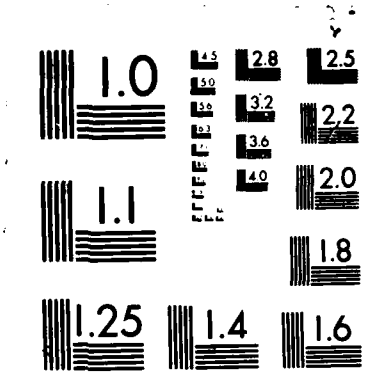


Figure 78. SEM Micrograph of a Polymer Fracture Surface for a CA/HF Anodized Ti-6Al-4V/Ultem® 1000 Polyetherimide Single Lap Bond (10,000X).

AD-A183 854 AN INTERDISCIPLINARY APPROACH TO PREDICTIVE MODELING OF 4/8
STRUCTURAL ADHESI (U) VIRGINIA TECH CENTER FOR
ADHESION SCIENCE BLACKSBURG J A SKILES ET AL JUN 87
UNCLASSIFIED CAS/CHEM-87-2 F/G 11/1 NL





MICROCOPY RESOLUTION TEST CHART
NATIONAL BUREAU OF STANDARDS 1963-A

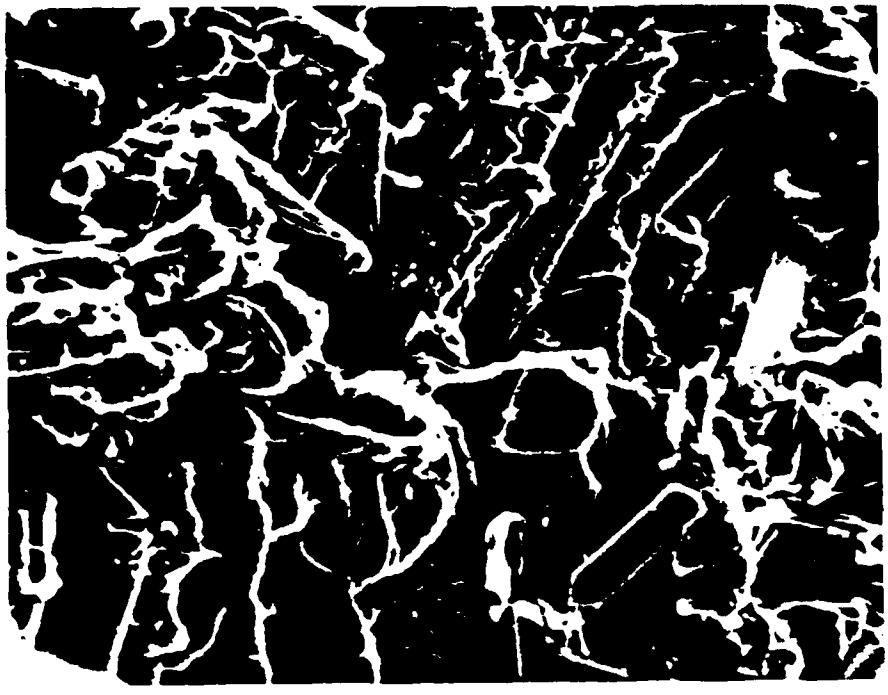


Figure 79. SEM Micrograph of a Polymer Fracture Surface for a CA/HF Anodized Ti-6Al-4V/Ultem® 2200, 20% Glass Filled Polyetherimide Single Lap Bond (500X).

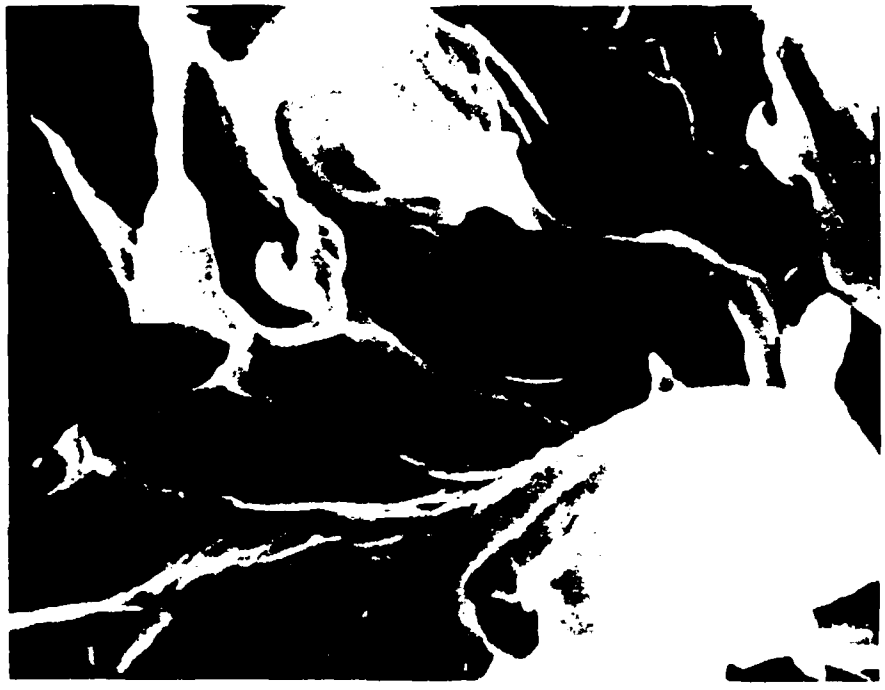


Figure 80. SEM Micrograph of a Polymer Fracture Surface for a CA/HF Anodized Ti-6Al-4V/Ultem® 2200, 20% Glass Filled Polyetherimide Single Lap Bond (10,000X).

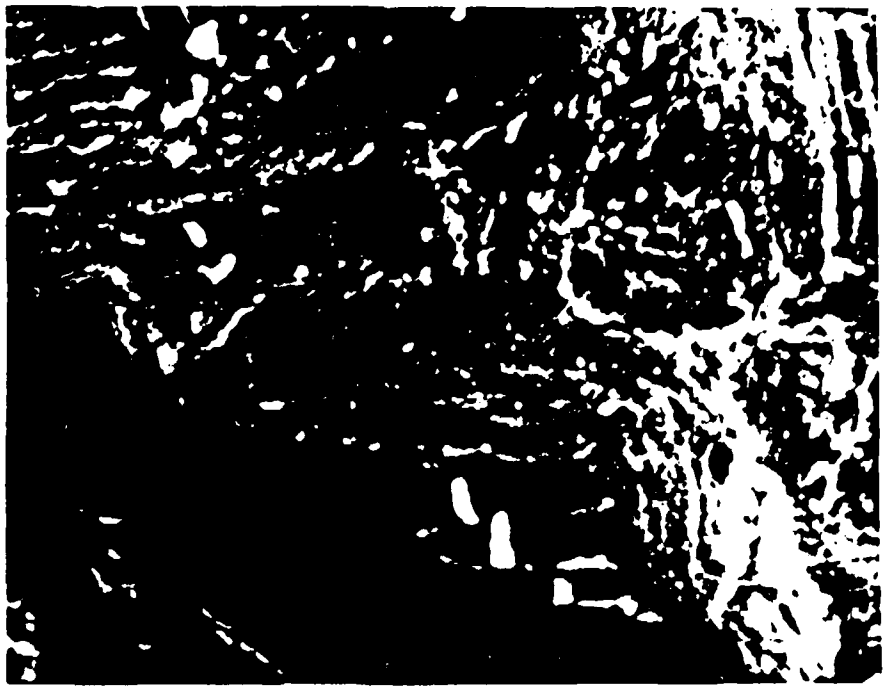


Figure 81. SEM Micrograph of a Polymer Fracture Surface for a CA/HF Anodized Ti-6Al-4V/Polyphenylquinoxaline Single Lap Bond (10,000X).



Figure 82. SEM Micrograph of a Polymer Fracture Surface for a CA/HF Anodized Ti-6Al-4V/Ablebond® 71-3, 50% $CaCO_3$ Filled Polyimide (5,000X).

three categories were suggested by Engel, et al.[51] and are based upon the polymer fibril length remaining on the fracture surface. The categories are:

1. high plastic deformation up to fracture, which results in polymer fibril lengths greater than 10μm;
2. low plastic deformation up to fracture, which results in polymer fibril lengths of 1-10μm; and,
3. brittle deformation up to fracture, which results in polymer fibrils less than 1 μm long with low levels of polymer deformation and relatively smooth polymer fracture surfaces.

Low plastic deformation up to fracture was evident, based upon SEM analyses for the following adhesives tested in single lap bonds: Udel® polysulfone, Victerex® polyethersulfone, Ultem® polyetherimide and Ultem® 20% glass filled polyetherimide. Brittle deformation up to fracture was observed for two adhesives tested, polyphenylquinoxaline and Ablebond® 71-3, 50% $CaCO_3$ filled polyimide.

The low plastic deformation and the brittle deformation observed for these heat resistant adhesives would be expected. In order to produce heat resistant adhesives, with continuous use temperatures described previously in Figure 1, from 423K to 505K, there must be a predominance of rigid, rather than flexible, chemical bonds in the polymer backbone structure. As a result, the polymer chain becomes more regular along its backbone, which

promotes strong interchain forces and thermal stability. Chemical structures for these adhesives have been illustrated earlier, in Table X. The high degree of aromaticity, and the presence of adjoining aromatic rings provided the rigidity to the polymer backbone necessary for high thermal stability. And, in the case of the polyimide thermoset, which had the highest reported continuous use temperature of the polymers tested, the polymer crosslinking is an added source of thermal stability.

The fibril microstructure was the evident polymer fracture response to absorb energy up to fracture for the polymers tested. The polymer flexibility necessary for this energy absorption mechanism of fibril formation to occur can, in part, be attributed to the presence in the polymer backbone of ether and/or aliphatic bonds.

CHAPTER V

SUMMARY

This work was conducted to identify anodization and bond process conditions which produce durable, structural single lap bonds ($\geq$ 6.9 MPa) for CA anodized Ti-6Al-4V/heat resistant adhesives, and to understand how and why these conditions are important to bond strength by describing the bond failure mechanisms. The conclusions are stated below.

1. Anodization without HF produced an average oxide thickness of 20 ± 10 nm. This was a sevenfold decrease in average thickness, compared to anodization with HF. CA anodization with HF increased the average bond strength by 30%, compared to anodization without HF, when polysulfone was the adhesive. Reasons for the strength differences may be described as follows. The thinner, less porous CA anodic oxide may have been inherently weaker than the thicker, more porous CA/HF oxide. The thickness and porosity of the CA/HF oxide may have promoted greater physical bonding and/or mechanical interlock of the adhesive to the oxide. The remainder of the study concentrated on CA/HF anodization conditions because of these bond strength results.
2. CA/HF anodization of Ti-6Al-4V for anodization conditions of: 10 V, 20 minutes, 20 ± 2 A/m^2 initial current density, at 298 ± 2K or 283 ± 2K, produced an anodic oxide with the following

characteristics: amorphous; follows the contours of the Ti-6Al-4V substrate; ≈ 170 nm peak-to-valley roughness, and pore diameters of 25 to 40 nm and wall thickness of 10 nm .

3. Oxide thickness did vary across the CA/HF anodized Ti-6Al-4V surface. MBI and TEM techniques used to determine average oxide thickness and range of values were in good agreement. For TEM, the measured average oxide thickness was 120 ± 20 nm, with values ranging from 95 to 150 nm. For MBI, the average oxide thickness was 160 ± 10 nm, with values ranging from 150 to 180 nm. CA/HF anodization conditions were: 10 V, 20 minutes, 20 A/m² initial current density, 283 ± 2K.
4. For the CA/HF anodization conditions examined, the following relationships were apparent: a direct, nonlinear relationship between oxide thickness and initial current density; an inverse, nonlinear relationship between oxide thickness and anodization solution temperature, and; increasing anodization time from 20 to 60 minutes doubled anodic oxide thickness.
5. CA/HF anodized Ti-6Al-4V/polysulfone single lap average bond strength and failure site were unaffected by average anodic oxide thickness in the range of 65 to 410 nm, for the anodization conditions tested. Changes in oxide thickness were produced by varying the initial current density (20 ± 2 A/m² or 30 ± 2 A/m²) and anodization solution temperature (283 ± 2K or 298 ± 2K) for 20 minute anodization at 10 V.

6. CA/HF anodized Ti-6Al-4V/polysulfone average bond strength was influenced by the choice of either a 20 ± 2 A/m^2 or 30 ± 2 A/m^2 anodization initial current density. The 20 ± 2 A/m^2 initial current density produced 20% higher average bond strengths than the 30 ± 2 A/m^2 initial current density. The polysulfone microstructure may have been degraded by the high fluoride content in the oxide resulting from the unnecessarily high initial current density.
7. In general, CA/HF anodized Ti-6Al-4V/heat resistant adhesive single lap bonds had good structural strengths, $\geq$ 18.6 MPa, when tested after 0.5 month aging at 298 ± 5K, or 9 months aging at 443 ± 5K. These values exceeded the structural single lap bond criterion by at least a factor of 2.7.
8. The CA/HF anodized Ti-6Al-4V/50% $CaCO_3$ filled polyimide single lap bond strengths were marginal, $\approx$ 6.0 MPa, when tested after 0.5 month aging at 298 ± 5K, or 9 months aging at 443 ± 5K. Low bond strength may be due to polyimide competition for the calcium carbonate filler and oxide.
9. In general, Lica® 44 titanate primer, applied to the CA/HF anodized Ti-6Al-4V, had no significant influence upon single lap bond strength. These bonds were thermally aged, unstressed, at 443 ± 5K for 9 months before testing.
10. Bond strengths were 45% higher for the isothermal vs. the isochronal bond process for CA/HF anodized Ti-6Al-4V/poly-

phenylquinoxaline bonds. Oxide degradation may have resulted from the isochronal bond process.

11. Single lap bond fracture initiation occurred in the adhesive fillet and propagation occurred in the anodic oxide/polymer interphase and/or cohesively in the polymer.
12. Structural bonds resulted for all the CA/HF anodization and bond process conditions tested.

CHAPTER VI

RECOMMENDATIONS FOR FUTURE STUDY

In this study, single lap bonds were subjected to unstressed thermal aging at a constant temperature. Future work should include single lap bonds characterized during and after repeated, cyclic thermal aging from 218K to 398K in a varying R.H. environment, which complies to military environmental test specifications. This testing should be conducted for both stressed and unstressed bonds. Single lap bonds should also be characterized after specific vibrations and gravitational forces induced by rapid changes in acceleration in the x, y, and z directions, which would simulate this aspect of aircraft operational conditions. Also, tests should be designed to select the proper sequential combinations of repeated cyclic thermal aging, relative humidity, vibration and acceleration for both unstressed and stressed bonds to simulate the combined effects of these environmental conditions upon the adhesive/metal bond. Strength should be determined for bonds subjected to constant strain. Tests should be conducted for a series of constant strains. The time dependent bond strength-strain relationship could then be determined. Future work should include thermoplastic polyimides and polyimide siloxanes which have good processability and good heat resistance, as well as the six adhesives tested in this study. A non-damaging bond test should be developed to assure some initial and/or long term minimum reliable bond strength in a realistic environment.

LITERATURE CITED

1. D. McCormick, Design Engineering, February, 1982, p. 85.

2. E. Oberg and F. D. Jones, Machinery's Handbook (18th ed.; Industrial Press, Inc., New York), p. 1219.

3. D. V. Edison, Design News, December 19, 1983, p. 46.

4. Modern Plastics Encyclopedia 1985-86, J. Agranoff, ed., (McGraw-Hill, Inc., New York, 1985), p. 505.

5. T. J. Aponyi, in Handbook of Adhesives, I. Skeist, ed., (Van Nostrand Reinhold Co., New York, 1977), p. 625.

6. Udel® Polysulfone Product Bulletin, Union Carbide Corporation.

7. Terry L. St. Clair and Donald J. Progar, Abstracts of Papers, 9th Annual Meeting of the Adhesion Society, Hilton Head, SC; Adhesion Society: Washington, D.C. Abstract No. 1.

8. W. A. Zisman, Ind. Eng. Chem. 55, No. 10, 19 (1963).

9. H. Schonborn and L. H. Sharpe, Pol. Letters 2, 719 (1964).

10. Handbook of Physics and Chemistry, C. D. Hodgman, ed., (Chemical Rubber Publishing Company, New York, 1962).

11. N. J. DeLollis, in Handbook of Adhesives, I. Skeist, ed., (Van Nostrand Reinhold Publishing Co., New York, 1962), p. 513.

12. D. H. Kaelble, Physical Chemistry of Adhesion, (John Wiley and Sons, Inc., New York, 1971), p. 450, 489 491-94.

13. A. F. Lewis and R. T. Natarajan, in Polymer Science and Technology, vol. 9A, L. H. Lee, ed., (Plenum Press, New York, 1975), pp. 563-577.

14. D. D. Eley, in Adhesion. (Oxford University Press, Fair Lawn, NJ, 1961), p. 32.

15. S. S. Voyutskii and V. L. Vakula, J. Appl. Polym. Sci. 7, 475 (1963).

16. W. L. Baun, Surface Technology 11, 421 (1980).

LITERATURE CITED (Continued)

17. B. M. Ditchek, K. R. Breen, T. S. Sun and J. D. Venables, 25th Nat. SAMPE Symp. and Exhibition, 13 (1980).

18. B. M. Ditchek, K. R. Breen, T. S. Sun and J. D. Venables, 12th Nat. SAMPE Tech. Conf., 882 (1980).

19. M. Natan, J. D. Venables and K. R. Breen, 27th Nat. SAMPE Symposium, 178 (1982).

20. J. J. Bickerman, Appl. Chem. 11, 81 (1961).

21. H. Schonborn and R. H. Hansen, J. Appl. Polym. Sci. 11, 1461 (1967).

22. J. M. Chen, T. S. Sun and J. D. Venables, 22nd Nat. SAMPE Symp. and Exhibition, 25 (1977).

23. B. M. Ditchek, K. R. Breen and J. D. Venables, Martin Marietta Laboratories Report MML TR-80-17-C, prepared for Naval Air Systems Command (1980).

24. M. R. Tant and G. L. Wilkes, Polym. Eng. and Sci. 21, 874 (1981).

25. M. Cizmecioglu, R. F. Fedors, S. D. Hong and J. Moachanin, Polym Eng. and Sci. 21, 940 (1981).

26. L. C. E. Struik, Physical Aging in Amorphous Polymers and Other Materials (Elsevier Scientific Publishing Co., Amsterdam, 1978), pp. 20, 26, 27, 69-83.

27. S. E. B. Petrie, J. Macromol., Sci. Phys. B. 12, 225 (1973).

28. S. Matsuoka, H. E. Bair, S. S. Bearder, H. E. Kern and S. T. Ryan, Polym. Eng. Sci. 18, 1073 (1978).

29. E. Kong, G. L. Wilkes, J. E. McGrath, A. K. Banthia, Y. Mohajer and M. R. Tant, Polym. Eng. Sci. 21, 943 (1981).

30. C. L. Brett, "The Effect of State of Cure on Bond Performance", in Adhesion 3, K. W. Allen, ed., (Applied Science Publishers, Ltd., London, 1983), p. 53.

31. M. Goland and E. Reissner, J. Appl. Mechan. 11, 17A 1944.

LITERATURE CITED (Continued)

31A. B. M. Barthelemy, M. P. Kamat, and H. F. Brinson, Virginia Polytechnic Institute and State University Report VPI-E-84-15, prepared for Office of Naval Research, (1984).

32. C. V. Cagle, in Handbook of Adhesive Bonding (McGraw-Hill, New York, 1973), pp. 11-14, 11-15, 31-9.

33. N. A. DeBruyne, Tech Notes (Aero Research Ltd., Duxford, England, 1948), as cited in C. V. Cagle, in Handbook of Adhesive Bonding (McGraw-Hill, New York, 1973), p. 31-9.

34. P. M. Hergenrother and D. J. Progar, 22nd Nat. SAMPE Symp. and Exhibition, 211 (1977).

35. Y. Moji and J. A. Marceau, U. S. Patent No. 3,959,091 The Boeing Company, (1976).

36. M. Natan, K. R. Breen and J. D. Venables, Martin Marietta Laboratories Report MML TR-81-42(C), prepared for Dept. of the Navy (1981).

37. A. Matthews, Am. Mineral 61, 419 (1976).

38. W. L. Baun, J. Adhesion 12, 81 (1981).

39. M. Natan and J. D. Venables, Martin Marietta Laboratories Report MML TR-82-20(C), prepared for Dept. of the Navy (1982).

40. W. Chen, R. Siriwardane and J. P. Wightman, 12th Nat. SAMPE Tech. Conf., 896 (1980).

41. M. Natan and J. Venables, Martin Marietta Laboratories Final Report MML TR-81-42(C), prepared for Dept. of the Navy (1981).

42. A. Cheng, "Anodic Oxide Formation on Ti-6Al-4V in Chromic Acid for Adhesive Bonding" M. S. Thesis, Virginia Polytechnic Institute and State University (1983).

43. J. Marceau. The Boeing Company, private communication November 25, 1983.

44. J. A. Filbey and J. P. Wightman, Virginia Polytechnic Institute and State University Report CAS/CHEM-4-86, prepared for Office of Naval Research, (1986).

LITERATURE CITED (Continued)

45. J. A. Filbey and J. P. Wightman, Virginia Polytechnic Institute and State University Report CAS/CHEM-6-86, prepared for Office of Naval Research, (1986).

46. KEN-REACT® Reference Manual No. KR-1084L, Kenrich Petrochemicals, Inc., Bayonne, NJ.

47. P. Hergenrother, J. Appl. Polym. Sci. 28, 355 (1983).

48. C. L. Hendrick, The Boeing Aerospace Company Contract Report #NAS1-15605, prepared for the National Aeronautics and Space Administration, (1980).

49. L. H. Sharpe, J. Adhesion 4, 51 (1972).

50. S. G. Hill, P. D. Peters and C. L. Hendricks, The Boeing Aerospace Company Contract Report #165944, prepared for the National Aeronautics and Space Administration (1982).

51. Lother Engel, Hermann Klingele, Gottfried Ehrenstein and Helmut Schaper, An Atlas of Polymer Damage (Prentice-Hall, Inc., Englewood Cliffs, NJ, 1981), pp. 152-197.

52. H. E. Klugh, Statistics: The Essentials of Research (John Wiley and Sons, Inc., New York, 1974), pp 250-264, p.396.

APPENDIX I

Approximation of the Titanate Monolayer Coverage on the Anodized Ti-6Al-4V Surface

Assumptions

1. The total volume for one titanate molecule is best described by a cone. The titanate chemical structure and the assumptions of a 0.3 nm atom diameter, a 0.1 nm covalent bond distance and a 1.0 nm van der Waals distance were used to approximate these cone dimensions. Cone dimensions were taken to be 3 nm in diameter and 5 nm in length.
2. The titanate molecules are packed on the anodized Ti-6Al-4V surface so that unoccupied volume is represented by the free volume of the cone.
3. The titanate primer was uniformly applied to the anodized Ti-6Al-4V surface.
4. Each of the 48 anodized Ti-6Al-4V coupons were primed with the same volume of titanate primer.
5. The titanate coverage can be calculated based upon the volume of titanate solution used to prime the anodized Ti-6Al-4V coupon. It is assumed that 75% of this volume of titanate primer remains soaked into the 25.4 mm X 50.8 mm sponge brush.

Given

1. Lica® 44 Structure: $RO\text{-}Ti(O\text{-}C_2H_4\text{-}NH\text{-}C_2H_4\text{-}NH_2)_3$, where R is composed of 12 carbon atoms, 21 hydrogen atoms and 2 oxygen atoms.
2. Lica® 44 molecular weight: 590 g/mole.
3. Lica® 44 density at 289K: 1.17 g/cm³.
4. A 0.2% V/V of Lica® 44/isopropanol solution was used to prime 48 anodized Ti-6Al-4V coupons. A total of 38.5 ml of the solution was used.
5. An anodized surface area of 2.54 cm X 2.54 cm was primed for each coupon.
6. The CA/HF anodized surface has pores over the entire surface. The pores have a 10 nm wall thickness, a 30 nm pore diameter and $\geq$ 100 nm height.

Calculations

1. The titanate solution volume applied to each anodized Ti-6Al-4V coupon is (0.25 X 38.5 ml)/48 coupons = 0.2 ml/coupon.
2. The titanate volume applied to each anodized Ti-6Al-4V coupon is:

$$\frac{0.2 \text{ ml solution}}{\text{coupon}} \times \frac{0.002 \text{ ml titanate}}{\text{ml solution}} = \frac{4.01 \times 10^{-4} \text{ ml titanate}}{\text{coupon}}$$

3. The titanate weight applied to each anodized Ti-6Al-4V coupon is:

$$\frac{4.01 \times 10^{-4} \text{ ml titanate}}{\text{coupon}} \times \frac{1.17 \text{ g}}{\text{ml}} = \frac{4.69 \times 10^{-4} \text{ g}}{\text{coupon}}$$

Calculations (Continued)

4. The number of titanate molecules applied to each anodized coupon is:

$$\frac{4.69 \times 10^{-4} \text{ g titanate}}{\text{coupon}} \times \frac{\text{mole}}{590 \text{ g}} \times \frac{6.02 \times 10^{23} \text{ molecules}}{\text{mole}} =$$

$$\frac{4.79 \times 10^{17} \text{ molecules}}{\text{coupon}}$$

5. Based upon the assumption that one titanate molecule sweeps out a cone 3 nm in diameter and 5 nm in length, the area of titanate molecules on each anodized Ti-6Al-4V coupon is:

$$\frac{4.79 \times 10^{17} \text{ titanate molecules}}{\text{coupon}} \times \frac{\pi (1.5)^2 \text{ nm}^2 \text{ titanate}}{\text{molecule}} =$$

$$\frac{3.39 \times 10^{18} \text{ nm}^2 \text{ of titanate}}{\text{coupon}}$$

6. The number of anodic oxide pores in a $(2.54 \times 10^7 \text{ nm})^2$ anodized surface area can be calculated as follows, given that each pore occupies 40 nm across the anodized surface:

$$\frac{\text{pore}}{40 \text{ nm length}} \times 2.54 \times 10^7 \text{ nm anodized surface length} =$$

$$6.35 \times 10^5 \text{ pores}$$

$(6.35 \times 10^5 \text{ pores})^2 = 4.0 \times 10^{11}$ pores on the anodized surface area.

7. The number of titanate monolayers on each anodized Ti-6Al-4V coupon is:

Calculations (Continued)

$$\frac{3.39 \times 10^{18}\ \text{nm}^2 \text{ of titanate}}{\text{coupon}} \times \frac{\text{coupon}}{(2.54 \times 10^{7}\ \text{nm})^2} +$$

$$\frac{\text{coupon}}{\frac{(30\ \text{nm})(100\ \text{nm})}{\text{pore}} \times (4.0 \times 10^{11}\ \text{pores})} =$$

$$\frac{7.63 \times 10^{2} \text{ titanate monolayers}}{\text{anodized Ti-6Al-4V coupon}}$$

8. The thickness of titanate is:

$$\frac{7.63 \times 10^{2} \text{ titanate monolayers}}{\text{coupon}} \times \frac{5\ \text{nm length}}{\text{titanate molecule}} =$$

3.8×10^{3} nm thick

APPENDIX II

T-Test Statistical Analysis

The t-test statistical analyses was used throughout this study whenever it was necessary to compare one set of single lap bond strength data against another set of single lap bond strength data to determine whether these data were significantly different. Specifically, the t-test compares the mean of one group of data against the mean of another group of data and tests whether or not these two sample means come from the same population.

The t-test is based upon several assumptions.[52] These assumptions are stated as follows:

(1) the sample means are drawn from normally distributed populations;

(2) the data in each sample group is randomly obtained;

(3) each observation is independent of all other observations; and,

(4) all samples taken from any one population should have the same variance.

For the purpose of these analyses, it is assumed that all of the t-test assumptions are met.

In order to determine whether or not the two sample groups being examined have been taken from the same population, the t-test computes the t statistic. The t statistic is defined as

follows:

$$t = (X_1 - X_2)/S_{X_1 - X_2} \qquad [1]$$

where:

X_1 = sample mean of group 1;

X_2 = sample mean of group 2; and,

$S_{X_1 - X_2}$ = estimate of the standard error of the difference between two means.

The standard error of the difference between two means is given by the formula

$$S_{X_1 - X_2} = \sqrt{(S_1^2/n_1) + (S_2^2/n_1)} \qquad [2]$$

where

S_1^2 = variance of group 1;

S_2^2 = variance of group 2;

n_1 = number of samples in group 1; and,

n_2 = number of samples in group 2.

The t statistic calculated from the data is compared to a table of critical values for t at the appropriate degrees of freedom and level of significance. A significance level of 99% was used. If the calculated t statistic is equal to or exceeds the critical t value, then it can be stated that the two groups of single lap bond strength data being tested do not come from the same population.

APPENDIX III

F-Test Statistical Analysis: The One Way Analysis of Variance Test

The One-Way Analysis of Variance statistical test is used whenever three or more groups of data are to be compared. This test examines the groups of data presented and determines:

(1) whether all of the groups were taken from the same population; and,

(2) which of the groups, if any, are to be considered part of different populations.

The One-Way Analysis of Variance answers the questions stated above at whatever confidence level is desired. A 99% confidence level was used in all analyses conducted for this study. The computer program "Statistical Package for the Social Sciences", or SPSS-X, was used to conduct these analyses, using the Scheffe test procedure.

The One-Way Analysis of Variance is based upon several assumptions.[52] These assumptions are:

(1) the samples are drawn from normally distributed populations;

(2) the data in each sample group is randomly obtained;

(3) each observation is independent from all other observations; and,

(4) all samples taken from any one population should have the same variance.

For purposes of these analyses, it was assumed that all of the One-Way Analysis of Variance assumptions were met.

In order to determine whether or not all of the samples have been taken from the same population, the One-Way Analysis of Variance calculates the F ratio. This F ratio is defined as follows:

$$F = S_w^2/S_b^2 \qquad [1]$$

where:

$$S_w^2 = \sum_1^k \sum_1^n (X - \bar{X}_k)^2/(k(n-1)) \qquad [2]$$

and:

$$S_b^2 = n \sum_1^k (\bar{X} - \bar{\bar{X}})^2/(k-1) \qquad [3]$$

In the formula stated above,

S_w^2 = the within samples estimate of the population variance;

S_b^2 = the between samples estimate of the population variance;

k = number of sample groups;

n = number of individual observations within each sample group;

X = individual observation;

$\bar{X}$ = average of any one sample group; and,

$\bar{\bar{X}}$ = average of all sample groups combined.

The F ratio calculated from the data is compared to a table of critical values for F at the appropriate degree of freedom and

level of significance.[52] If the calculated F ratio is equal to or exceeds the critical value, then it can be stated that all of the sample groups do not come from the same population.

The One-Way Analysis of Variance package also permitted the comparison of every sample group mean with every other sample group mean in order to identify the group or groups, if any, that do not come from the same population. This procedure calculates a slightly modified F ratio that is defined as follows:

$$F = (\bar{X}_1 - \bar{X}_2)^2/(S_w^2((n_1 + n_2)/(n_1 \times n_2))) \qquad [4]$$

where:

$\bar{X}_1$ = sample mean of the first group being examined;

$\bar{X}_2$ = sample mean of the second group being examined;

S_w^2 = the within samples estimate of population variance, which was described above;

n_1 = sample size of the first group being examined; and,

n_2 = sample size of the second group being examined.

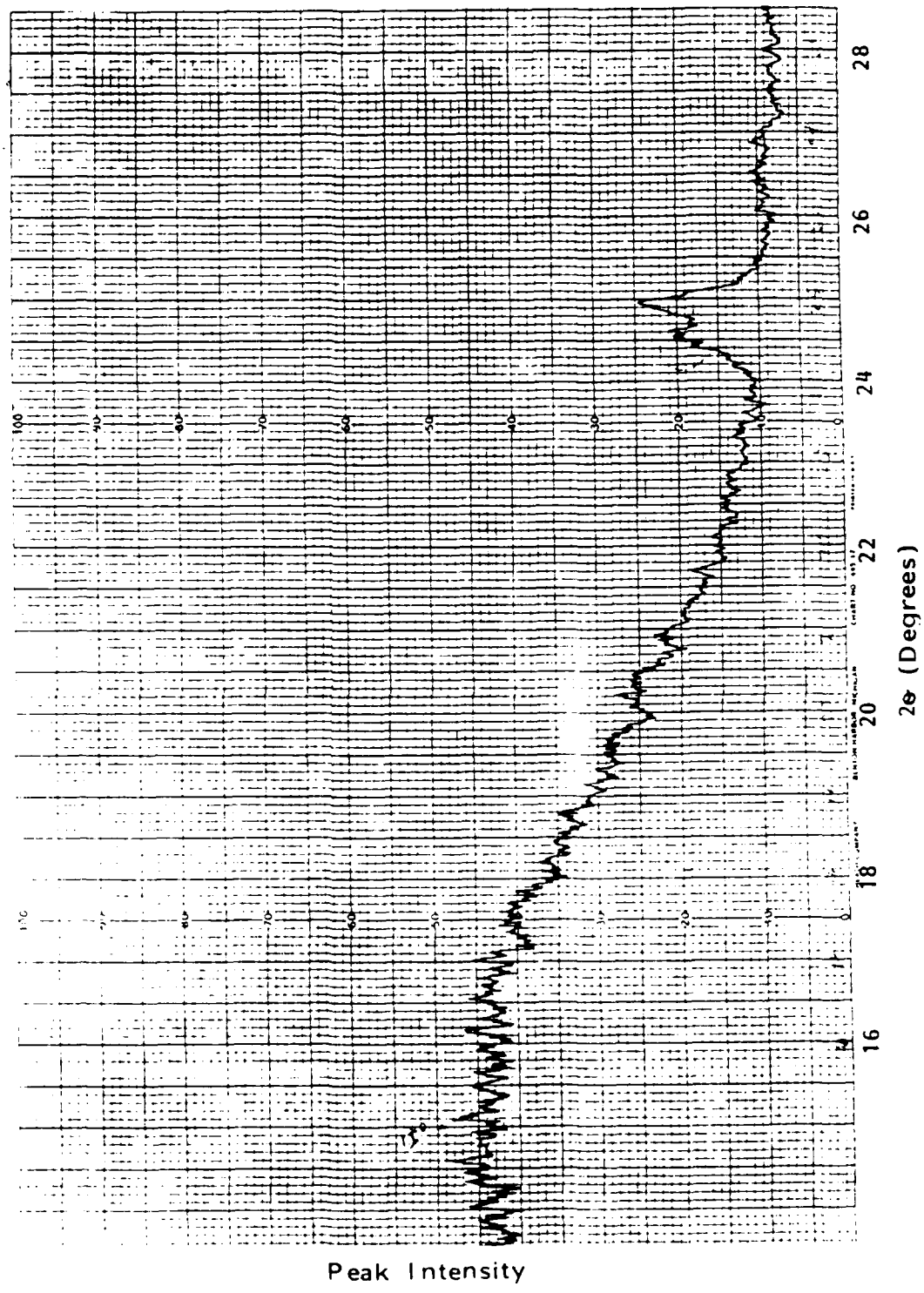
The calculated F ratio is then compared to the table of critical values of F at the desired degree of freedom and significance level.[52] If the calculated F ratio is equal to or exceeds the critical value, then the two samples examined have means that do not come from the same population.

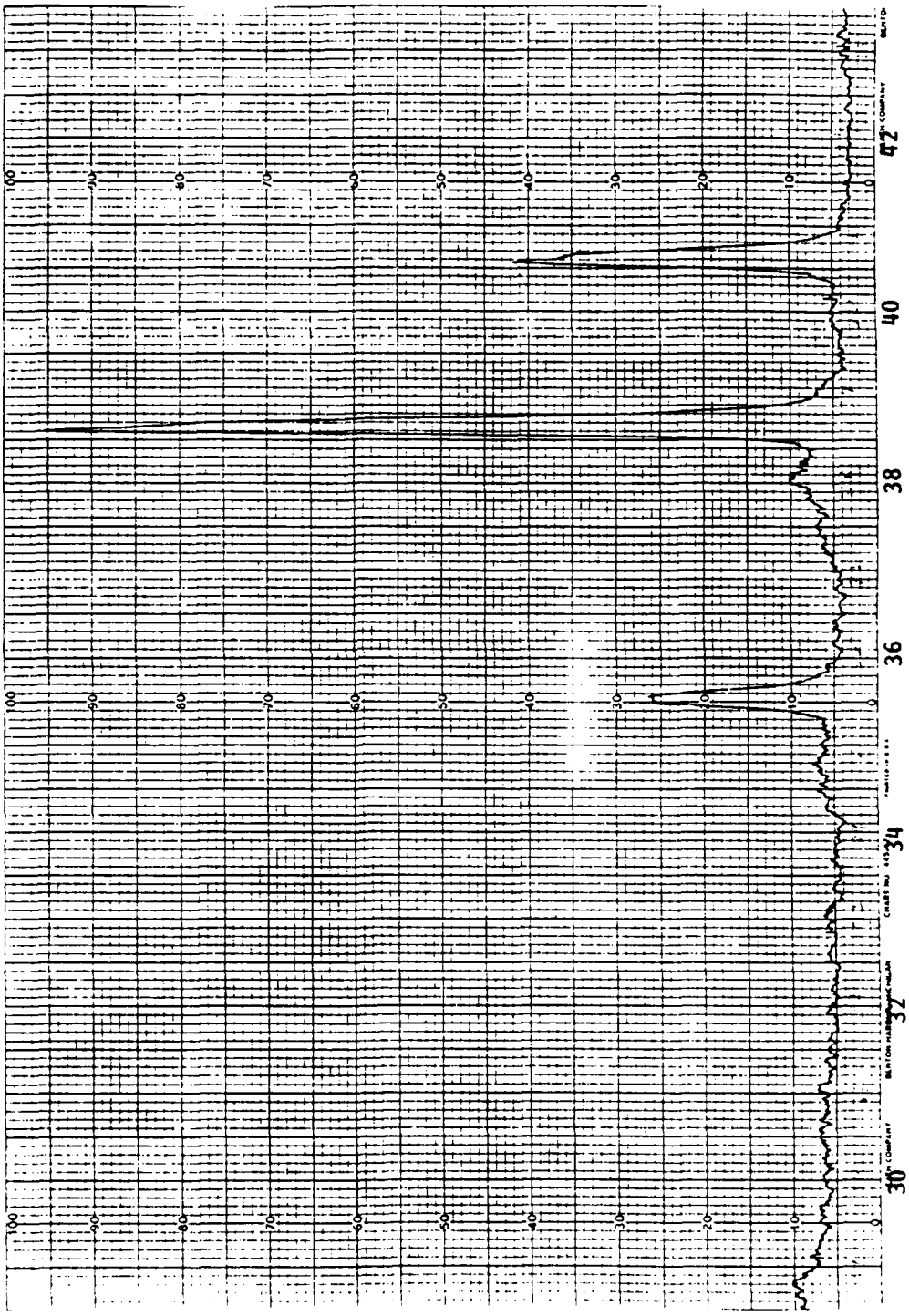
APPENDIX IV

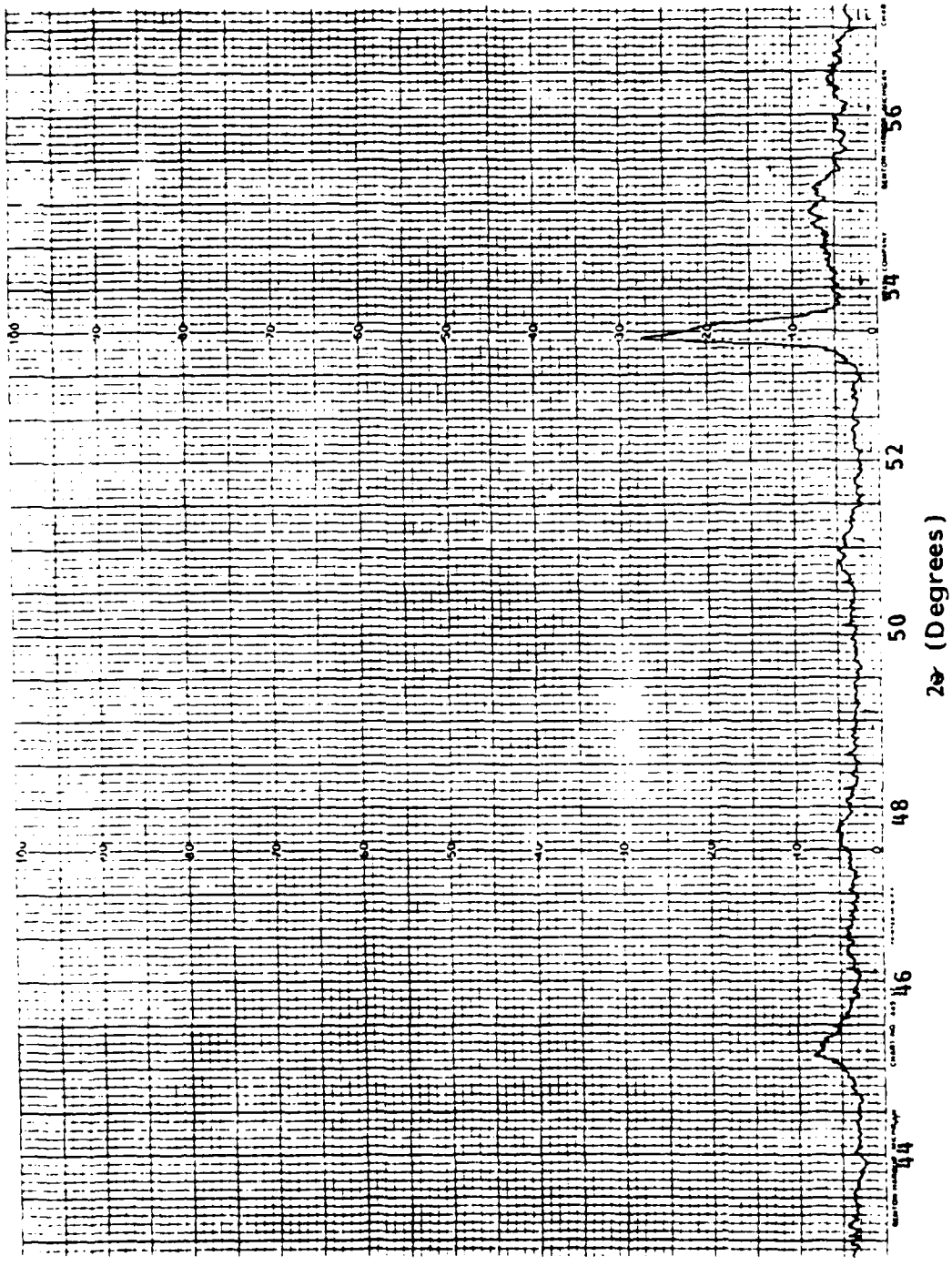
X-Ray Diffraction Spectra for CA/HF Anodized Ti-6Al-4V.

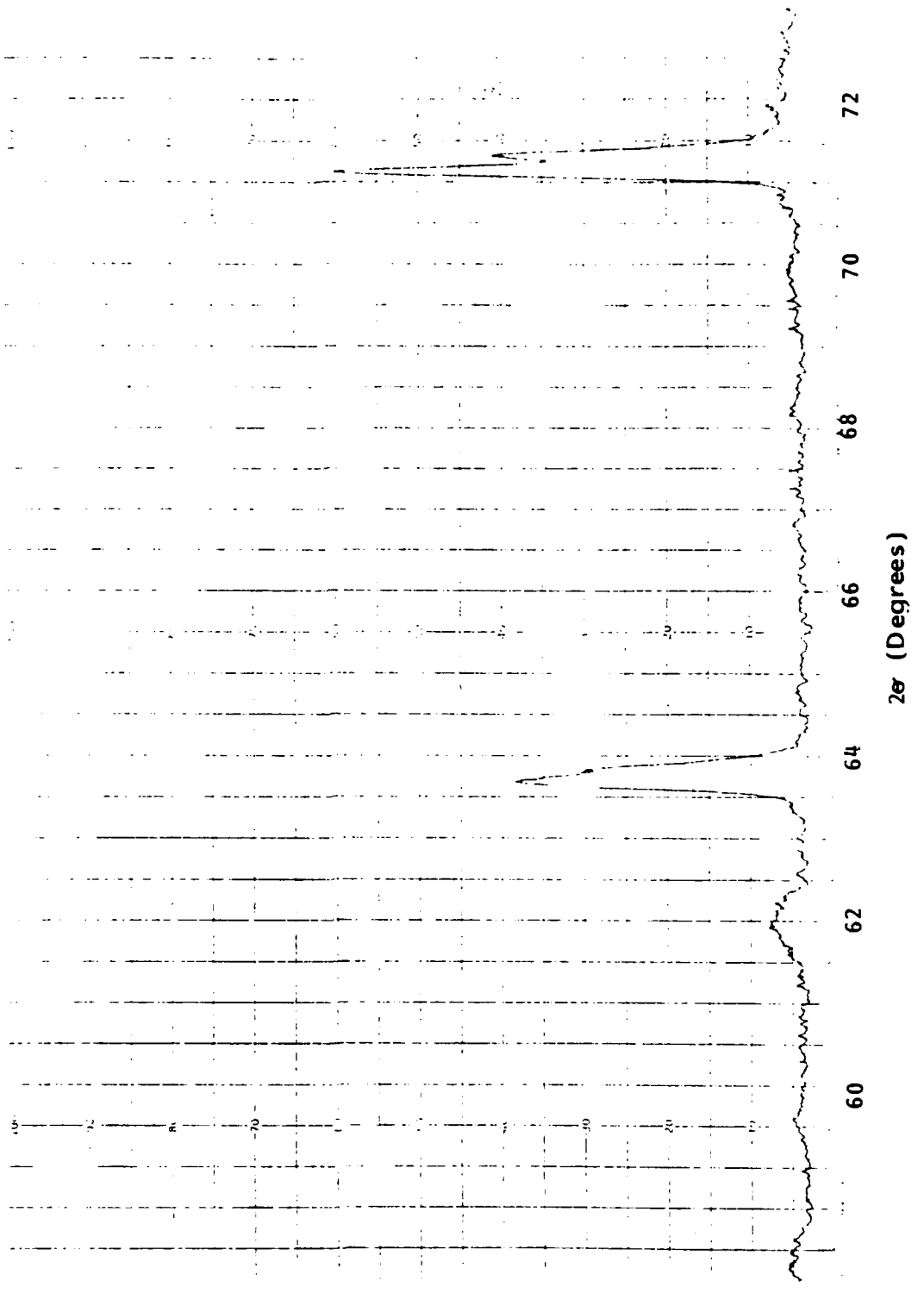
Anodization Conditions were: 20 Minutes, 298 ± 2K,

30 ± 2 A/m^2 Initial Current Density, 10 Volts.


28
26
24
22
20
18
16
2θ (Degrees)
Peak Intensity

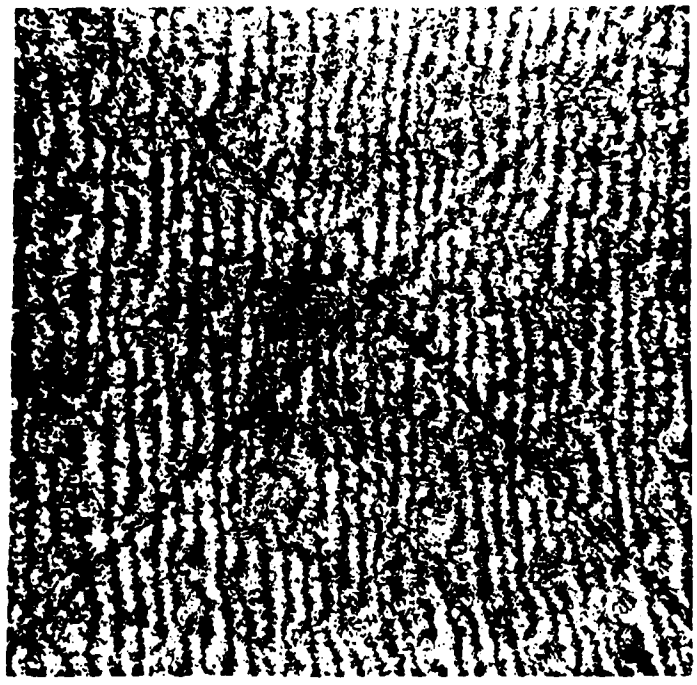

100
90
80
70
60
50
40
30
20
10
0
30
32
34
36
38
40
42
2θ (Degrees)
Peak Intensity


44
46
48
50
52
54
56
2θ (Degrees)
Peak Intensity

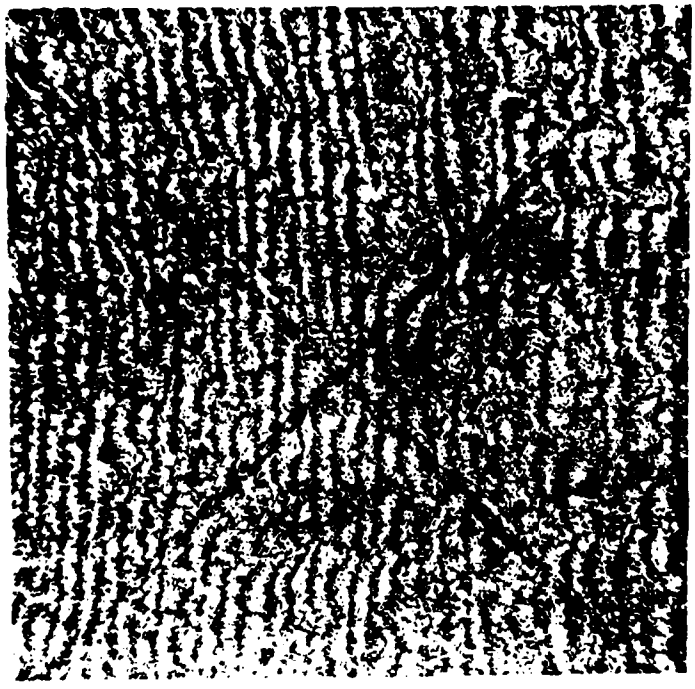

72
70
68
66
64
62
60
2θ (Degrees)
Peak Intensity

APPENDIX V

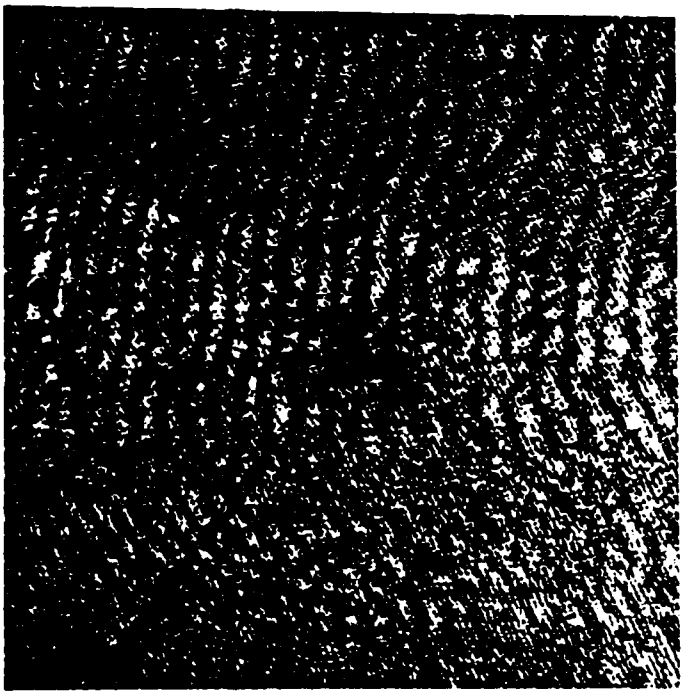
Multiple Beam Interferograms for Anodic Oxide Thickness Determination



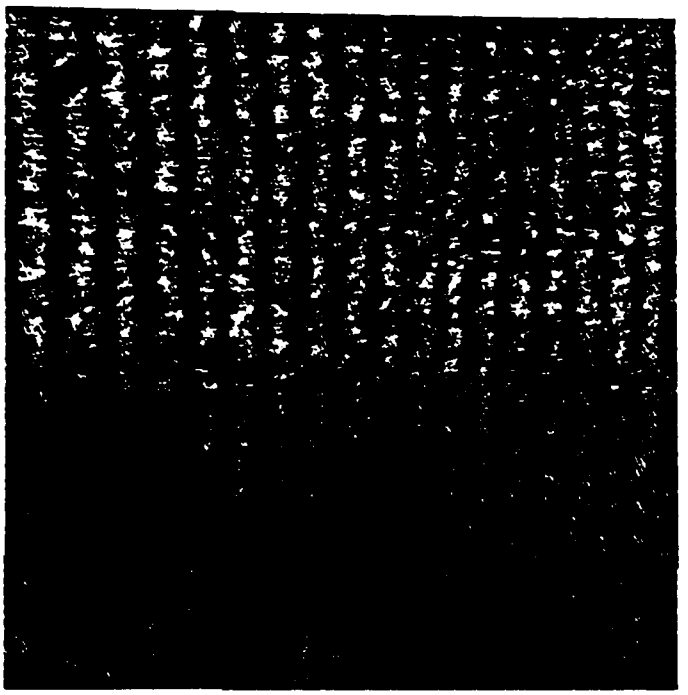
Interferogram of Fringe Pattern Used to Measure Ti-6Al-4V Anodic Oxide Thickness (28.4X). CA/HF Anodization Conditions: 20 Minutes, 298 ± 2K Solution Temperature, 10 Volts, 54 ± 2 A/m^2 Initial Current Density, Area #1 on Anodized Ti-6Al-4V Coupon



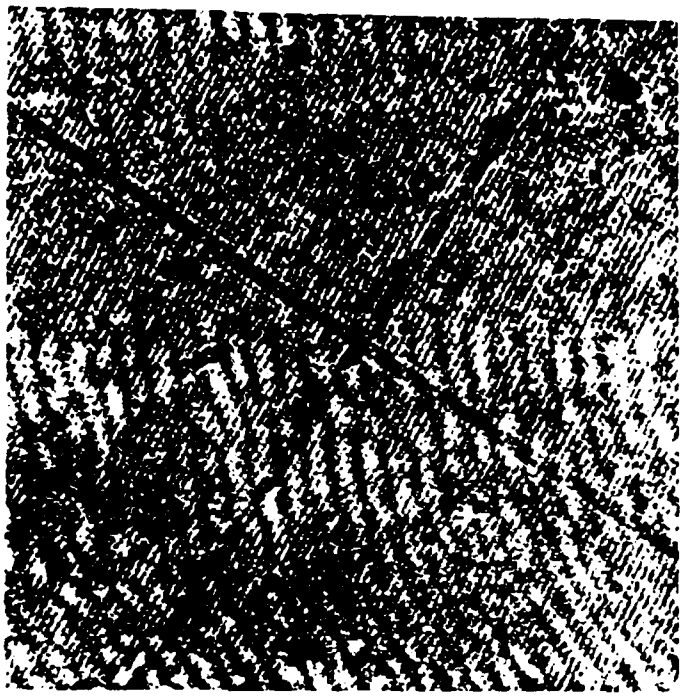
Interferogram of Fringe Pattern Used to Measure Ti-6Al-4V Anodic Oxide Thickness (28.4X). CA/HF Anodization Conditions: 20 Minutes, 298 ± 2K Solution Temperature, 10 Volts, 54 ± 2 A/m^2 Initial Current Density, Area #2 on Anodized Ti-6Al-4V Coupon



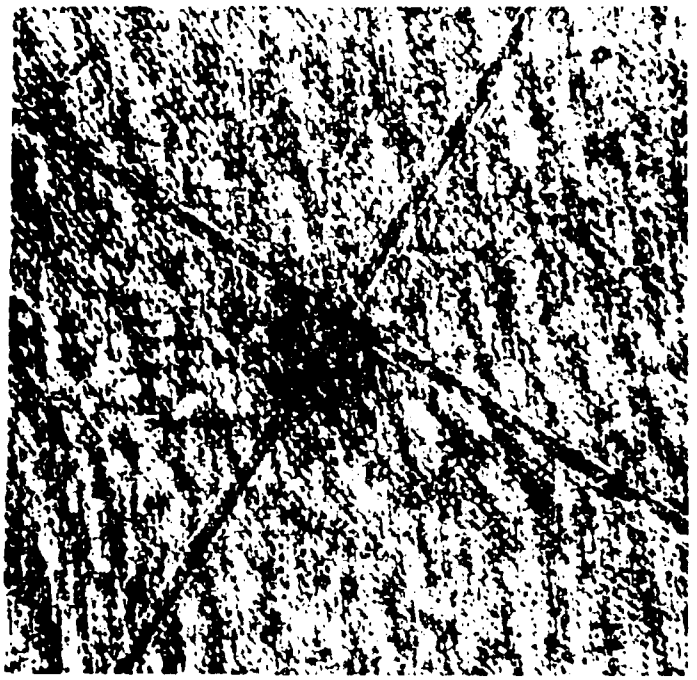
Interferogram of Fringe Pattern Used to Measure Ti-6Al-4V Anodic Oxide Thickness (28.4X). CA/HF Anodization Conditions: 60 Minutes, 298 ± 2K Solution Temperature, 10 Volts, 30 ± 2 A/m² Initial Current Density,



Interferogram of Fringe Pattern Used to Measure Ti-6Al-4V Anodic Oxide Thickness (28.4X). CA Without HF Anodization Conditions: 20 Minutes, 298 ± 2K Solution Temperature, 39 Volts, 30 ± 2 A/m² Initial Current Density,



Interferogram of Fringe Pattern Used to Measure Ti-6Al-4V Anodic Oxide Thickness (28.4X). CA/HF Anodization Conditions: 20 Minutes, 298 ± 2K Solution Temperature, 10 Volts, 30 ± 2 A/m^2 Initial Current Density,



Interferogram of Fringe Pattern Used to Measure Ti-6Al-4V Anodic Oxide Thickness (28.4X). CA/HF Anodization Conditions: 20 Minutes, 283 ± 2K Solution Temperature, 10 Volts, 20 ± 2 A/m² Initial Current Density,

APPENDIX VI

Anodic Oxide Electrical Property Characterization: Preliminary Results

I. INTRODUCTION

The electrical properties of oxides produced on a Ti-6Al-4V substrate by two different chromic acid (CA) anodization procedures are discussed in this appendix. The oxide electrical properties determined were capacitance, dielectric constant and bulk resistivity. This appendix describes the preliminary data obtained.

II. EXPERIMENTAL

A. Chromic Acid Anodization Materials and Methods

The metal used in this study was Ti-6Al-4V. The dimensions of a metal coupon was 15.2 cm X 2.5 cm X 0.1 cm.

The Ti-6Al-4V coupons were 1,1,1 trichloroethane vapor degreased in a standard degreaser set-up. The vapor degreaser cleaning schedule was: 15 minutes in the vapor of a 325K solvent sump, 5 minutes immersed in 298K solvent, followed by another 5 minutes in the solvent vapors. The 1,1,1 trichloroethane cleaning procedure removes the organic contamination. This cleaning procedure is a standard industrial method used for cleaning metals.

After vapor degreasing, the Ti-6Al-4V coupons were pickled to remove the natural oxide. The procedure is described as preanodization treatment #2 in Table III. The coupons were then anodized; the anodization apparatus is illustrated in Figure 2. A 750 cc, 5% solution of CrO_3 was used to anodize 6 coupons connected in a parallel circuit. A 50% hydrofluoric acid was added to the anodization solution in a 0.3% V/V to obtain the desired initial current density at 10 volts. The anodization cathode was a Ti-6Al-4V coupon also. Distilled, deionized water was used in all solutions.

Two different anodization methods were used to produce the oxide on the Ti-6Al-4V substrate in this study. They are described in Table XXI. Hydrofluoric acid (HF) was used in one

CA anodization method, whereas it was deleted in the second method. A second difference between these two methods is the voltage used during anodization; in CA anodization without HF, the voltage was 39 volts, whereas in CA/HF anodization the voltage was 10 volts. Each voltage was necessary to obtain the same initial current density, 30 ± 2 A/m^2, for the respective anodization procedures.

B. Chromic Acid Anodized Ti-6Al-4V Oxide Electrical Properties

1. Methods and Materials

The dielectric constant, capacitance and bulk resistivity were determined for the CA anodized Ti-6Al-4V oxide produced by the anodization procedures described in Table XXI.

The oxide thickness data, necessary for the determination of oxide electrical properties, are also reported in Table XXI. The oxide thickness data were determined by multiple beam interferometry.

The electrical property measurements were conducted at 298 ± 2K in a dry nitrogen environment. Contact probes for these measurements were designed to apply 85.1 grams of force to the contact surface. A schematic of the contact probe is shown in Figure 83. Contact probes were obtained from Assembly and Test Equipment Corporation of Pomona, California.

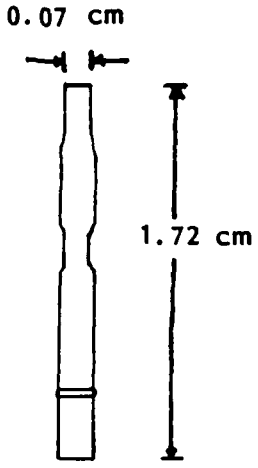


Figure 83a. Probe Receptacle

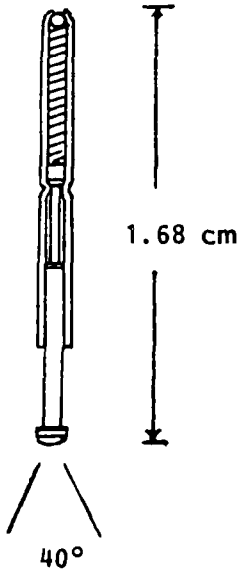


Figure 83b. Probe

Figure 83. Schematic of a Contact Probe.

2. Bulk Resistivity Determination

In order to determine oxide bulk resistivity, approximately 70 nm of pure silver was evaporated onto the anodized Ti-6Al-4V surface. The silver was deposited as equidistantly spaced rectangles by using a template. A schematic of the template is shown in Figure 84.

The oxide bulk resistivity determination is described in Figure 85. A current of 161.4 mA at a constant voltage of 3.3 volts was applied to the silver rectangles at each end of the sample. The potential was measured as a function of distance, relative to one end rectangle.

Based upon the applied current, the slope of the potential vs. distance data, and the distance between the end rectangles, ℓ, the bulk resistance, R, was calculated. The oxide cross-sectional area was then calculated based upon (1) the length of a single silver rectangle, which is the oxide length, and (2) the oxide thickness data. The oxide bulk resistivity, ρ, was then calculated by:

$$\rho = \frac{R\ A}{\ell} \qquad [1]$$

A schematic of the Plexiglas contact probe fixture used for these measurements is shown in Figure 86. Figure 87 is a schematic of the test apparatus used in the CA anodized Ti-6Al-4V oxide bulk resistivity determination.

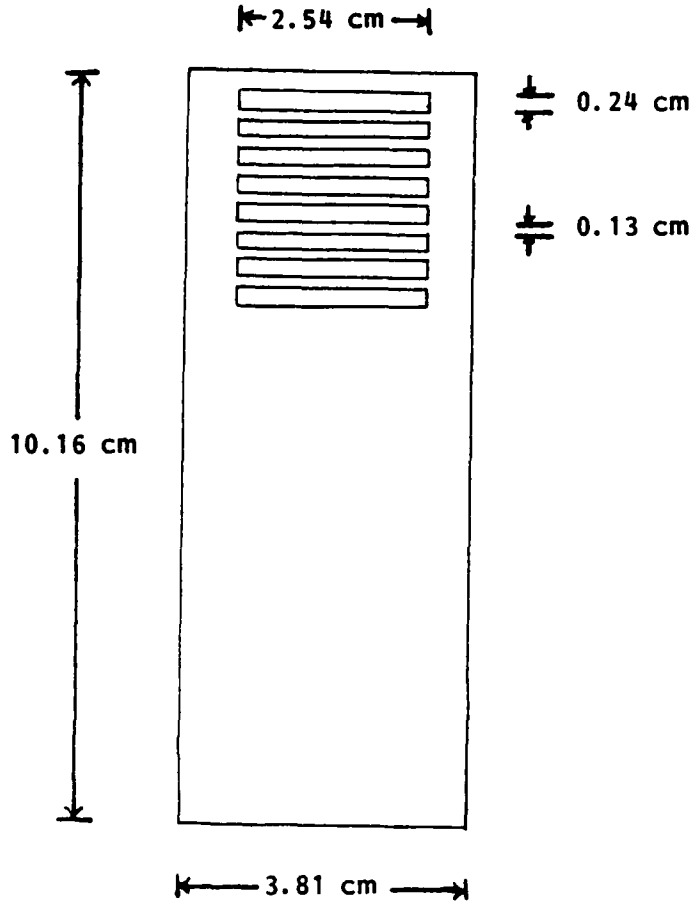
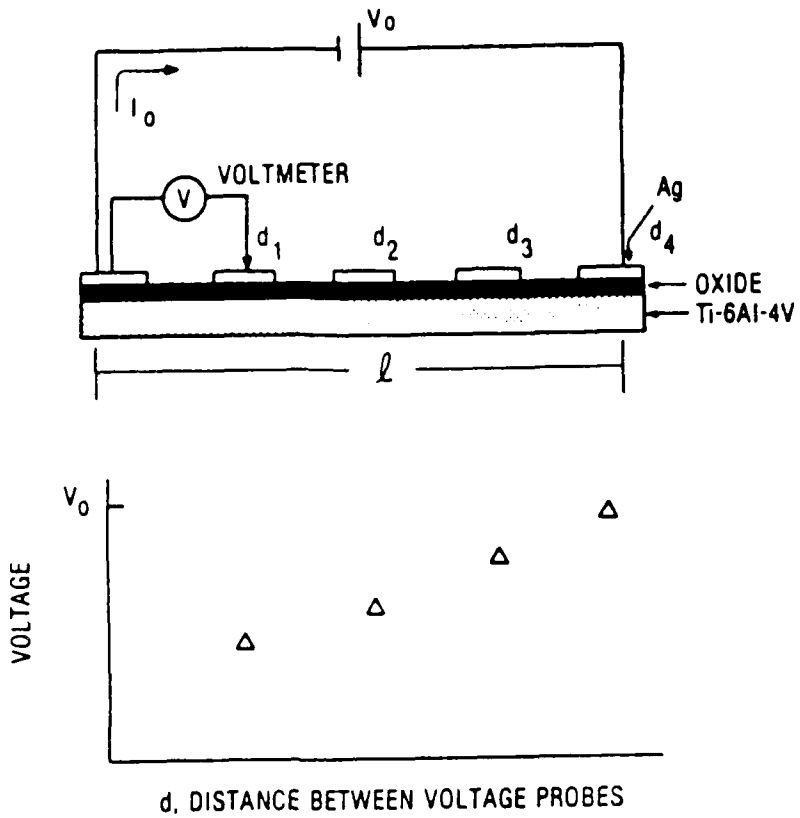


Figure 84. Schematic of the Template Used to Evaporate Silver Onto Anodized Ti-6Al-4V for the Oxide Bulk Resistivity Determination.



R, OXIDE BULK RESISTANCE, IS CALCULATED BASED UPON, THE KNOWN APPLIED CURRENT, I_0, THE SLOPE OF THE VOLTAGE VS. DISTANCE GRAPH, AND THE DISTANCE BETWEEN END VOLTAGE PROBES, ℓ THE OXIDE BULK RESISTIVITY, ρ, IS CALCULATED BY:

$$\rho = \frac{RA}{\ell}$$

WHERE A IS THE CROSS-SECTIONAL AREA OF THE OXIDE

Figure 85. Schematic of the Method for Ti-6Al-4V Anodic Oxide Bulk Resistivity Determination.

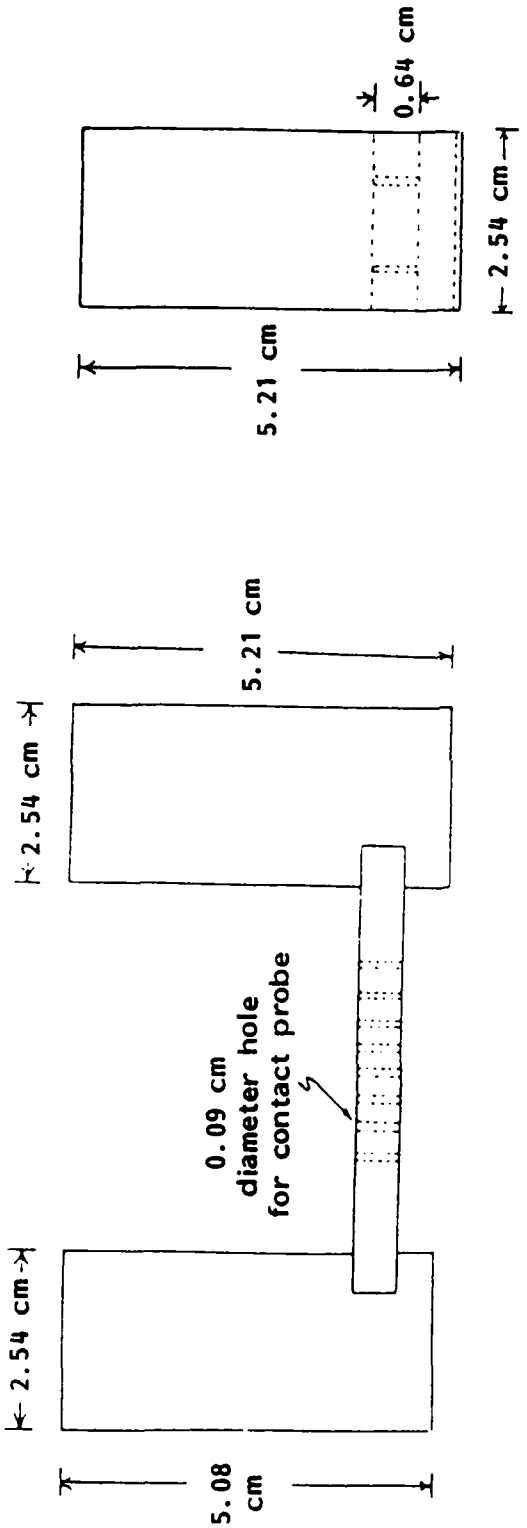


Figure 86. Schematic of the Plexiglas Contact Probe Fixture Used in the Anodic Oxide Bulk Resistivity Determination.

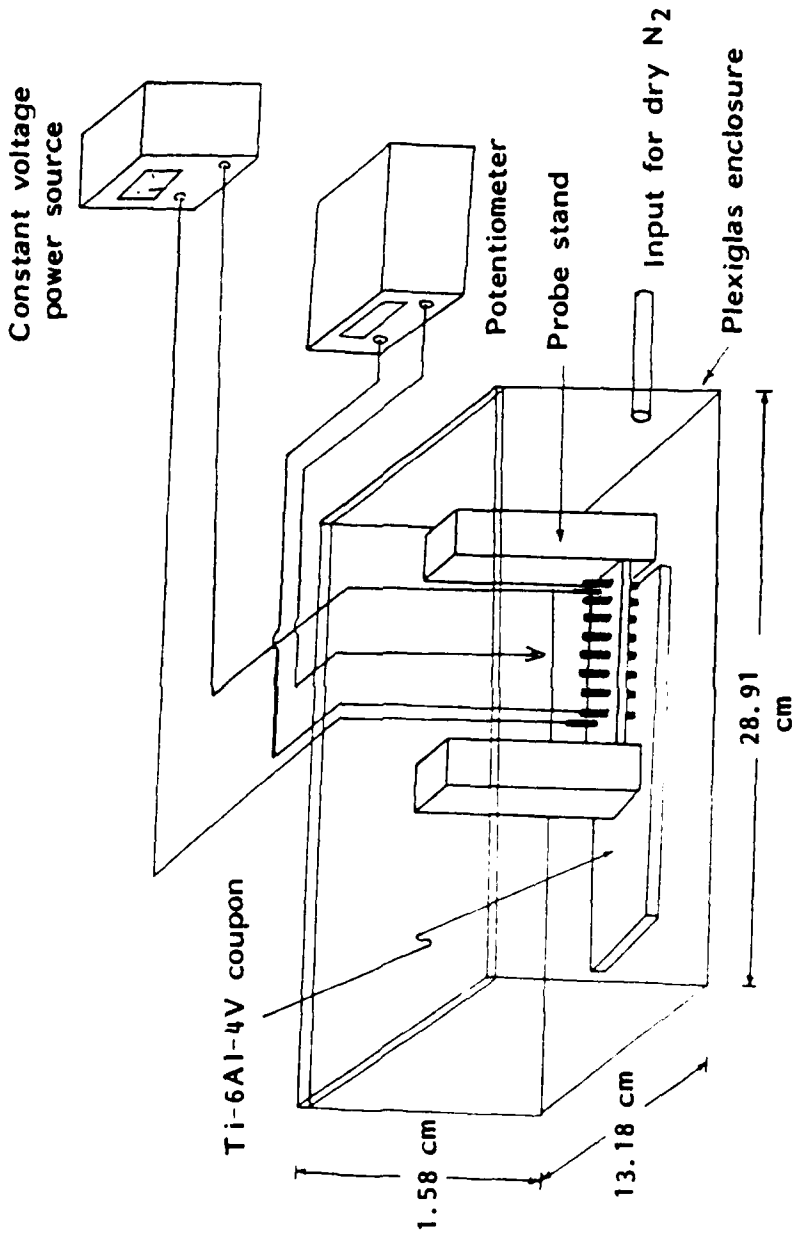


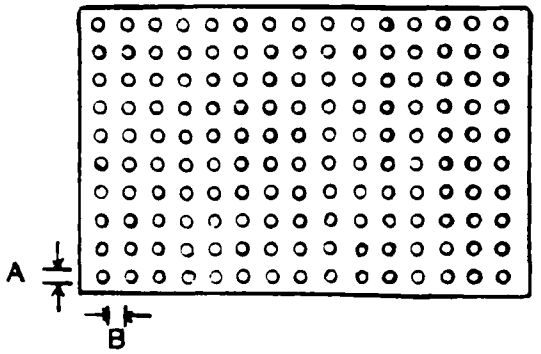
Figure 87. Schematic of the Test Apparatus Used in the Ti-6Al-4V Anodic Oxide Bulk Resistivity Determination.

3. Capacitance Measurements

Silver disks approximately 70 nm thick were evaporated onto the anodized Ti-6Al-4V surface by means of a template. A schematic of the template is shown in Figure 88. The geometry of the silver disks was chosen so as to minimize electrical field edge effects in the capacitance measurements.

Capacitance measurements, with the oxide as the dielectric, were determined as described in Figure 89. An evaporated silver disk, oxide and metal substrate form a parallel plate capacitor. Capacitance for two adjacent parallel plate capacitors in series was measured at 1 MHz, 1 KHz and 120 Hz. A GR 1687-B LC Digi-bridge® impedance meter from GenRad, Inc. was used for capacitance measurements at 1 MHz. A GR 1657 RLC Digibridge® from GenRad, Inc. was used for capacitance measurements at 1 KHz and 120 Hz.

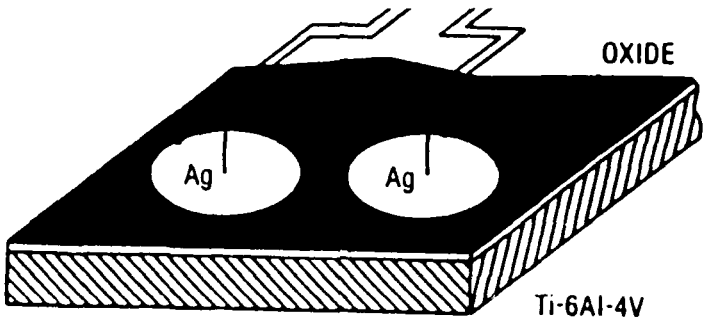
A pair of Kelvin probes were attached to each digibridge for oxide capacitance measurements. The Kelvin probe pair, as shown in Figure 90, were four-wire probes that nullify the lead bulk resistance up to the single-stranded silver wire, which was crimped onto each contact probe. Each single-stranded silver wire was approximately 12.7 cm in length and was 0.02 cm in diameter. The wire was required, since the Kelvin probes were too large to attach directly to adjacent contact probes. The contact probe geometry was described earlier in this appendix.



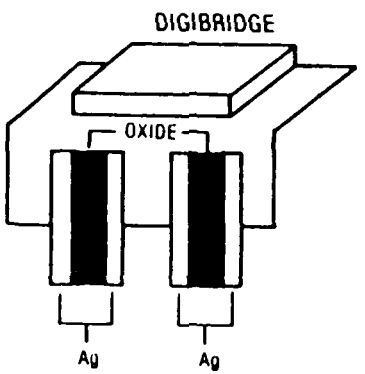
Template is drawn to full scale.

For A, $\bar{X}$ = 0.24 ± 0.00 cm. For B, $\bar{X}$ = 0.13 ± 0.01 cm.

Figure 88. A Schematic of the Template Used to Evaporate Silver Disks Onto Anodized Ti-6Al-4V for the Anodic Oxide Capacitance Determination.



SIDE VIEW OF TEST DESIGN



CIRCUIT DIAGRAM OF TEST DESIGN

Figure 89. Schematic of the Set-Up for the Ti-6Al-4V Anodic Oxide Capacitance Determination.

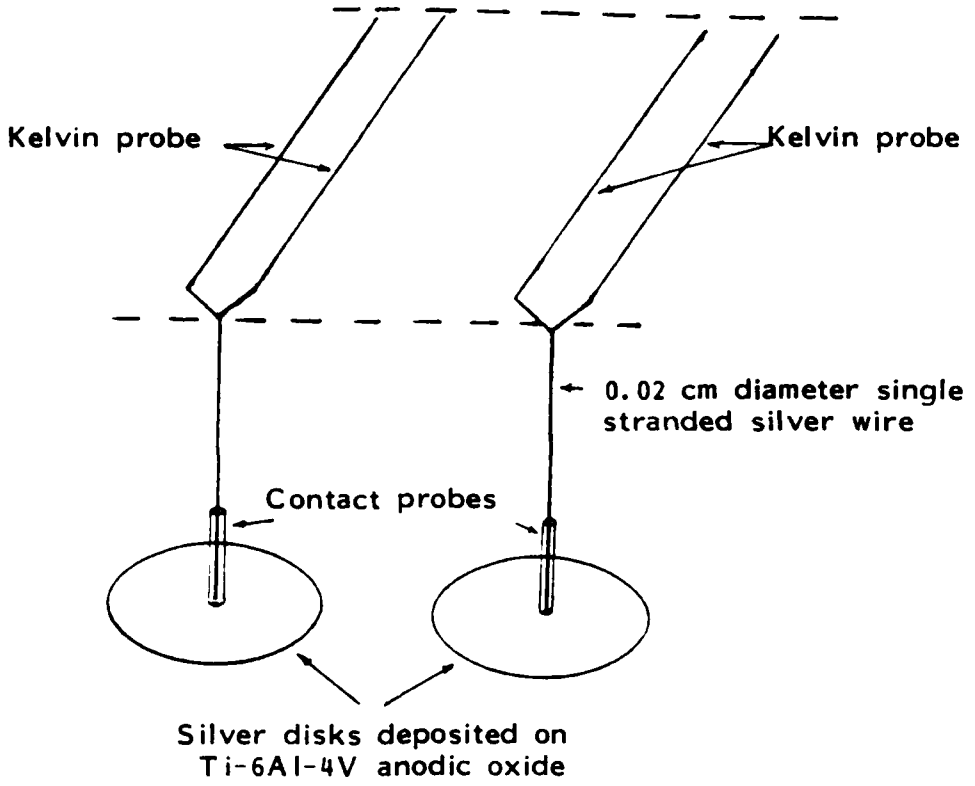


Figure 90. Schematic of Probe Set-Up Used in Ti-6Al-4V Anodic Oxide Capacitance Measurements.

A schematic of the contact probe fixture used for these measurements is shown in Figure 91. The 3.2 cm X 1.3 cm contact probe holder was Plexiglas. The remainder of the fixture was phenolic. Figure 92 is a schematic of the test apparatus used in the CA anodized Ti-6Al-4V oxide capacitance determination.

Capacitance measurements were made for at least four different adjacent silver disks for each type of anodic oxide. Stray capacitance or inductance from the probe apparatus was subtracted from the capacitance measurements to determine the actual parallel plate capacitance with the oxide as the dielectric. Stray capacitance or inductance from the probe apparatus was measured by placing the measurement probe apparatus on a brass coupon which had been scrubbed immediately prior to measurements so as to remove surface contaminants.

4. Oxide Dielectric Constant Determination

The oxide dielectric constant at 1 MHz was calculated based upon the capacitance measurements at this frequency. The oxide dielectric constant can be determined for a parallel plate capacitor by using the following relationship:

$$C_x = \frac{E_o K A}{d} \qquad [2]$$

where E_o is the permittivity of free space, 8.85×10^{-12} F/m, K is the dielectric constant, A is the measured area of one silver disk, which is equivalent to the oxide area, and d is the oxide thickness. C_x is the capacitance of one parallel plate capacitor. C_x is cal-

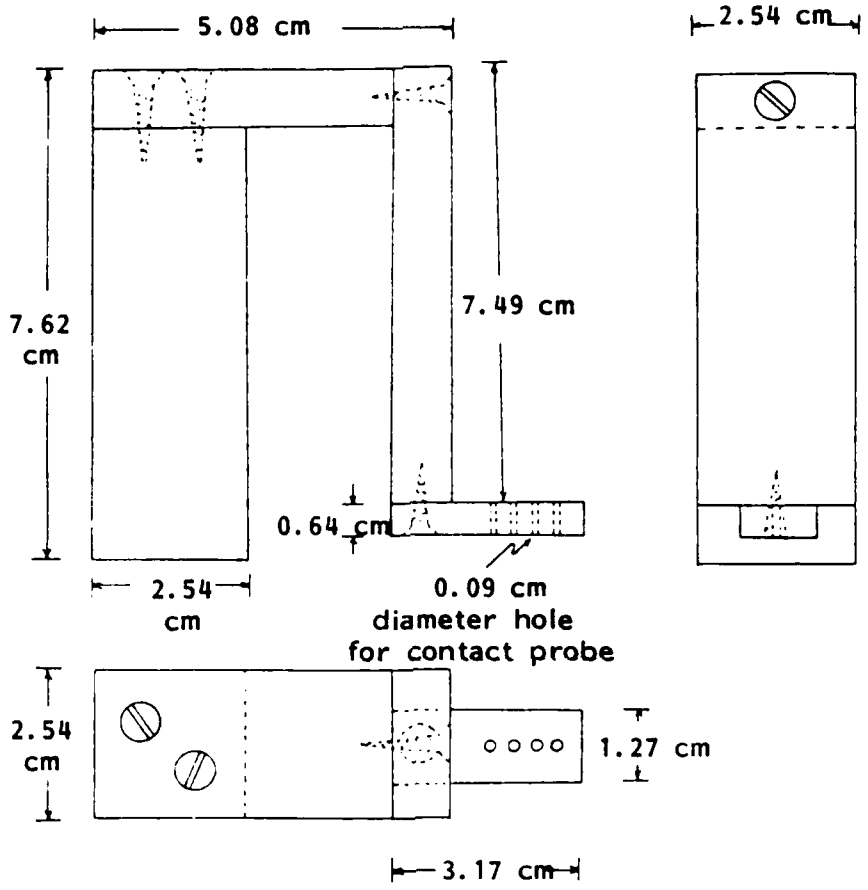


Figure 91. Schematic of the Contact Probe Fixture Used in the Ti-6Al-4V Anodic Oxide Capacitance Determination.

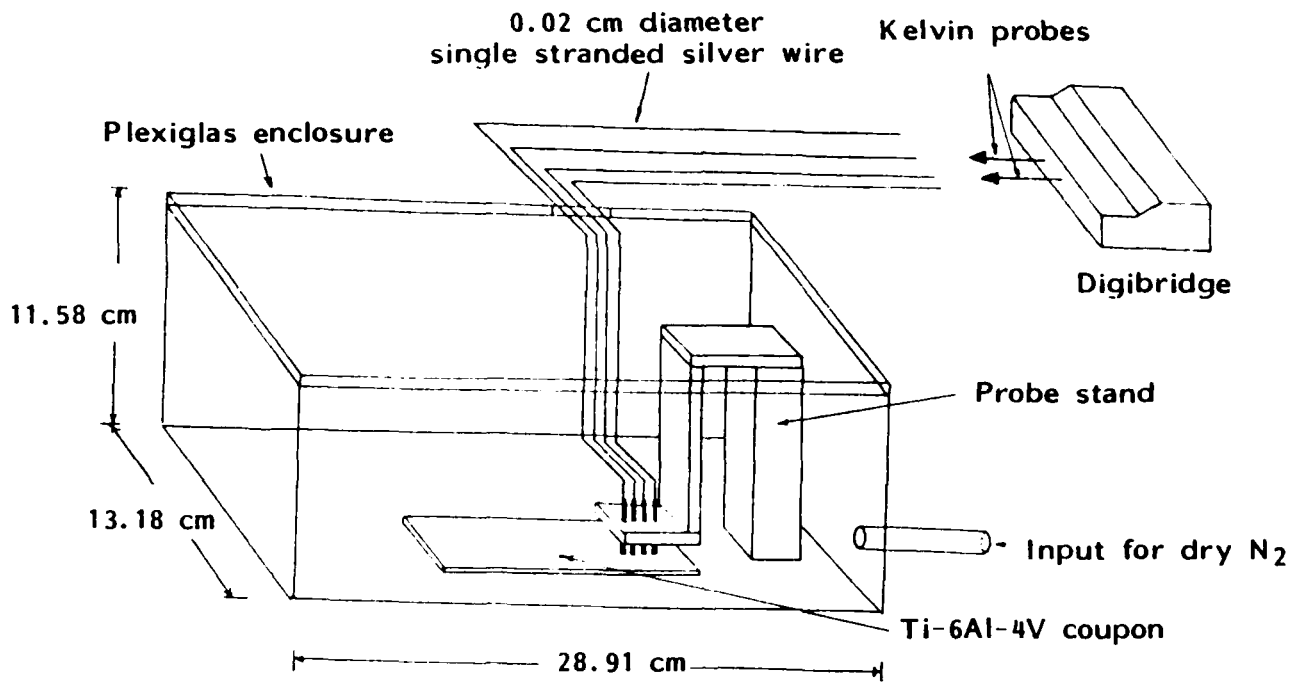


Figure 92. Schematic of the Test Apparatus Used in the Ti-6Al-4V Anodic Oxide Capacitance Determination.

culated based upon the following relationship:

$$C_x = 2\ C_s \qquad [3]$$

where C_s is the measured capacitance for two parallel plate capacitors tested in series. Equation 3 assumes equivalent parallel plate capacitors tested in series.

III. RESULTS AND DISCUSSION

A. Electrical Properties of Anodic Oxide Produced by CA Anodized Without HF

1. Capacitance of Oxide Produced by CA Anodization Without HF

Table XLI contains the test apparatus measurements. Also, Table XLI contains the combined measurements of both the test apparatus and two parallel plate capacitors in series, with the dielectric being the CA anodic oxide produced without HF. Test apparatus measurements were made before and after each oxide capacitance measurement; these values remained constant. All measurements were conducted in dry nitrogen at 298 ± 2K.

It can be seen in Table XLI the test apparatus was inductive. It can also be seen that the combined test apparatus and sample were capacitive. C_x, the parallel plate capacitance with the CA anodic oxide as a dielectric, can be calculated from the measured inductance of the test apparatus, L_{ts}, the measured capacitance of the sample plus test apparatus, C_t, and the known frequency, w. This calculation of C_x is described in Table XLII.

In the oxide capacitance calculations described in Table XLII, it is assumed that the stray capacitance between any pair of silver disks in the measurement circuit is low, and the stray capacitance does not contribute significantly to the oxide capacitance. This assumption is based upon the small distance ($\leq$ 140 nm) from

TABLE XLI

Test Apparatus Measurements and the Measurements for Two Parallel Plate Capacitors in Series With the Dielectric Being Anodic Oxide Produced by Chromic Acid Anodization Without HF

Frequency	Test Apparatus (Henries)	Test Apparatus and Sample (Farads)
120 Hz	0	159.71×10^{-6}
	0	149.49×10^{-6}
	0	128.11×10^{-6}
	0	169.14×10^{-6}
1 KHz	300.0×10^{-9}	152.07×10^{-6}
	300.0×10^{-9}	180.00×10^{-6}
	300.0×10^{-9}	34.40×10^{-6}
	300.0×10^{-9}	13.85×10^{-6}

Note: Each test apparatus measurement was for a specific pair of probes. Each test apparatus datum in Column 2 corresponds specifically to the adjacent datum in Column 3.

TABLE XLI (Continued)

Frequency	Test Apparatus (Henries)	Test Apparatus and Sample (Farads)
1 MHz	254.0×10^{-9}	190.72×10^{-11}
	208.0×10^{-9}	730.80×10^{-12}
	190.0×10^{-9}	390.30×10^{-12}
	190.0×10^{-9}	655.84×10^{-12}

Note: Each test apparatus measurement was for a specific pair of probes. Each test apparatus datum in Column 2 corresponds specifically to the adjacent datum in Column 3.

TABLE XLII

Equations to Determine Parallel Plate Capacitance

Test Conditions: Test apparatus is inductive. Test apparatus plus two parallel plate capacitors test in series are capacitive.

Definitions:

Z = impedance

R_t = test apparatus resistance

X_t = complex reactance of test apparatus plus two parallel plate capacitors in series

X_{ts} = complex reactance of test apparatus

$X = X_t - X_{ts}$

$w = 2 \pi f$

f = frequency, in Hz

C_t = capacitance of test apparatus plus two parallel plate capacitors in series

C_{ts} = capacitance of the test apparatus

C_s = capacitance of two parallel plate capacitors in series

$C_x = 2C_s$ = Capacitance of one parallel plate capacitor

L_t = inductance of test apparatus plus two parallel plate capacitors in series

L_{ts} = inductance of the test apparatus

$j = -1 = 1/j$

TABLE XLII (Continued)

Equations: [1] $Z = R_t - R_{ts} + X_t - X_{ts}$

[2] $X_t = -j/wC_t$ or $X_t = jwL_t$

$X_{ts} = -j/wC_{ts}$ or $X_{ts} = jwL_{ts}$

[3] $X = X_t - X_{ts}$

[4] $X = -j(1/wC_t + wL_{ts})$

[5] $X = 1/jwC_s$

[6] $1/jwC_s = -j(1/wC_t + wL_{ts})$

[7] Once the vector direction has been determined by the sign on j, then only the vector magnitude need be considered in the capacitance calculation.

$1/wC_s = 1/wC_t + wL_{ts}$

[8] $1/C_s = 1/C_t + w^2L_{ts}$

[9] $C_s = 1/(1/C_t + w^2L_{ts})$

[10] $C_s = C_t/(1 + w^2L_{ts}C_t)$

[11] $C_x = 2C_s$

one silver disk to the metal substrate, compared to the relatively large 0.4 cm center to center distance between adjacent disks.

The calculated parallel plate capacitance, with this CA anodic oxide as the dielectric, is shown in Table XLIII for 120 Hz, 1 KHz, and 1 MHz. The trend indicated by this data appears to show that as frequency is increased, parallel plate capacitance decreased. Apparently, as frequency is increased, the alignment of the polarizable oxide between the oppositely charged metal substrates is disrupted, thereby reducing oxide capacitance.

2. Dielectric Constant of Oxide Produced by CA Anodization Without HF

The CA anodic oxide average dielectric constant was calculated based upon the average of the four C_x capacitance data described in Table XLIII, and the 20 nm oxide thickness, determined by interferometry.

The average dielectric constant at 1 MHz was 0.88. Based upon the range of calculated C_x values shown in Table XLIII, the dielectric constant ranged from 1.5 to 0.2.

B. Electrical Properties of Anodic Oxide Produced by CA Anodization With HF

1. Capacitance of Oxide Produced by CA Anodization with HF

The test data for two parallel plates tested in series with the oxide as the dielectric are shown in Table XLIV. The data for the

TABLE XLIII

C_x, Parallel Plate Capacitance, With the Dielectric Anodic Oxide Produced by Chromic Acid Anodization Without HF

Frequency	C_x (Farads)
120 Hz	3.20×10^{-4}
	3.00×10^{-4}
	2.60×10^{-4}
	3.40×10^{-4}
1 KHz	3.04×10^{-4}
	3.59×10^{-4}
	6.88×10^{-5}
	2.77×10^{-5}
1 MHz	3.74×10^{-9}
	1.46×10^{-9}
	0.78×10^{-9}
	1.30×10^{-9}

Note: C_x calculations were based upon equations in Table XLII, and data measured at 298 ± 2K in a dry nitrogen environment per the method shown in Table XLI.

TABLE XLIV

Test Apparatus Measurements and Measurements for Two Parallel Plates in Series With the CA/HF Anodic Oxide Between the Plates

Frequency	Test Apparatus (Henries)	Test Apparatus and Sample (Henries)
120 Hz	0	0
	0	0
	0	0
	0	0
1 KHz	300×10^{-9}	300×10^{-9}
	300×10^{-9}	300×10^{-9}
	300×10^{-9}	300×10^{-9}
	300×10^{-9}	300×10^{-9}
1 MHz	254×10^{-9}	229×10^{-9}
	208×10^{-9}	197×10^{-9}
	208×10^{-9}	204×10^{-9}
	208×10^{-9}	176×10^{-9}

Note: Each test apparatus measurement was for a specific pair of probes. Each test apparatus datum in Column 2 corresponds specifically to the adjacent datum in Column 3.

test apparatus used in this experiment are also included in Table XLIV.

It can be seen that the CA/HF anodic oxide is neither capacitive nor inductive at 1 MHz, 1 KHz, or 120 Hz. At 1 MHz, the test apparatus inductance, L_{ts}, was similar to the measured inductance of the test apparatus plus sample, L_t, within experimental error. At 1 KHz and at 120 Hz, the test apparatus inductance, L_{ts}, was equal to the inductance of the test apparatus plus sample, L_t.

These data suggest that the CA/HF anodic oxide would behave like a conductor rather than an inductor or capacitor. This is substantiated by the bulk resistivity data to be discussed below.

2. Dielectric Constant of Oxide Produced by CA Anodization with HF

Since the CA/HF anodic oxide was not capacitive, no determination of the dielectric constant was made.

3. Bulk Resistivity of Oxide Produced by CA Anodization with HF

Figure 93 is the voltage vs. distance data obtained when a known potential and current were applied to the end test probes. Two sets of measurements were made. These measurements were obtained in a dry nitrogen environment at 298 ± 2K. There was a linear relationship between potential and distance. This indicates that there was no contact resistance which could interfere with any of the electrical property measurements.

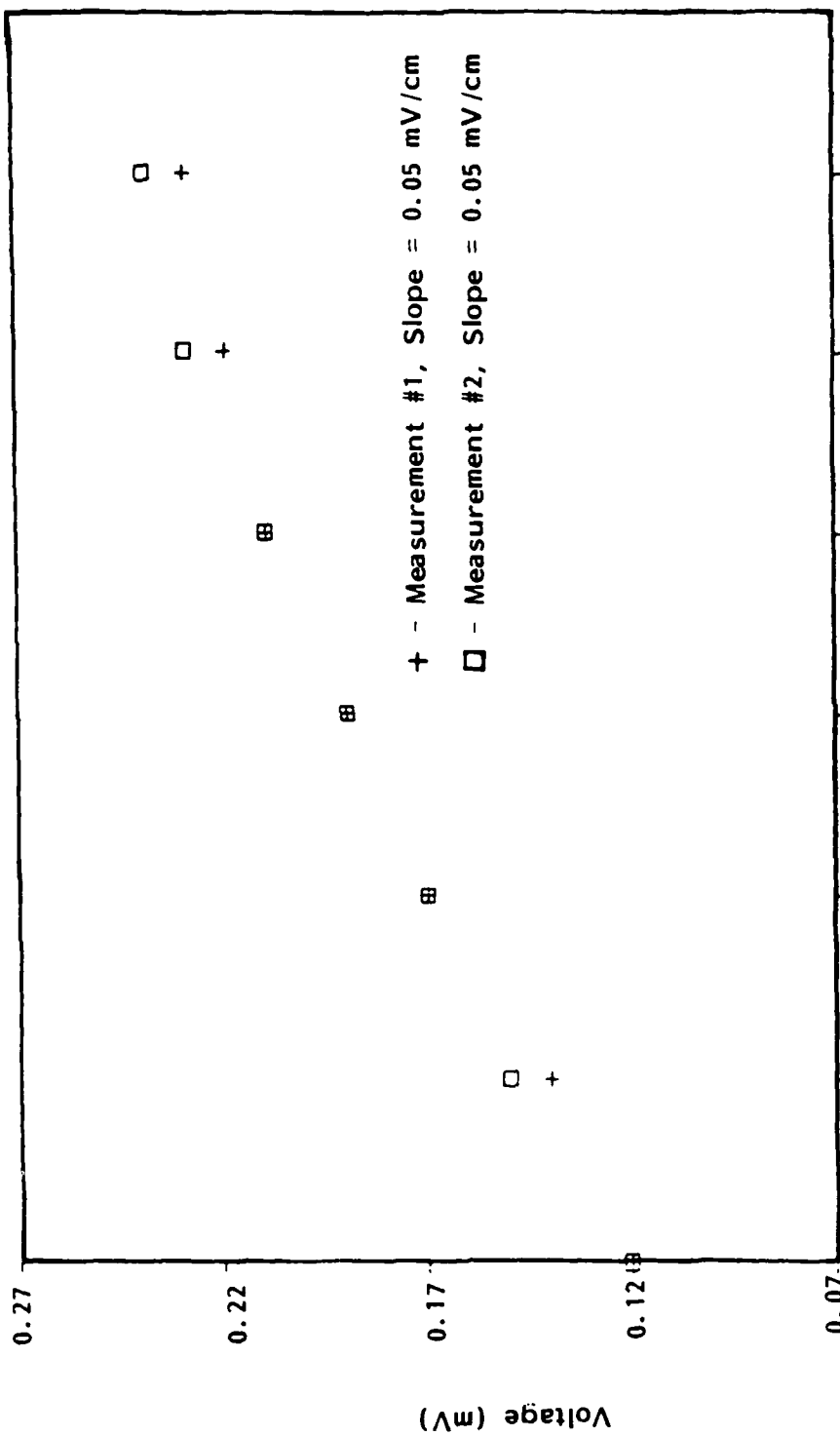


Figure 93. Voltage vs. Distance Data Used in Ti-6Al-4V Anodic Oxide Bulk Resistivity Determination. CA/HF Anodization Procedure for Ti-6Al-4V was Used.

The oxide bulk resistivity in dry nitrogen at 298 ± 2K was calculated based upon: (1) the average of the slope data in Figure 93, (2) the oxide cross sectional area, and (3) an oxide thickness of 140 nm, based upon interferometric measurements.

The oxide bulk resistivity was calculated to be 1×10^{-8} Ω -cm. The value of 1×10^{-8} Ω-cm is 100X lower than for the most highly conductive metal, silver. In fact, the value of 1×10^{-8} Ω-cm would be valid for a superconductor at 15K, but not for $(TiO)_x$ at 298K.

The unrealistically low oxide bulk resistivity may be attributed to:

(1) fluorine in the oxide, and/or

(2) oxide pores, and/or

(3) oxide flaws or cracks.

The anodic oxide produced by the CA/HF anodization procedure has inorganic and organic fluorine in the oxide surface ($\leq$ 10 nm) as described by surface analyses discussed earlier in this text. The fluorine compounds would be expected to be distributed throughout the oxide and not just in the surface, however. It is generally accepted that when HF is added to the chromic acid solution, the oxide is built up from the metal substrate as the HF etches the metal substrate. The fluoride ions could provide a conductive path to the metal surface and result in the unrealistically low oxide bulk resistivity.

The oxide produced by CA/HF anodization is more porous than the oxide produced by anodization without HF. Oxide pores may provide a conductive path to the metal surface if the contact probe force of 8.5 grams breaks through the barrier oxide to the adjacent metal surface.

Recall that silver was evaporated onto the oxide in the oxide bulk resistivity measurement method. The evaporated silver could have penetrated into an oxide pore or oxide crack or flaw. If the silver coated oxide crack or flaw extended to the metal surface, a low resistivity path to the metal surface would exist, resulting in the unrealistically low bulk resistivity. And, if the silver coated oxide pore, crack or flaw extended only to the barrier oxide, the contact probe force could break through the barrier oxide and expose the metal oxide and thereby create a low resistance path.

Suggested experiments to determine the cause of the unrealistically low oxide resistance measurements, and prevent them, if possible, are as follows.

(1) Use indium strips, which are applied to the oxide surface, rather than silver evaporation. This should eliminate silver penetration into the oxide pores, cracks and/or flaws.

(2) Reduce the 85.1 gram probe contact pressure to minimize any chance of penetrating the barrier oxide to expose the metal surface.

(3) Determine oxide bulk resistivity using indium strips and low contact pressure for a CA/HF anodic oxide 140 mm thick and also for a 400 nm thick oxide. The anodization methods are described in this text. The thicker oxide may reduce the likelihood that a crack or flaw extends to the barrier oxide or to the metal surface.

(4) Characterize all oxide studied in cross section by Transmission Electron Microscopy (TEM) before and after oxide bulk resistivity measurements. These data will determine the effects of measurement methods upon oxide morphology.

IV CONCLUSIONS

(1) The following electrical properties were determined for the anodic oxide produced on Ti-6Al-4V by chromic acid anodization without HF. The CA anodization procedure was: 298 ± 2K solution temperature, 30 ± 2 A/m^2 initial current density, 20 minute anodization time, and 39 volt potential.

1. The CA anodic oxide was capacitive.
2. The average dielectric constant at 1 MHz was 0.88, based upon oxide capacitance measurements in a dry nitrogen environment at 298 ± 2K.

(2) The following electrical properties were determined for the anodic oxide produced on Ti-6Al-4V by chromic acid anodization with HF. The CA/HF anodization procedure was the same as described above, except that a 10 volt potential was used.

1. The CA/HF anodic oxide was conductive.
2. Since the CA/HF anodic oxide was not capacitive, no dielectric constant determination was made.
3. The CA/HF anodic oxide bulk resistivity was measured as 1×10^{-8} Ω-cm and is unrealistically low. The low value may be attributed to the porosity of, or fluorine in, the CA/HF oxide, or to flaws or cracks in the oxide which extend to the metal surface. Also, the silver evaporated onto the

oxide for the resistivity measurements could have penetrated a flaw, pore or crack and created a low resistance path to the metal surface. Suggested experiments to determine the cause of these electrical shorts, and prevent them if possible, were discussed in this appendix.

APPENDIX VII

ESCA Data for:

(1) Ti-6Al-4V Before and After Anodization;

(2) Lica® 44 Titanate Primer;

(3) Polysulfone, Polyphenylquinoxaline, Polyethersulfone, 50% Calcium Carbonate Filled Polyimide, Unfilled and 20% Glass Fiber Filled Polyetherimide; and,

(4) Anodized Ti-6Al-4V/Heat Resistant Adhesive Single Lap Bond Fracture Surfaces

Sample Description: Unbonded Anodized Ti-6Al-4V, Preanodization Treatment #1, Anodized 20 Minutes, CA Anodized With HF, 30 A/m², 10 V, 298K

Element	Corrected Binding Energy C: 285.0 eV	Atomic Concentration (%)	% Conc. X / % Conc. Ti
C (1s)	285.0	32	2.3
O (1s)	530.4	49	3.5
F (1s)	685.0	3	0.2
F (A)	596.2		
Ti ($2p\frac{1}{2}$)	464.4	14	1.0
Ti (2p3/2)	458.8		
Cr (2p3/2)	577.6	1	0.1
V (2p3/2)	NSP		
Al ($2p\frac{1}{2}$)	74.6	1	0.1
S (2s)	NSP		
S (2p3/2)	NSP		
N (1s)	NSP		
Si (2p3/2)	NSP		
Cl (2p3/2)	NSP		
Na (1s)	NSP		

NSP: No Significant Peak

Sample Description: Unbonded, Anodized Ti-6Al-4V, Preanodization Treatment #2, Anodized 20 Minutes, CA Anodized With HF, 20 A/m², 10 V, 283K

Element	Corrected Binding Energy C: 285.0 eV	Atomic Concentration (%)	% Conc. X / % Conc. Ti
C (1s)	285.0	63	10.5
O (1s)	530.6	25	4.2
F (1s)	685.4	1	0.2
Ti ($2p\frac{1}{2}$)	464.6	6	1.0
Ti (2p3/2)	458.8		
Cr (2p3/2)	NSP		
V (2p3/2)	NSP		
Al ($2p\frac{1}{2}$)	74.2	2	0.3
S (2s)	NSP		
S (2p3/2)	NSP		
N (1s)	NSP		
Si (2p3/2)	104.0	3	0.5
Cl (2p3/2)	NSP		
Na (1s)	NSP		

NSP: No Significant Peak

Sample Description: Unbonded, Anodized Ti-6Al-4V, Preanodization Treatment #1, Anodized 60 Minutes, CA Anodized With HF, 30 A/m², 10 V, 298K

Element	Corrected Binding Energy C: 285.0 eV	Atomic Concentration (%)	% Conc. X / % Conc. Ti
C (1s)	285.0	59	8.4
O (1s)	530.4	27	3.9
F (1s)	688.8	2	0.3
F (1s)	685.4		
Ti (2p½)	464.6	7	1.0
Ti (2p3/2)	458.8		
Cr (2p3/2)	NSP		
V (2p3/2)	NSP		
Al (2p½)	74.6	2	0.3
S (2s)	NSP		
S (2p3/2)	NSP		
N (1s)	400.0	2	0.3
Si (2p3/2)	100.8	1	0.1
Cl (2p3/2)	NSP		
Na (1s)	NSP		

NSP: No Significant Peak

Sample Description: Unbonded, Anodized Ti-6Al-4V, Preanodization Treatment #1, No Yellow Stain, Anodized 20 Minutes, CA Anodized Without HF, 30 A/m², 39 V, 298K

Element	Corrected Binding Energy C: 285.0 eV	Atomic Concentration (%)	% Conc. X / % Conc. Ti
C (1s)	285.0	63	10.5
O (1s)	531.4	24	4.0
F (1s)	NSP		
Ti (2p½)	464.4	6	1.0
Ti (2p3/2)	458.8		
Cr (2p3/2)	NSP		
V (2p3/2)	NSP		
Al (2p½)	74.2	3	0.5
S (2s)	NSP		
S (2p3/2)	NSP		
N (1s)	400.0	2	0.3
Si (2p3/2)	102.2	2	0.3
Cl (2p3/2)	NSP		
Na (1s)	NSP		

NSP: No Significant Peak

Sample Description: Unbonded, Anodized Ti-6Al-4V, Preanodization Treatment #1, In Yellow Stain Region, Anodized 20 Minutes, CA Anodized Without HF, 30 A/m², 39 V, 298K

Element	Corrected Binding Energy C: 285.0 eV	Atomic Concentration (%)	% Conc. X / % Conc. Ti
C (1s)	285.0	54	5.4
O (1s)	530.4	33	3.3
F (1s)	NSP		
Ti (2p½)	464.6	10	1.0
Ti (2p3/2)	458.8		
Cr (2p3/2)	NSP		
V (2p3/2)	NSP		
Al (2p½)	74.0	2	0.2
S (2s)	NSP		
N (1s)	NSP		
Si (2p3/2)	102.0	1	0.1
Cl (2p3/2)	NSP		
Na (1s)	NSP		

NSP: No Significant Peak

Sample Description: UDEL® Unfilled Polysulfone Compression Molded Film

Element	Corrected Binding Energy C: 285.0 eV	Atomic Concentration (%)	% Conc. X / % Conc. Ti
C (1s)	285.0	80	N/A
O (1s)	532.4	13	N/A
F (1s)	689.2	1	N/A
Ti (2p½)	NSP		
Ti (2p3/2)	NSP		
Cr (2p3/2)	NSP		
V (2p3/2)	NSP		
Al (2p½)	75.6	2	N/A
S (2s)	232.2	1	N/A
S (2p½)	168.4		
N (1s)	NSP		
Si (2p3/2)	102.4	3	N/A
Cl (2p3/2)	NSP		
Na (1s)	NSP		

NSP: No Significant Peak

Sample Description: UDEL® Unfilled Polysulfone Beads After Vacuum Bake at 373K for 16 Hours

Element	Corrected Binding Energy C: 285.0 eV	Atomic Concentration (%)	% Conc. X / % Conc. Ti
C (1s)	285.0	81	N/A
O (1s)	532.6	13	N/A
F (1s)	NSP		
Ti ($2p\frac{1}{2}$)	NSP		
Ti (2p3/2)	NSP		
Cr (2p3/2)	NSP		
V (2p3/2)	NSP		
Al ($2p\frac{1}{2}$)	75.6	2	N/A
S (2s)	232.2	2	N/A
S ($2p\frac{1}{2}$)	168.4		
N (1s)	NSP		
Si (2p3/2)	102.2	2	N/A
Cl (2p3/2)	NSP		
Na (1s)	NSP		

NSP: No Significant Peak

Sample Description: Unfilled Polyphenylquinoxaline Adhesive

Element	Corrected Binding Energy C: 285.0 eV	Atomic Concentration (%)	% Conc. X / % Conc. Ti
C (1s)	285.0	78	N/A
O (1s)	532.8	15	N/A
F (1s)	NSP		
Ti (2p½)	NSP		
Ti (2p3/2)	NSP		
Cr (2p3/2)	NSP		
V (2p3/2)	NSP		
Al (2p½)	NSP		
S (2s)	NSP		
S (2p3/2)	NSP		
N (1s)	399.3	4	N/A
Si (2p3/2)	102.1	3	N/A
Cl (2p3/2)	NSP		
Na (1s)	NSP		

NSP: No Significant Peak

Sample Description: Victerex® Unfilled Polyethersulfone, Compression Molded Film

Element	Corrected Binding Energy C: 285.0 eV	Atomic Concentration (%)	% Conc. X / % Conc. Ti
C (1s)	285.0	74	N/A
O (1s)	532.4	15	N/A
F (1s)	689.5	6	N/A
Ti (2p½)	NSP		
Ti (2p3/2)	NSP		
Cr (2p3/2)	NSP		
V (2p3/2)	NSP		
Al (2p½)	NSP		
S (2s)	232.2	4	N/A
S (2p½)	168.2		
N (1s)	NSP		
Si (2p½)	102.2	1	N/A
Cl (2p3/2)	NSP		
Na (1s)	NSP		

NSP: No Significant Peak

Sample Description: Ablebond® 71-3 50% Calcium Carbonate Filled Polyimide, Thermally Cured

Element	Corrected Binding Energy C: 285.0 eV	Atomic Concentration (%)	% Conc. X / % Conc. Ti
C (1s)	285.0	61	N/A
O (1s)	531.8	32	N/A
F (1s)	NSP		
Ti (2p½)	NSP		
Ti (2p3/2)	NSP		
Cr (2p3/2)	NSP		
V (2p3/2)	NSP		
Al (2p½)	NSP		
S (2s)	NSP		
S (2p3/2)	NSP		
Ca (2p3/2)	NSP		
N (1s)	399.8	4	N/A
Si (2p3/2)	102.5	3	N/A
Cl (2p3/2)	NSP		
Na (1s)	NSP		

NSP: No Significant Peak

Sample Description: Ultem®, Unfilled Polyetherimide Compression Molded Film

Element	Corrected Binding Energy C: 285.0 eV	Atomic Concentration (%)	% Conc. X / % Conc. Ti
C (1s)	285.0	75	N/A
O (1s)	532.4	12	N/A
F (1s)	689.7	11	N/A
Ti (2p½)	NSP		
Ti (2p3/2)	NSP		
Cr (2p3/2)	NSP		
V (2p3/2)	NSP		
Al (2p½)	NSP		
S (2s)	NSP		
S (2p3/2)	NSP		
N (1s)	400.6	2	N/A
Si (2p3/2)	NSP		
Cl (2p3/2)	NSP		
Na (1s)	NSP		

NSP: No Significant Peak

Sample Description: Ultem®, 20% Glass Filled, Polyetherimide
Compression Molded Film

Element	Corrected Binding Energy C: 285.0 eV	Atomic Concentration (%)	% Conc. X / % Conc. Ti
C (1s)	285.0	66	N/A
O (1s)	532.3	11	N/A
F (1s)	689.8	20	N/A
Ti (2p½)	NSP		
Ti (2p3/2)	NSP		
Cr (2p3/2)	NSP		
V (2p3/2)	NSP		
Al (2p½)	NSP		
S (2s)	NSP		
S (2p3/2)	NSP		
N (1s)	400.6	3	N/A
Si (2p3/2)	NSP		
Cl (2p3/2)	NSP		
Na (1s)	NSP		

NSP: No Significant Peak

Sample Description: Fractured Bond, Anodized Ti-6Al-4V/UDEL® Unfilled Polysulfone, 18.2 MPa, Side #2, Preanodization Treatment #1, Anodized 20 Minutes, CA Anodized Without HF, 30 A/m², 39 V, 298K

Element	Corrected Binding Energy C: 285.0 eV	Atomic Concentration (%)	% Conc. X / % Conc. Ti
C (1s)	285.0	75	25.0
O (1s)	531.6	18	6.0
F (1s)	NSP		
Ti (2p½)	464.8	3	1.0
Ti (2p3/2)	459.2		
Cr (2p3/2)	NSP		
V (2p3/2)	NSP		
Al (2p½)	74.4	1	0.3
S (2s)	231.8	2	0.7
S (2p½)	168.2		
N (1s)	NSP		
Si (2p3/2)	102.4	1	0.3
Cl (2p3/2)	NSP		
Na (1s)	NSP		

NSP: No Significant Peak

Sample Description: Fractured Bond, Anodized Ti-6Al-4V/UDEL® Unfilled Polysulfone, 18.2 MPa, Side #1, Preanodization Treatment #1, Anodized 20 Minutes, CA Anodized Without HF, 30 A/m², 39 V, 298K

Element	Corrected Binding Energy C: 285.0 eV	Atomic Concentration (%)	% Conc. X / % Conc. Ti
C (1s)	285.0	81	81.1
O (1s)	532.6	13	13.0
F (1s)	689.2	1	1.0
F (1s)	686.6		
Ti ($2p_{\frac{1}{2}}$)	465.8	1	1.0
Ti (2p3/2)	460.2		
Cr (2p3/2)	NSP		
V (2p3/2)	NSP		
Al ($2p_{\frac{1}{2}}$)	74.8	1	1.0
S (2s)	232.2	2	2.0
S ($2p_{\frac{1}{2}}$)	168.2		
N (1s)	NSP		
Si (2p3/2)	102.4	1	1.0
Cl (2p3/2)	NSP		
Na (1s)	NSP		

NSP: No Significant Peak

Sample Description: Fractured Bond, Anodized Ti-6Al-4V/UDEL® Unfilled Polysulfone Bond, 28.2 MPa, Preanodization Treatment #1, Anodized 20 Minutes, CA Anodized With HF, 30 A/m², 10 V, 298K

Element	Corrected Binding Energy C: 285.0 eV	Atomic Concentration (%)	% Conc. X / % Conc. Ti
C (1s)	285.0	75	37.5
O (1s)	532.6	17	8.5
F (1s)	685.0	2	1.0
F (1s)	689.0		
Ti (2p½)	465.2	2	1.0
Ti (2p3/2)	459.4		
Cr (2p3/2)	NSP		
V (2p3/2)	NSP		
Al (2p½)	75.6	1	0.5
S (2p½)	168.2	1	0.5
S (2p3/2)	164.2		
N (1s)	NSP		
Si (2p3/2)	102.8	2	1.0
Cl (2p3/2)	NSP		
Na (1s)	NSP		

NSP: No Significant Peak

Sample Description: Fractured Bond, Anodized Ti-6Al-4V/UDEL® Unfilled Polysulfone, 27.5 MPa, Side #2, Preanodization Treatment #1, Anodized 60 Minutes, CA Anodized With HF, 30 A/m², 10 V, 298K

Element	Corrected Binding Energy C: 285.0 eV	Atomic Concentration (%)	% Conc. X / % Conc. Ti
C (1s)	285.0	77	77.0
O (1s)	532.2	14	14.0
F (1s)	NSP		
Ti (2p½)	465.2	1	1.0
Ti (2p3/2)	459.6		
Cr (2p3/2)	NSP		
V (2p3/2)	NSP		
Al (2p½)	74.4	5	5.0
S (2s)	231.8	2	2.0
S (2p½)	168.4		
N (1s)	NSP		
Si (2p3/2)	101.4	1	1.0
Cl (2p3/2)	NSP		
Na (1s)	NSP		

NSP: No Significant Peak

Sample Description: Fractured Bond, Anodized Ti-6Al-4V/UDEL® Unfilled Polysulfone, 27.5 MPa, Side #1, Preanodization Treatment #1, Anodized 60 Minutes, CA Anodized With HF, 30 A/m², 10 V, 298K

Element	Corrected Binding Energy C: 285.0 eV	Atomic Concentration (%)	% Conc. X / % Conc. Ti
C (1s)	285.0	77	38.5
O (1s)	532.0	15	7.5
F (1s)	NSP		
Ti (2p½)	464.3	2	1.0
Ti (2p3/2)	458.6		
Cr (2p3/2)	NSP		
V (2p3/2)	NSP		
Al (2p½)	74.4	2	1.0
S (2s)	231.8	1	0.5
S (2p½)	168.2		
N (1s)	400.4	2	1.0
Si (2p3/2)	102.2	1	0.5
Cl (2p3/2)	NSP		
Na (1s)	NSP		

NSP: No Significant Peak

Sample Description: Fractured Bond, Anodized Ti-6Al-4V/UDEL® Unfilled Polysulfone, 21.5 MPa, Preanodization Treatment #1, Anodized 20 Minutes, CA Anodized With HF, 30 A/m², 10 V, 283K

Element	Corrected Binding Energy C: 285.0 eV	Atomic Concentration (%)	% Conc. X / % Conc. Ti
C (1s)	285.0	59	9.8
O (1s)	530.6	28	4.7
F (1s)	689.3	3	0.5
Ti ($2p\frac{1}{2}$)	464.8	6	1.0
Ti (2p3/2)	458.8		
Cr (2p3/2)	NSP		
V (2p3/2)	NSP		
Al ($2p\frac{1}{2}$)	NSP		
S (2s)	232.1	4	0.7
S ($2p\frac{1}{2}$)	168.1		
N (1s)	NSP		
Si (2p3/2)	NSP		
Cl (2p3/2)	NSP		
Na (1s)	NSP		

NSP: No Significant Peak

Sample Description: Fractured Bond, Anodized Ti-6Al-4V/UDEL® Unfilled Polysulfone, 31.6 MPa, Preanodization Treatment #1, Anodized 20 Minutes, CA Anodized With HF, 20 A/m², 10 V, 298K

Element	Corrected Binding Energy C: 285.0 eV	Atomic Concentration (%)	% Conc. X / % Conc. Ti
C (1s)	285.0	72	24.0
O (1s)	532.2	17	5.7
F (1s)	689.3	4	1.3
Ti (2p½)	464.8	3	1.0
Ti (2p3/2)	459.0		
Cr (2p3/2)	NSP		
V (2p3/2)	NSP		
Al (2p½)	NSP		
S (2s)	232.2	4	1.3
S (2p½)	168.2		
N (1s)	NSP		
Si (2p3/2)	NSP		
Cl (2p3/2)	NSP		
Na (1s)	NSP		

NSP: No Significant Peak

Sample Description: Fractured Bond, Anodized Ti-6Al-4V/UDEL® Unfilled Polysulfone, 34.2 MPa, Side #1, Preanodization Treatment #2, Anodized 20 Minutes, CA Anodized With HF, 20 A/m², 10 V, 283K

Element	Corrected Binding Energy C: 285.0 eV	Atomic Concentration (%)	% Conc. X / % Conc. Ti
C (1s)	285.0	82	N/A
O (1s)	532.8	11	N/A
F (1s)	689.2	2	N/A
Ti ($2p\frac{1}{2}$)	NSP		
Ti (2p3/2)	NSP		
Cr (2p3/2)	NSP		
V (2p3/2)	NSP		
Al ($2p\frac{1}{2}$)	74.2	1	N/A
S (2s)	232.0	2	N/A
S ($2p\frac{1}{2}$)	168.2		
N (1s)	NSP		
Si (2p3/2)	104.0	2	N/A
Cl (2p3/2)	NSP		
Na (1s)	NSP		

NSP: No Significant Peak

Sample Description: Fractured Bond, Anodized Ti-6Al-4V/UDEL® Unfilled Polysulfone, 34.2 MPa, Side #2, Preanodization Treatment #2, Anodized 20 Minutes CA Anodized With HF, 20 A/m², 10 V, 283K

Element	Corrected Binding Energy C: 285.0 eV	Atomic Concentration (%)	% Conc. X / % Conc. Ti
C (1s)	285.0	82	N/A
O (1s)	533.2	14	N/A
F (1s)	NSP		
Ti ($2p\frac{1}{2}$)	NSP		
Ti (2p3/2)	NSP		
Cr (2p3/2)	NSP		
V (2p3/2)	NSP		
Al ($2p\frac{1}{2}$)	75.6	2	N/A
S (2s)	232.2	2	N/A
S ($2p\frac{1}{2}$)	168.2		
N (1s)	NSP		
Si (2p3/2)	NSP		
Cl (2p3/2)	NSP		
Na (1s)	NSP		

NSP: No Significant Peak

Sample Description: Fractured Bond, Anodized Ti-6Al-4V/UDEL® Unfilled Polysulfone, Aged 9 Months @ 443K, 19.7 MPa, Preanodization Treatment #1, Anodized 20 Minutes, CA Anodized With HF, 30 A/m², 10 V, 298K

Element	Corrected Binding Energy C: 285.0 eV	Atomic Concentration (%)	% Conc. X / % Conc. Ti
C (1s)	285.0	70	23.3
O (1s)	532.3	23	7.7
F (1s)	NSP		
Ti ($2p\frac{1}{2}$)	464.9	3	1.0
Ti (2p3/2)	459.1		
Cr (2p3/2)	NSP		
V (2p3/2)	NSP		
Al ($2p\frac{1}{2}$)	NSP		
S (2s)	232.3	4	1.3
S (2p3/2)	168.3		
N (1s)	NSP		
Si (2p3/2)	NSP		
Cl (2p3/2)	NSP		
Na (1s)	NSP		

NSP: No Significant Peak

Sample Description: Fractured Bond, Anodized Ti-6Al-4V/UDEL® Unfilled Polysulfone, Aged 9 Months @ 378K, 20.2 MPa, Preanodization Treatment #1, Anodized 20 Minutes, CA Anodized With HF, 30 A/m², 10 V, 298K

Element	Corrected Binding Energy C: 285.0 eV	Atomic Concentration (%)	% Conc. X / % Conc. Ti
C (1s)	285.0	70	23.3
O (1s)	532.1	21	7.0
F (1s)	689.2	2	0.7
Ti (2p½)	464.7	3	1.0
Ti (2p3/2)	459.0		
Cr (2p3/2)	NSP		
V (2p3/2)	NSP		
Al (2p½)	NSP		
S (2s)	232.2	4	1.3
S (2p½)	168.3		
N (1s)	NSP		
Si (2p3/2)	NSP		
Cl (2p3/2)	NSP		
Na (1s)	NSP		

NSP: No Significant Peak

Sample Description: Fractured Bond, Anodized Ti-6Al-4V/UDEL® Unfilled Polysulfone, Aged 11 Months @ 298K, 8.2 MPa, Preanodization Treatment #1, Anodized 20 Minutes, CA Anodized With HF, 30 A/m², 10 V, 298K

Element	Corrected Binding Energy C: 285.0 eV	Atomic Concentration (%)	% Conc. X / % Conc. Ti
C (1s)	285.0	78	78.0
O (1s)	532.3	16	16.0
F (1s)	NSP		
Ti (2p½)	465.2	1	1.0
Ti (2p3/2)	459.3		
Cr (2p3/2)	NSP		
V (2p3/2)	NSP		
Al (2p½)	NSP		
S (2s)	232.2	5	5.0
S (2p3/2)	168.3		
N (1s)	NSP		
Si (2p3/2)	NSP		
Cl (2p3/2)	NSP		
Na (1s)	NSP		

NSP: No Significant Peak

Sample Description: Fractured Bond, Anodized Ti-6Al-4V (UDEL®
Unfilled Polysulfone, Bonded 2 Days After
Anodization, Aged 9 Months @ 298K, 19.7 MPa,
Preanodization Treatment #1, Anodized 20 Minutes
CA Anodized With HF, 30 A m^{-2}, 10 V, 2 9K

Element	Corrected Binding Energy C: 285.0 eV	Atomic Concentration (%)	% Conc. / % Conc. Ti
C (1s)	285.0	76	38.0
O (1s)	532.3	18	9.0
F (1s)	NSP		
Ti (2p½)	465.1	2	1.0
Ti (2p3/2)	459.1		
Cr (2p3/2)	NSP		
V (2p3/2)	NSP		
Al (2p½)	NSP		
S (2s)	232.2	4	2.0
S (2p½)	168.3		
N (1s)	NSP		
Si (2p3/2)	NSP		
Cl (2p3/2)	NSP		
Na (1s)	NSP		

NSP: No Significant Peak

Sample Description: Fractured Bond, Anodized Ti-6Al-4V/UDEL® Unfilled Polysulfone, Aged 2 Months @ 298K, 29.2 MPa, Preanodization Treatment #1, Anodized 20 Minutes, CA Anodized With HF, 30 A/m², 10 V, 298K

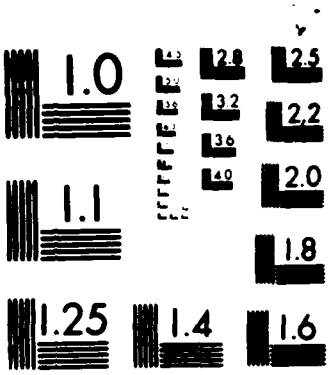
Element	Corrected Binding Energy C: 285.0 eV	Atomic Concentration (%)	% Conc. X / % Conc. Ti
C (1s)	285.0	76	76.0
O (1s)	530.7	17	17.0
F (1s)	689.5	1	1.0
Ti (2p½)	465.0	1	1.0
Ti (2p3/2)	459.6		
Cr (2p3/2)	NSP		
V (2p3/2)	NSP		
Al (2p½)	NSP		
S (2s)	232.2	5	5.0
S (2p½)	168.2		
N (1s)	NSP		
Si (2p3/2)	NSP		
Cl (2p3/2)	NSP		
Na (1s)	NSP		

NSP: No Significant Peak

AD-A183 854 AN INTERDISCIPLINARY APPROACH TO PREDICTIVE MODELING OF STRUCTURAL ADHESI (U) VIRGINIA TECH CENTER FOR ADHESION SCIENCE BLACKSBURG J A SKILES ET AL JUN 87 5/5

UNCLASSIFIED CAS/CHEM-87-2 F/G 11/1 NL





MICROCOPY RESOLUTION TEST CHART
NATIONAL BUREAU OF STANDARDS 1963-A

Sample Description: Fractured Bond, Anodized Ti-6Al-4V/Unfilled Polyphenylquinoxaline, Isochronally Bonded, 16.1 MPa, Side #1, Preanodization Treatment #2, Anodized 20 Minutes, CA Anodized With HF, 20 A/m², 10 V, 283K. Apparent anodic oxide/metal failure.

Element	Corrected Binding Energy C: 285.0 eV	Atomic Concentration (%)	% Conc. X / % Conc. Ti
C (1s)	285.0	37	2.5
O (1s)	530.2	38	2.5
F (1s)	686.1	7	0.5
Ti ($2p_{\frac{1}{2}}$)	464.5	15	1.0
Ti (2p3/2)	458.7		
Cr (2p3/2)	NSP		
V (2p3/2)	NSP		
Al ($2p_{\frac{1}{2}}$)	NSP		
S (2s)	NSP		
S ($2p_{\frac{1}{2}}$)	NSP		
N (1s)	399.6	3	0.2
Si (2p3/2)	NSP		
Cl (2p3/2)	NSP		
Na (1s)	NSP		

NSP: No Significant Peak

Sample Description: Fractured Bond, Anodized Ti-6Al-4V/Unfilled Polyphenylquinoxaline, Isothermally Bonded, 32.5 MPa, Preanodization Treatment #2, Anodized 20 Minutes, CA Anodized With HF, 20 A/m², 10 V, 283K

Element	Corrected Binding Energy C: 285.0 eV	Atomic Concentration (%)	% Conc. X / % Conc. Ti
C (1s)	285.0	81	40.5
O (1s)	532.8	12	6.0
F (1s)	NSP		
Ti (2p½)	465.1	2	1.0
Ti (2p3/2)	459.4		
Cr (2p3/2)	NSP		
V (2p3/2)	NSP		
Al (2p½)	NSP		
S (2s)	NSP		
S (2p3/2)	NSP		
N (1s)	399.2	5	2.5
Si (2p3/2)	NSP		
Cl (2p3/2)	NSP		
Na (1s)	NSP		

NSP: No Significant Peak

Sample Description: Fractured Bond, Anodized Ti-6Al-4V/Unfilled Polyphenylquinoxaline, Isothermally Bonded, 28.6 MPa, Preanodization Treatment #2, Anodized 20 Minutes, CA Anodized With HF, 30 A/m², 10 V , 283K

Element	Corrected Binding Energy C: 285.0 eV	Atomic Concentration (%)	% Conc. X / % Conc. Ti
C (1s)	285.0	80	40.0
O (1s)	533.6	14	7.0
F (1s)	NSP		
Ti (2p½)	464.7	2	1.0
Ti (2p3/2)	459.0		
Cr (2p3/2)	NSP		
V (2p3/2)	NSP		
Al (2p½)	NSP		
S (2s)	NSP		
S (2p½)	NSP		
N (1s)	399.3	4	2.0
Si (2p3/2)	NSP		
Cl (2p3/2)	NSP		
Na (1s)	NSP		

NSP: No Significant Peak

Sample Description: Fractured Bond, Anodized Ti-6Al-4V/Unfilled Polyphenylquinoxaline, Isothermally Bonded, 46.0 MPa, Side #2, Preanodization Treatment #1, Anodized 20 Minutes, CA Anodized With HF, 20 A/m², 10 V, 298K

Element	Corrected Binding Energy C: 285.0 eV	Atomic Concentration (%)	% Conc. X / % Conc. Ti
C (1s)	285.0	88	88.0
O (1s)	533.5	6	6.0
F (1s)	NSP		
Ti (2p½)	465.4	1	1.0
Ti (2p3/2)	459.7		
Cr (2p3/2)	NSP		
V (2p3/2)	NSP		
Al (2p½)	NSP		
S (2s)	NSP		
S (2p½)	NSP		
N (1s)	399.2	5	5.0
Si (2p3/2)	NSP		
Cl (2p3/2)	NSP		
Na (1s)	NSP		

NSP: No Significant Peak

Sample Description: Fractured Bond, Anodized Ti-6Al-4V/Unfilled Polyphenylquinoxaline, Isothermally Bonded, 46.0 MPa, Side #1, Preanodization Treatment #2, Anodized 20 Minutes, CA Anodized With HF, 20 A/m², 10 V, 298K

Element	Corrected Binding Energy C: 285.0 eV	Atomic Concentration (%)	% Conc. X / % Conc. Ti
C (1s)	285.0	86	86.0
O (1s)	533.5	7	7.0
F (1s)	NSP		
Ti ($2p\frac{1}{2}$)	464.9	1	1.0
Ti (2p3/2)	459.2		
Cr (2p3/2)	NSP		
V (2p3/2)	NSP		
Al ($2p\frac{1}{2}$)	NSP		
S (2s)	NSP		
S ($2p\frac{1}{2}$)	NSP		
N (1s)	399.3	6	6.0
Si (2p3/2)	NSP		
Cl (2p3/2)	NSP		
Na (1s)	NSP		

NSP: No Significant Peak

Sample Description: Fractured Bond, Anodized Ti-6Al-4V/Ablebond® 50% Calcium Carbonate Filled Polyimide, 6.0 MPa, Preanodization Treatment #2, Anodized 20 Minutes, CA Anodized With HF, 20 A/m², 10 V, 283K

Element	Corrected Binding Energy C: 285.0 eV	Atomic Concentration (%)	% Conc. X / % Conc. Ti
C (1s)	285.0	59	7.3
O (1s)	529.5	29	3.6
F (1s)	NSP		
Ti (2p½)	465.5	8	1.0
Ti (2p3/2)	459.8		
Cr (2p3/2)	NSP		
V (2p3/2)	NSP		
Al (2p½)	75.3	1	0.1
S (2s)	NSP		
S (2p3/2)	NSP		
N (1s)	400.4	3	0.4
Si (2p3/2)	NSP		
Cl (2p3/2)	NSP		
Na (1s)	NSP		

NSP: No Significant Peak

Sample Description: Fractured Bond, Anodized Ti-6Al-4V/Ultem® Unfilled Polyetherimide, 35.2 MPa, Preanodization Treatment #2, Anodized 20 Minutes, CA Anodized With HF, 20 A/m², 10 V, 283K

Element	Corrected Binding Energy C: 285.0 eV	Atomic Concentration (%)	% Conc. X / % Conc. Ti
C (1s)	285.0	45	4.1
O (1s)	530.5	41	3.7
F (1s)	NSP		
Ti (2p½)	464.7	11	1.0
Ti (2p3/2)	458.9		
Cr (2p3/2)	NSP		
V (2p3/2)	NSP		
Al (2p½)	74.3	1	0.1
S (2s)	NSP		
S (2p3/2)	NSP		
N (1s)	400.5	2	0.2
Si (2p3/2)	NSP		
Cl (2p3/2)	NSP		
Na (1s)	NSP		

NSP: No Significant Peak

Sample Description: Fractured Bond, Anodized Ti-6Al-4V/Ultem® 20% Glass Filled Polyetherimide, 31.2 MPa, Preanodization Treatment #2, Anodized 20 Minutes, CA Anodized With HF, 20 A/m², 10 V, 283K

Element	Corrected Binding Energy C: 285.0 eV	Atomic Concentration (%)	% Conc. X / % Conc. Ti
C (1s)	285.0	57	9.5
O (1s)	530.4	28	4.7
F (1s)	689.7	5	0.8
Ti (2p½)	464.7	6	1.0
Ti (2p3/2)	458.9		
Cr (2p3/2)	NSP		
V (2p3/2)	NSP		
Al (2p½)	74.2	2	0.3
S (2s)	NSP		
S (2p½)	NSP		
N (1s)	400.4	2	0.3
Si (2p3/2)	NSP		
Cl (2p3/2)	NSP		
Na (1s)	NSP		

NSP: No Significant Peak

Sample Description: Fractured Bond, Anodized Ti-6Al-4V/Victrex® Unfilled Polyethersulfone, 24.3 MPa, Preanodization Treatment #2, Anodized 20 Minutes, CA Anodized With HF, 20 A/m², 10 V, 283K

Element	Corrected Binding Energy C: 285.0 eV	Atomic Concentration (%)	% Conc. X / % Conc. Ti
C (1s)	285.0	51	7.3
O (1s)	530.5	34	4.9
F (1s)	689.5	2	0.3
Ti (2p½)	464.6	7	1.0
Ti (2p3/2)	458.9		
Cr (2p3/2)	NSP		
V (2p3/2)	NSP		
Al (2p½)	74.5	2	0.3
S (2s)	230.9	4	0.6
S (2p½)	167.9		
N (1s)	NSP		
Si (2p3/2)	NSP		
Cl (2p3/2)	NSP		
Na (1s)	NSP		

NSP: No Significant Peak

BIBLIOGRAPHIC DATA SHEET	1. Report No.	2.	3. Recipient's Accession No.

4. Title and Subtitle
An Interdisciplinary Approach to Predictive Modeling of Structural Adhesive Bonding/Chromic Acid Anodized Ti-6Al-4V: Its Characterization and Its Single Lap Bond Strength to Heat Resistant Adhesives

5. Report Date
June 1987

6.

7. Author(s)
Skiles, Jean Ann and Wightman, J. P.

8. Performing Organization Rept. No. CAS/CHEM-87-2

9. Performing Organization Name and Address
Virginia Polytechnic Institute and State University
Center for Adhesion Science and Department of Chemistry
Blacksburg, VA 24061

10. Project/Task/Work Unit No.

11. Contract/Grant No.
N00014-82-K-0185

12. Sponsoring Organization Name and Address
Office of Naval Research
800 N. Quincy Street
Arlington, VA 22217

13. Type of Report & Period Covered
Summary Report
1/82 - 6/87

14.

15. Supplementary Notes

16. Abstracts

Single lap bond strength and the fracture mechanism were determined for unprimed and Lica® 44 titanate primed chromic acid/hydrofluoric acid (CA/HF) anodized Ti-6Al-4V/heat resistant bonds. Adhesives tested had reported service temperatures $\geq$ 423K. Bonds were tested in ambient and also after exposure to thermal aging conditions. Anodic oxide morphology, structure, and thickness were also characterized as a function of anodization procedure.

17. Key Words and Document Analysis. 17a. Descriptors

17b. Identifiers/Open-Ended Terms

17c. COSATI Field/Group

18. Availability Statement	19. Security Class (This Report)	21. No. of Pages
Unlimited	UNCLASSIFIED	364
	20. Security Class (This Page) UNCLASSIFIED	22. Price

FORM NTIS-35 (REV. 10-73) ENDORSED BY ANSI AND UNESCO. THIS FORM MAY BE REPRODUCED USCOMM-DC 8265-P74

END

9-87

DTIC